NASA Contractor Report 3846

Experimental Investigation of Shock-Cell Noise Reduction for Dual-Stream Nozzles in Simulated Flight

B. A. Janardan, K. Yamamoto,
R. K. Majjigi, and J. F. Brausch

CONTRACT NAS3-23166
NOVEMBER 1984

NASA

NASA Contractor Report 3846

Experimental Investigation of Shock-Cell Noise Reduction for Dual-Stream Nozzles in Simulated Flight

B. A. Janardan, K. Yamamoto,
R. K. Majjigi, and J. F. Brausch
General Electric Company
Cincinnati, Ohio

Prepared for
Lewis Research Center
under Contract NAS3-23166

National Aeronautics
and Space Administration

**Scientific and Technical
Information Branch**

1984

TABLE OF CONTENTS

TABLE OF CONTENTS (Concluded)

1.0 INTRODUCTION

1.1 BACKGROUND

Whenever a jet from a convergent nozzle operating at supercritical pressure ratios exhausts into the ambient environment, the static pressure at the nozzle exit is greater than the ambient pressure. The expansion from the higher exit-plane pressure to the ambient pressure occurs outside the nozzle in the form of oblique expansion waves radiating from the nozzle lip which, on striking the opposite boundary of the jet, are reflected as a family of compression waves as shown in Figure 1-1. These compression waves converge to form a normal shock-wave. This cycle then is repeated resulting in a pattern of regularly spaced shock formations as shown in Figure 1-2. The spacing and strength of these shocks diminish in the downstream direction due to the mixing of the jet plume with the ambient air. The mixing process also produces turbulence in the form of statistically regular eddies which convect downstream with the flow. As these eddies pass through (or by) the shock fronts, they disturb the shocks causing them to emit acoustic waves. The acoustic waves from the various shock-cells can constructively or destructively interfere depending on the shock spacing, the eddy convection velocity, and the lifetime of a given eddy.

The eddies, produced in the mixing layers of the plume, are themselves unsteady so that the emitted acoustic waves from each of the shocks have characteristics which are related to the unsteadiness of the turbulent disturbances (e.g., their characteristic frequency and amplitude). The far-field time-average correlation of this emission, after summing the contributions from all the shocks, produces a spectrum made up of two basic components. First, the sum of the mean-square pressure signals from each shock produces a "group spectrum" which is rather broadband in character, similar to a jet mixing noise spectrum. The second component, referred to as the "interference spectrum," results from the selective reinforcement and cancellation which occurs between emitted waves from neighboring shocks. The superposition of these two components results in the rather "peaky" spectrum that is identified generally as the shock-cell noise spectrum. This is illustrated in Figure 1-3.

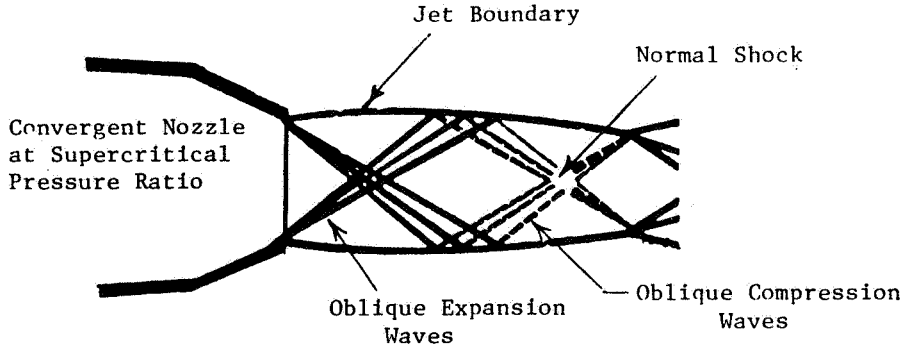

Figure 1-1. Development of a Shock-Cell.

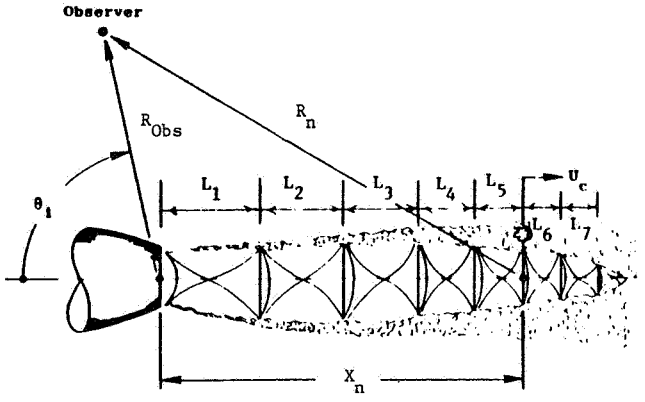

Figure 1-2. Representation of a Family of Shock-Cells

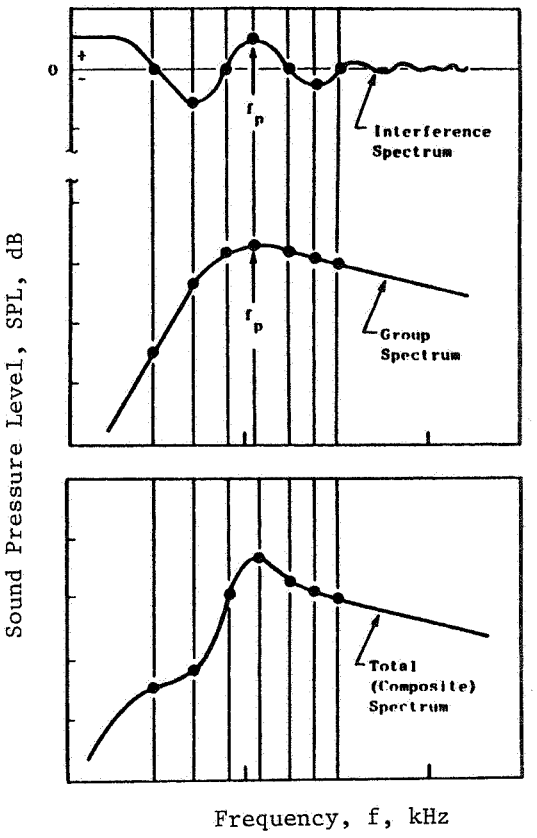

Figure 1-3. Illustration of Primary Components of a Convergent Circular Nozzle Shock-Cell Noise Spectrum.

The above described physical process by which the shock-cell noise is generated was first proposed by Harper-Bourne and Fisher (Reference 1). Employing measured data, they proposed a semi-empirical model to predict the peak frequency and spectra associated with the shock-cell noise. Important aspects of this model have been verified through experiments with a convergent circular nozzle operating at supercritical pressure ratios (References 1 through 3). One such verification is presented in Figure 1-4. An examination of this figure also indicates that in the forward quadrant, the shock-cell noise of a model scale nozzle tends to dominate the total jet noise spectrum at middle to high frequencies. This model scale data when extrapolated to be applicable to a typical engine size nozzle would indicate that shock-cell noise would be the dominant front quadrant noise at low to middle frequencies.

Experimental measurements (References 2 and 4 through 7) indicate that the basic shock-cell noise is amplified in the forward quadrant due to aircraft motion and the jet mixing noise is reduced in flight in the aft quadrant. To illustrate this flight effect, static and simulated-flight measured convergent circular nozzle directivity and spectral acoustic data are presented in Figure 1-5. The significant amplification of the shock-cell noise observed in flight, therefore, indicates the potential problems associated with shock-cell noise and the need to reduce or eliminate it.

1.2 SINGLE-FLOW PROGRAM REVIEW

As briefly described above, shock-cell associated noise is a significant contributor to the total noise radiated from jets operating at supercritical pressure ratios. In addition, the shock-cell noise is the dominant component in the forward quadrant and is amplified in flight. References 3 and 8 through 11 have demonstrated, under static conditions, the use of convergent-divergent (C-D) nozzle passages for circular nozzles as one means of effecting shock-cell noise reduction. Figure 1-6, from References 9 and 11, illustrates typical benefits measured under static tests from the use of convergent-divergent circular nozzles. Over the recent years, the General Electric Company, under NASA-Lewis sponsored contracts (References 6 and 7) has tested in both static and simulated flight conditions, a family of convergent and C-D circular and annular plug nozzles. A brief summary of the acoustic and diagnostic data obtained with circular and annular plug nozzles are presented in this introduction in order to demonstrate the effectiveness

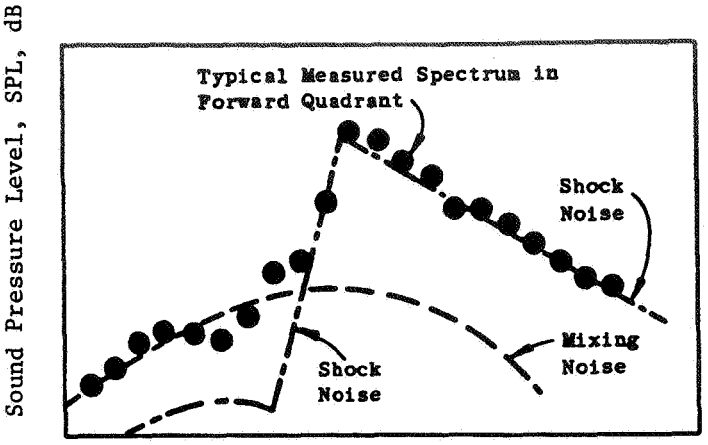

a) Typical Fordward-Quadrant Spectrum

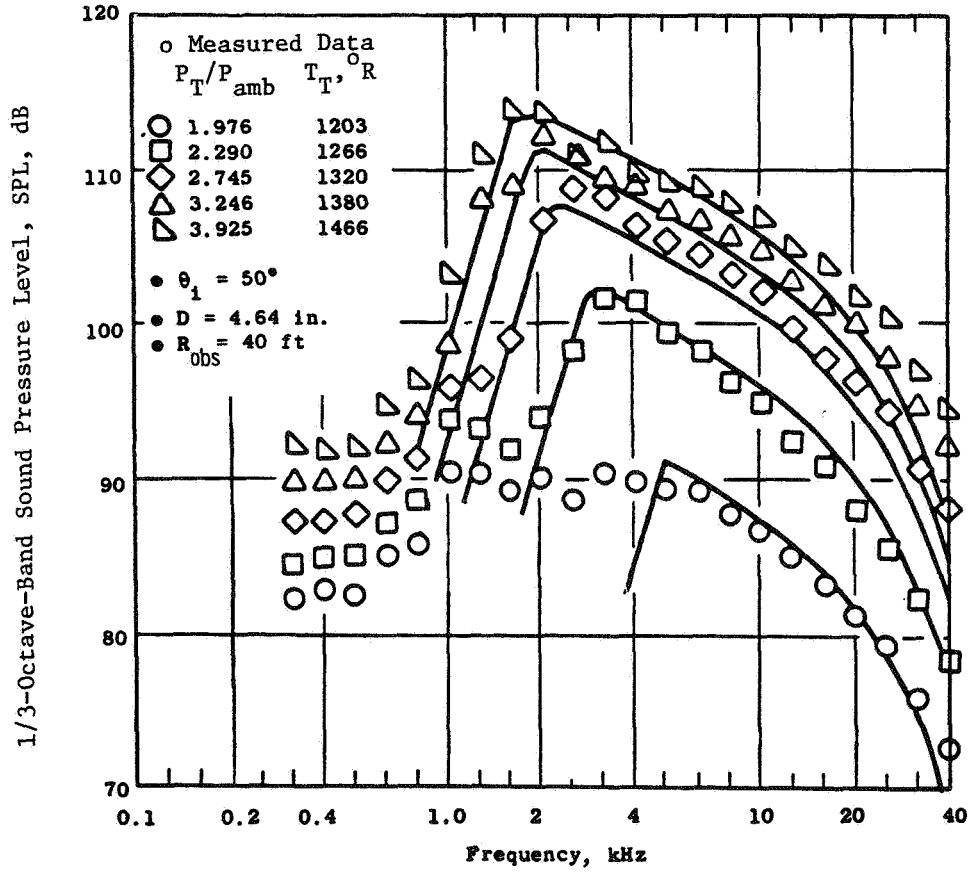

b) Spectrum Over a Range of Operating Conditions

FIGURE 1-4. COMPARISON OF PREDICTED SHOCK-CELL NOISE WITH MEASURED CONVERGENT CIRCULAR NOZZLE SPECTRA (REFERENCE 2).

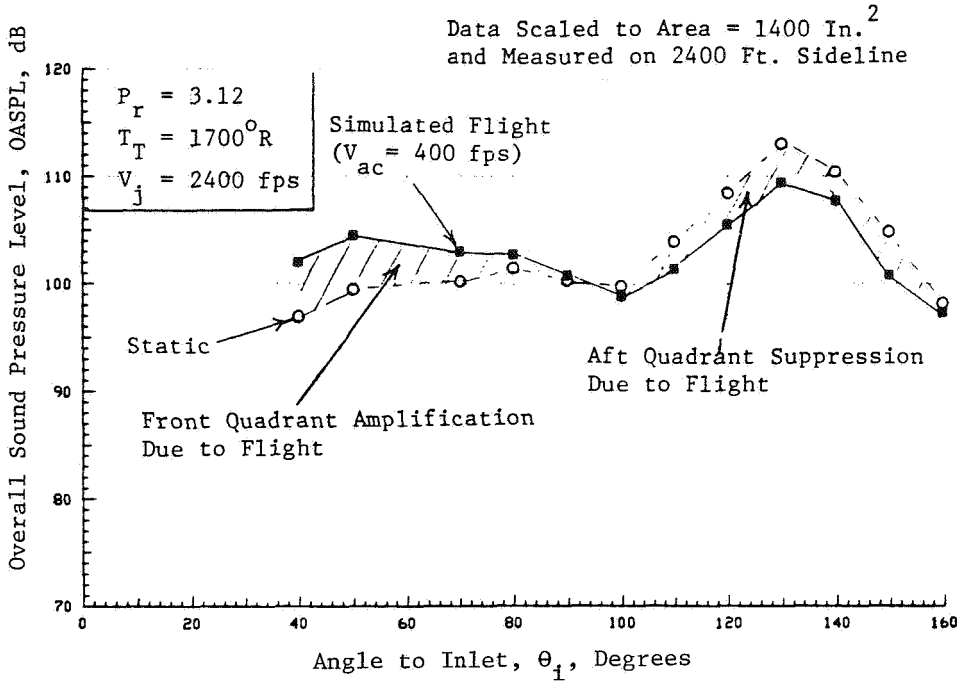

a) OASPL Directivity

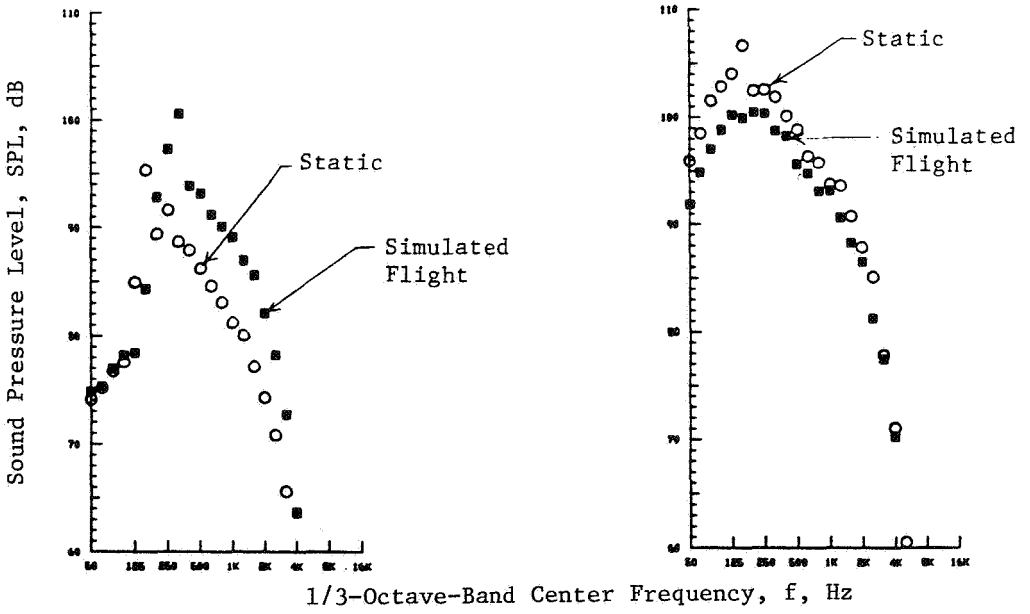

b) Front Quadrant Spectra
(Directivity Angle θ_i= 50°)

c) Aft Quadrant Spectra
(Directivity Angle θ_i= 130°)

Figure 1-5. Effects of Flight on OASPL Directivity and Typical Front and Aft Quadrant Spectra of Convergent Circular Nozzle. (Data from Reference 5)

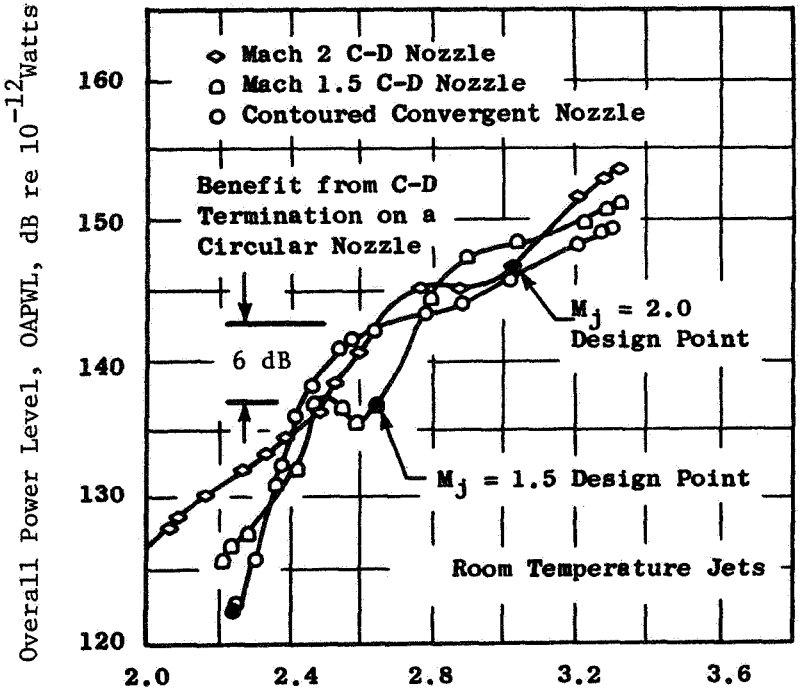

a) FROM REFERENCE 9

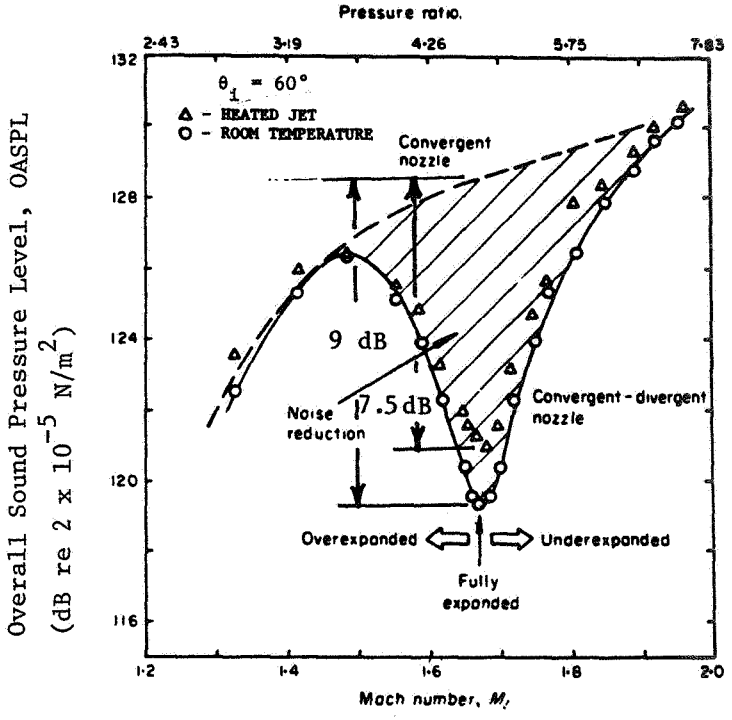

b) FROM REFERENCE 11

FIGURE 1-6. REDUCTION IN THE FORWARD QUADRANT NOISE OBTAINED BY USING CONVERGENT-DIVERGENT NOZZLES (STATIC TESTS).

of C-D flowpaths in the reduction/elimination of shock-cell noise and also to provide the needed background that preceded the present work on coannular plug nozzles. Unless otherwise stated, the results presented are measured data that are scaled to a size of 1,400 in^2, extrapolated to a sideline of 2,400 ft, and corrected to a standard day (59° F and 70% relative humidity) atmospheric attenuation (Shields and Bass method, Reference 12).

1.2.1 Circular Nozzles

The convergent-divergent circular nozzle was designed for a shock-free flow at an exit jet Mach number, M_j, of 1.40 (P_r = 3.12 and T_T = 1700° R). To demonstrate the effectiveness of the C-D contour in the control of the shock-cell noise at and in the vicinity of the shock-free condition, acoustic tests were conducted over a pressure ratio range of 2.6 to 3.9. The OASPL data measured at a typical forward quadrant angle of Θ_i = 50° are plotted in Figure 1-7 as a function of shock strength parameter β (which is defined as equal to $\sqrt{M_j^2 - 1}$). The data are compared in this figure with the acoustic data measured with a convergent circular nozzle. An examination of this figure indicates a significant broad region of effectiveness of the C-D design in reducing the forward quadrant shock-cell associated noise under both static and simulated flight conditions. In addition, this figure indicates that, at Θ_i = 50°, a maximum reduction of 7.5 dB and 11 dB is obtained in the OASPL under static and simulated flight conditions, respectively, with the use of the C-D circular nozzle relative to the convergent circular nozzle.

Diagnostic data are presented in Figure 1-8 to substantiate that the significant acoustic benefit noted in Figure 1-7 with the C-D nozzle at its design condition is due to the absence of the shock structure downstream of its exit. The data presented compare the axial mean velocity traces, obtained with a laser velocimeter (LV), along the centerlines of convergent and C-D circular nozzles and shadowgraphs taken in the vicinity of the nozzle exits including the region of the first shock-cell location. An examination of mean velocity traces indicates the presence of 9 shock-cells (located at each of the velocity minimums) within the first 11 diameters from the exit of the convergent nozzle and an absence of a similar shock-cell pattern for the C-D configuration, with both nozzles operating at the same aerodynamic

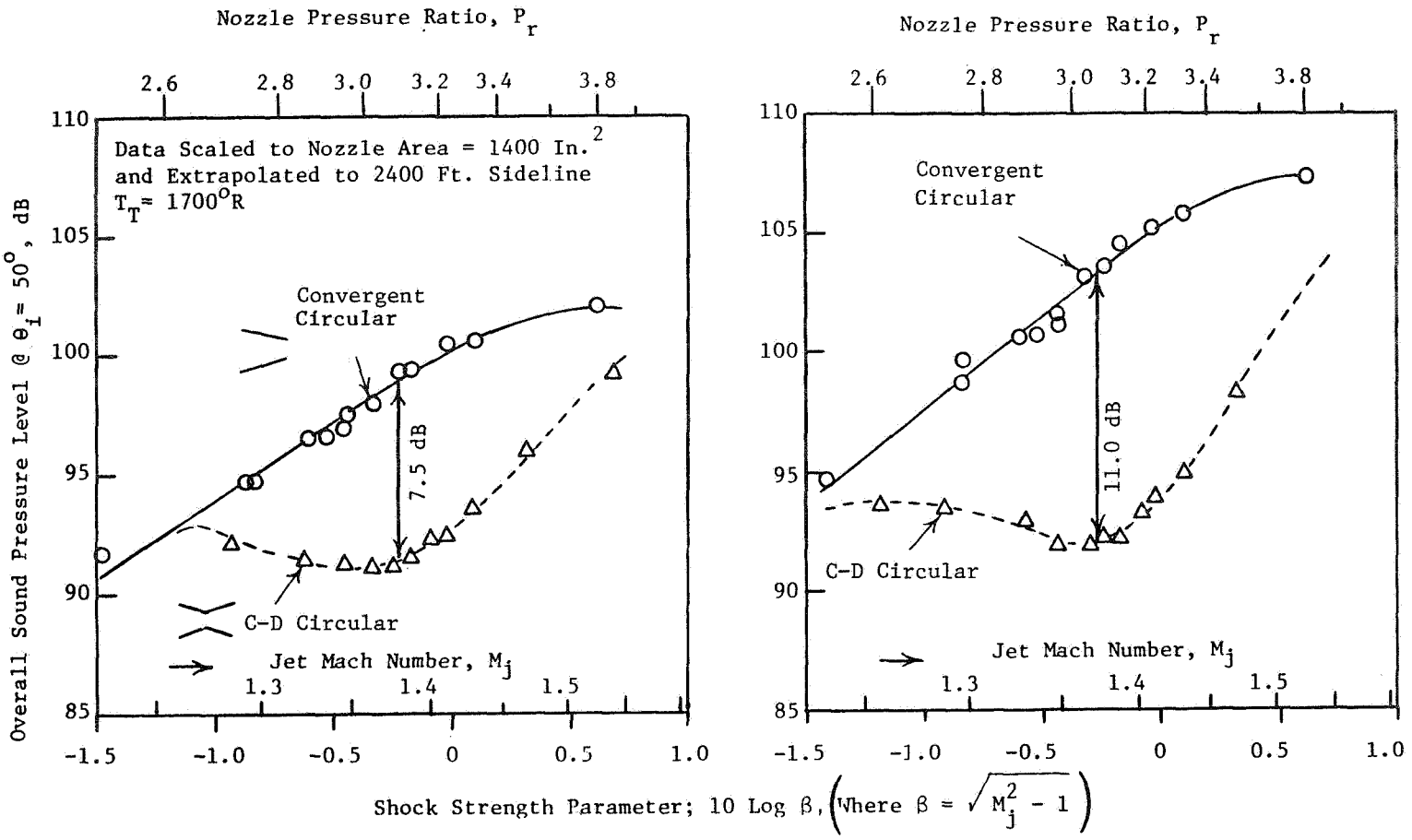

Figure 1-7. Effectiveness of C-D Flowpath on Circular Nozzle in Shock-Cell Noise Reduction. (Data from Reference 7)

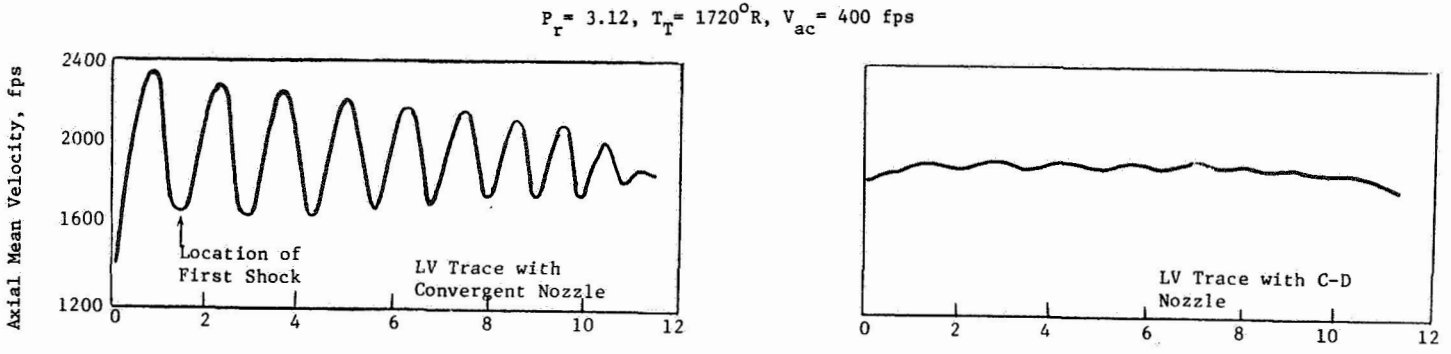

a) Mean Velocity Distribution Along the Nozzle Axis

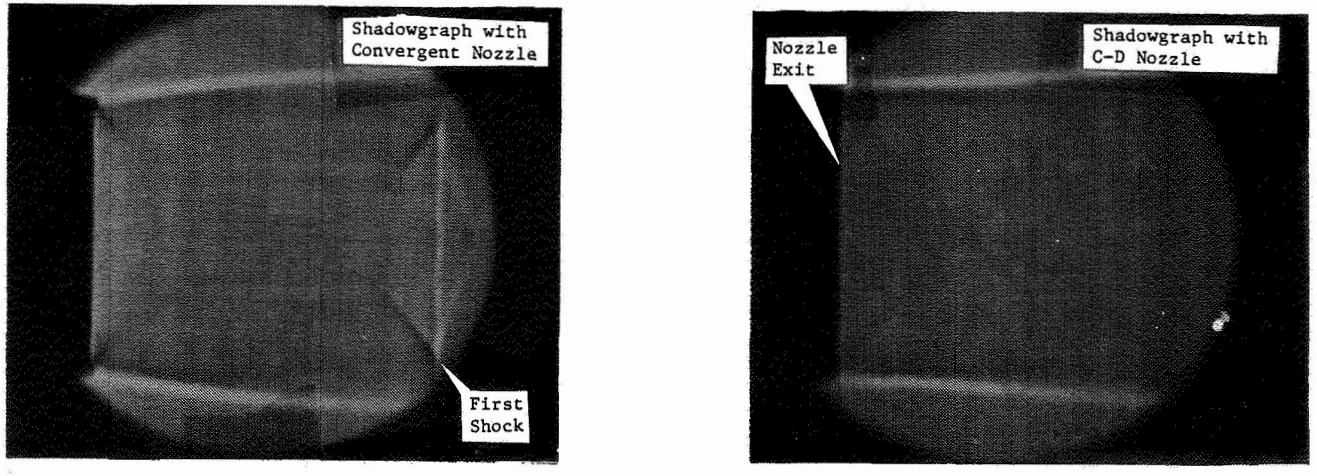

b) Shadowgraphs Near the Nozzle Exit

FIGURE 1-8. COMPARISON BETWEEN CONVERGENT AND C-D CIRCULAR NOZZLES DIAGNOSTIC (LV AND SHADOWGRAPH) DATA AT C-D NOZZLE DESIGN CONDITION (DATA FROM REFERENCE 7).

conditions. Similarly, the shadowgraphs taken in the vicinity of the nozzle exits indicate the presence and absence of the first shock-cell for the convergent and C-D nozzles, respectively.

Comparison of static and simulated flight OASPL-directivity and selected front quadrant spectra of the C-D nozzle at its design condition with the corresponding convergent nozzle data are presented in Figures 1-9 and 1-10, respectively. The data presented in Figure 1-9 indicate the significant OASPL benefit observed with the C-D nozzle at all angles in the front quadrant under both static and simulated flight conditions. Similarly, the data of Figure 1-10 indicate the significant spectral benefit obtained over the entire frequency range for a given front quadrant location with the C-D nozzle.

It was earlier noted from the convergent nozzle static and simulated flight data presented in Figure 1-5 that the basic shock-cell noise in the front quadrant is amplified due to aircraft motion. A similar comparison of the static with simulated flight OASPL-directivity data of the C-D circular nozzle at the shockless condition, presented in Figure 1-11, indicates no significant noise amplification in the front quadrant due to flight. This provides additional confirmation to the absence of the shock structure with the convergent-divergent nozzle and indicates that the front quadrant acoustic signature and benefit associated with such a configuration is unaltered due to flight.

1.2.2 Annular Plug Nozzles

The convergent-divergent annular plug nozzle, the details of which are presented in Figure 1-12, is designed for a shock-free flow at an exit jet Mach number, M_j, of 1.44 (P_r = 3.3 and T_T = 1760° R). The radius ratio, R_r, at the throat and exit are 0.855 and 0.789, respectively. To demonstrate the effectiveness of the design C-D contour in the control of shock-cell noise at and in the vicinity of its shock-free condition, static and simulated flight (V_{ac} = 400 fps) tests were conducted over a pressure ratio range of 2.94 to 3.54 (and Mach number range of M_j = 1.34 to 1.48). The PNL data measured at a typical forward quadrant angle of Θ_i = 60° are plotted in Figure 1-12, as a function of shock strength parameter (which is defined as equal to $\sqrt{M_j^2 - 1}$). The data are compared in this figure with

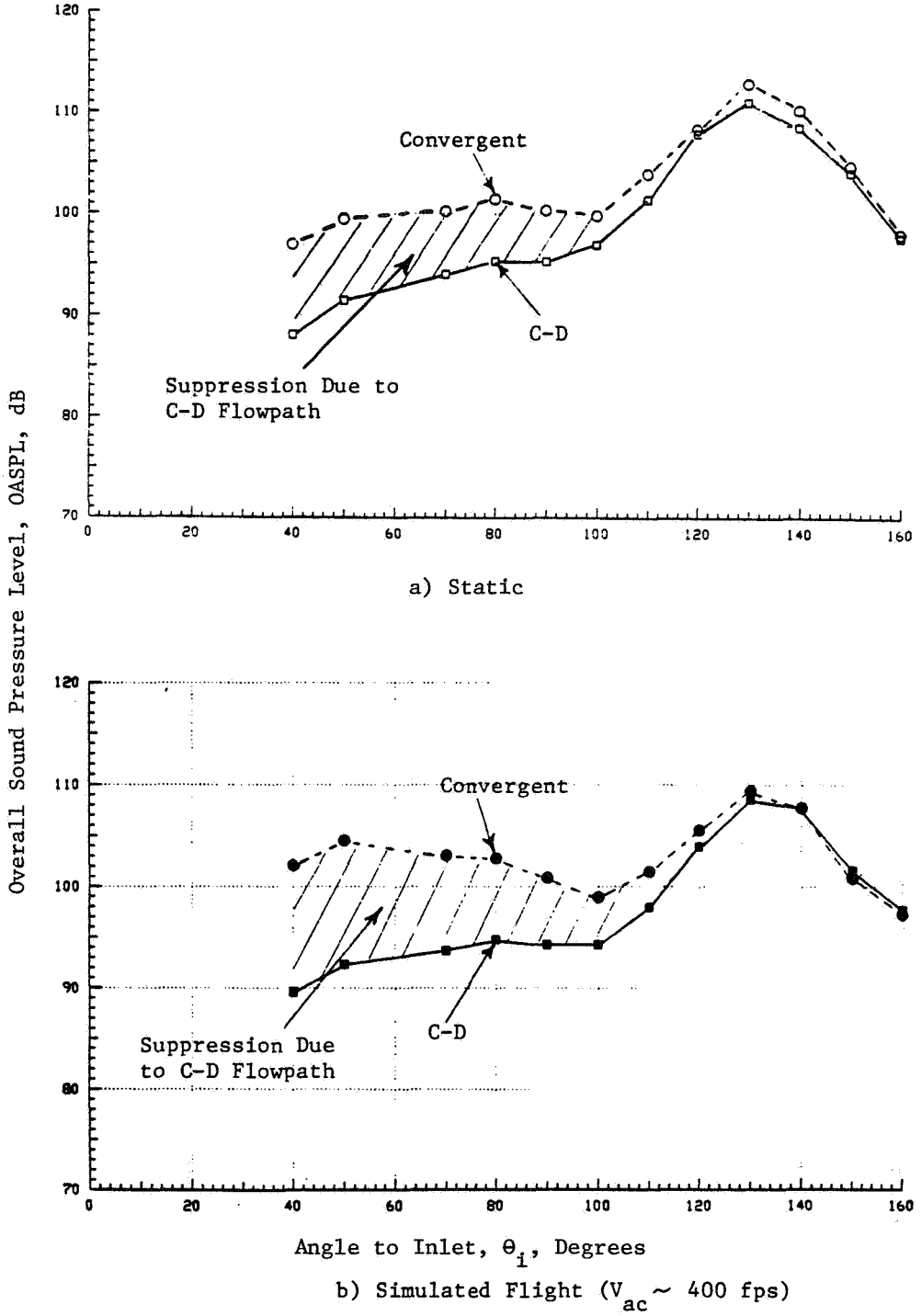

Figure 1-9. Comparison of OASPL Directivity of Convergent and C-D Nozzle at the C-D Nozzle Design Conditions. (Data from Reference 7)

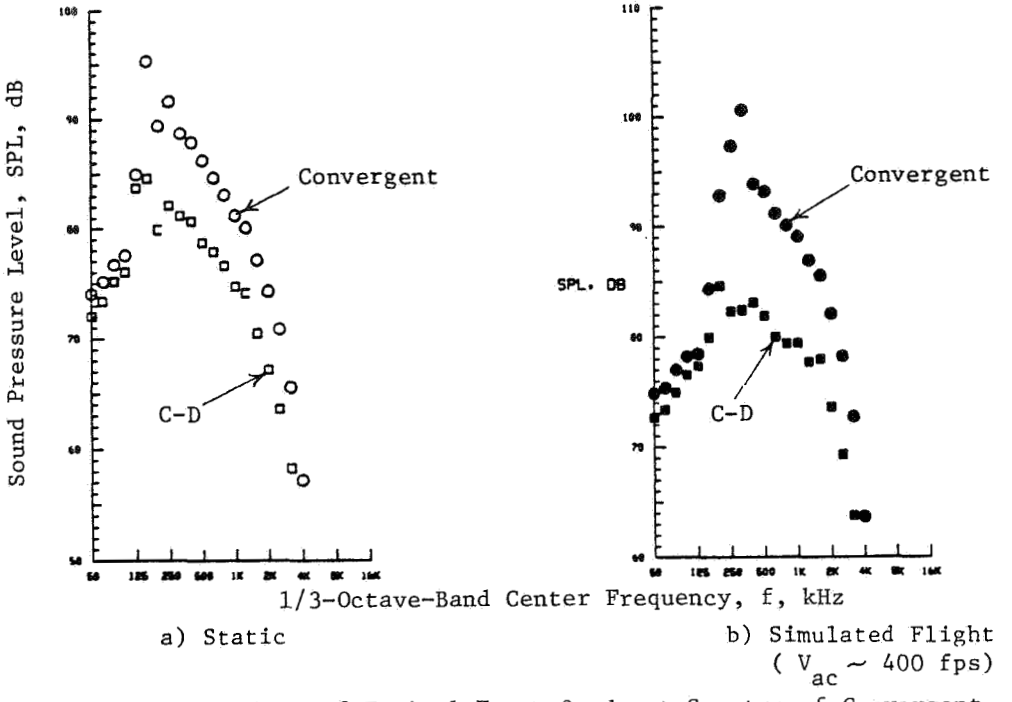

Figure 1-10. Comparison of Typical Front Quadrant Spectra of Convergent and C-D Nozzles at the C-D Nozzle Design Conditions, θ_i = 50°. (Data from Reference 7)

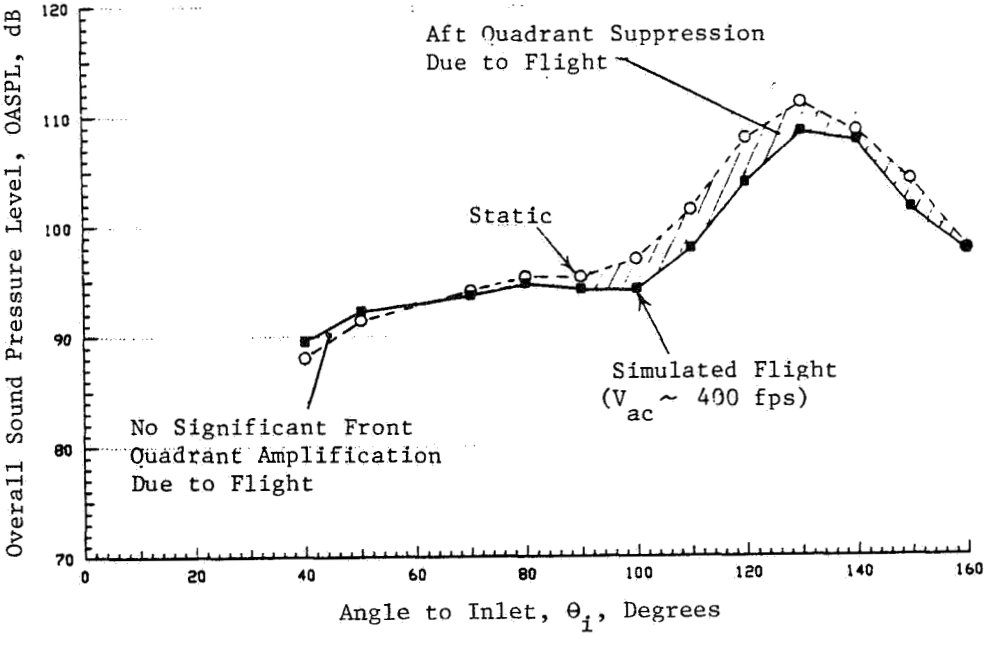

Figure 1-11. Effect of Flight on OASPL Directivity of the C-D Nozzle at Its Design Condition. (Data from Reference 7)

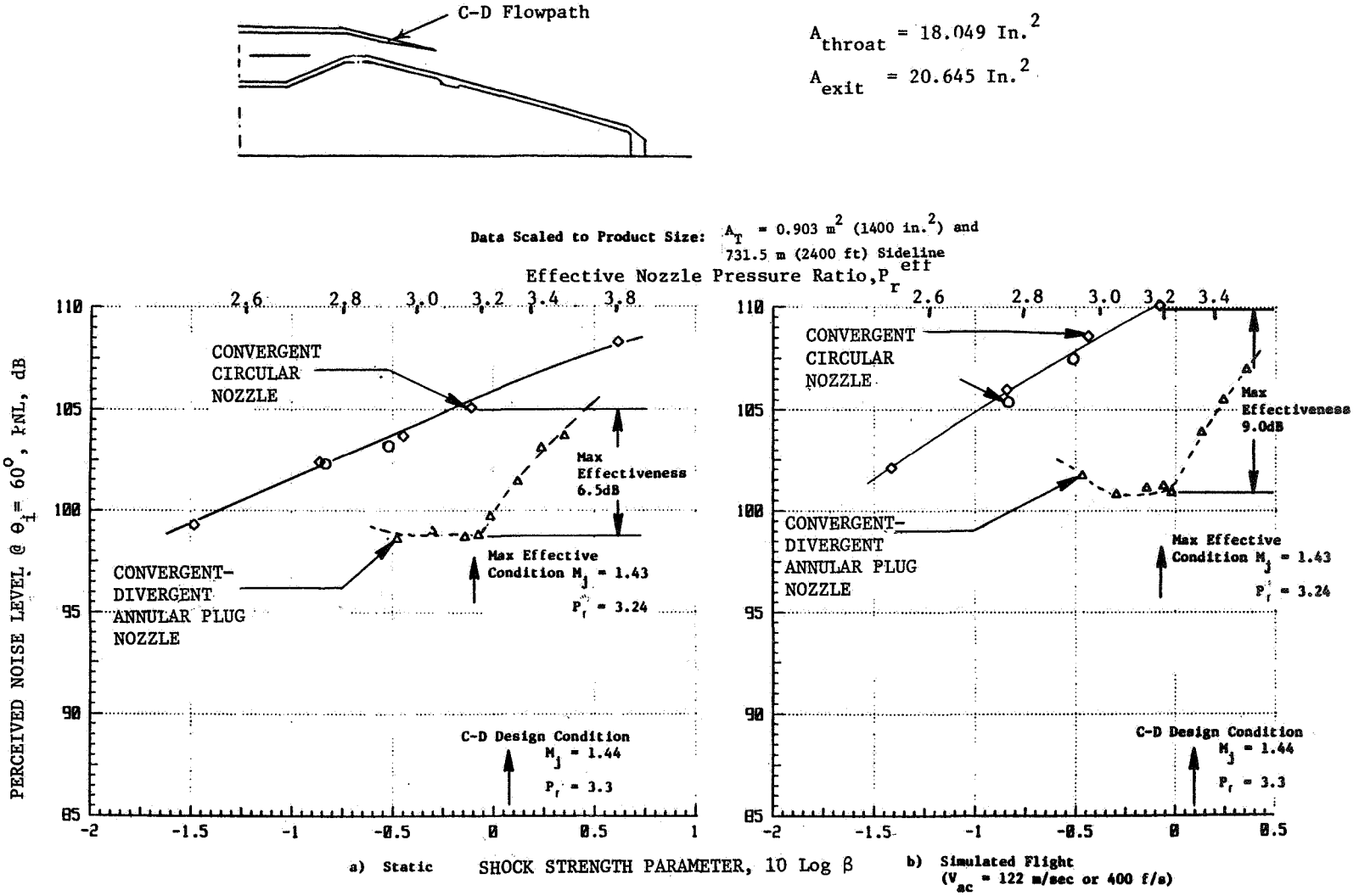

Figure 1-12. C-D Effectiveness in Shock Noise Reduction for a C-D Annular Plug Nozzle; Static and Simulated Flight PNL_{60} Data. (Reference 6)

the results of the convergent circular nozzle. An examination of the figure indicates a broad region of effectiveness of C-D design in reducing the forward quadrant shock noise. In addition, this figure indicates that, at $\Theta_i = 60°$, a maximum reduction of 6.5 and 9 dB is obtained with the use of the C-D annular plug nozzle relative to a convergent circular nozzle under static and simulated flight conditions, respectively. The jet Mach number corresponding to this maximum effective condition is observed, under both static and simulated flight conditions, to be $M_j = 1.43$ ($P_r = 3.24$) which is close to the C-D design condition of $M_j = 1.44$ ($P_r = 3.3$).

Diagnostic mean velocity data obtained during LV traverses parallel to the plug and along the nozzle centerlines of convergent annular and C-D annular plug nozzles are presented in Figures 1-13 and 1-14, respectively. The aerodynamic flow conditions for both of the test cases correspond to the design condition of the C-D annular nozzle. A comparison of the presented data indicates that while no significant differences are seen in the mean velocity variations along the axes of the two nozzle configurations (and hence no change in the shock-structure) significant differences in the mean velocity distributions (and hence the shock strengths) are noted along the plug. This observed presence of the shock-cell downstream of the C-D annular plug nozzle, therefore, indicates that all of the shock-cell noise has not been eliminated with this nozzle operating at its design condition and a greater reduction in the front quadrant shock-cell noise could be obtained provided the downstream of shock-cell structure could be eliminated.

1.3 DUAL-FLOW PROGRAM SCOPE

Detailed acoustic and diagnostic data that describe the effectiveness of C-D flow passages with coannular nozzles are not available except for the very limited acoustic data of Reference 6. This program was initiated with the objective to obtain such data at elevated exhaust nozzle temperatures and pressure ratios that are typical of operating conditions of a variable cycle engine and applicable for an advanced supersonic transport. The test configurations included high-radius-ratio convergent and C-D unsuppressed coannular nozzles both with truncated and extended plugs, and convergent and C-D coannular plug nozzles with convergent and C-D 20-chute mechanical suppressor in the outer stream, respectively. A total of 153 acoustic test points were completed. In addition, velocity profile measurements for selected

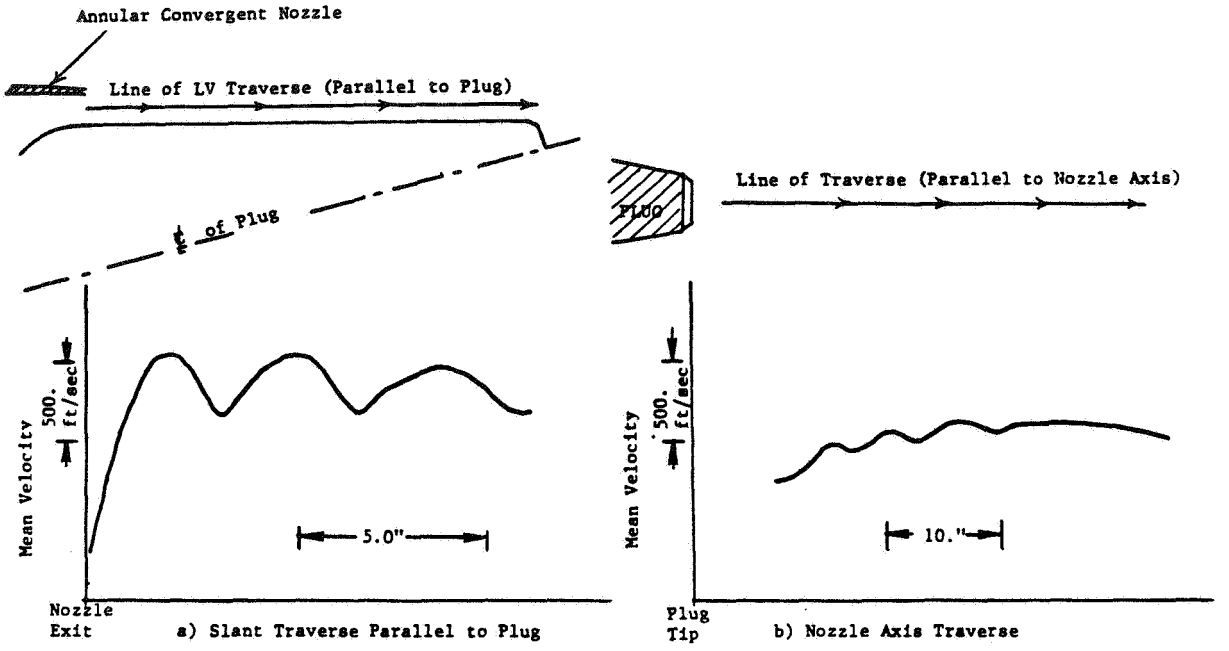

Figure 1-13. Mean Velocity Data Measured with a Convergent Annular Plug Nozzle at Aerodynamic Conditions that Match the Design Conditions of the C-D Annular Nozzle.

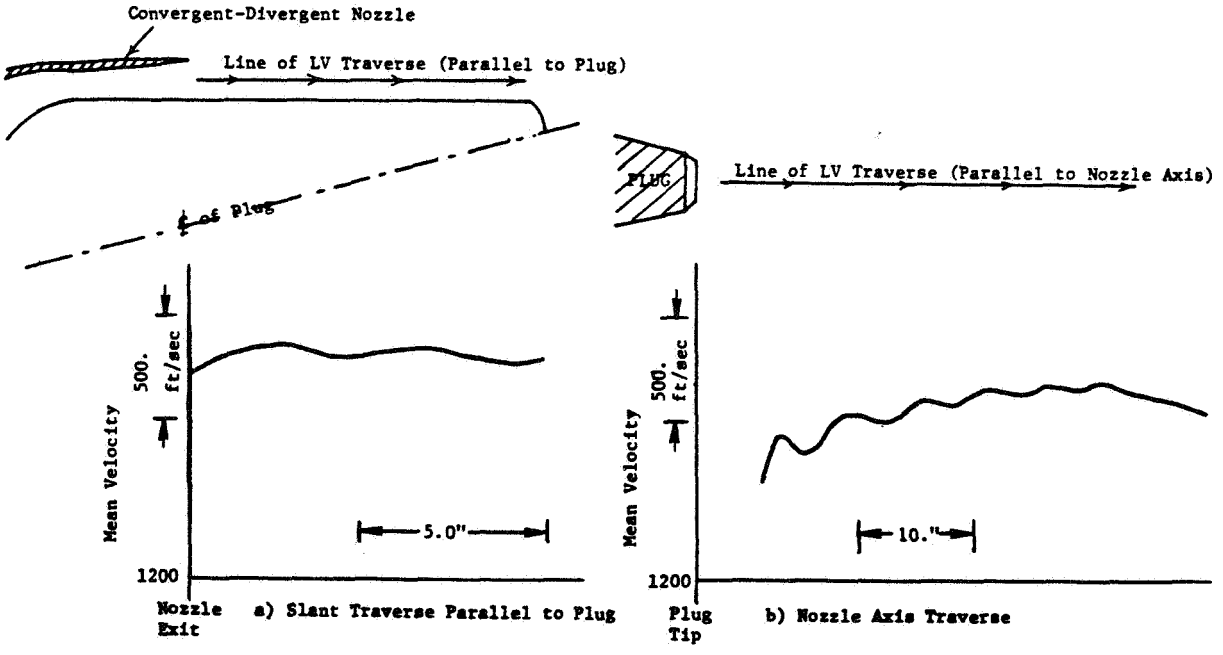

Figure 1-14. Mean Velocity Data Measured with the Convergent-Divergent Nozzle Operating at Its Design Condition.

acoustic test points of each of the configurations and diagnostic shadowgraphs of convergent and C-D nozzles at C-D design conditions were obtained under both static and simulated flight conditions. Detailed descriptions of the model nozzle configurations, tabulations that summarize the aerodynamic flow conditions of the acoustic, laser velocimeter and shadowgraph test points, and brief descriptions of the test facility are provided in Section 2.0 of this report.

Measured acoustic and diagnostic LV and shadowgraph data are presented and discussed in Section 3.0 with the objective to demonstrate the usefulness of C-D passages on unsuppressed coannular plug nozzles for the reduction of shock-cell associated noise at and in the vicinity of the C-D design conditions. Under these conditions, as with the unsuppressed annular plug nozzle of Reference 7, the C-D flowpaths on unsuppressed coannular nozzles with truncated plug were observed to eliminate shock-cells on the plug only. The flow expansion at the plug tip and the resulting downstream shock-cell structure of the unsuppressed C-D coannular nozzle were eliminated by replacing the truncated plug with an extended sharp plug. While the benefit of C-D passages in significantly reducing the shock-cell noise of unsuppressed coannular nozzle near the C-D design conditions was noted, an alternative approach is demonstrated in Section 3.0 to reduce the front quadrant noise over an entire operational range of the outer stream. This was achieved by keeping the inner stream of a convergent coannular plug nozzle subsonic for all underexpanded outer stream conditions. Finally in that section, the acoustic and diagnostic data of coannular configurations with convergent and C-D 20-chute mechanical suppressor in the outer stream are presented and the significantly different spectral characteristics between the two nozzles are indicated.

Based on measured diagnostic data of the flowfield of unsuppressed convergent and C-D coannular plug nozzles, appropriate parameters that characterize the length scale and strength associated with the shock-cells on the plug and downstream of the plug were identified. An existing shock-cell noise predictive program (Reference 5), based on the Harper-Bourne and Fisher model for circular nozzles (Reference 1), was modified to account for the two shock-cell structures. Descriptions of the modifications along with typical measured and predicted acoustic data comparisons, indicating acceptable agreement between the two sets of data, are provided in Section 4.0.

2.0 TEST FACILITIES, MODEL NOZZLES AND TEST MATRICES

All of the acoustic and diagnostic tests of this program were conducted in the General Electric Anechoic Free-Jet Facility located in Evendale, Ohio. Brief descriptions of the facility, data acquisition and reduction procedures, and scale model test nozzles are presented in this section. Detailed descriptions of the facility plus acoustic data acquisition, reduction and flight transformation procedures are provided in References 7, 13 and 14. Tabulations that summarize the aerodynamic flow conditions of the conducted acoustic, laser velocimeter and shadowgraph tests and brief descriptions of the scale-model nozzles of this investigation are provided in this section. Measured acoustic and diagnostic data are summarized in Reference 15.

2.1 ANECHOIC FREE-JET FACILITY

The facility, schematically shown in Figure 2-1, is a cylindrical chamber 13.1 meters (43 feet) in diameter and 21.95 meters (72 feet) high. The inner surfaces of the chamber are lined with anechoic wedges made of fiberglass wool to yield a low frequency cutoff below 220 Hz and an absorption coefficient of 0.99 above 220 Hz. Descriptions and results of the tests conducted in order to determine the acoustic characteristics of the anechoic chamber (such as inverse square law tests) and the mean velocity and turbulence intensity distributions in the free jet are presented in Reference 14.

The facility can accommodate model configurations up to a size of 17.3 cm (6.8 inch) in equivalent flow diameter. The required streams of heated air for a dual-flow arrangement, produced by two separate burners, flow through silencers and plenum chambers before entering the test nozzle.

The tertiary air system consists of a 250,000-scfm (50 inches water column static pressure) fan and a 3,500-hp electric motor. The transition duct work and silencer route the air from the fan discharge to the tertiary silencer plenum chamber. The air is then discharged through the 1.2-m (48 inch) free-jet exhaust. Tertiary flow at its maximum permits simulation up to a Mach number of 0.41. Mach number variation is obtained by changing

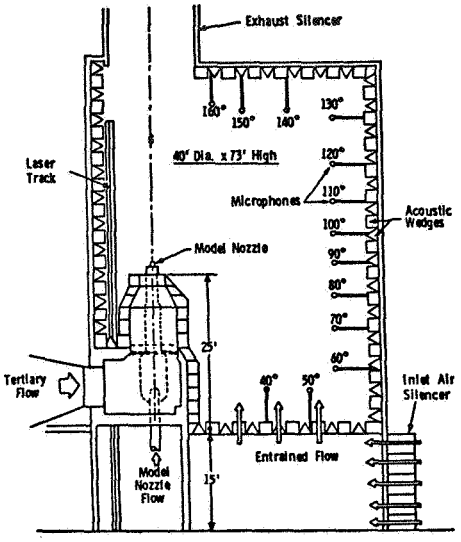

Angle (Degrees)	Radial Distance m	ft
40	7.92	26.0
50	9.48	31.1
60	9.50	31.18
70	8.76	28.73
80	8.36	27.42
90	8.23	27.00
100	8.36	27.42
110	8.76	28.73
120	9.5	31.18
130	10.74	35.25
140	9.17	30.17
150	8.23	27.0
160	7.92	26.0

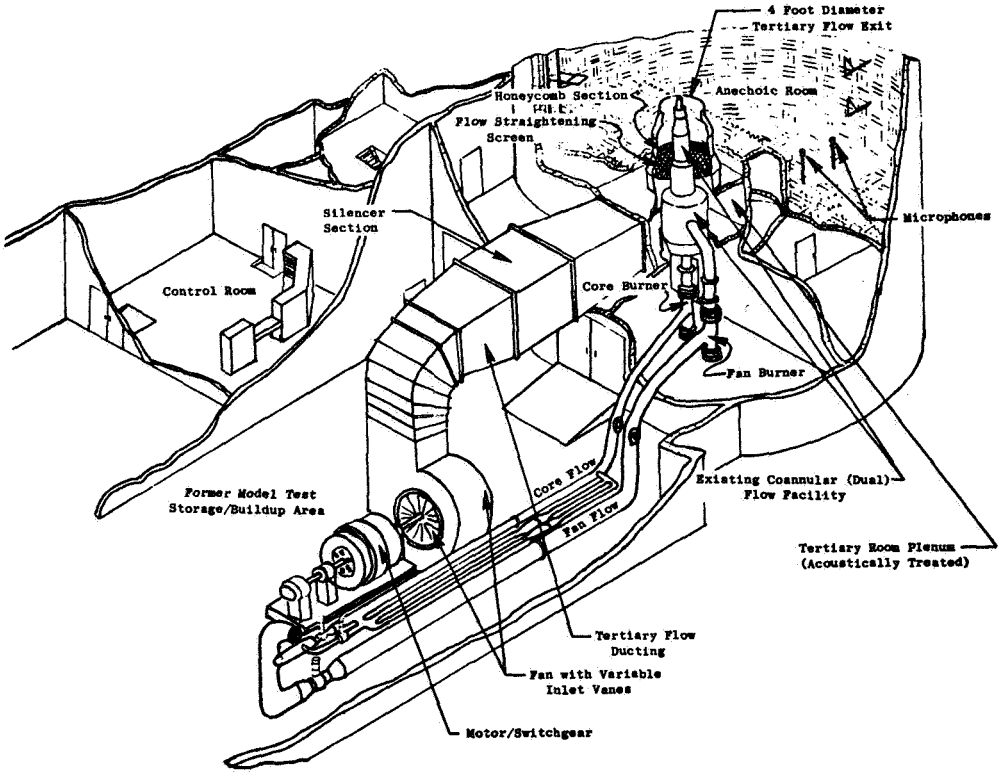

Figure 2-1. Anechoic Free-Jet/Jet Noise Facility Schematic.

the tertiary airflow rate achieved by adjusting the fan inlet vanes. The combined airflow is exhausted through a "T" stack directly over the nozzles in the ceiling of the chamber.

2.1.1 Aerodynamic Data Acquisition and Reduction Procedures

Facility Operational Method

The facility operating parameters are monitored during testing at the control console to (1) ensure that prescribed facility limits are not exceeded and (2) set the test-point conditions.

The core and fan discharge pressures are measured on rakes at the metering station and are used for setting the desired nozzle pressure ratios. These parameters also are routed through the Dymec scanning system and recorded along with nozzle performance data by the aerodynamic data handling (ADH) system.

Facility temperatures are monitored at the control console using a Doric multichannel temperature indicator. The unit has a 24-channel capability and is designed for use with Type K thermocouples (chromel-alumel). It is used for safety monitoring and setting test-point temperatures for the dual-flow system. A system schematic is shown in Figure 2-2.

Nozzle Pressure and Temperature Measurement

A critical parameter used in evaluating acoustic test results is nozzle exhaust velocity. Determination of this velocity depends on an accurate measurement of the exhaust temperature and pressure which, in turn, depends on adequate sampling across the stream to account for profile effects. Special multi-element rakes have been designed for use on the single and dual flow systems.

The dual flow system uses four rakes, two on each stream, each having three pressure and three temperature elements with spacing of the elements corresponding to centers of six equal area annular segments of the flow stream. These rakes use shielded Type K thermocouples (chromel-alumel) which have a recovery factor very close to unity.

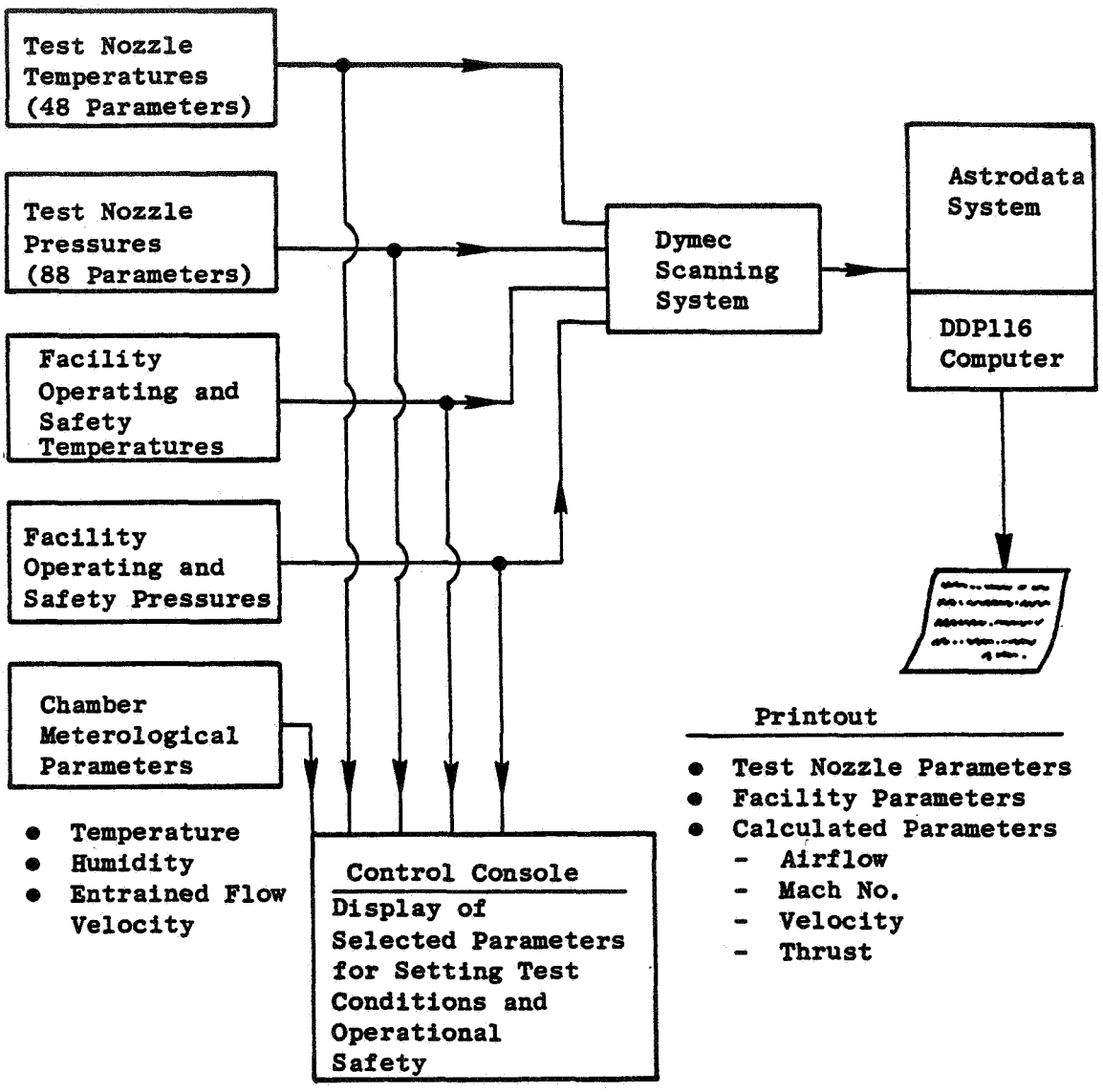

Figure 2-2. General Electric Anechoic Chamber Aerodynamic Data Processing System.

Pressure measurement accuracy is controlled by the accuracy of the transducer used for the measurement. The scanivalve tranducers that are used are rated 0.1% of full-scale range.

Performance Data Processing

Aerodynamic parameters are calculated based on the acquired temperature and pressure information. The input information for nozzle performance consists of ambient pressure (P_{amb}), nozzle discharge total temperature (T_T), and nozzle total pressure (P_T). For the case of dual flow and tertiary flow, similar parameters are required for each stream.

Output of the processing program consists of tabulations of the individual input parameters with their identification, averages of similar parameters (e.g., P_T rake average), and calculated parameters such as flow rates, Mach number, ideal velocity, and ideal thrust.

2.1.2 Acoustic Data Acquisition and Reduction Procedures

A flow chart of the acoustic data acquisition and reduction system is shown in Figure 2-3. This system has been optimized for obtaining the acoustic data up to the 80 kHz 1/3-octave-band center frequency. The microphones used to obtain 80 kHz data are the B&K 4135, 0.64 cm (1/4 inch), condenser microphones with the microphone grid caps removed to obtain the best frequency response. The cathode followers used in the chamber are transistorized B&K 2619 for optimum frequency response and lower inherent system noise characteristics. All systems utilize the B&K 2801 power supply operated in the direct mode.

The output of the power supply is connected to a line driver adding 10 dB of amplification to the signal as well as adding "preemphasis" to the high frequency portion of the spectrum. The net effect of this amplifier is a 10 dB gain at all frequencies, plus an additional 3 dB at 40 kHz and 6 dB at 80 kHz due to pre-emphasis. This increases the ability to measure low amplitude, high frequency data. In order to remove low frequency noise, high pass filters with attenuations of approximately 26 dB at 12.5 Hz, decreasing to 0 dB at 200 Hz, are installed in the system.

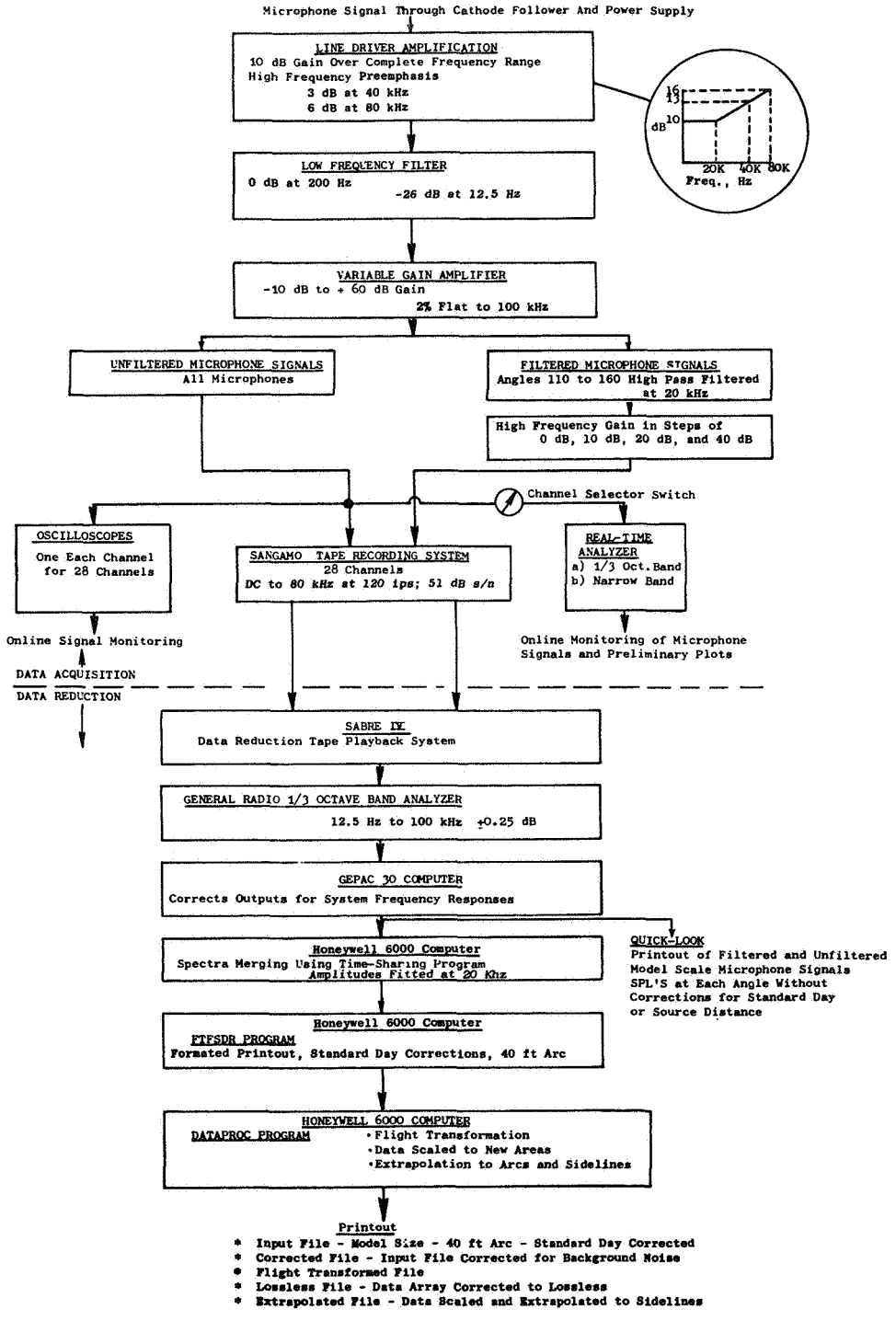

Figure 2-3. Acoustic Data Acquisition and Reduction System.

The tape recorder amplifers have a variable gain from -10 dB to +60 dB in 10 dB steps and a gain trim capability for normalizing incoming signals. High pass filters are incorporated in the acoustic data acquisition systems for microphones from 110° to 160° to enhance high frequency data otherwise potentially lost in the tape recorder electronic noise floor. The microphone signal below the 20-Hz 1/3-octave band is filtered out, and the gain is increased to boost the "signal-to-noise" ratio of the remaining high frequency signal. For microphones from 110° to 160°, both the filtered and unfiltered signals are recorded on tape. The sound pressure levels for frequencies below 20 kHz are obtained using the unfiltered signal; above 20 kHz the filtered and de-emphasized signal is used. The final jet noise spectra at a given angle is obtained by computationally merging these two spectra.

The prime system used for recording acoustic data is a Sangamo/Sabre IV, 28-track FM recorder. The system is set up for wide band Group I (intermediate band double extended) at 120-ips tape speed. Operating at 120-ips tape speed provides the improved dynamic range necessary for obtaining the high frequency/low amplitude portion of the acoustic signal. The tape recorder is set up for $\pm$40% carrier deviation with a recording level of 8 volts peak-to-peak. During recording, the signal gain is adjusted to maximum without exceeding the 8 volt peak-to-peak level.

Individual monitor scopes are used for observing signal characteristics during operation. On-line data monitoring is available through a Rockland narrow band analyzer or a General Radio 1921 1/3-octave analyzer with their outputs on display scopes or hard copy through a Tektronic plotter.

Standard data reduction is conducted in the General Electric AEBG Instrumentation Data Room (IDR). The analog data tapes are played back on a CDC3700B tape deck with electronics capable of reproducing signal characteristics within the specifications indicated for wide band Groups I and II. An automatic shuttling control is incorporated in the system. In normal operation, a tone is inserted on the recorder in the time slot designed for data analysis. Tape control automatically shuttles the tape, initiating an integration start signal to the analyzer at the tone as the tape moves in its forward motion. This motion continues until an "integration complete" is

received from the analyzer at which time the tape direction is reversed and the tape restarts at the tone in the forward direction, advancing to the next channel to be analyzed until all the channels have been processed. A time code generator is also utilized to signal the tape position of the readings as directed by the computer program control. After each total reading is completed, the tape is advanced to the next reading.

All 1/3-octave analyses are performed on a General Radio 1921 analyzer. Normal intergration time is set for 32 seconds to ensure good integration for the low frequency content. The analyzer has 1/3-octave filter sets from 12.5 Hz to 100 kHz with a rated accuracy of $\pm$1/4 dB in each band. Each data channel is passed through an interface to the GEPAC 30 computer where the data are corrected for microphone frequency response. Also, the data are corrected to standard day (59° F, 70% RH) atmospheric attenuation conditions using the Shields and Bass model (Reference 12) and then processed to calculate the perceived noise level and OASPL from the spectra. For calculation of the acoustic power, or scaling to other nozzle sizes, or extrapolation to different farfield distances, the data are sent to the Honeywell 6000 computer for data processing. This step is accomplished by transmitting the SPL's through a direct time-share link to the 6000 computer through a 1200 Band Modem. In the 6000 computer, the data are processed through the Flight-Transformed Full-Scale Data Reduction (FTFSDR) program where the appropriate calculations are performed. The data printout is accomplished on a high-speed "remote" terminal.

The detailed FTFSDR program flow chart is shown in Figure 2-4. The as-measured data are first extrapolated from the measured distance to a common 40 foot arc. This is accomplished by subtracting both the distance correction [that is, 20 log (40-foot distance/measured distance)] and the atmospheric attenuation correction over the measured distance R_{obs}, where R_{obs} is measured in feet. The Shields and Bass Pure Tone Method (Reference 12) is used for all atmospheric attenuation corrections. The data are then converted to standard day at the 40-foot arc location by adding in the standard day correction. The data are printed in tabulated form for SPL, OASPL, and PWL (for full sphere and based on the lossless data). For this program, scale model data below the chamber cutoff frequency of 250 Hz should be ignored.

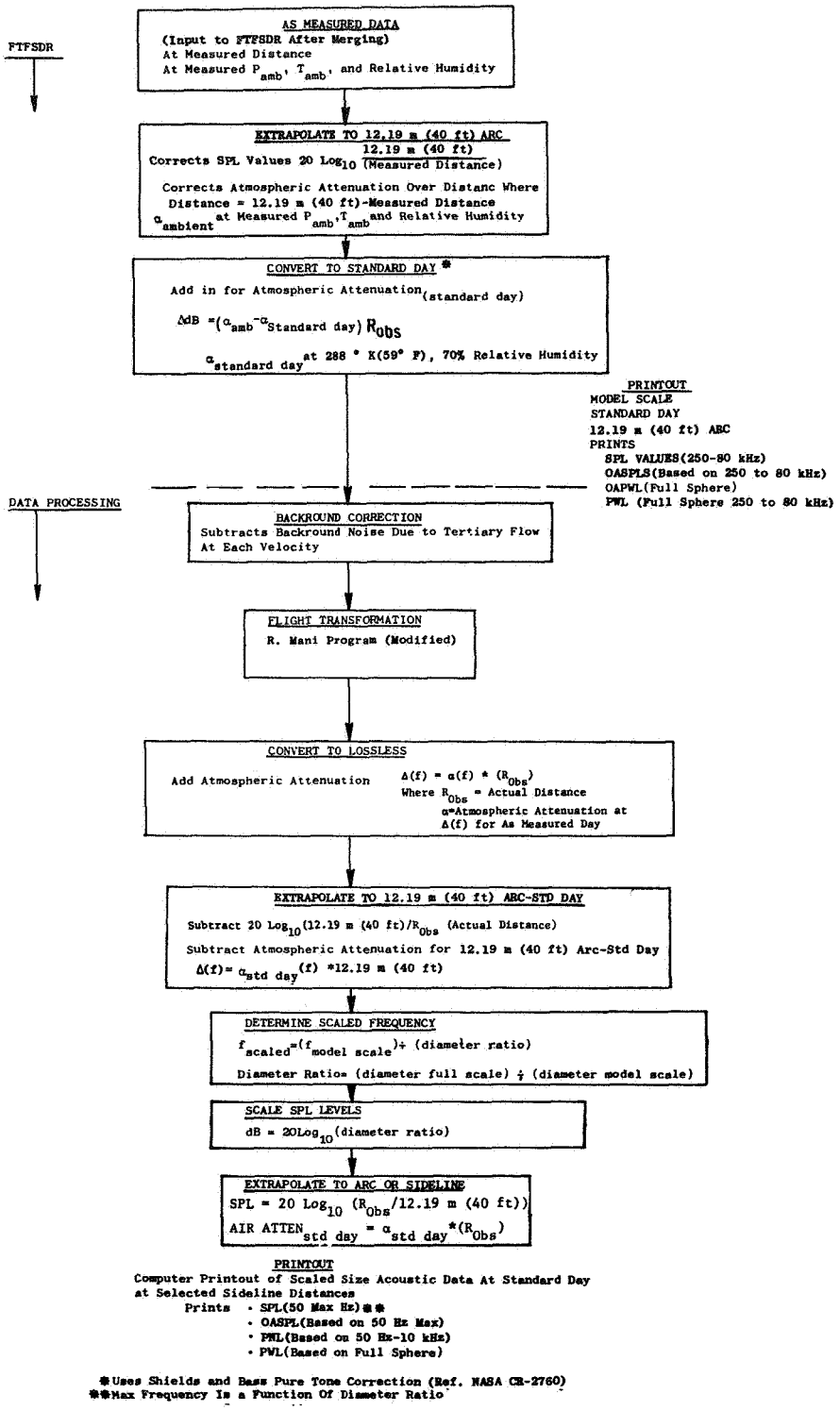

Figure 2-4. Acoustic Data Processing Flow Chart.

The scale model data are corrected next for background noise using the background noise spectra obtained with the tertiary jet at the required simulated flight velocity. The corrected scale model data are processed next through a flight transformation procedure to obtain results that are representative of the noise produced in actual flight.

2.2 LASER VELOCIMETER SYSTEM

2.2.1 General Arrangement

The laser velocimeter (LV) available for use during this program is a system developed under a USAF/DOT-sponsored program and reported in detail in Reference 16. The basic optics system is a differential Doppler, backscatter, single-package arrangement that has the proven feature of ruggedness for the severe environments encountered in close proximity to high velocity, high temperature jets. Figure 2-5 shows a photograph of the LV system in the General Electric Anechoic Test Facility. The dimensions of the control volume are 0.636 cm (0.25 inch) for the major axis and 0.518 cm (0.020 inch) for the minor axis. The range of the LV control volume from the laser hardware is 2.16 m (85.0 inches). The three steering mirrors and the beam splitter are mounted on adjustable supports, all of the same aluminum alloy, which minimizes temperature-alignment problems.

2.2.2 LV Actuator and Seeding

A remotely actuated platform is used which has three axes: vertical, horizontal, and axial. Travel capabilities are 0.813 m (32 inches), 0.813 m (32 inches) and 5.79 m (228 inches), respectively. Resolution is $\pm$.16 cm ($\pm$1/16 inch) for each axis except for the last 5.28 m (208 inches) of axial travel, which has a resolution of $\pm$.32 cm ($\pm$1/8 inch).

Seeding is by injection of aluminum oxide (Al_2O_3) powder, nominal 1-micron diameter, into the supply air to the burner and into the region of the nozzle to seed the entrained air. The powder-feeder equipment used is

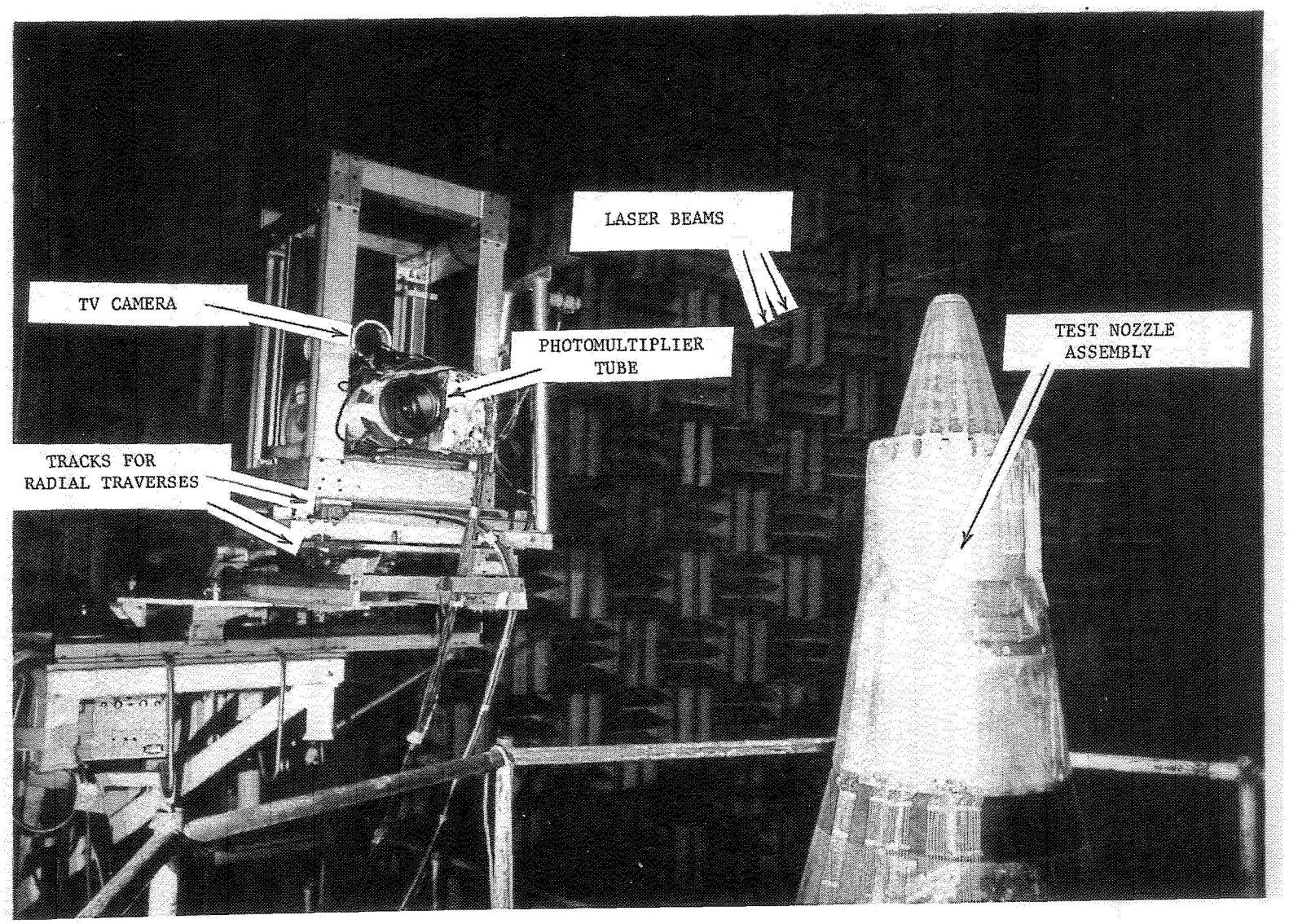

FIGURE 2-5. A PHOTOGRAPH SHOWING THE LASER VELOCIMETER SYSTEM AND A TEST NOZZLE ASSEMBLY FOR PLUME SURVEY IN THE ANECHOIC FACILITY.

described in Reference 17, except that the fluidized bed column supply air is currently heated to about 394.1 K (250° F) to prevent powder aggregation by moisture absorption.

2.2.3 Signal Processing and Recording

The LV signal processor used is a direct-counter (time-domain) type similar to that reported in References 16 and 18 but with improvements. These improvements result in a lowered rate of false validations and improved linearity and resolution. Turbulent-velocity probability distributions (histograms) are recorded by a 256-channel NS633 pulse-height analyzer. All the data acquired from the laser unit is transmitted to a minicomputer system which stores the data on diskettes and performs all the necessary data reduction functions.

The processing capabilities of the General Electric LV system are as follows:

- Velocity range - 10.7 to 1,524 mps (35 to 5,000 fps)
- Random error for single particle accuracy (error associated with system inaccuracies such as fringe spacing, linearity, stability, burst noise) - 0.75%
- Bias error for mean velocity - 0.5%
- False data rejection capability (possibility of accepting bad data) - <0.0002%.

The system uses a 16-fringe control volume where all of the eight center fringes are used in the data acceptance/rejection testing.

2.2.4 LV Data Reduction Procedures

The concept of using LV measurements for obtaining the mean and turbulent velocity profiles may be described as follows: Two beams of monochromatic light intersect at a point in space and set up a fringe pattern of known spacing (Figure 2-6). The flow is seeded with small particles which pass through the measuring volume. The light scattered from the particles is collected, and the laser signal processor measures the time it takes for the

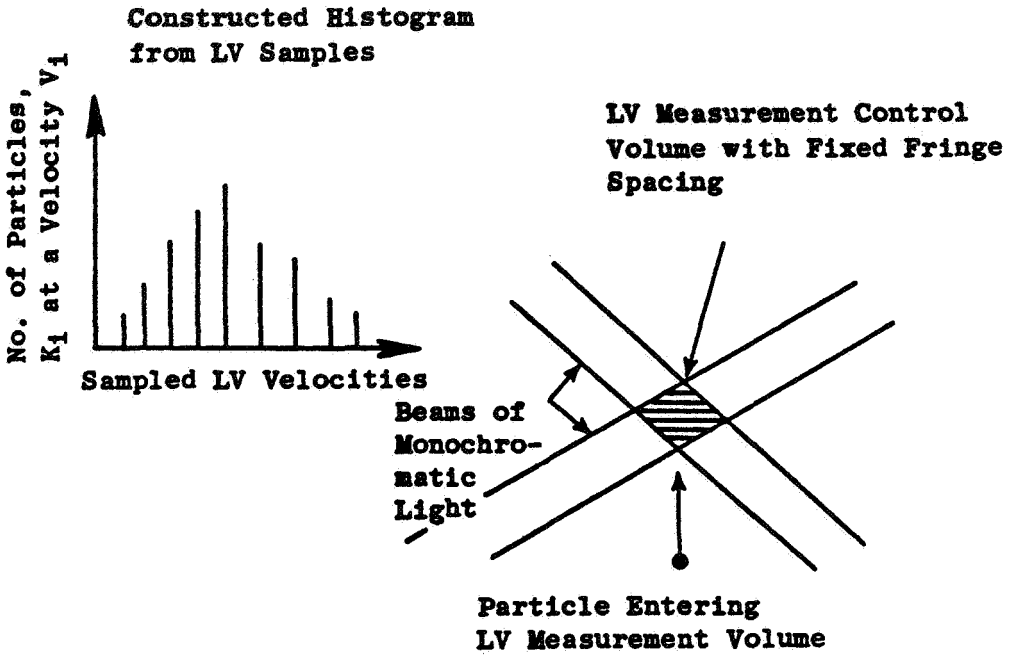

Figure 2-6. Schematic of Laser Velocity Measurements.

particles to pass through each fringe. Knowing the distance and time for each validated particle enables the construction of the usual histogram (see insert on Figure 2-6). Then by statistical techniques, the mean value (which corresponds to the mean velocity) and the standard deviation (which corresponds to the turbulent velocity) are constructed. The method of calculation used to obtain the mean and turbulent velocities from LV measurements is described below.

2.2.5 Histogram

A histogram is an estimate of the first-order probability density of the amplitude of a given sample. To obtain a velocity histogram, the time-dependent LV velocity, V(t), is accumulated and divided into classes bounded by values of velocity increments V_i. For each independent sample of velocity, a class interval is formed such that $V_i \leq V(t) \leq V_{i+1}$. During a measurement period, k_i number of velocity samples are accumulated in each sample class V_i. From the total sample of measured velocity points, the histogram is constructed as shown in Figure 2-6. The mean velocity and turbulent velocity derived from the histogram are obtained as described below.

2.2.6 Mean Velocity

The mean velocity of the jet, V_j, obtained from the discrete velocity sample is calculated by:

$$\bar{V}_j = \sum_{\substack{\text{All Class} \\ \text{Intervals}}} \left(\frac{V_{i+1} + V_i}{2} \right) \frac{k_i}{N}$$

where

$\frac{V_{i+1} + V_i}{2}$ is the value of the sampled axial velocity component at the center of the class interval

k_i is the number of velocity samples in the class interval

N is the total number of velocity samples ($= \Sigma\, k_i$) in the histogram

2.2.7 Turbulent Velocity

To obtain the turbulent velocity, v', from the sampled data contained in the histogram, the standard square root of the statistical variance is performed. This calculation is performed using the following equation:

$$v' = \left\{ \sum_{\substack{\text{All Class} \\ \text{Intervals}}} \left(\frac{\frac{V_{i+1} + V_i}{2} - \bar{V}_j}{N} \right)^2 k_i \right\}^{1/2}$$

2.2.8 Statistical Errors For LV Mean and Turbulent Velocity Measurements

With any large data sample, as obtained through the collection of velocity samples in an LV histogram, guidelines for estimating the accuracy of each measurement are required. Table 2-I provides estimates of the percent error obtained for a mean velocity or turbulent velocity LV measurement.

Table 2-I lists the percent error for a 95% confidence statement of mean velocity measurement as a function of the total number, N, of velocity samples contained in the histogram and the turbulence level, $v'/\bar{V}_j$. Table 2-I also gives the percent error for a 95% confidence statement of the turbulent velocity estimate as a function of N, the total number of velocity samples. As can be seen from Table 2-I, a fairly small sample of velocity measurements is required to obtain a good estimate of the mean velocity. For the turbulent velocity, the number of data samples required for a good estimate increases substantially. The usual number of samples obtained with the General Electric LV during a routine data-taking measurement performed during this program is approximately 1,000 samples. For a simple and quick diagnostic-type information, this amount of samples is sufficient.

Table 2-I. Estimates of Error in Mean and Turbulent Velocities Measured by LV.

(a) **Estimated Percent Error in the LV Measurement of Mean Velocity with 95% Confidence.**

N	$v'/\bar{V}j$			
	0.2	0.1	0.05	0.025
10	14.1	7	3.5	1.76
20	9.3	4.7	2.3	1.20
30	7.4	3.7	1.9	0.93
40	6.3	3.2	1.6	0.80
60	5.0	2.6	1.3	0.65
120	3.6	1.8	0.9	0.45

(b) **Estimated Percent Error for LV Turbulent Velocity Measurements with 95% Confidence.**

N	Percent Error
20	31.5
40	21.8
60	17.8
120	12.6
240	9.12
480	6.45
960	4.56
5000	2.0
25000	0.89

2.2.9 LV Traverses For Mean Velocity Profiles

In addition to the above described stationary mode of LV operation for the determination of mean and turbulent velocities at discrete points, the LV can be operated also in a traversing mode to obtain continuous profiles of mean velocities. These traverses are possible along any of the three LV axes. During these traverses, the data describing the velocity levels and the location of the measurement volume are recorded continuously on an X-Y plotter. The traversing speeds are adjusted as well as traverses repeated for obtaining well-defined mean velocity profiles. While exact sampling rates during these traverses are not recorded in any way, it is felt that an estimated rate of approximately 250 samples per inch of traverse is needed for a well-defined smooth profile.

2.2.10 Recent LV System Modifications; Minihistograms

The LV System that has been used successfully in previous NASA-supported programs (References 5 and 6) has recently been modified to have the following additional features in a traversing mode:

- A modified slant traverse mechanism that enables LV traverses to be made along an axis that is other than truly vertical (i.e., parallel to the plug surface) of an annular plug nozzle.

- A fine traverse mechanism (10 revolutions on a potentiometer for 33 inches of total travel; usable fine traverse distance is 20 inches) that is available during both the slant and vertical movements. This new drive system allows for more smoothly controlled vertical traverses required for obtaining minihistograms.

- Modified software that enables mean velocity data to be obtained during any of the traverses (that is, axial or vertical, radial and slant) from minihistograms in the form of plots of mean velocity data points plotted as a function of their traverse location. During the current program, the mean velocity data measured with the minihistograms have been obtained from the acceptable data

samples set to 20. This number of acceptable samples yields an estimated 5% error in the LV mean velocity measurements with a statistical 95% confidence level within a given flow regime having a turbulent velocity ratio ($v'/\bar{V}_j$) of 10%.

2.3 DIAGNOSTIC SHADOWGRAPH SYSTEM

A shadowgraph system, illustrated in Figure 2-7, has been employed in the anechoic free-jet facility to accomplish flow visualization and documentation. The system includes:

- A mounting in close proximity to the free jet nozzle for good resolution
- A steady-state light system
- A 10-inch-diameter mirror system to collimate the light through the test volume
- A backdrop screen of sufficient size to encompass the total test section
- A mounting platform for the light source, mirror, and camera system so as to control remotely and record the position of the shadowgraph system for an approximate 3-foot vertical plume definition.

2.4 SCALE MODEL NOZZLE CONFIGURATIONS

The primary objective of this program is to determine means by which supersonic jet shock noise could be reduced to acceptable levels for advanced supersonic aircraft. This was accomplished principally by experimentally evaluating the influence of select nozzle flow passages on the acoustic behavior of inverted-velocity-profile coannular nozzles. Two basic coannular nozzle categories, namely, non-mechanically suppressed and outer stream mechanically suppressed configurations, were investigated. Particular emphasis was placed on determining the usefulness of convergent-divergent (C-D) nozzle flow passages designed for ideal isentropic shock-free expansion

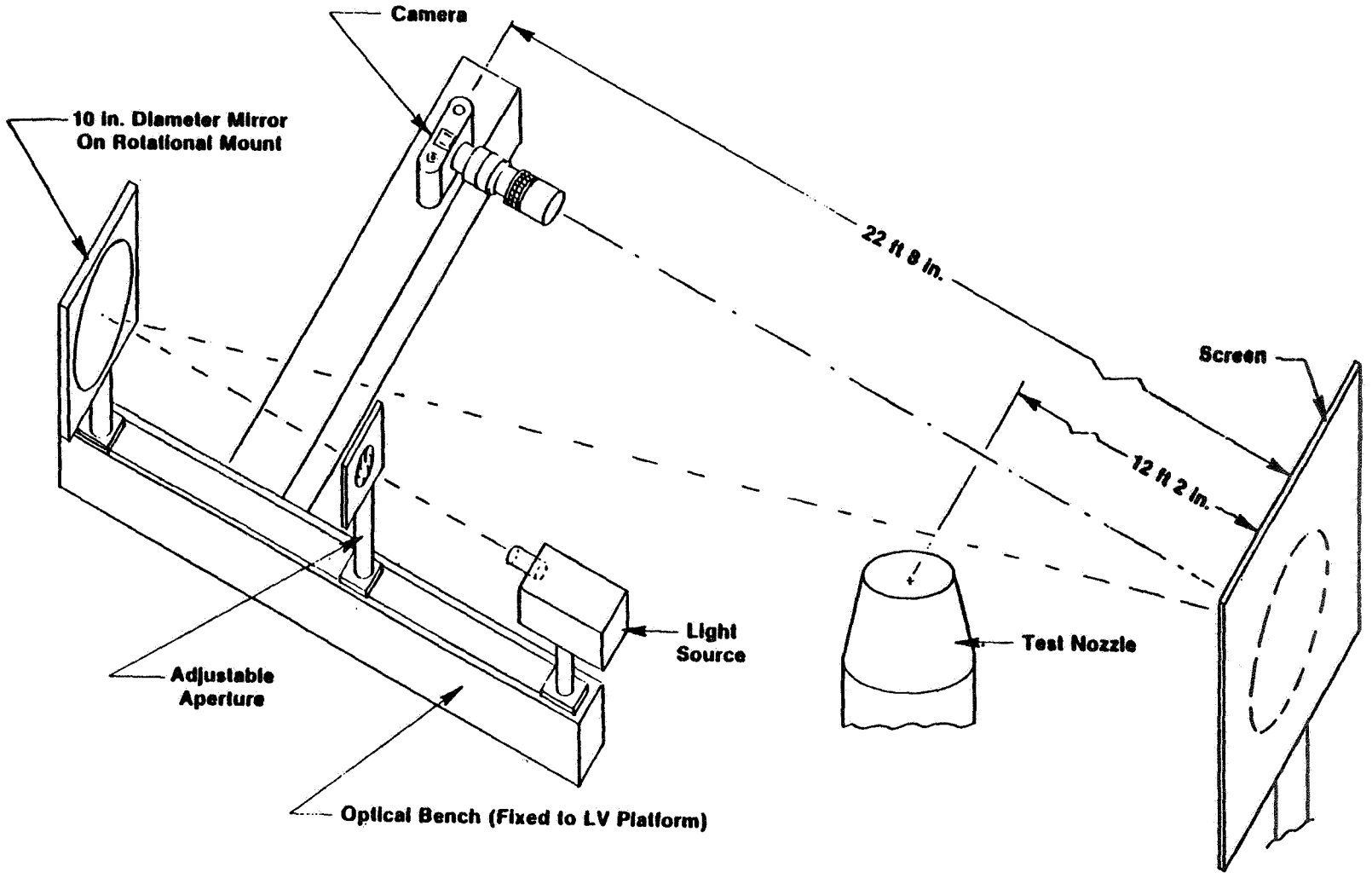

Figure 2-7. Schematic Arrangement of the Shadowgraph System in the Anechoic Jet Facility.

at selected Mach numbers. C-D flow passages were employed on both of the basic coannular systems and on each of the outer and inner nozzles. For evaluation of the C-D effectiveness, comparable convergent nozzles with convergent inner and outer flow passages were tested for both nozzle categories.

The following six nozzle configurations were selected and tested within the General Electric Anechoic Free-Jet/Jet Noise Facility:

- Configuration DFSC-1 — Coannular plug nozzle, inner and outer convergent flowpaths, truncated plug closure, Figures 2-8 and 2-9.
- Configuration DFCS-6 — Same as DFSC-1, but with extended, sharp-tipped plug closure, Figure 2-10.
- Configuration DFCS-2 — Coannular plug nozzle, inner and outer convergent-divergent (C-D) flowpaths, truncated plug closure, Figure 2-11.
- Configuration DFCS-3 — Same as DFCS-2, but with extended, sharp-tipped closure, Figures 2-12 and 2-13.
- Configuration DFCS-4 — Coannular plug nozzle, 20-chute outer stream suppressor with convergent flow elements, annular inner stream of convergent flowpath, truncated plug closure, Figures 2-14 and 2-15.
- Configuration DFCS-5 — Coannular plug nozzle, 20-chute outer stream suppressor with C-D flow elements, annular inner stream of C-D flowpath, truncated plug closure, Figures 2-16 and 2-17.

The significant geometric characteristics of the test configurations are summarized in Table 2-II. From the above descriptions of the configurations, the following model sets and nozzle categories are grouped for a comparative study later in Section 3.0:

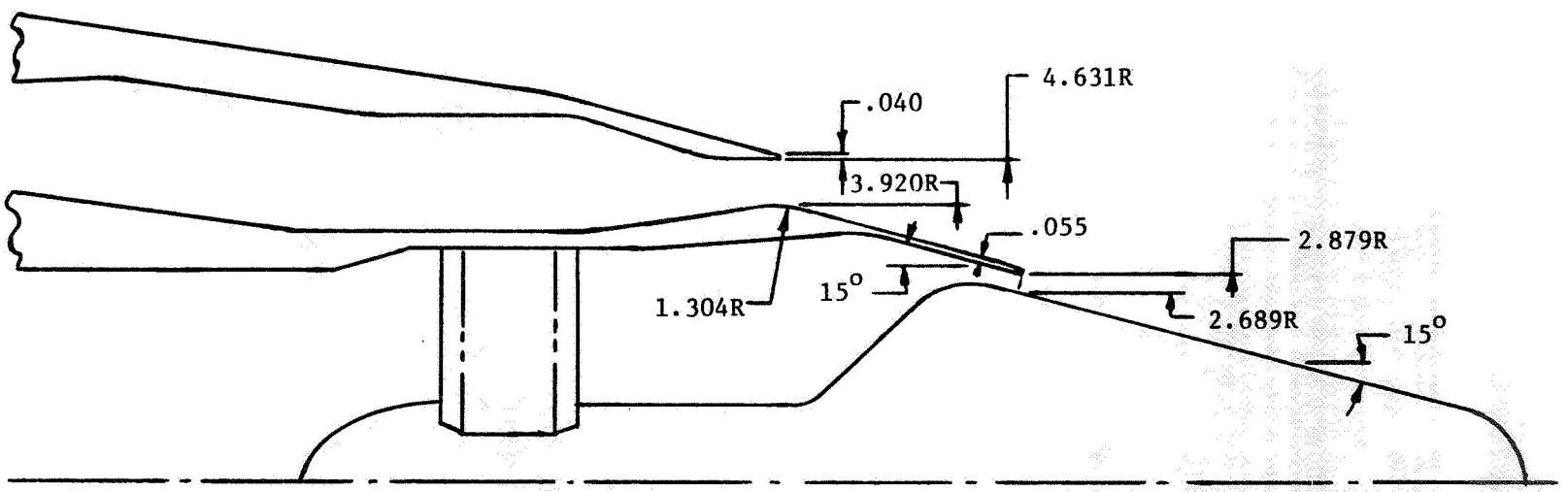

FIGURE 2-8. CONFIGURATION DFSC-1; COANNULAR PLUG NOZZLE, INNER AND OUTER CONVERGENT FLOWPATHS, TRUNCATED PLUG CLOSURE.

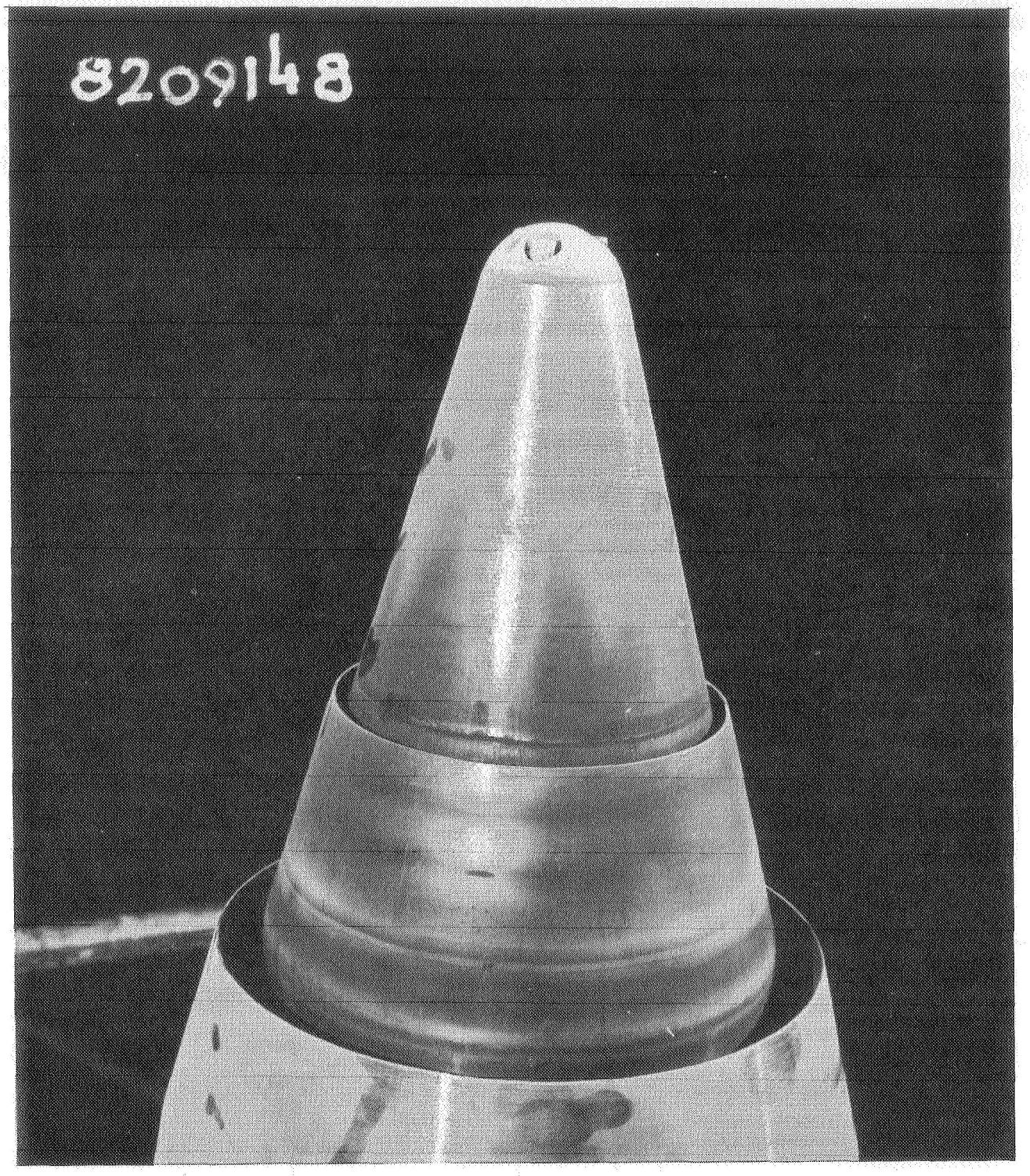

FIGURE 2-9. AN OVERVIEW OF CONFIGURATION DFSC-1; COANNULAR PLUG NOZZLE, INNER AND OUTER CONVERGENT FLOWPATHS, TRUNCATED PLUG CLOSURE.

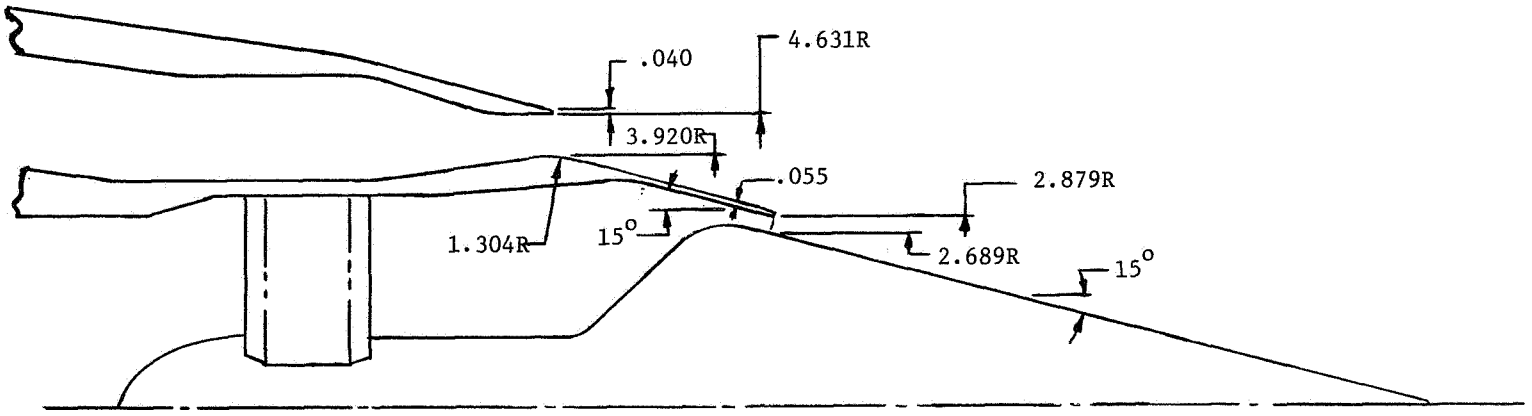

FIGURE 2-10. CONFIGURATION DFSC-6; COANNULAR PLUG NOZZLE, INNER AND OUTER CONVERGENT FLOWPATHS, SHARP-TIPPED PLUG CLOSURE.

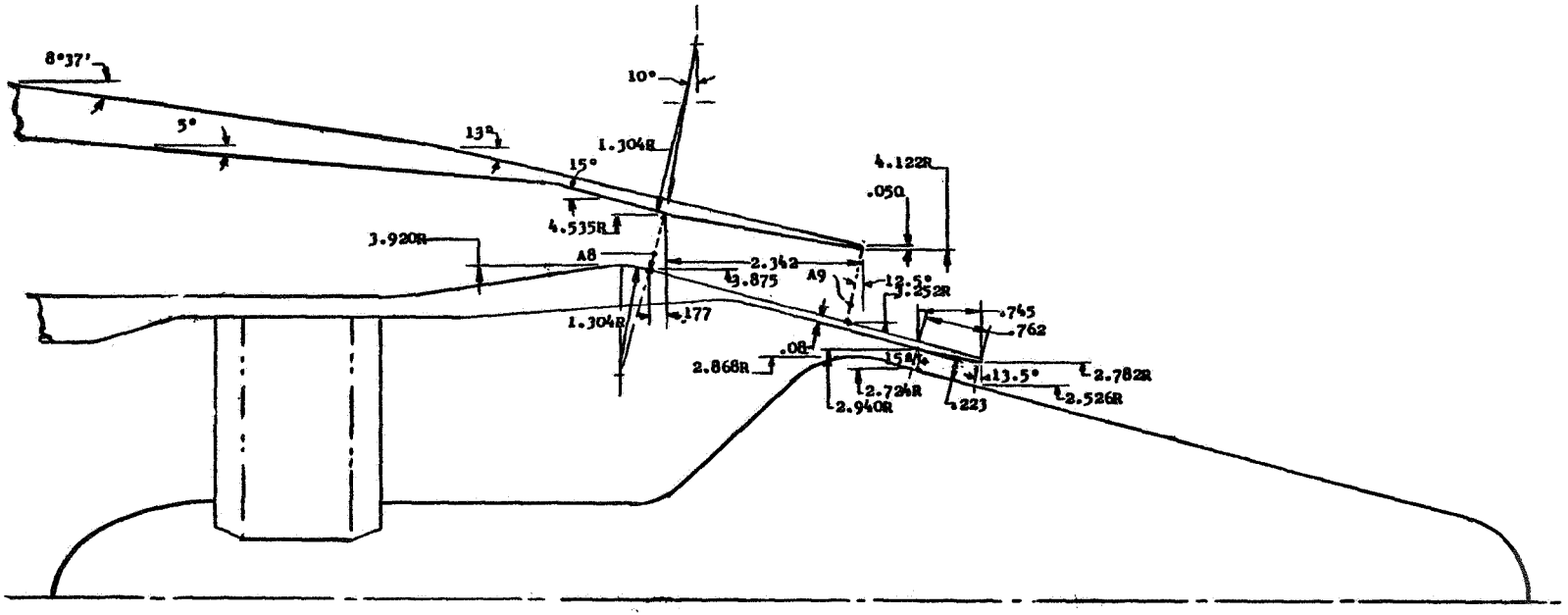

FIGURE 2-11. CONFIGURATION DFSC-2; COANNULAR PLUG NOZZLE, INNER AND OUTER CONVERGENT-DIVERGENT FLOWPATHS, TRUNCATED PLUG CLOSURE.

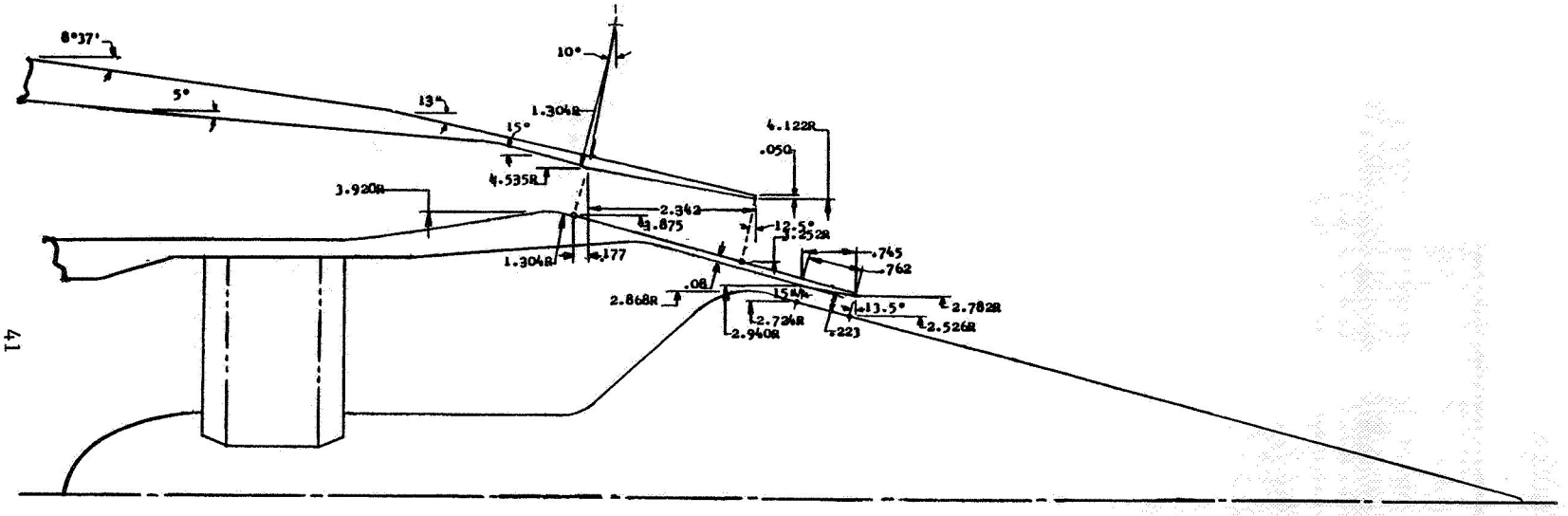

FIGURE 2-12. CONFIGURATION DFSC-3; COANNULAR PLUG NOZZLE, INNER AND OUTER CONVERGENT-DIVERGENT FLOWPATHS, SHARP-TIPPED PLUG CLOSURE.

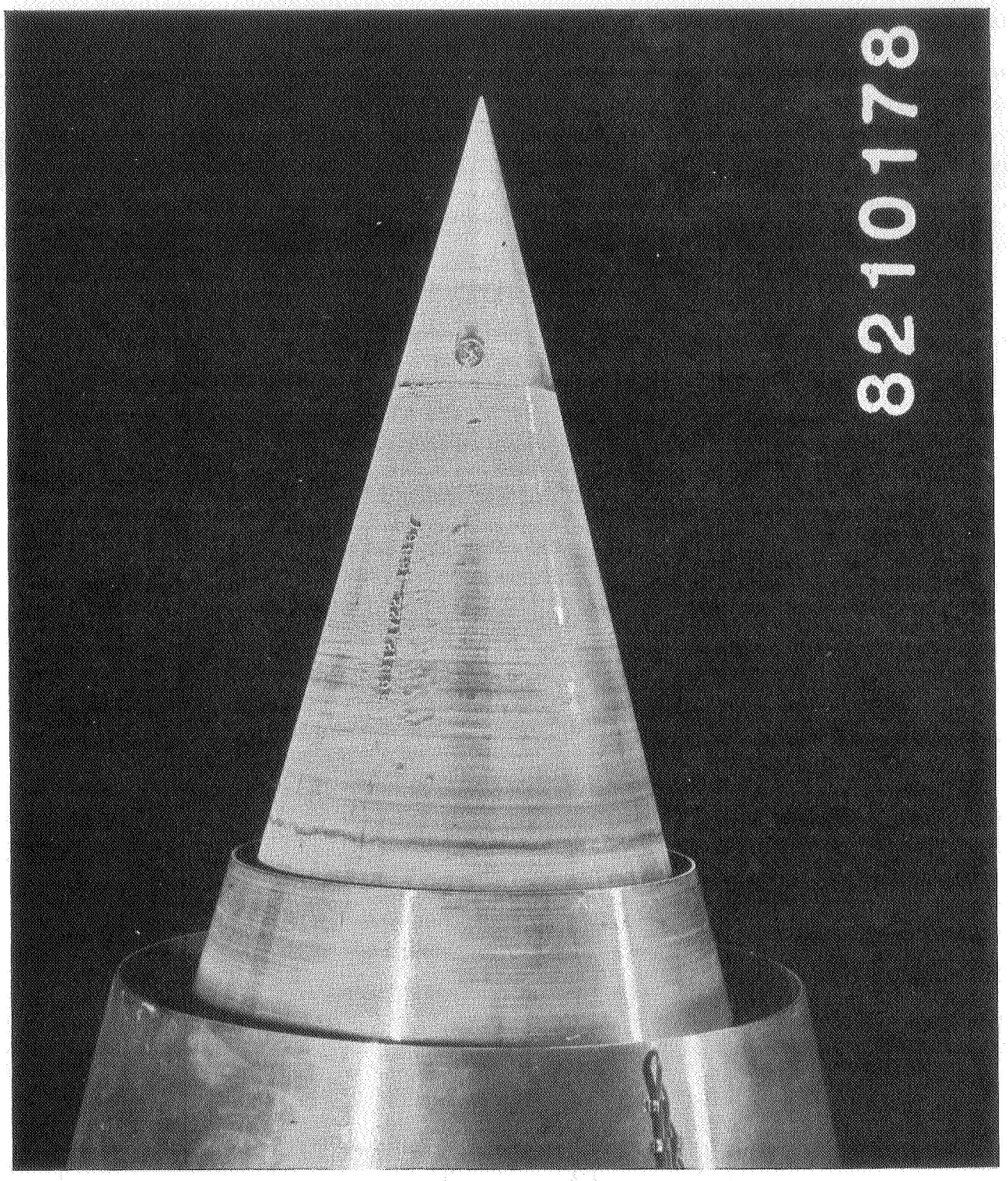

FIGURE 2-13. AN OVERVIEW OF DFSC-3; COANNULAR PLUG NOZZLE, INNER AND OUTER CONVERGENT-DIVERGENT FLOWPATHS, SHARP-TIPPED PLUG CLOSURE.

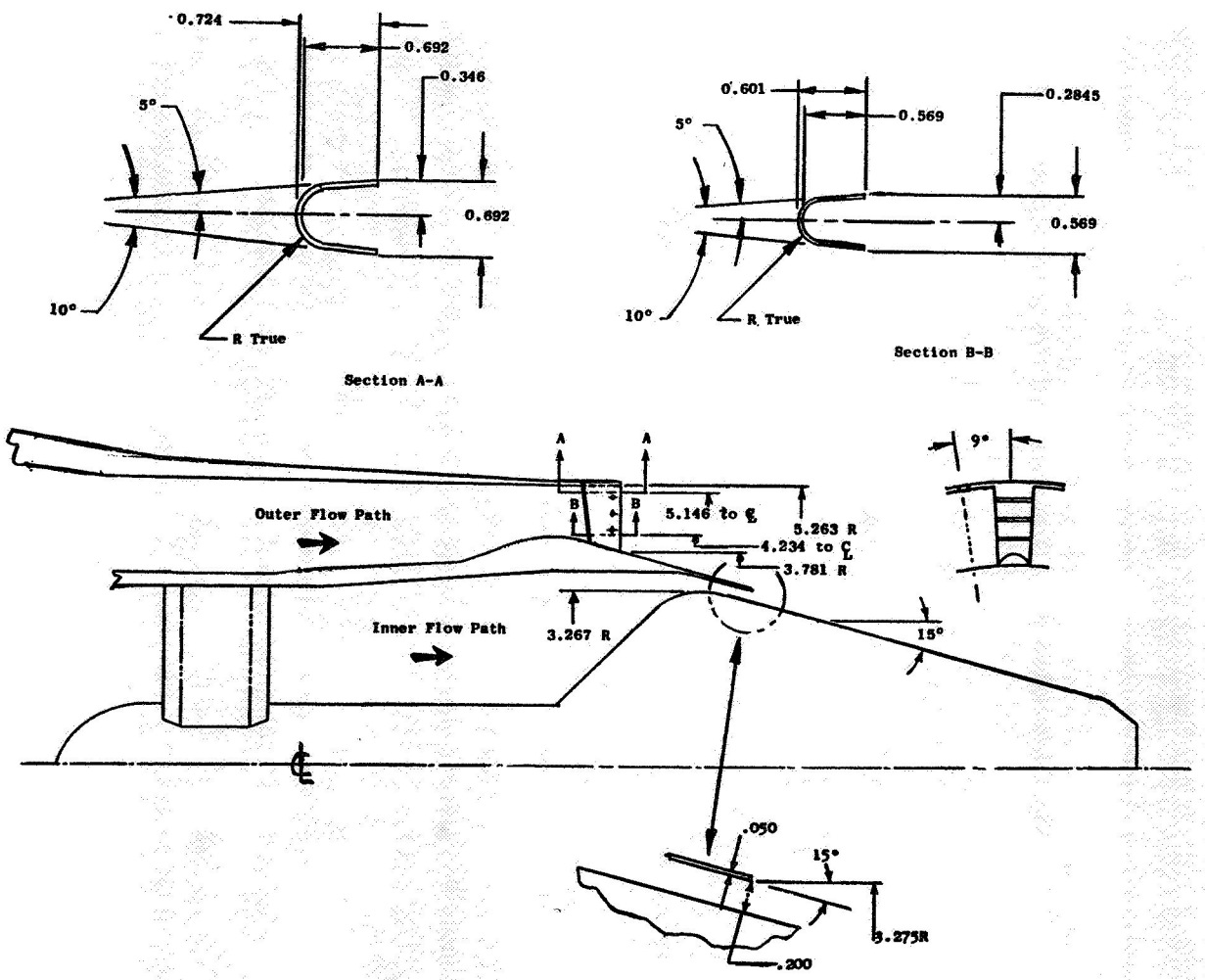

FIGURE 2-14. CONFIGURATION DFSC-4; COANNULAR PLUG NOZZLE, 20-CHUTE OUTER STREAM SUPPRESSOR WITH CONVERGENT FLOW ELEMENTS, ANNULAR INNER STREAM OF CONVERGENT FLOWPATH, TRUNCATED PLUG CLOSURE.

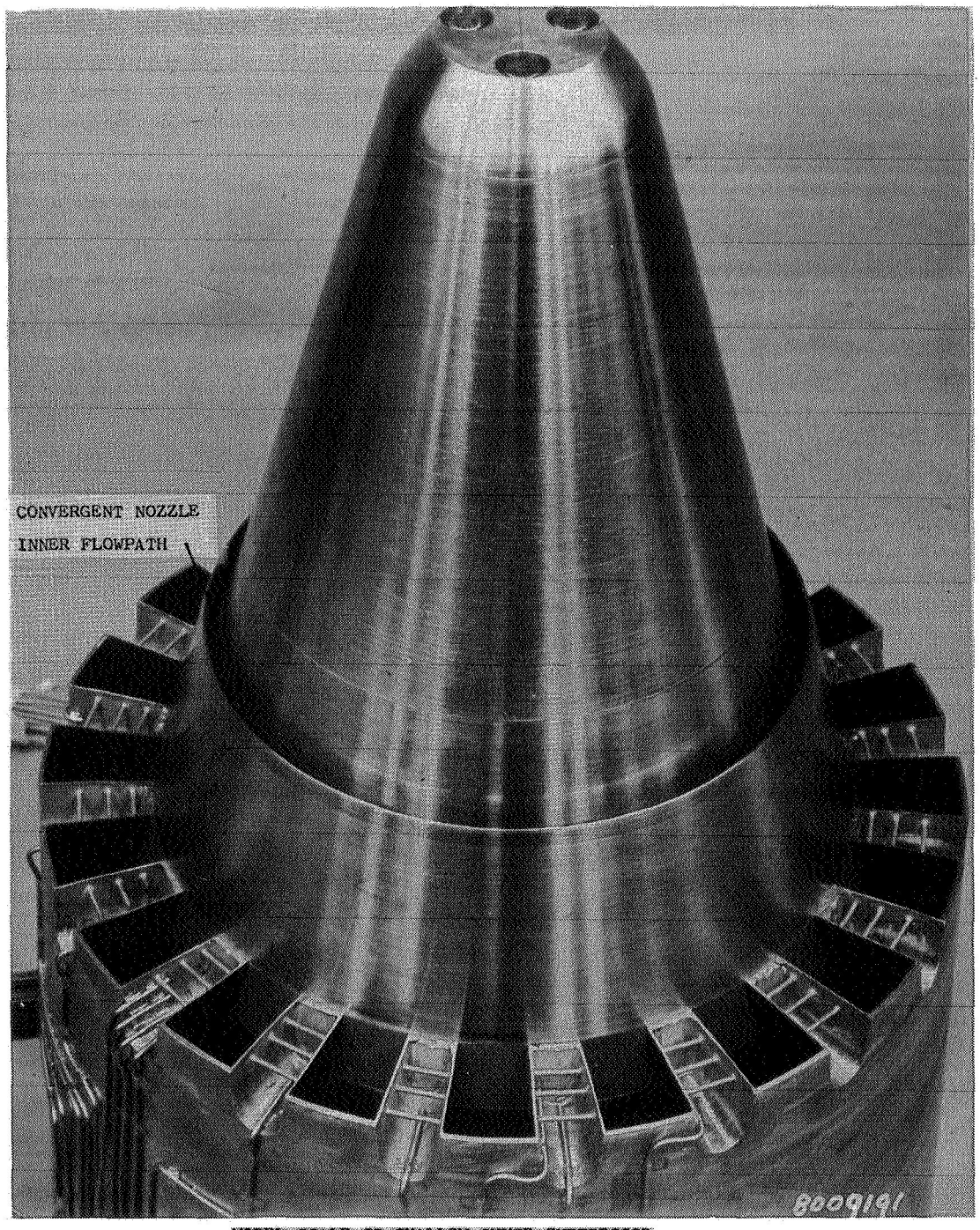

FIGURE 2-15. CONFIGURATION DFSC-4; CONVERGENT 20-SHALLOW CHUTE SUPPRESSOR NOZZLE WITH CONVERGENT INNER FLOWPATH.

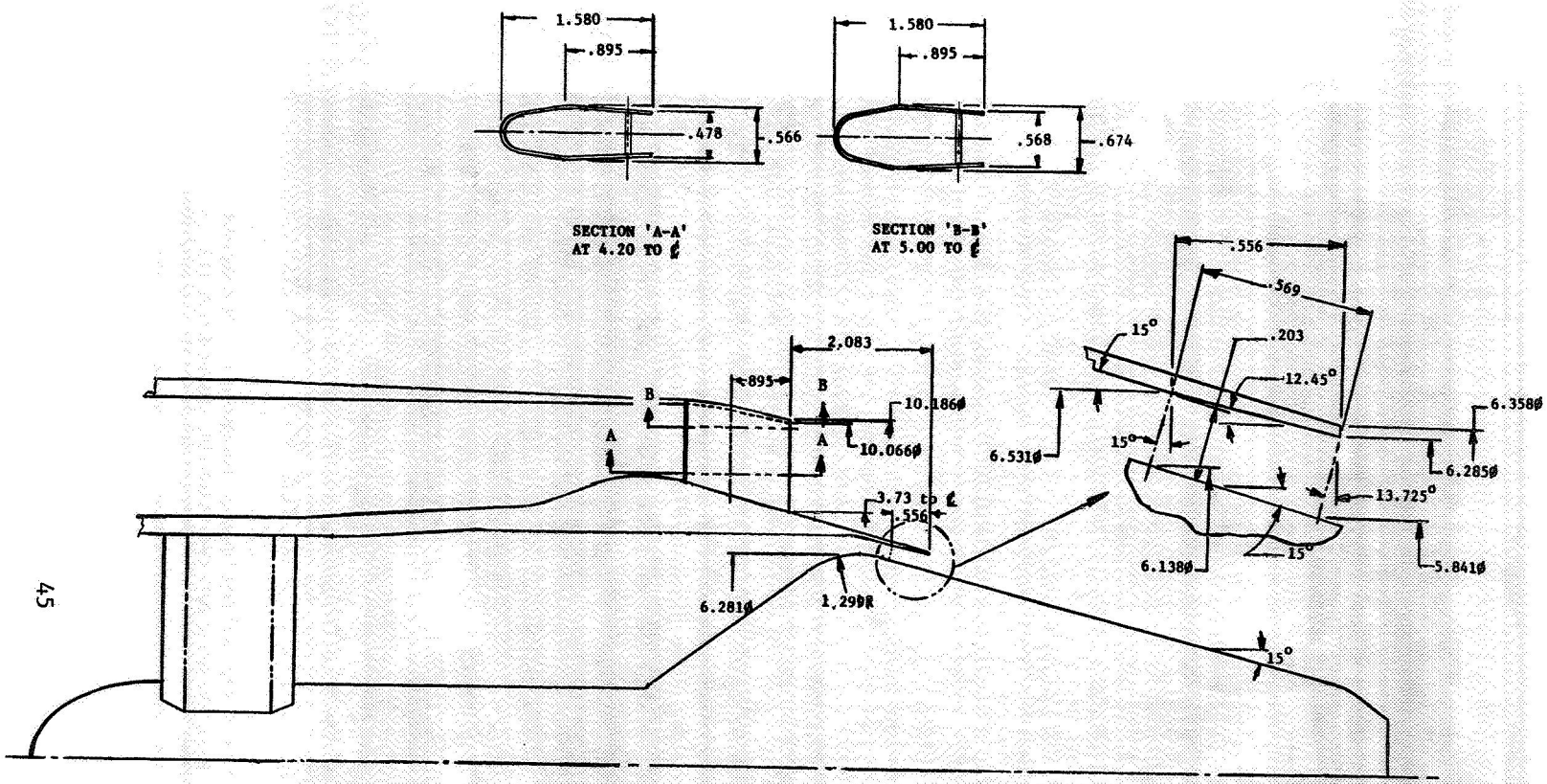

FIGURE 2-16. CONFIGURATION DFSC-5; COANNULAR PLUG NOZZLE, 20-CHUTE OUTER STREAM SUPPRESSOR WITH CONVERGENT-DIVERGENT FLOW ELEMENTS, ANNULAR INNER STREAM OF CONVERGENT-DIVERGENT FLOWPATH, TRUNCATED PLUG CLOSURE.

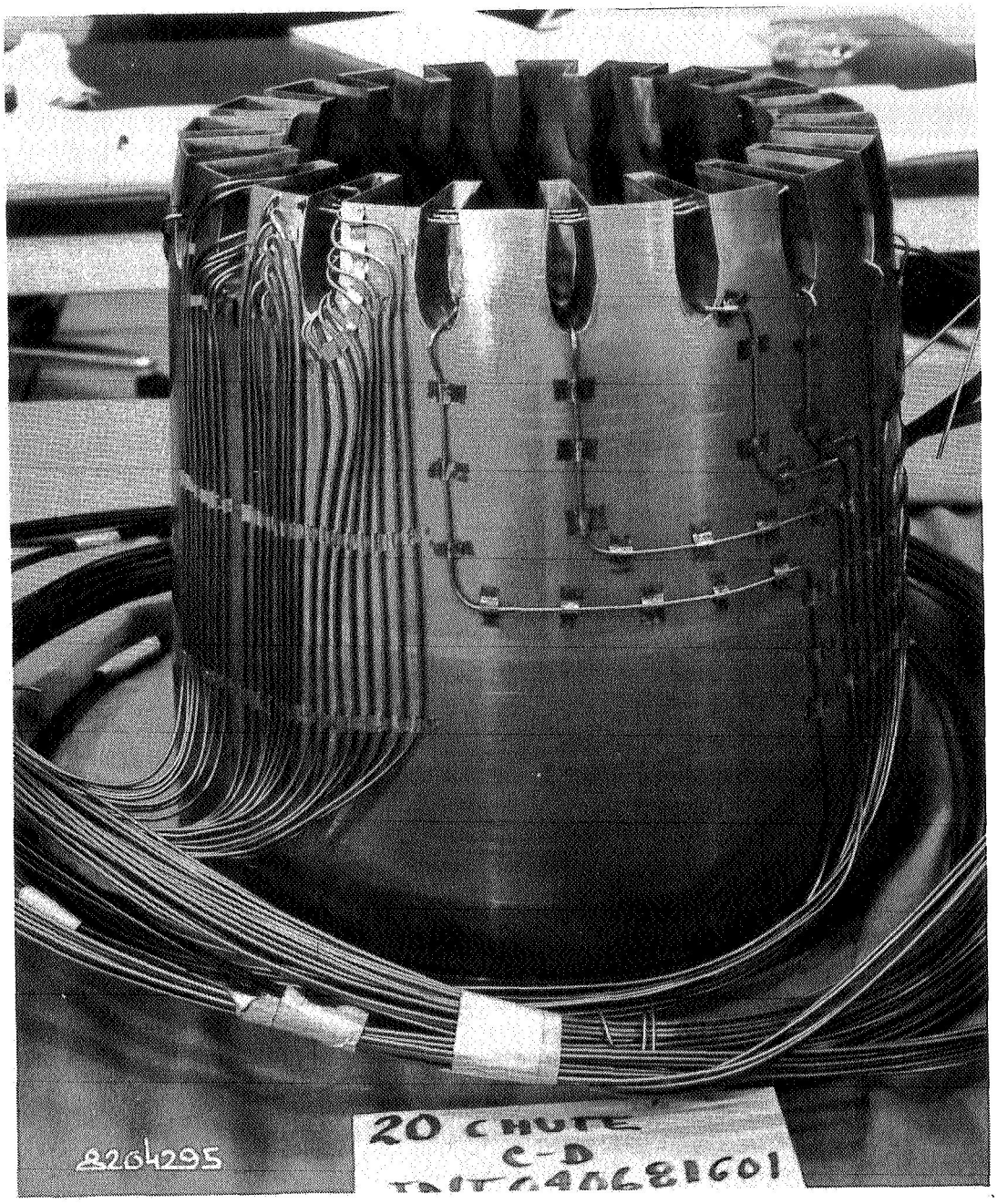

FIGURE 2-17. OVERVIEW OF CONFIGURATION DFSC-5; 20-CHUTE C-D SUPPRESSOR SHOWING BASE PRESSURE AND C-D FLOWPATH INSTRUMENTATION APPLICATION.

TABLE 2-II. SUMMARY OF SIGNIFICANT GEOMETRIC CHARACTERISTICS OF TEST NOZZLES

NOZZLE CATEGORY		NON-MECHANICALLY SUPPRESSED				MECHANICALLY SUPPRESSED	
MODEL DESCRIPTION		COANNULAR PLUG NOZZLE, INNER & OUTER CONVERGENT FLOWPATHS		COANNULAR PLUG NOZZLE, INNER & OUTER C-D FLOWPATHS		20-CHUTE CONVERGENT OUTER SUPPRESSOR, ANNULAR CONVERGENT INNER	20-CHUTE C-D OUTER SUPPRESSOR, ANNULAR C-D INNER
CONFIGURATION NUMBER		DFSC-1	DFSC-6	DFSC-2	DFSC-3	DFSC-4	DFSC-5
PLUG CLOSURE		TRUNCATED	SHARP-TIPPED	TRUNCATED	SHARP-TIPPED	TRUNCATED	TRUNCATED
NOZZLE PARAMETER							
THROAT AREA, cm^2 (in^2)	OUTER	116.5 (18.05)		116.5 (18.05)		131.4 (20.36)	130.5 (20.23)
	INNER	22.2 (3.44)		25.6 (3.97)		25.7 (3.99)	26.1 (4.05)
THROAT EQUIVALENT DIAMETER, cm (in)	OUTER	12.2 (4.79)		12.2 (4.79)		12.9 (5.09)	12.8 (5.08)
	INNER	5.3 (2.09)		5.7 (2.25)		5.7 (2.25)	5.8 (2.27)
THROAT RADIUS RATIO	OUTER	.85		.855		.764	.764
	INNER	.93		.927		.941	.940
EXIT AREA OF DIVERGENT FLOWPATH, cm^2 (in^2)	OUTER	-		133.2 (20.65)		-	147.9 (22.92)
	INNER	-		28.3 (4.39)		-	28.1 (4.36)
EXIT RADIUS RATIO OF DIVERGENT FLOWPATH	OUTER	-		.789		-	.743
	INNER	-		.908		-	.929
A_{exit}/A_{throat} OF C-D FLOWPATH	OUTER	-		1.144		-	1.133
	INNER	-		1.105		-	1.077
SUPPRESSOR AREA RATIO	AT THROAT	-		-		1.75	1.75
	AT EXIT	-		-		-	1.56
C-D DESIGN MACH NO.	OUTER	-		1.44		-	1.425
	INNER	-		1.38		-	1.327
A_{inner}/A_{outer}	SYSTEM	.19		.22		.20	.20

- DFSC-2 and DFSC-1: Compares coannular C-D to convergent flow passages, respectively, for unsuppressed nozzles.

- DFSC-6 and DFSC-1: Compares sharp-tipped to truncated plug closures, respectively, for coannular convergent nozzles.

- DFSC-3 and DFSC-2: Compares sharp-tipped to truncated plug closures, respectively, for coannular C-D nozzles.

- DFSC-5 and DFSC-4: Compares coannular C-D to convergent flow passages, respectively, for nozzles employing a 20-chute mechanical suppressor in the outer stream.

Details of the test configurations are summarized in the following sections. Further details on nozzle design, physical dimensions, fabrication and instrumentation application are provided in Reference 19 and in the comprehensive data report of this program (Reference 15).

2.4.1 Coannular Plug Nozzles, Non-Mechanically Suppressed

Within this category fall Configurations DFSC-1, -6, -2 and -3, discussed separately as follows:

Configuration DFSC-1; Coannular Plug Nozzle, Inner and Outer Convergent Flowpaths, Truncated Plug Closure

This configuration, shown in Figures 2-8 and 2-9, was selected as the baseline coannular convergent nozzle in order to evaluate the effectiveness of C-D flowpaths of DFSC-2. Specifications of this dual stream inverted-velocity-profile nozzle are as follows:

- Outer Flow Throat Plane Area, $in.^2$	18.05
- Outer Flow Equivalent Flow Diameter, in.	4.79
- Outer Flow Radius Ratio	0.85
- Inner Flow Throat Plane Area, $in.^2$	3.44
- Inner Flow Equivalent Flow Diameter, in.	2.09
- Inner Flow Radius Ratio	0.93
- Inner to Outer Flow Area Ratio	0.19

Configuration DFSC-6; Coannular Plug Nozzle, Inner and Outer Convergent Flowpaths, Sharp-Tipped Plug Closure

This configuration, shown in Figure 2-10, is identical to Configuration DFSC-1 except that it has a sharp plug tip that replaces the truncated tip plug closure. This extended 15° half angle plug maintains an aerodynamically clean flow closure aft of the plug tip such that downstream flow disturbances and shock structure are minimized.

Configuration DFSC-2; Coannular Plug Nozzle, Inner and Outer Convergent-Divergent Flowpath, Truncated Plug Closure

This coannular C-D nozzle system, shown in Figure 2-11, has physical details and design point aerodynamic cycle conditons as follows:

	OUTER NOZZLE	INNER NOZZLE
- Throat Plane Area, $in.^2$	18.05	3.97
- Equivalent Throat Diameter, in.	4.79	2.25
- Exit Plane Area, $in.^2$	20.65	4.39
- Radius Ratio at Throat	0.855	0.927
- Radius Ratio at Exit Plane	0.789	0.908
- A_{exit}/A_{throat}	1.144	1.105
- M, Mach Number-Design Point	1.44	1.38
- P_T/P_{amb}, Nozzle Pressure Ratio	3.3	3.1
- T_T, Nozzle Total Temp., °R	1760	860
- γ, Gamma	1.345	1.4
- θ_1, Divergent Flap Angle, degrees	10	12
- θ_2, Plug Angle, degrees	15	15
- ℓ/S, Divergent Flowpath Length/ Throat Slant Height	3.4	3.42

	SYSTEM
- Total Throat Plane Area, $in.^2$	22.02
- Total Equivalent Throat Diameter, in.	5.295
- System Area Ratio, Inner-to-Outer	0.22

The configuration has outer and inner flowpaths designed for isentropic expansion at nozzle pressure ratios of 3.3 and 3.1, respectively.

Configuration DFSC-3; Coannular Plug Nozzle, Inner and Outer Convergent-Divergent Flowpaths, Sharp-Tipped Plug Closure

This configuration, shown in Figures 2-12 and 2-13, is identical to Configuration DFSC-2 except that the truncated plug tip is replaced with a sharp-tipped plug closure that was discussed previously.

2.4.2 Coannular Plug Nozzles, Mechanically Suppressed

Within this category fall Configurations DFSC-4 and DFSC-5 that are discussed as follows:

Configuration DFSC-4; Coannular Plug Nozzle, 20-Chute Outer Stream Suppressor with Convergent Flow Elements, Annular Inner Stream of Convergent Flowpath, Truncated Plug Closure

This nozzle system, shown in Figures 2-14 and 2-15, was available from an earlier NASA-Lewis/GE program (Reference 6). It had produced identifiable shock-cell radiated noise and, therefore, was selected as a baseline configuration against which the effectiveness of redesigned chutes in the form of C-D flow elements could be evaluated. The suppressor was a scale model of the YJ101 AST/VCE-size 20-chute configuration, developed under NASA-Lewis/GE Contract NAS3-20582 (Reference 20). Details of the configuration are as follows:

OUTER NOZZLE

- Number of Suppressor Elements	20
- Elemental Planform Shape	Radial
- Suppressor Area Ratio	1.75
- Suppressor Radius Ratio	0.764
- Angle Subtended by Each Chute, Θ_{chute}, degrees	7.714
- Angle Subtended by Each Flow Element, Θ_{flow}, degrees	10.286
- Chute Depth-to-Width Ratio	1.0
- Chute Entrance Design Mach Number	0.7
- Throat Plane Area, $in.^2$ (Design)	20.36
- Equivalent Throat Diameter, in. (Design)	5.09

INNER NOZZLE

- Throat Plane Area, $in.^2$	3.99
- Equivalent Throat Diameter, in.	2.25
- Throat Radius Ratio	0.941

SYSTEM

- Total Throat Plane Area, $in.^2$ (Design)	24.348
- Total Equivalent Throat Diameter, in. (Design)	5.568
- System Area Ratio, Inner to Outer (Design)	0.20

Configuration DFSC-5; Coannular Plug Nozzle, 20-Chute Outer Stream Suppressor with Convergent-Divergent Flow Elements, Annular Inner Stream of Convergent-Divergent Flowpath, Truncated Plug Closure

This nozzle, having an outer stream mechanical suppressor with C-D flow elements and shown in Figures 2-16 and 2-17, was designed and fabricated under the NASA-Lewis/GE Contract NAS3-22514, "Investigation of Shock-Cell Noise Reduction for Single Stream Nozzles in Simulated Flight." Details of the C-D flowpath suppressor design are discussed in References 7 and 21. The inner nozzle C-D flowpath was designed and implemented during this program. Specific design values are as follows:

OUTER NOZZLE

- Mach No. (Design)	1.425	-C-D DESIGN POINT CYCLE
- P_T/P_{amb}	3.238	
- T_T, °R	1730	
- T_s, °R	1271	
- γ	1.354	
- V_j, ft/sec	2448	
- Number of Suppressor Elements	20	
- Elemental Planform Shape	Radial	
- A_{exit}/A_{throat}	1.133	

	AT THROAT	AT EXIT PLANE
- Suppressor Area Ratio	1.752	1.56
- Suppressor Radius Ratio	0.764	0.743
- Angle Subtended by Each Chute, θ_{Chute}, degrees	7.72	6.44
- Angle Subtended by Each Flow Element θ_{flow}, degrees	10.28	11.56
- Flow Area, $in.^2$ (Design)	20.23	22.92
- Equivalent Flow Diameter, in. (Design)	5.08	5.403
- Chute Blockage Area, $in.^2$	15.20	12.77

INNER NOZZLE

- Mach No. (Design)	1.327	
- P_T/P_{amb}	2.90	
- T_T, °R	850	-C-D DESIGN POINT CYCLE
- T_s, °R	620	
- γ	1.424	
- V_j, ft/sec	1633	
- A_{exit}/A_{throat}	1.077	
- θ_1, Divergent Flap Angle, degrees	12.45	
- θ_2, Plug Angle, degrees	15	
- ℓ/S, Divergent Flowpath Length/Throat Slant Height	2.80	

	AT THROAT	AT EXIT PLANE
- Flow Area, $in.^2$	4.05	4.36
- Equivalent Flow Diameter, in.	2.27	2.36
- Radius Ratio	0.940	0.929

SYSTEM

- $A_{Throat, Inner}/A_{Throat, Outer}$	0.20
- Total Throat Flow Area, Inner & Outer, $in.^2$	24.272
- Total Equivalent Flow Diameter at Throat, Inner & Outer, in.	5.559

2.5 ACOUSTIC AND DIAGNOSTIC TEST MATRICES

A summary of acoustic and diagnostic tests conducted with the six coannular configurations, described in Section 2.4, is presented in Table 2-III. The aerodynamic flow conditions corresponding to these tests are tabulated in this section.

2.5.1 Acoustic Tests

A total of 153 acoustic test points distributed as per Table 2-III among the test nozzles were conducted during this program. The flow conditions of the test points for configurations DFSC-1 through DFSC-6 are presented in Tables 2-IV through 2-IX, respectively. In addition to the outer and inner stream flow parameters, the tabulated data contain mass-averaged velocities and temperatures of the mixed streams that are calculated as follows:

$$V_j^{mix} = \frac{W^o V_j^o + W^i V_j^i}{W^o + W^i} \quad \text{and}$$

$$T_T^{mix} = \frac{W^o T_T^o + W^i T_T^i}{W^o + W^i}$$

The mixed stream data are employed to calculate the mixed jet velocity parameter (LVM) and mixed shock strength parameter (LBM) that are defined as follows:

$$LVM = 10 \log \left(V_j^{mix} / a_{amb}\right)$$

$$LBM = 10 \log \beta^{eff}$$

$$\beta^{eff} = \left[\left(M_j^{eff}\right)^2 - 1\right]^{1/2}$$

$$M_j^{eff} = \frac{2}{\gamma - 1}\left[\left(P_r^{eff}\right)^{\frac{\gamma-1}{\gamma}} - 1\right] \quad ; \quad \gamma = 1.4$$

TABLE 2- III SUMMARY OF ACOUSTIC AND DIAGNOSTIC TESTS

CONFIGURATION DESCRIPTION	DESIGNATION	NUMBER OF ACOUSTIC TEST POINTS		NUMBER OF LV PLUMES		NUMBER OF SHADOWGRAPH PLUMES		REMARKS
		STATIC	FLIGHT	STATIC	FLIGHT	STATIC	FLIGHT	
UNSUPPRESSED COANNULAR NOZZLE WITH TRUNCATED PLUG AND HAVING BOTH INNER AND OUTER FLOW-PATHS CONVERGENT	DFSC-1	17	12	3	2	2	2	BASELINE CONVERGENT COANNULAR NOZZLE TESTED AT TWO OUTER STREAM TEMPERATURES (1700°R AND 870°R) OVER A RANGE OF OUTER STREAM PRESSURE RATIOS OF $2.5 < P_r^o < 4.0$
UNSUPPRESSED COANNULAR NOZZLE WITH TRUNCATED PLUG AND HAVING BOTH INNER AND OUTER FLOW-PATHS CONVERGENT-DIVERGENT (C-D)	DFSC-2	15	13	3	2	2	2	C-D COANNULAR NOZZLE TESTED AT $T_T^o \sim 1700°R$ AND $2.2 < P_r^o < 4.0$ TO DETERMINE BENEFIT OF CONVERGENT-DIVERGENT TERMINATION
UNSUPPRESSED COANNULAR NOZZLE WITH EXTENDED PLUG AND HAVING BOTH INNER AND OUTER FLOW-PATHS CONVERGENT-DIVERGENT (C-D)	DFSC-3	9	8	3	2	2	2	C-D COANNULAR NOZZLE WITH EXTENDED PLUG TESTED AT $T_T^o \sim 1700°R$ AND $2.8 < P_r^o < 4.0$ TO DETERMINE ADDITIONAL BENEFIT OF SHARP PLUG OVER TRUNCATED PLUG
COANNULAR PLUG NOZZLE WITH 20 ELEMENT CONVERGENT SUPPRESSOR IN THE OUTER AND AN ANNULAR CONVERGENT INNER	DFSC-4	20	10	2	2	2	2	BASELINE CONVERGENT SUPPRESSOR COANNULAR NOZZLE TESTED AT TWO OUTER STREAM TEMPERATURES (1700°R AND 870°R) OVER PRESSURE RATIO RANGE OF $2.0 < P_r^o < 4.0$
COANNULAR PLUG NOZZLE WITH 20 ELEMENT C-D SUPPRESSOR IN THE OUTER AND AN ANNULAR C-D INNER	DFSC-5	10	10	2	2	2	2	C-D SUPPRESSOR COANNULAR NOZZLE TESTED AT $T_T^o \sim 1700°R$ AND $2.7 < P_r^o < 3.5$ TO DETERMINE BENEFIT OF CONVERGENT DIVERGENT TERMINATION
UNSUPPRESSED COANNULAR NOZZLE WITH EXTENDED PLUG AND HAVING BOTH INNER AND OUTER FLOW-PATHS CONVERGENT	DFSC-6	16	13	3	2	-	-	CONVERGENT COANNULAR NOZZLE WITH EXTENDED PLUG TESTED AT $T_T^o \sim 1700°R$ AND $2.5 < P_r^o < 4.0$ WITH INNER STREAM AT (1) SUPERSONIC AND (2) SUBSONIC TO DETERMINE BENEFIT OF SHARP PLUG OVER TRUNCATED PLUG AND SUBSONIC OVER SUPERSONIC INNER STREAM
	TOTAL	87	66	16	12	10	10	
		153		28		20		

TABLE 2- IV. ACOUSTIC TEST MATRIX OF UNSUPPRESSED COANNULAR NOZZLE WITH TRUNCATED PLUG AND CONVERGENT INNER AND OUTER FLOWPATHS (DFSC-1).

NOZZLE - DFSC-1 AREA [MODEL SIZE - INNER = 3.44 , OUTER = 18.05 ; FULL SIZE - TOTAL = 1400.00] SQ.IN.

TEST POINT	V_{ac} FT/SEC	P_r^o	T_T^o DEG R	V_j^o FT/SEC	W^o LB/SEC	P_r^i	T_T^i DEG R	V_j^i FT/SEC	W^i LB/SEC	P_r^{mix}	T_T^{mix} DEG R	V_j^{mix} FT/SEC	F LB	V_j^i/V_j^o	NF dB	LVM	LBM	COMMENTS
*101	0	1.00	519	0	0.	3.13	846	1681	1135.1	3.13	846	1681	60299	0.00	-10.1	1.75	-0.17	INNER ONLY
102	400	1.00	519	0	0.	3.13	873	1708	1151.6	3.13	873	1708	60427	0.00	-10.1	1.78	-0.16	
109	0	2.59	1697	2215	558.0	3.12	864	1697	182.6	2.62	1491	2087	48039	0.77	-6.3	2.68	-1.04	
110	400	2.54	1707	2203	545.4	3.12	868	1701	181.9	2.59	1497	2077	46956	0.77	-6.3	2.63	-1.14	
111	0	2.80	1697	2294	604.3	3.12	855	1689	183.5	2.80	1501	2153	52724	0.74	-6.8	2.81	-0.64	
112	400	2.80	1710	2302	601.3	3.12	872	1705	181.8	2.80	1515	2163	52651	0.74	-6.8	2.79	-0.64	
113	0	3.05	1697	2372	657.4	3.12	853	1686	183.7	3.00	1513	2222	58105	0.71	-7.2	2.95	-0.28	
114	400	3.05	1702	2378	657.9	3.12	862	1696	182.8	3.01	1519	2230	58273	0.71	-7.3	2.94	-0.27	
115	0	3.23	1700	2427	695.9	3.12	863	1697	182.5	3.15	1525	2275	62124	0.70	-7.6	3.04	-0.04	
*119+	0	3.32	1686	2441	719.2	3.12	855	1688	183.4	3.23	1517	2287	64185	0.69	-7.8	3.07	0.06	
*120+	400	3.33	1699	2452	717.5	3.13	869	1703	182.2	3.23	1530	2300	64331	0.69	-7.8	3.07	0.06	
123	0	3.50	1687	2486	757.9	3.12	861	1694	182.7	3.38	1527	2332	68189	0.68	-8.1	3.15	0.24	
125	0	3.61	1682	2508	783.5	3.12	865	1698	182.4	3.47	1527	2354	70701	0.68	-8.3	3.19	0.35	
126	400	3.62	1696	2519	779.3	3.13	869	1704	182.2	3.47	1539	2364	70663	0.68	-8.3	3.19	0.35	
127	0	3.82	1694	2562	824.8	3.13	865	1701	182.9	3.65	1543	2405	75352	0.66	-8.6	3.28	0.52	
129	0	4.02	1721	2622	858.4	3.12	876	1710	181.1	3.81	1574	2462	79577	0.65	-8.8	3.38	0.67	
130	400	4.01	1695	2600	866.2	3.13	866	1700	182.6	3.80	1550	2443	79653	0.65	-8.9	3.34	0.67	
1109	0	2.60	868	1579	794.9	3.13	853	1688	184.1	2.69	865	1599	48670	1.07	-9.1	1.53	-1.00	
1110	400	2.61	882	1593	791.9	3.13	863	1698	183.1	2.69	878	1612	48876	1.07	-9.1	1.53	-0.99	
1111	0	2.88	864	1645	882.3	3.13	854	1689	184.0	2.92	862	1653	54783	1.03	-9.6	1.67	-0.51	
1112	400	2.88	868	1649	881.9	3.13	869	1704	182.1	2.92	868	1658	54854	1.03	-9.7	1.65	-0.51	
1113	0	3.13	874	1708	951.9	3.13	846	1682	184.8	3.13	869	1703	60187	0.98	-10.0	1.80	-0.17	
*1119+	0	3.41	864	1753	1043.9	3.13	844	1680	184.5	3.37	861	1741	66497	0.96	-10.6	1.89	0.15	
*1120+	400	3.41	880	1768	1037.3	3.13	866	1701	182.9	3.37	878	1758	66686	0.96	-10.6	1.90	0.15	
1123	0	3.59	869	1787	1097.8	3.12	862	1695	182.8	3.51	867	1773	70599	0.95	-10.8	1.97	0.32	
1125	0	3.69	863	1797	1133.2	3.12	855	1689	183.7	3.60	862	1782	72950	0.94	-11.0	1.99	0.41	
1126	400	3.69	887	1822	1119.4	3.13	869	1704	182.5	3.60	884	1805	73073	0.94	-11.0	2.02	0.42	
1127	0	3.93	865	1833	1203.7	3.13	857	1691	183.4	3.80	863	1814	78223	0.92	-11.4	2.07	0.60	
1128	400	3.92	886	1855	1188.5	3.13	871	1707	182.3	3.80	884	1835	78202	0.92	-11.3	2.09	0.60	

FIXED SUPERSONIC INNER STREAM

$T_T^o \sim 1700^oR$, $2.5 < P_r^o < 4.0$

$T_T^o \sim 870^oR$, $2.6 < P_r^o < 4.0$

NOTE: * INDICATES LV PLUME MEASUREMENTS
+ INDICATES DIAGNOSTIC SHADOWGRAPHS

SUPERSCRIPTS
o = OUTER STREAM
i = INNER STREAM
mix = MIXED STREAM

P_r = PRESSURE RATIO
T_T = TOTAL TEMPERATURE, ^oR
V_j = FULLY EXPANDED JET EXIT VELOCITY, fps

V_{ac} = FREE JET VELOCITY, fps
W = WEIGHT FLOW RATE, lbs/sec

TABLE 2- V.. ACOUSTIC TEST MATRIX OF UNSUPPRESSED COANNULAR NOZZLE WITH TRUNCATED PLUG AND C-D INNER AND OUTER FLOWPATHS (DFSC-2).

NOZZLE - DFSC-2 AREA [MODEL SIZE - INNER = 3.97 , OUTER = 18.05 ; FULL SIZE - TOTAL = 1400.00] SQ.IN.

TEST POINT	V_{ac} FT/SEC	P_r^o	T_T^o DEG R	V_j^o FT/SEC	W^o LB/SEC	P_r^i	T_T^i DEG R	V_j^i FT/SEC	W^i LB/SEC	P_r^{mix}	T_T^{mix} DEG R	V_j^{mix} FT/SEC	F LB	V_j^i/V_j^o	NF dB	LVM	LBM	COMMENTS
*201	0	1.00	519	0	0.	3.13	873	1708	1135.1	3.13	873	1708	60259	0.00	-10.1	1.78	-0.17	INNER
202	400	1.00	519	0	0.	3.12	849	1682	1151.6	3.12	849	1682	60219	0.00	-10.1	1.75	-0.18	ONLY
205	0	2.22	1691	2046	468.4	3.12	856	1689	206.1	2.34	1435	1937	40615	0.83	-5.7	2.33	-1.95	
209	0	2.53	1704	2198	531.3	3.12	856	1689	206.3	2.59	1466	2055	47118	0.77	-6.4	2.59	-1.12	
210	400	2.52	1708	2194	529.0	3.11	871	1703	204.7	2.58	1474	2057	46915	0.78	-6.3	2.60	-1.16	
211	0	2.81	1683	2288	592.6	3.12	857	1691	206.1	2.81	1469	2133	52969	0.74	-6.9	2.75	-0.61	
212	400	2.77	1696	2281	583.4	3.12	869	1702	205.0	2.77	1481	2130	52203	0.75	-6.8	2.75	-0.68	
213	0	3.04	1695	2370	641.2	3.12	858	1691	205.9	2.99	1491	2205	58057	0.71	-7.4	2.89	-0.28	
214	400	3.07	1702	2382	645.9	3.12	874	1707	204.9	3.01	1502	2219	58690	0.72	-7.4	2.93	-0.25	
215	0	3.23	1680	2412	683.2	3.12	859	1693	206.3	3.14	1489	2245	62066	0.70	-7.7	2.97	-0.05	
216	400	3.23	1702	2429	681.1	3.12	866	1700	205.6	3.15	1508	2260	62288	0.70	-7.6	3.01	-0.05	
217	0	3.27	1685	2427	691.3	3.12	865	1699	205.5	3.18	1497	2260	62991	0.70	-7.8	3.00	-0.00	
218	400	3.27	1712	2446	685.7	3.12	869	1702	205.0	3.17	1517	2274	62974	0.70	-7.7	3.03	-0.01	
*219+	0	3.32	1679	2436	703.2	3.12	862	1696	205.6	3.22	1494	2268	64087	0.70	-7.9	3.01	0.05	
*220+	400	3.33	1695	2450	703.4	3.12	873	1705	204.8	3.23	1509	2282	64415	0.70	-7.8	3.05	0.06	
221	0	3.40	1687	2461	716.0	3.12	869	1702	204.6	3.28	1505	2292	65582	0.69	-8.0	3.06	0.13	
222	400	3.40	1691	2463	718.3	3.12	878	1711	204.4	3.28	1510	2296	65864	0.69	-8.0	3.07	0.13	
223	0	3.49	1676	2475	740.5	3.12	852	1685	206.7	3.36	1495	2302	67795	0.68	-8.2	3.08	0.22	
224	400	3.51	1697	2495	740.8	3.12	880	1713	204.3	3.37	1520	2326	68322	0.69	-8.1	3.13	0.24	
225	0	3.63	1684	2512	766.1	3.12	857	1690	206.2	3.46	1508	2337	70653	0.67	-8.3	3.15	0.34	
226	400	3.62	1708	2529	760.0	3.13	885	1719	203.6	3.46	1534	2358	70621	0.68	-8.3	3.19	0.34	
227	0	3.82	1697	2563	802.9	3.12	860	1694	206.0	3.62	1526	2385	74814	0.66	-8.6	3.24	0.50	
228	400	3.81	1715	2577	800.0	3.12	872	1705	205.0	3.61	1543	2399	74936	0.66	-8.5	3.26	0.50	
229	0	4.02	1708	2611	840.8	3.12	870	1703	204.1	3.78	1544	2433	79046	0.65	-8.8	3.32	0.66	
230	400	4.02	1696	2604	849.6	3.12	873	1706	205.0	3.79	1536	2429	79620	0.66	-8.9	3.32	0.66	
231	0	3.16	1690	2400	666.8	3.12	859	1693	206.1	3.09	1494	2233	60587	0.71	-7.6	2.95	-0.13	
*1219+	0	3.40	877	1764	1010.7	3.13	851	1687	207.5	3.36	872	1750	66285	0.96	-10.5	1.89	0.14	
*1220+	400	3.41	875	1763	1017.4	3.13	852	1687	207.6	3.36	870	1750	66645	0.96	-10.5	1.91	0.15	

FIXED SUPERSONIC INNER STREAM

$T_T^o \sim 1700^oR$, $2.2 < P_r^o < 4.0$

$T_T^o \sim 870^oR$

NOTE: * INDICATES LV PLUME MEASUREMENTS
+ INDICATES DIAGNOSTIC SHADOWGRAPHS

SUPERSCRIPTS
o = OUTER STREAM
i = INNER STREAM
mix = MIXED STREAM

P_r = PRESSURE RATIO
T_T = TOTAL TEMPERATURE, ^oR
V_j = FULLY EXPANDED JET EXIT VELOCITY, fps
V_{ac} = FREE JET VELOCITY, fps
W = WEIGHT FLOW RATE, lbs/sec

TABLE 2- VI. ACOUSTIC TEST MATRIX OF UNSUPPRESSED COANNULAR NOZZLE WITH EXTENDED PLUG AND C-D INNER AND OUTER FLOWPATHS (DFSC-3).

NOZZLE - DFSC-3 AREA (MODEL SIZE - INNER = 3.97 , OUTER = 18.05 ; FULL SIZE - TOTAL = 1400.00) SQ.IN.

TEST POINT	V_{ac} FT/SEC	P_r^o	T_T^o DEG R	V_j^o FT/SEC	W^o LB/SEC	P_r^i	T_T^i DEG R	V_j^i FT/SEC	W^i LB/SEC	P_r^{mix}	T_T^{mix} DEG R	V_j^{mix} FT/SEC	F LB	V_j^i/V_j^o	NF dB	LVM	LBM	COMMENTS
*301	0	1.00	519	0	0.	3.13	864	1699	1135.1	3.13	864	1699	60509	0.00	-10.1	1.77	-0.17	INNER ONLY
302	400	1.00	519	0	0.	3.13	877	1712	1151.6	3.13	877	1712	60460	0.00	-10.0	1.80	-0.17	
311	0	2.80	1692	2289	591.1	3.13	857	1692	207.1	2.80	1475	2134	52943	0.74	-6.9	2.77	-0.63	
312	400	2.80	1694	2293	591.9	3.13	856	1690	207.3	2.80	1476	2136	53081	0.74	-6.9	2.76	-0.62	
315	0	3.22	1678	2408	683.3	3.12	865	1700	205.9	3.14	1489	2244	62025	0.71	-7.7	2.99	-0.06	
316	400	3.23	1688	2418	683.4	3.13	863	1698	206.6	3.15	1496	2250	62249	0.70	-7.7	2.99	-0.05	
*319+	0	3.32	1688	2442	702.7	3.13	861	1696	206.6	3.22	1500	2272	64232	0.69	-7.8	3.04	0.05	$T_T^o \sim 1700^oR$, $2.8 < P_r^o < 4.0$
*320+	400	3.33	1698	2451	701.7	3.13	875	1710	205.2	3.23	1511	2283	64367	0.70	-7.8	3.04	0.06	
321	0	3.39	1685	2459	718.1	3.13	871	1705	205.3	3.28	1504	2291	65757	0.69	-7.9	3.07	0.13	
322	400	3.39	1689	2461	717.1	3.13	870	1705	205.5	3.28	1506	2292	65734	0.69	-7.9	3.06	0.12	
325	0	3.62	1691	2515	764.0	3.13	872	1707	205.6	3.46	1517	2343	70640	0.68	-8.3	3.18	0.34	
326	400	3.62	1692	2517	765.0	3.13	876	1711	204.9	3.46	1520	2346	70749	0.68	-8.3	3.16	0.34	
329	0	4.03	1692	2601	850.0	3.13	869	1704	205.7	3.79	1531	2425	79602	0.66	-8.9	3.32	0.66	
330	400	4.03	1688	2597	852.2	3.13	866	1701	206.2	3.79	1527	2422	79703	0.65	-8.9	3.31	0.66	
331	0	3.16	1683	2396	670.1	3.13	858	1692	207.1	3.09	1488	2230	60798	0.71	-7.6	2.96	-0.13	
*1319+	0	3.42	871	1761	1021.0	3.12	854	1688	207.1	3.37	868	1748	66745	0.96	-10.5	1.92	0.15	$T_T^o \sim 870^oR$
*1320+	400	3.42	878	1767	1016.6	3.13	856	1692	207.5	3.37	874	1754	66754	0.96	-10.6	1.90	0.15	

FIXED SUPERSONIC INNER STREAM

NOTE: * INDICATES LV PLUME MEASUREMENTS
+ INDICATES DIAGNOSTIC SHADOWGRAPHS

SUPERSCRIPTS
o = OUTER STREAM
i = INNER STREAM
mix = MIXED STREAM

P_r = PRESSURE RATIO
T_T = TOTAL TEMPERATURE, ^oR
V_j = FULLY EXPANDED JET EXIT VELOCITY, fps

V_{ac} = FREE JET VELOCITY, fps
W = WEIGHT FLOW RATE, lbs/sec

TABLE 2-VII.ACOUSTIC TEST MATRIX OF SUPPRESSED COANNULAR PLUG NOZZLE WITH CONVERGENT FLOW PATHS (DFSC-4).

NOZZLE - DFSC-4 AREA [MODEL SIZE - INNER = 3.99 , OUTER = 20.36 ; FULL SIZE - TOTAL = 1400.00] SQ.IN.

TEST POINT	V_{ac} FT/SEC	P_r^o	T_T^o DEG R	V_j^o FT/SEC	W^o LB/SEC	P_r^i	T_T^i DEG R	V_j^i FT/SEC	W^i LB/SEC	P_r^{mix}	T_T^{mix} DEG R	V_j^{mix} FT/SEC	F LB	V_j^i/V_j^c	NF dB	LVM	LBM	COMMENTS
401	0	1.98	1714	1920	424.2	2.90	851	1637	175.4	2.10	1461	1837	34241	0.85	-4.9	2.08	-3.44	
403	0	2.02	1722	1948	430.7	2.90	865	1651	173.9	2.13	1475	1862	35002	0.85	-4.9	2.14	-3.18	
404	400	2.09	1722	1992	446.7	2.90	858	1645	174.9	2.19	1479	1894	36597	0.83	-5.1	2.22	-2.76	
405	0	2.22	1711	2059	476.7	2.90	864	1650	174.1	2.30	1484	1949	39444	0.80	-5.4	2.33	-2.16	
407	0	2.38	1707	2132	510.9	2.90	868	1654	173.9	2.42	1493	2011	42800	0.78	-5.8	2.47	-1.64	
408	400	2.37	1714	2135	509.5	2.90	855	1642	175.5	2.42	1494	2009	42772	0.77	-5.8	2.48	-1.66	
409	0	2.54	1716	2210	544.5	2.90	871	1656	173.5	2.56	1511	2076	46329	0.75	-6.2	2.61	-1.22	
411	0	2.80	1720	2311	599.1	2.90	862	1648	174.2	2.77	1527	2161	51951	0.71	-6.7	2.78	-0.71	
412	400	2.79	1710	2300	599.4	2.91	857	1645	175.4	2.76	1516	2151	51807	0.72	-6.7	2.77	-0.72	
413	0	3.05	1711	2384	654.2	2.90	871	1656	173.3	2.97	1535	2231	57386	0.70	-7.2	2.93	-0.33	
* 415 +	0	3.14	1715	2411	672.1	2.90	872	1658	173.4	3.04	1541	2256	59312	0.69	-7.4	2.97	-0.21	
* 416 +	400	3.14	1708	2407	673.9	2.91	866	1654	174.6	3.04	1535	2251	59393	0.69	-7.4	2.96	-0.21	
417	0	3.32	1695	2447	714.9	2.90	874	1660	173.0	3.20	1534	2293	63296	0.68	-7.7	3.05	0.01	
419	0	4.04	1727	2631	862.0	2.90	876	1662	173.0	3.79	1585	2468	79422	0.63	-8.8	3.37	0.65	
420	400	4.03	1747	2644	855.6	2.91	869	1656	174.3	3.78	1598	2476	79279	0.63	-8.8	3.36	0.65	
1401	0	2.01	845	1357	624.0	2.93	850	1643	177.3	2.17	846	1420	35379	1.21	-8.0	0.98	-3.15	
1403	0	2.16	854	1424	665.8	2.93	855	1647	176.8	2.29	854	1470	38512	1.16	-8.3	1.13	-2.40	
1404	400	2.14	869	1428	654.6	2.90	853	1641	175.6	2.27	865	1473	38017	1.15	-8.2	1.11	-2.50	
1405	0	2.29	847	1466	710.5	2.93	834	1627	178.9	2.40	844	1498	41417	1.11	-8.6	1.21	-1.89	
1407	0	2.45	859	1526	752.6	2.92	859	1651	176.2	2.53	859	1549	44736	1.08	-8.8	1.36	-1.44	
1408	400	2.45	868	1533	749.0	2.90	853	1640	175.6	2.52	864	1553	44640	1.07	-8.9	1.34	-1.46	
1409	0	2.61	849	1564	807.0	2.93	851	1644	177.2	2.66	849	1578	48287	1.05	-9.2	1.44	-1.06	
1411	0	2.88	854	1636	887.5	2.92	853	1643	176.1	2.89	853	1636	54111	1.01	-9.7	1.59	-0.57	
1412	400	2.88	865	1646	884.1	2.91	847	1635	176.5	2.89	861	1644	54212	0.99	-9.7	1.59	-0.57	
1413	0	3.13	859	1695	963.1	2.91	858	1646	175.3	3.10	859	1687	59710	0.97	-10.1	1.72	-0.22	
* 1415 +	0	3.22	844	1697	999.7	2.90	848	1634	175.5	3.17	844	1688	61655	0.96	-10.4	1.72	-0.11	
* 1416 +	400	3.22	871	1725	984.9	2.91	846	1634	176.5	3.17	867	1711	61770	0.95	-10.3	1.76	-0.10	
1417	0	3.41	845	1732	1055.3	2.89	851	1636	175.0	3.32	845	1718	65700	0.94	-10.7	1.79	0.10	
1419	0	4.15	851	1848	1280.9	2.90	854	1640	175.0	3.96	851	1822	82491	0.89	-11.8	2.05	0.73	
1420	400	4.15	892	1892	1251.9	2.91	853	1642	176.1	3.96	887	1861	82607	0.87	-11.6	2.12	0.73	

FIXED SUPERSONIC INNER STREAM

$T_T^o \sim 1700^oR$, $2.0 < P_r^o < 4.0$

$T_T^o \sim 870^oR$, $2.0 < P_r^o < 4.2$

NOTE: * INDICATES LV PLUME MEASUREMENTS

+ INDICATES DIAGNOSTIC SHADOWGRAPHS

SUPERSCRIPTS

o = OUTER STREAM

i = INNER STREAM

mix = MIXED STREAM

P_r = PRESSURE RATIO

T_T = TOTAL TEMPERATURE, ^oR

V_j = FULLY EXPANDED JET EXIT VELOCITY, fps

V_{ac} = FREE JET VELOCITY, fps

W = WEIGHT FLOW RATE, lbs/sec

TABLE 2-VIII.ACOUSTIC TEST MATRIX OF SUPPRESSED COANNULAR PLUG NOZZLE WITH C-D FLOWPATHS (DFSC-5).

NOZZLE - DFSC-5 AREA (MODEL SIZE - INNER = 4.05 , OUTER = 20.23 ; FULL SIZE - TOTAL = 1400.00) SQ.IN.

TEST POINT	V_{ac} FT/SEC	P_r^o	T_T^o DEG R	V_j^o FT/SEC	W^o LB/SEC	P_r^i	T_T^i DEG R	V_j^i FT/SEC	W^i LB/SEC	P_r^{mix}	T_T^{mix} DEG R	V_j^{mix} FT/SEC	F LB	V_j^i/V_j^o	NF dB	LVM	LBM	COMMENTS
501	0	2.73	1700	2273	587.7	2.91	884	1672	176.3	2.72	1512	2134	50683	0.74	-6.6	2.75	-0.82	
502	400	2.71	1710	2272	580.2	2.91	852	1640	178.9	2.69	1507	2122	50084	0.72	-6.5	2.73	-0.86	
505	0	2.96	1727	2367	629.9	2.92	848	1639	180.1	2.89	1531	2205	55519	0.69	-6.9	2.92	-0.45	
506	400	2.96	1715	2359	632.8	2.91	848	1637	179.4	2.89	1523	2199	55521	0.69	-7.0	2.89	-0.45	
507	0	3.03	1728	2389	644.9	2.92	846	1636	180.4	2.95	1535	2224	57074	0.69	-7.1	2.95	-0.35	
508	400	3.03	1716	2380	647.2	2.91	849	1637	179.3	2.95	1527	2218	57003	0.69	-7.1	2.93	-0.36	
509	0	3.08	1723	2401	656.4	2.92	849	1640	180.1	2.99	1534	2236	58152	0.68	-7.2	2.98	-0.28	
510	400	3.08	1724	2401	657.1	2.90	853	1641	178.8	2.99	1537	2238	58165	0.68	-7.2	2.97	-0.29	
*511 +	0	3.13	1725	2419	667.1	2.92	852	1644	179.6	3.04	1540	2254	59336	0.68	-7.3	3.01	-0.21	
*512 +	400	3.13	1718	2412	668.2	2.91	857	1646	178.7	3.03	1536	2250	59244	0.68	-7.3	3.00	-0.22	
513	0	3.18	1710	2421	680.7	2.91	861	1648	178.0	3.08	1534	2260	60339	0.68	-7.4	3.02	-0.16	
514	400	3.18	1724	2431	679.3	2.91	856	1644	178.6	3.07	1543	2267	60455	0.68	-7.4	3.03	-0.16	
515	0	3.23	1711	2435	691.3	2.91	849	1638	179.4	3.12	1533	2271	61464	0.67	-7.5	3.04	-0.09	
516	400	3.23	1724	2444	689.5	2.91	858	1646	178.5	3.11	1545	2280	61517	0.67	-7.5	3.05	-0.10	
517	0	3.32	1707	2456	711.6	2.91	850	1639	179.3	3.19	1534	2292	63465	0.67	-7.7	3.08	0.01	
518	400	3.32	1726	2470	708.1	2.91	865	1653	177.8	3.19	1553	2306	63502	0.67	-7.6	3.10	0.01	
519	0	3.52	1723	2518	750.5	2.91	867	1656	177.5	3.36	1559	2353	67879	0.66	-7.9	3.19	0.22	
520	400	3.53	1742	2533	748.4	2.91	874	1661	176.9	3.36	1576	2366	68065	0.66	-7.9	3.22	0.22	
*1511 +	0	3.23	877	1732	980.0	2.91	861	1651	178.6	3.18	874	1719	61909	0.95	-10.2	1.83	-0.10	
*1514 +	400	3.22	876	1729	978.6	2.91	837	1627	181.1	3.17	870	1712	61742	0.94	-10.2	1.81	-0.11	

$T_T^o \sim 1700^oR$, $2.7 < P_r^o < 3.5$

$T_T^o \sim 870^oR$

FIXED SUPERSONIC INNER STREAM

NOTE: * INDICATES LV PLUME MEASUREMENTS
+ INDICATES DIAGNOSTIC SHADOWGRAPHS

SUPERSCRIPTS
o = OUTER STREAM
i = INNER STREAM
mix = MIXED STREAM

P_r = PRESSURE RATIO
T_T = TOTAL TEMPERATURE, ^oR
V_j = FULLY EXPANDED JET EXIT VELOCITY, fps

V_{ac} = FREE JET VELOCITY, fps
W = WEIGHT FLOW RATE, lbs/sec

TABLE 2- IX. ACOUSTIC TEST MATRIX OF UNSUPPRESSED COANNULAR NOZZLE WITH EXTENDED PLUG AND CONVERGENT INNER AND OUTER FLOWPATHS (DFSC-6).

NOZZLE - DFSC-6 AREA (MODEL SIZE - INNER = 3.44 , OUTER =18.05 ; FULL SIZE - TOTAL = 1400.00) SQ.IN.

TEST POINT	V_{ac} FT/SEC	P_r^o	T_T^o DEG R	V_j^o FT/SEC	W^o LB/SEC	P_r^i	T_T^i DEG R	V_j^i FT/SEC	W^i LB/SEC	P_r^{mix}	T_T^{mix} DEG R	V_j^{mix} FT/SEC	F LB	V_j^i/V_j^o	NF dB	LVM	LBM	COMMENTS
607	0	2.04	1675	1936	439.2	3.13	850	1685	191.9	2.19	1424	1860	36488	0.87	-4.9	2.28	-2.75	
609	0	2.55	1720	2217	541.7	3.13	839	1676	193.1	2.60	1488	2075	47390	0.76	-6.1	2.75	-1.09	
610	400	2.53	1684	2184	545.3	3.12	860	1694	191.3	2.58	1470	2056	47087	0.78	-6.2	2.64	-1.14	
611	0	2.79	1680	2280	599.3	3.14	841	1678	192.8	2.80	1475	2133	52529	0.74	-6.6	2.87	-0.64	
612	400	2.80	1681	2281	603.1	3.13	854	1690	192.3	2.80	1480	2138	52861	0.74	-6.8	2.82	-0.64	
613	0	3.06	1677	2362	657.2	3.14	850	1687	191.9	3.01	1490	2209	58317	0.71	-7.1	3.03	-0.25	
614	400	3.06	1713	2387	652.4	3.14	856	1693	192.2	3.01	1517	2229	58517	0.71	-7.2	3.00	-0.26	
*619	0	3.33	1672	2432	716.9	3.14	866	1703	190.6	3.24	1502	2279	64294	0.70	-7.6	3.15	0.07	$T_T^o \sim 1700^oR$, $2.0 < P_r^o < 4.0$
*620	400	3.32	1692	2446	714.7	3.14	867	1703	191.0	3.23	1517	2289	64440	0.70	-7.7	3.12	0.06	
625	0	3.65	1701	2531	778.0	3.13	867	1703	189.7	3.50	1537	2368	71240	0.67	-8.0	3.32	0.38	
626	400	3.61	1683	2508	777.4	3.13	848	1684	192.9	3.46	1517	2344	70694	0.67	-8.2	3.22	0.34	
627	0	3.83	1678	2551	822.2	3.14	883	1719	188.3	3.65	1529	2395	75235	0.67	-8.4	3.37	0.53	
629	0	4.03	1681	2593	864.1	3.14	888	1724	187.6	3.82	1540	2438	79693	0.67	-8.6	3.45	0.68	
630	400	4.02	1681	2591	867.3	3.13	870	1705	190.3	3.81	1535	2431	79930	0.66	-8.8	3.40	0.67	SUPERSONIC INNER
*1619	0	3.39	862	1746	1031.9	3.13	833	1668	193.6	3.35	857	1733	66038	0.96	-10.3	1.98	0.13	$T_T^o \sim 870^oR$
*1620	400	3.39	856	1740	1040.9	3.13	853	1687	192.3	3.35	855	1732	66389	0.97	-10.5	1.93	0.13	
7609	0	2.53	1691	2190	542.8	1.81	1163	1478	94.1	2.41	1612	2084	41271	0.67	-5.0	2.77	-1.83	
7610	400	2.53	1675	2178	546.4	1.81	1175	1487	94.1	2.41	1601	2076	41339	0.68	-5.2	2.68	-1.84	
7611	0	2.80	1698	2295	597.2	1.81	1178	1490	93.6	2.63	1627	2185	46936	0.65	-5.6	2.97	-1.12	
7612	400	2.80	1683	2283	602.6	1.81	1226	1520	92.2	2.63	1622	2181	47117	0.67	-5.8	2.90	-1.14	
7613	0	3.05	1702	2377	649.9	1.82	1208	1512	92.8	2.84	1640	2269	52375	0.64	-6.2	3.13	-0.66	
7614	400	3.05	1681	2362	658.0	1.81	1243	1529	91.4	2.85	1627	2260	52644	0.65	-6.4	3.05	-0.66	
*7619	0	3.32	1695	2447	708.7	1.80	1279	1545	89.0	3.08	1648	2346	58171	0.63	-6.7	3.26	-0.26	$T_T^o \sim 1700^oR$, $2.5 < P_r^o < 4.0$
7620	400	3.32	1710	2459	710.1	1.81	1263	1543	90.7	3.08	1659	2355	58622	0.63	-6.8	3.23	-0.25	
7625	0	3.62	1704	2525	769.1	1.81	1334	1587	87.5	3.34	1666	2429	64685	0.63	-7.2	3.43	0.09	
7626	400	3.61	1748	2558	763.9	1.81	1379	1614	86.7	3.33	1710	2461	65084	0.63	-7.3	3.41	0.09	
7627	0	3.82	1710	2573	810.4	1.80	1253	1527	89.7	3.50	1664	2468	69074	0.59	-7.6	3.50	0.28	
7629	0	4.04	1721	2625	854.8	1.82	1258	1542	90.6	3.69	1676	2521	74079	0.59	-7.9	3.60	0.48	
7630	400	4.02	1697	2603	863.1	1.81	1372	1609	86.9	3.68	1667	2512	74177	0.62	-8.1	3.51	0.46	SUBSONIC INNER

NOTE: * INDICATES LV PLUME MEASUREMENTS
+ INDICATES DIAGNOSTIC SHADOWGRAPHS

SUPERSCRIPTS
o = OUTER STREAM
i = INNER STREAM
mix = MIXED STREAM

P_r = PRESSURE RATIO
T_T = TOTAL TEMPERATURE, ^oR
V_j = FULLY EXPANDED JET EXIT VELOCITY, fps
V_{ac} = FREE JET VELOCITY, fps
W = WEIGHT FLOW RATE, lbs/sec

$$P_r^{eff} = \frac{P_r^o A_r + P_r^i}{A_r + 1}$$

In the above expressions P_r is the pressure ratio and A_r is the inner to outer stream area ratio of the nozzle. The superscripts i and o refer to inner and outer streams, respectively.

The normalization factor (NF) found in Tables 2-IV through 2-IX can be employed to normalize the acoustic data on a reference thrust (F_{ref} = 5130 lbs) and reference ambient density basis. For example, normalized perceived noise level can be obtained as follows:

Normalized PNL = PNLN = PNL + NF where

$$NF = -10 \log \left[\left(\frac{F}{F_{ref}} \right) \quad \left(\frac{\rho^{mix}}{\rho_{amb}} \right) \quad \omega-1 \right]$$

2.5.2 Laser Velocimeter Tests

The laser velocimeter was used to determine the mean and turbulent velocity distributions in 28 selected plumes of the six nozzle configurations as per Table 2-III. In order to determine the C-D effectiveness, the aerodynamic test conditions for both convergent and convergent-divergent configurations were selected to match the shock-free design conditions of the corresponding C-D nozzles. In addition, the LV tests of configurations DFSC-1 through -5 were conducted at two outer stream temperatures, namely, T_T^o ~ 1700° R and 870° R to determine the effect of temperature on shock-cell structure. In order to determine the effect of supersonic and subsonic inner streams on the shock structure downstream of the plug of a coannular nozzle operating at a given supersonic outer stream condition, LV tests were conducted with configuration DFSC-6. The test conditions of the LV plumes are identified in the acoustic test matrices (Tables 2-IV through 2-IX) by their matching acoustic test points.

2.5.3 Shadowgraph Tests

In order to substantiate the expected shock noise benefit with convergent-divergent nozzles at their design conditions, flow visualization shadowgraph photos were taken on selected plumes of configurations DFSC-1 through DFSC-5 as per Table 2-III. The selected aerodynamic test conditions for both convergent and convergent-divergent configurations match the design Mach numbers of the C-D nozzles. The shadowgraphs on plumes heated to 870° R were observed to have better clarity than those heated to 1700° R. Hence, the required photos were taken at both of the above-mentioned outer stream temperatures for each configuration, at the matching C-D design Mach number.

The flow conditions of the shadowgraph tests are identified also in the acoustic test matrices (Tables 2-IV through 2-IX) by their matching acoustic test points.

The experimentally obtained acoustic, LV and shadowgraph test data are presented in detail in the Comprehensive Data Report of this program (Reference 15).

3.0 ACOUSTIC AND DIAGNOSTIC TEST RESULTS

The acoustic and diagnostic laser velocimeter and shadowgraph test results obtained with the model configurations described in Section 2.4 as per the aerodynamic conditions summarized in Section 2.5 are analyzed and presented in this section.

This section is subdivided into six major subsections. General acoustic characteristics of the baseline unsuppressed and suppressed convergent coannular configurations (DFSC-1 and DFSC-4, respectively) are presented and the repeatability of the measured data is demonstrated in Subsection 3.1. The effectiveness of the convergent-divergent flow passages on the unsuppressed coannular plug nozzle (DFSC-2) for the reduction of shock-cell associated noise at and in the vicinity of the C-D design conditions is discussed in Subsection 3.2. This subsection also contains analyses of the data to demonstrate the additional front quadrant noise reduction obtained within the modification of the plug of the DFSC-2 nozzle (i.e., with DFSC-3 configuration). An alternative concept for the reduction of the front quadrant noise over an entire underexpanded operational range of the outer stream of a convergent coannular plug nozzle (DFSC-6) is demonstrated in Subsection 3.3. The acoustic and diagnostic data of convergent and C-D coannular configurations (i.e., DFSC-4 and DFSC-5, respectively) that employ 20-chute mechanical suppressors in the outer stream are presented in Subsection 3.4. Subsections 3.5 and 3.6 contain brief discussions on the effect of jet plume temperature on shock-cell associated noise and the effect of simulated flight on the location of sonic line near the jet exit.

Unless otherwise stated, the presented acoustic results are measured data that are scaled to a typical product size of A_T = 0.903 square meters (1,400 square inches) and extrapolated to a sideline of 731.5 meters (2,400 feet) and corrected to a standard day [15°C (59°F) and 70% relative humidity] atmospheric attenuation (Shields and Bass method, Reference 12).

3.1 UNSUPPRESSED AND SUPPRESSED CONVERGENT COANNULAR BASELINE NOZZLE DATA

The two baseline configurations of this study are the unsuppressed coannular nozzle with truncated plug and having convergent inner and outer flowpaths (DFSC-1) and the suppressed coannular nozzle with a convergent 20-element suppressor in the outer and a convergent annular inner (DFSC-4). These two configurations have been tested as Models 8 and 10.1 during an earlier NASA-Lewis supported program (Reference 6). To broaden the data base of these baseline coannular configurations, they were tested during this program as per test matrices presented in Tables 2-IV and 2-VII. The static and simulated flight (V_{ac} = 400 fps) measured perceived noise level data of DFSC-1 and DFSC-4 at a typical forward quadrant angle of Θ_i = 60° are presented in Figures 3-1 and 3-2, respectively. The data are plotted as a function of effective mixed shock strength parameter β^{eff} that was defined in Subsection 2.5.1. The repeatability of the data of the two configurations is demonstrated in these figures by comparing the data obtained during this program with those obtained from the previous tests (Reference 6). For reference, the corresponding static and simulated flight data of a convergent circular nozzle (References 6 and 7) are presented also in these figures.

3.2 UNSUPPRESSED CONVERGENT-DIVERGENT COANNULAR NOZZLE DATA

This section summarizes the acoustic and diagnostic data of unsuppressed C-D coannular nozzles with truncated and extended plugs (DFSC-2 and DFSC-3). The data are compared with the corresponding results obtained with the unsuppressed convergent coannular nozzle configuration (DFSC-1) to demonstrate the effect of C-D flow passages on the front and aft quadrant acoustic results.

3.2.1 Reduction of Shock-Cell Noise Due to C-D Flowpaths

The unsuppressed convergent-divergent coannular plug nozzle (DFSC-2), details of which are presented in Figure 2-11, has been designed for a shock-free flow at the following nominal conditions:

DATA SCALED TO TOTAL NOZZLE AREA OF 0.903 m^2 (1400 $In.^2$)
AND EXTRAPOLATED TO 731.5 m (2400 Ft.) SIDELINE

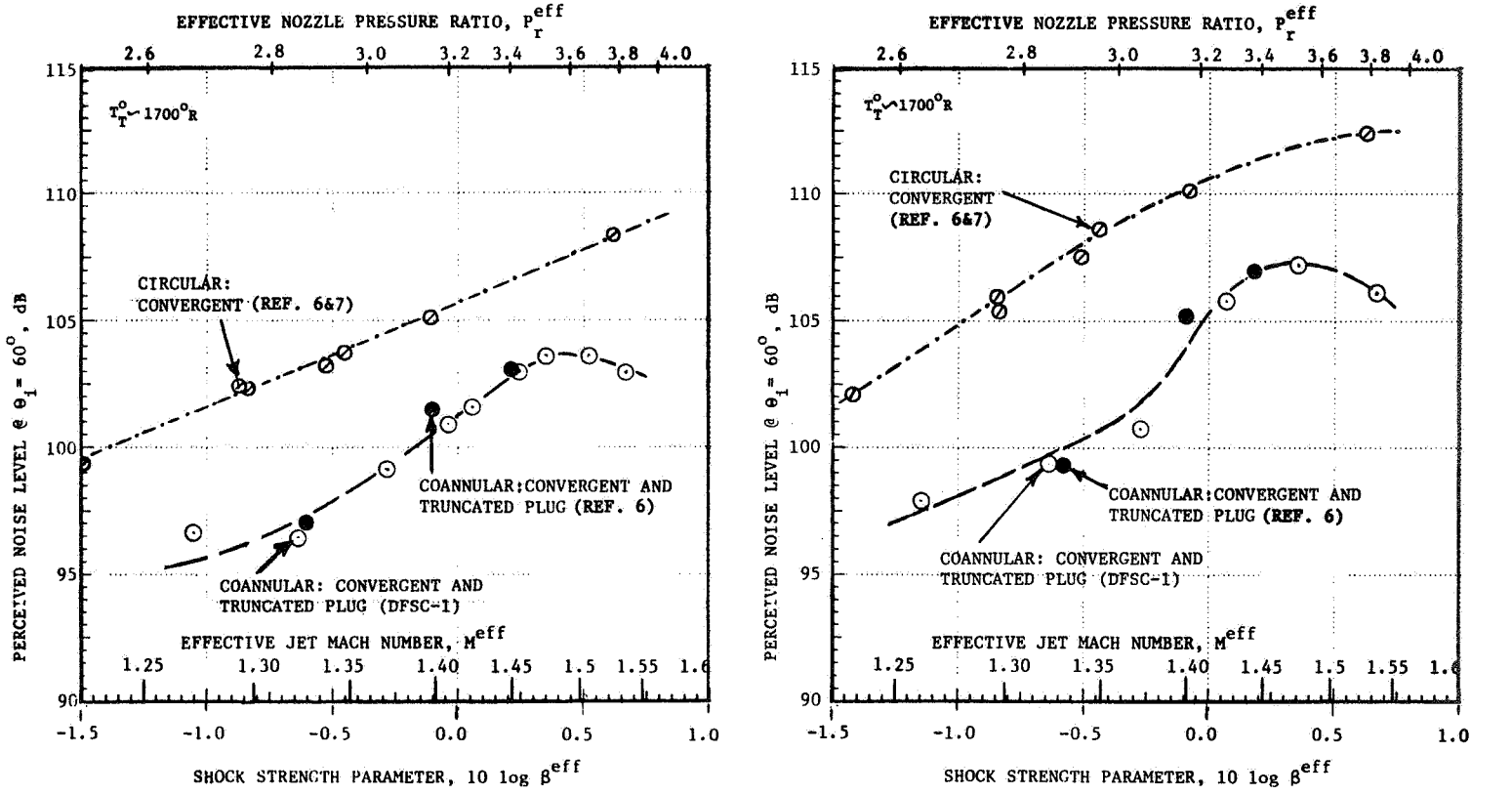

FIGURE 3-1. COMPARISON OF FORWARD QUADRANT PERCEIVED NOISE LEVEL DATA (AT $\theta_i = 60^o$) OF THE CONVERGENT COANNULAR NOZZLE WITH TRUNCATED PLUG (DFSC-1) WITH THAT OF A CONVERGENT BASELINE CIRCULAR NOZZLE.

DATA SCALED TO TOTAL NOZZLE AREA OF 0.903 m^2 (1400 $In.^2$)
AND EXTRAPOLATED TO 731.5 m (2400 Ft.) SIDELINE

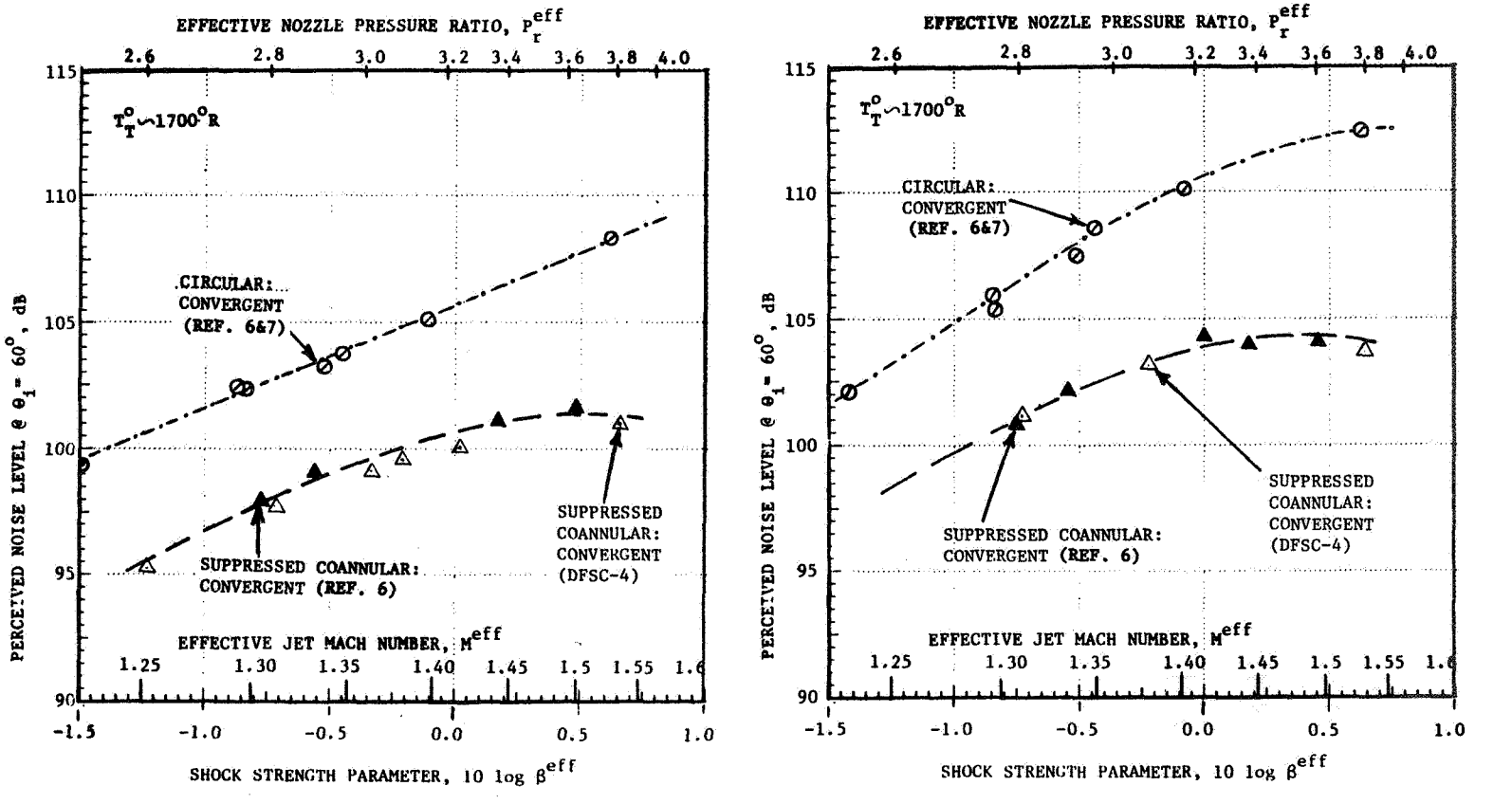

FIGURE 3-2. COMPARISON OF FORWARD QUADRANT PERCEIVED NOISE LEVEL DATA (AT $\theta_i = 60^o$) OF CONVERGENT SUPPRESSED COANNULAR NOZZLE (DFSC-4) WITH THAT OF A CONVERGENT BASELINE CIRCULAR NOZZLE.

$P_r^o = 3.3$ $\quad T_T^o = 1760°R$ $\quad M_j^o = 1.44$

$P_r^i = 3.1$ $\quad T_T^i = 860°R$ $\quad M_j^i = 1.38$

To determine the effectiveness of the convergent-divergent flowpaths in the control of shock-cell noise at and in the vicinity of their design conditions, static and simulated flight (V_{ac} = 122 m/sec or 400 fps) acoustic tests were conducted over an outer stream pressure ratio range of $2.2 < P_r^o < 4.0$ with its temperature at $T_T^o \simeq 1700°R$ and the inner stream maintained constant at the design condition of its flow passages (see Table 2-V for the test matrix). The measured PNL data at $\Theta_i = 60°$ are plotted in Figure 3-3 as a function of the effective shock strength parameter. The data are compared in this figure with the eariler presented (Figure 3-1) data of convergent terminated coannular nozzle (DFSC-1) and convergent circular nozzle. An examination of this figure indicates:

- A broad region of effectiveness of the C-D terminations in reducing the forward quadrant shock noise under both static and simulated flight conditions,

- The flow conditions at the region of maximum effectiveness are in the vicinity of the design conditions of C-D flowpaths,

- A maximum reduction of 2.3 dB and 4.2 dB relative to the convergent terminated coannular nozzle (DFSC-1) under static and simulated flight conditions, respectively, and

- A maximum reduction of 6.5 dB and 9.2 dB relative to convergent circular nozzle under static and simulated flight conditions, respectively.

3.2.2 Additional Reduction of Shock-Cell Noise Because of Plug Modification

As described earlier in the introduction, the diagnostic mean velocity data obtained during LV traverses parallel to the plug and along the centerline of the C-D annular nozzle with truncated plug (refer to Figure 1-14) operating at its C-D design condition indicated (1) absence of shock structure

DATA SCALED TO TOTAL NOZZLE AREA OF 0.903 m^2 (1400 $In.^2$)
AND EXTRAPOLATED TO 731.5 m (2400 Ft.) SIDELINE

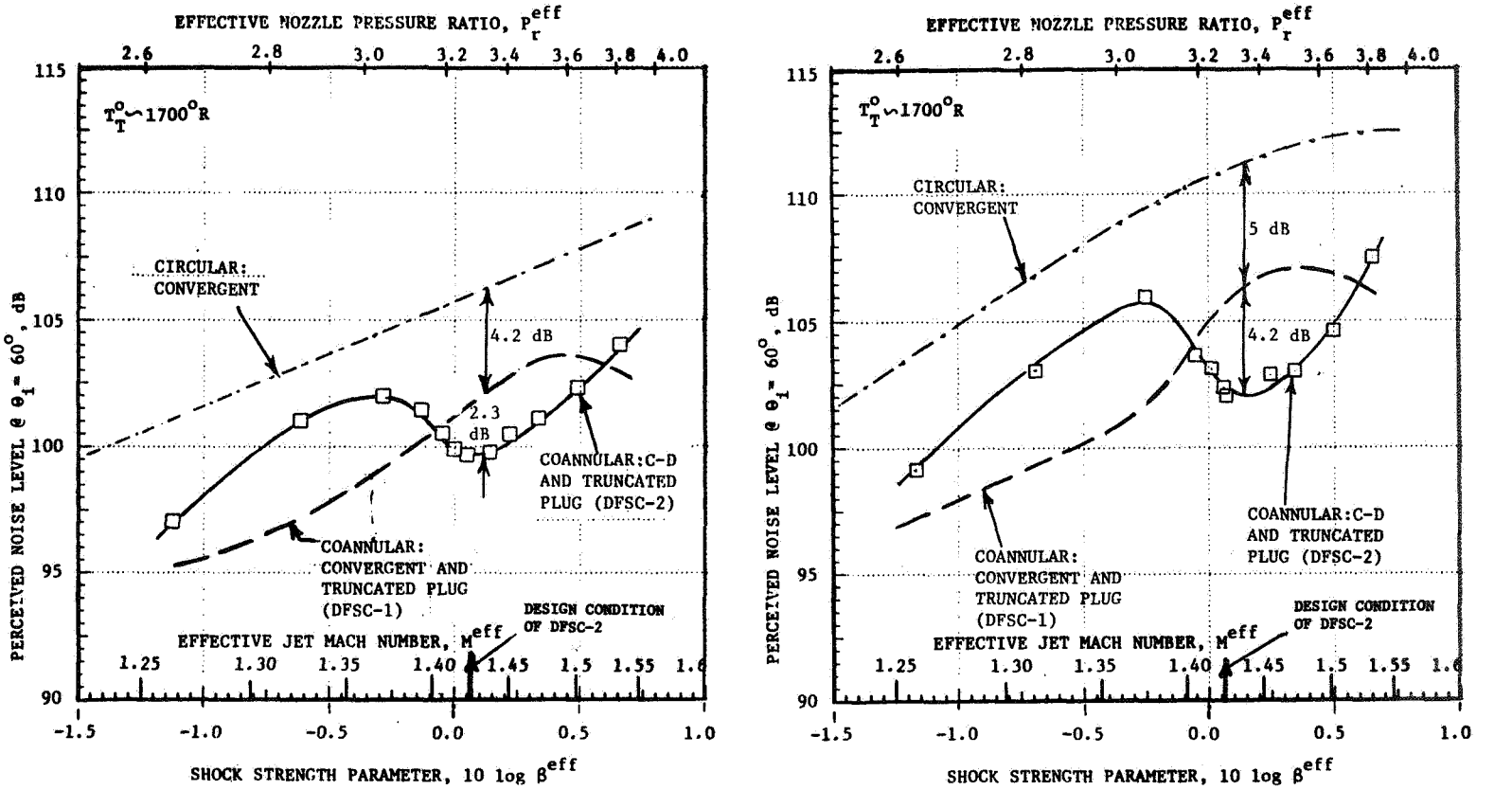

FIGURE 3-3. EFFECTIVENESS OF CONVERGENT-DIVERGENT INNER AND OUTER FLOWPATHS IN SHOCK-CELL NOISE REDUCTION FOR A COANNULAR NOZZLE WITH TRUNCATED PLUG (DFSC-2).

on the plug and (2) presence of the shocks downstream of the plug. This is due to the fact that the supersonic flow on the plug undergoes an expansion at the blunt plug termination resulting in a series of expansion and compression regions downstream of the plug. The presence of a strong expansion fan at the blunt plug termination had been confirmed with the shadowgraphs on C-D annular nozzle with truncated plug (Reference 7). Since the C-D coannular nozzle (DFSC-2) of this study has a similar truncated center plug, it was anticipated at the outset (and later confirmed during diagnostic tests) that shock-cells could be present downstream of the plug and hence more than C-D terminations would be necessary for complete shock-cell elimination. Therefore, as a part of this study, an effort was made to eliminate the downstream shock-cells of C-D coannular nozzles with truncated plug by designing a smooth extension to the plug. The acoustic and diagnostic test results obtained with the resulting configuration (DFSC-3), details of which are given in Figure 2-12, are presented in this section and compared with those of DFSC-1 and -2.

To determine additional reduction, if any, due to the plug modification of the C-D coannular plug nozzle, static and simulated flight (V_{ac} = 122 m/sec or 400 fps) acoustic tests were conducted with DFSC-3 over an outer stream pressure ratio range of $2.8 < P_r^o < 4.0$ (T_T^o was held fixed at 1700°R) and the inner stream maintained constant at the C-D design condition (see Table 2-VI for the test matrix). The measured PNL data at Θ_i = 60° are plotted in Figure 3-4 as a function of the effective shock strength parameter. The data are compared in the figure with the earlier presented (Figure 3-3) data of convergent (DFSC-1) and C-D (DFSC-2) coannular nozzles with truncated plugs. An examination of this figure indicates:

- An additional shock-cell noise reduction of 2.4 dB and 3 dB with DFSC-3, relative to the unsuppressed C-D coannular nozzle with truncated plug (DFSC-2) at its design condition, under static and simulated flight conditions, respectively,

- A maximum reduction of 4.7 dB and 7.2 dB with DFSC-3 at the C-D design conditions, under static and simulated flight conditions, respectively, relative to the unsuppressed convergent coannular nozzle with truncated plug (DFSC-1), and

DATA SCALED TO TOTAL NOZZLE AREA OF 0.903 m^2 (1400 $In.^2$)
AND EXTRAPOLATED TO 731.5 m (2400 Ft.) SIDELINE

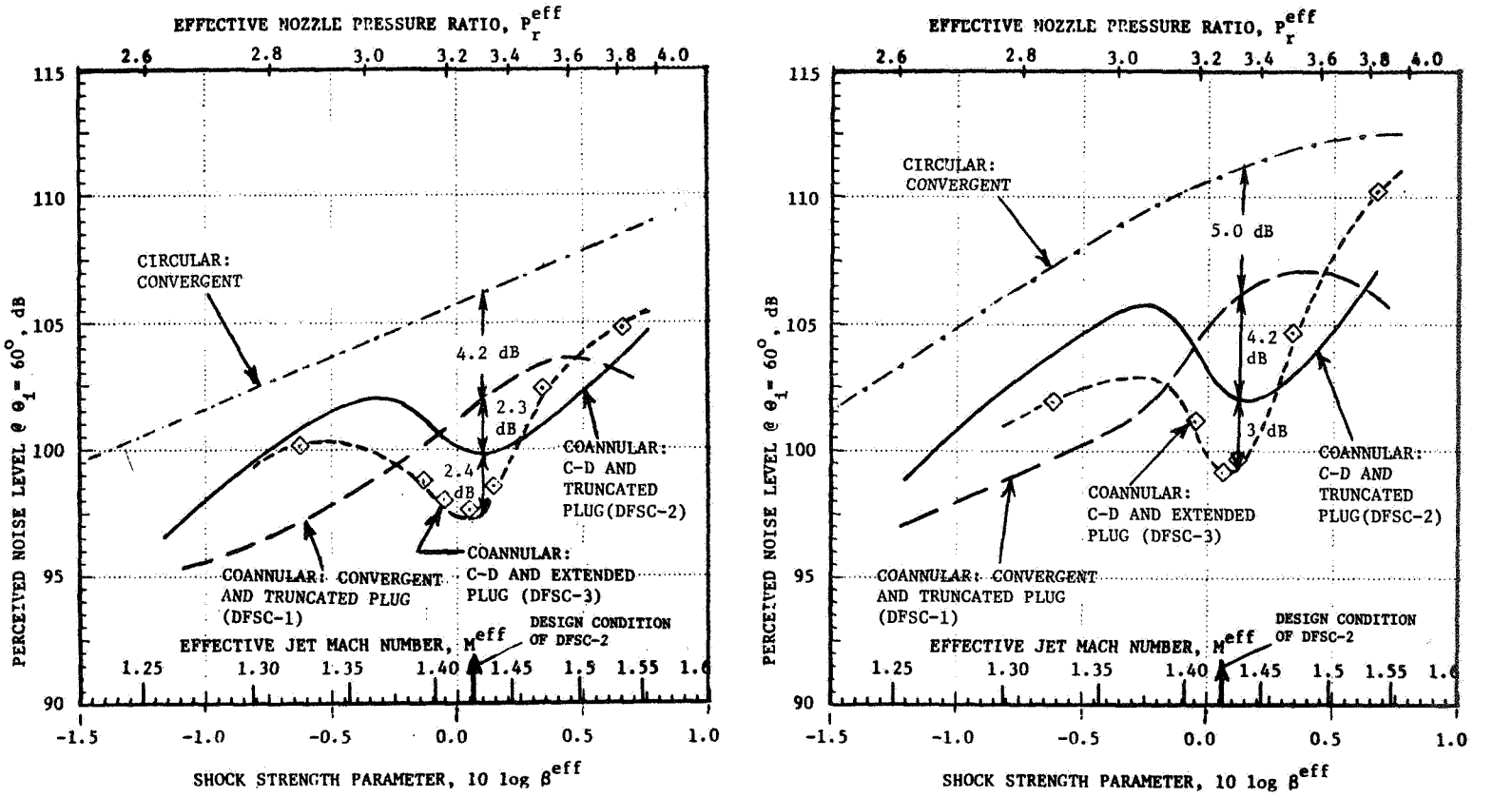

a) STATIC

b) SIMULATED FLIGHT, $V_{ac} \approx 122$m/sec (400 fps)

FIGURE 3-4. EFFECTIVENESS OF EXTENDED PLUG IN SHOCK-CELL NOISE REDUCTION FOR A COANNULAR NOZZLE WITH CONVERGENT-DIVERGENT INNER AND OUTER FLOWPATHS (DFSC-3).

- A maximum reduction of 8.9 dB and 12.2 dB with DFSC-3 at the C-D design conditions, under static and simulated flight conditions, respectively, relative to convergent circular nozzle.

An explanation to this additional shock-cell noise reduction is obtained from a comparison between some of the diagnostic data of configurations DFSC-1, -2 and -3. The diagnostic data are presented in Figures 3-5 through 3-7 and they consist of mean velocity data on and downstream of the plugs, shadowgraphs in the vicinity of the plugs and on-line narrowband acoustic data as measured by the 60° microphone, respectively. The aerodynamic flow conditions for the diagnostic tests match the design conditions of the C-D flowpaths of DFSC-2 and -3.

The laser velocimeter data of Figure 3-5 compare the mean velocity traces obtained along two axial traverses (one on the nozzle centerline and the other on a parallel to the centerline but offset by $R/D_{eq} = 0.5$) and a traverse parallel to the plugs for each of the three configurations. An examination of this figure indicates:

a) Elimination of shock structure on the plug surface of DFSC-2 and DFSC-3 configurations because of the use of convergent-divergent terminations,

b) Not a very significant difference in the mean velocity variations and hence minimal change in the shock-cell structure downstream of the truncated plug of the convergent-divergent DFSC-2 nozzle relative to that of convergent DFSC-1 nozzle data,

c) Elimination of the above-mentioned downstream shock-cell structure of the DFSC-2 nozzle by the use of the extended plug on the DFSC-3 configuration,

d) Observations a) and c), therefore, indicate complete absence of all shock-cells with the unsuppressed convergent-divergent coannular nozzle with extended plug (DFSC-3) operating at its design conditions, and

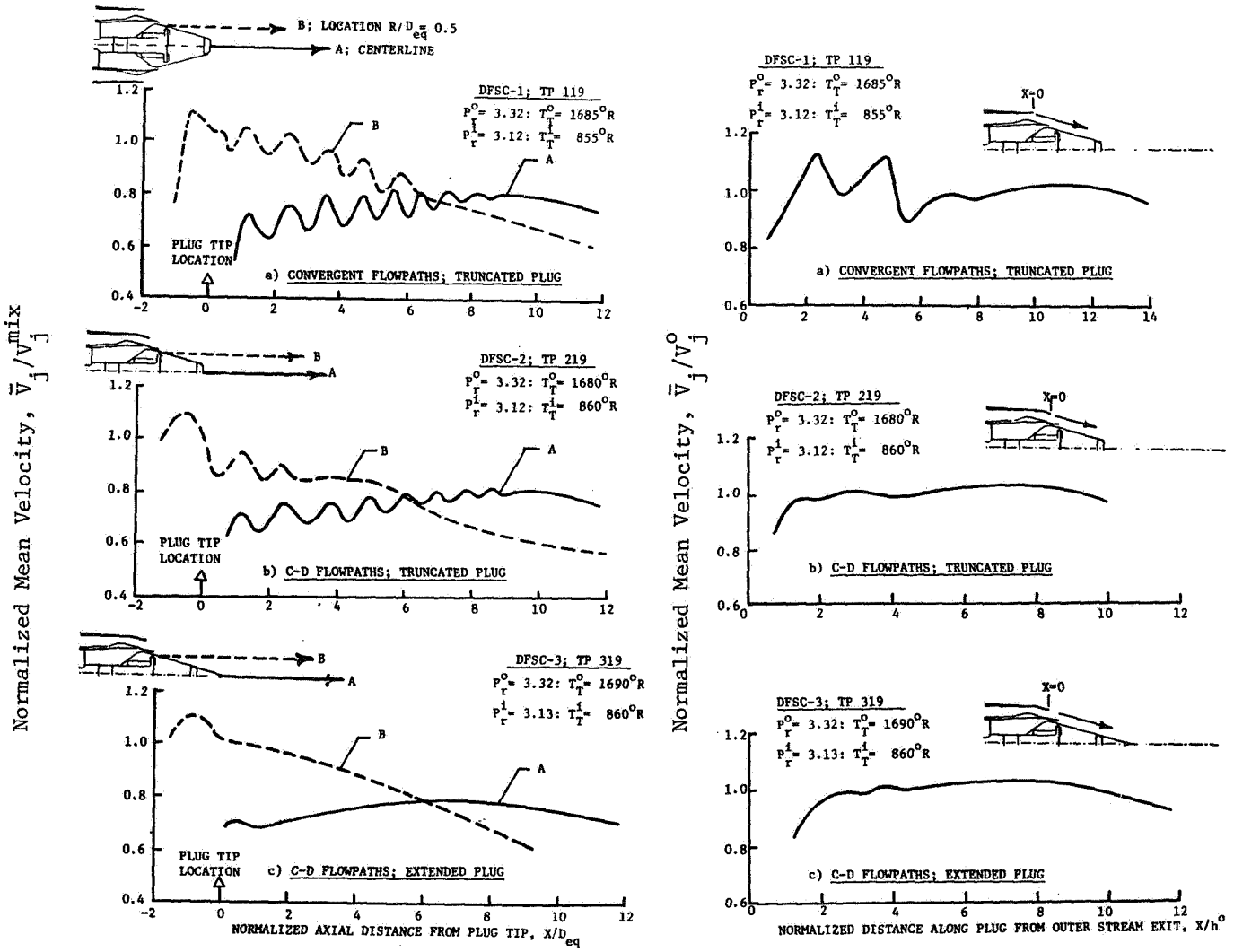

i) Axial Mean Velocity Distributions

ii) Mean Velocity Distributions Parallel to Plug Surface

FIGURE 3-5. COMPARISON OF MEAN VELOCITY DISTRIBUTIONS OF CONVERGENT COANNULAR NOZZLE WITH TRUNCATED PLUG (DFSC-1) WITH THOSE OF CONVERGENT-DIVERGENT COANNULAR NOZZLES WITH TRUNCATED (DFSC-2) AND EXTENDED (DFSC-3) PLUGS (STATIC TEST).

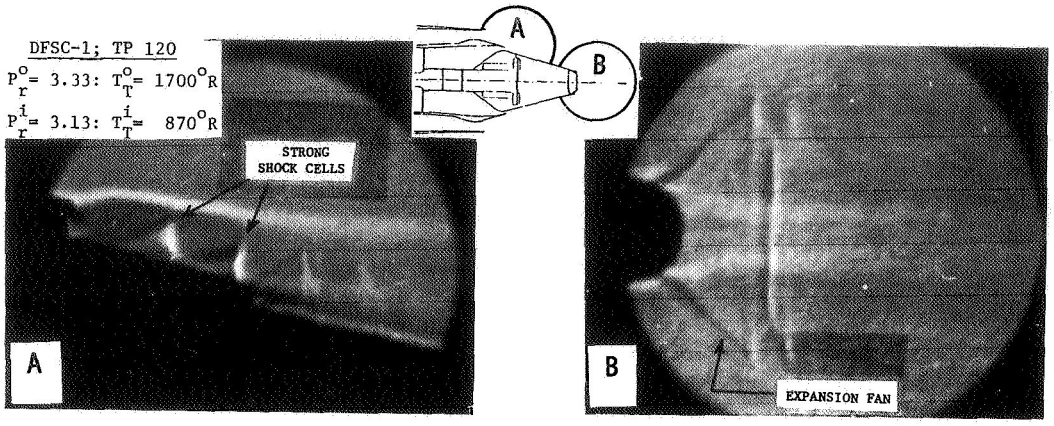

a) CONVERGENT FLOWPATHS; TRUNCATED PLUG

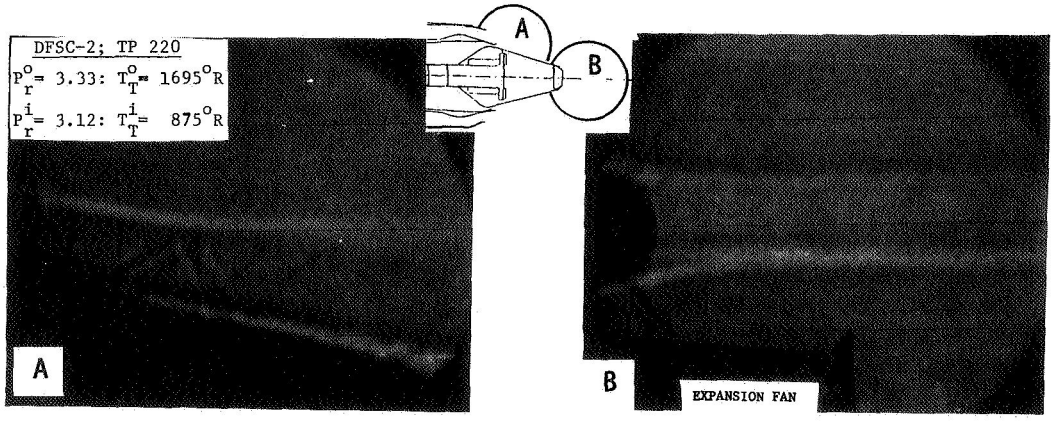

b) C-D FLOWPATHS; TRUNCATED PLUG

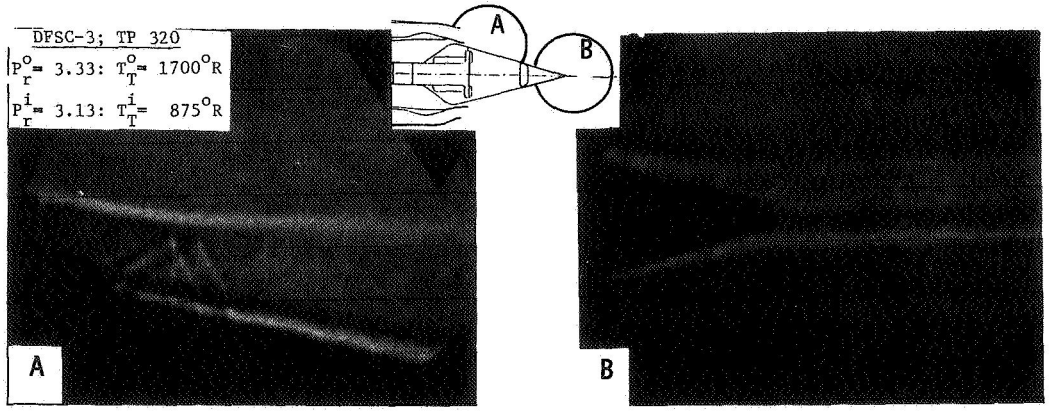

c) C-D FLOWPATHS; EXTENDED PLUG

FIGURE 3-6. COMPARISON OF THE PLUG REGION SHADOWGRAPHS OF CONVERGENT COANNULAR NOZZLE HAVING TRUNCATED PLUG (DFSC-1) WITH THOSE OF C-D COANNULAR NOZZLE HAVING TRUNCATED (DFSC-2) AND EXTENDED (DFSC-3) PLUGS (SIMULATED FLIGHT TEST).

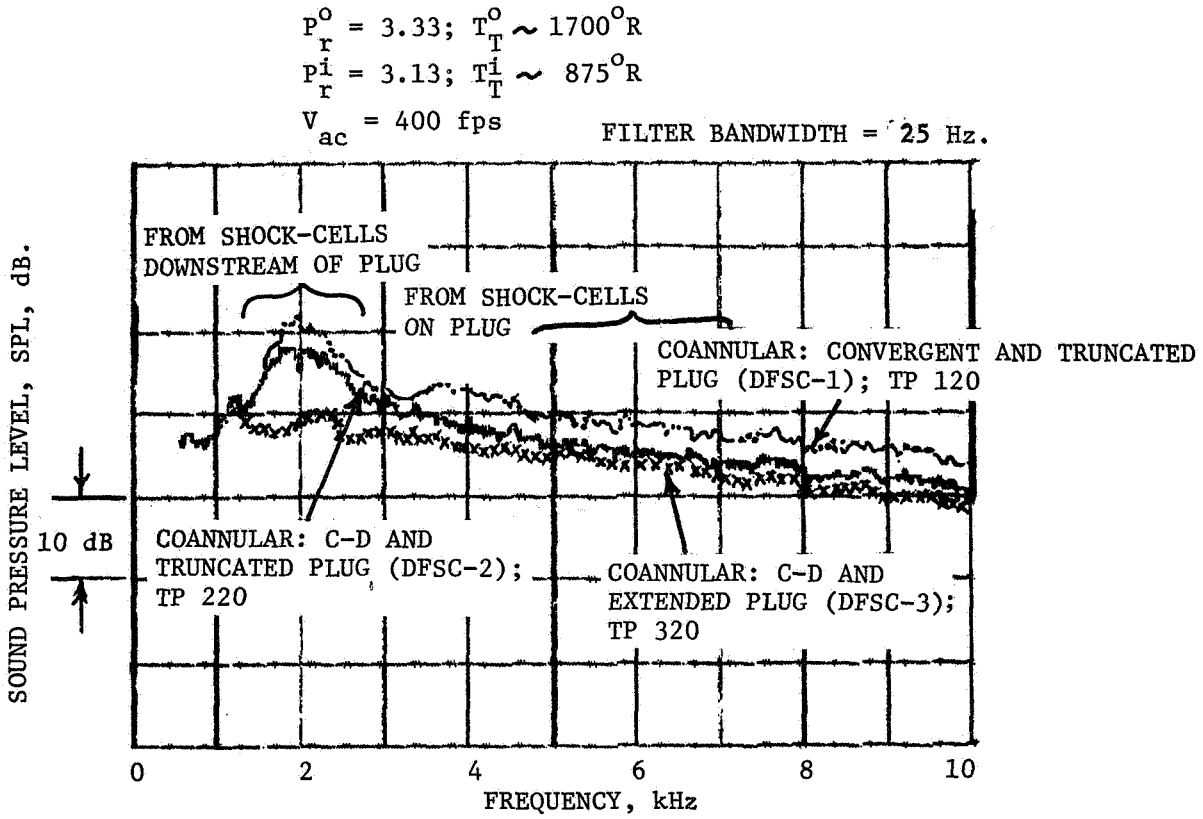

FIGURE 3-7. COMPARISON OF ON-LINE NARROWBAND SPECTRAL DATA OF CONVERGENT COANNULAR NOZZLE WITH TRUNCATED PLUG (DFSC-1) WITH THOSE OF C-D NOZZLES WITH TRUNCATED PLUG (DFSC-2) AND EXTENDED PLUG (DFSC-3). (SIMULATED FLIGHT TESTS)

e) The average shock-cell spacing on the plug and downstream of the plug for the test static case with convergent coannular nozzle (DFSC-1) was determined to be 1.778 inch (2.5 h°) and 5.623 inch (1.08 D_{eq}), respectively. (This data is employed in Section 3.2.4 to calculate the broadband peak frequencies associated with the observed shock-cells.)

The supersonic flow near the plug truncation of DFSC-1 and DFSC-2 nozzles undergoes an expansion resulting in the observed downstream shock structure. This expansion is eliminated by the use of the extended plug. This is confirmed further by the shadowgraphs summarized in Figure 3-6. The presented pictures were taken in the plug region of the three configurations. They confirm the presence/absence of an expansion fan at the tip of the truncated/extended plugs. The shadowgraphs also substantiate the elimination of the shock-cells on the plug of the C-D terminated DFSC-2 and DFSC-3 nozzles that was noted earlier with the LV data of Figure 3-5.

On-line diagnostic narrowband data (filter bandwidth = 25 Hz) of the three unsuppressed coannular configurations at flow conditions that match the design conditions of the C-D terminations are presented in Figure 3-7 to demonstrate the spectral shock-noise benefit of C-D termination and extended plug. An examination of the data, measured by the 60° microphone, indicates:

- Two identifiable broadband peaks in the spectra of the convergent coannular nozzle (DFSC-1),

- Elimination of the higher frequency broadband and minimal changes in the lower frequency broadband due to the C-D termination on the truncated plug configuration (DFSC-2), and

- Significant SPL reduction of the lower frequency broadband peak with the extended plug relative to the truncated plug of the C-D coannular nozzle. Detailed spectral and directivity data comparisons are presented and discussed later in Subsection 3.2.4.

3.2.3 Effect of C-D Flowpaths on Aft Quadrant Noise

Acoustic data measured in the front quadrant were presented in Subsections 3.2.1 and 3.2.2 to demonstrate the region of C-D effectiveness and

to indicate the magnitude of shock noise reduction observed with the tested C-D nozzles (DFSC-2 and -3). In this section, typical aft angle acoustic data measured during the course of those tests are presented and discussed.

The normalized PNL data measured at θ_i = 130° with the coannular plug nozzles having C-D flowpaths on both the outer and inner supersonic streams (DSFC-2 and -3) as a function of mixed jet velocity parameter, 10 log (V_j^{mix}/a_{amb}), are presented in Figure 3-8. The data are compared in this figure with data obtained with the coannular plug nozzle with convergent flowpaths (DFSC-1) on both the outer and inner supersonic streams. An examination of this figure indicates that, over the range of test conditions, the measured data of DFSC-2 and DFSC-3 nozzles agree with each other. This indicates no jet mixing noise benefit due to the extended plug with the C-D coannular nozzle. The data also indicate that, for a given V_j^{mix}, the C-D coannular nozzle resulted in a higher noise level in the aft quadrant than the convergent coannular plug nozzle. This trend in data is opposite to the observation made earlier using the front quadrant data of these configurations wherein the C-D configuration resulted in a shock noise reduction (Figure 3-3). A probable explanation for this trend in aft quadrant data is provided in the next paragraph.

It is to be recalled that the C-D design for the outer and inner nozzles of the C-D coannular plug configuration resulted in lower radius ratios (R_r^o = 0.789, R_r^i = 0.908) compared to those of the coannular plug nozzle having convergent terminations (R_r^o = 0.846, R_r^i = 0.933). It has been shown in Reference 17 that a decrease in the outer stream radius ratio, for a given area ratio of coannular plug nozzles, results in an increase in the aft angle jet noise. This conclusion has been reached in Reference 21 after comparing the measured aft angle data of a series of coannular plug nozzles with convergent terminations and having outer stream radius ratios in the range of 0.853 to 0.902. A similar radius ratio effect has been reported in Reference 17 by comparing the aft angle acoustic data of convergent terminated annular plug nozzles with radius ratios in the range of 0.59 to 0.853. In addition, it is shown in Reference 5 that a decrement in the outer stream radius ratio from say, $(R_r)_1$ to $(R_r)_2$ results in an increment in the high frequency SPL's of the source spectrum by 50 log $[(R_r)_1/(R_r)_2]$. This empirical expression was derived from the measured

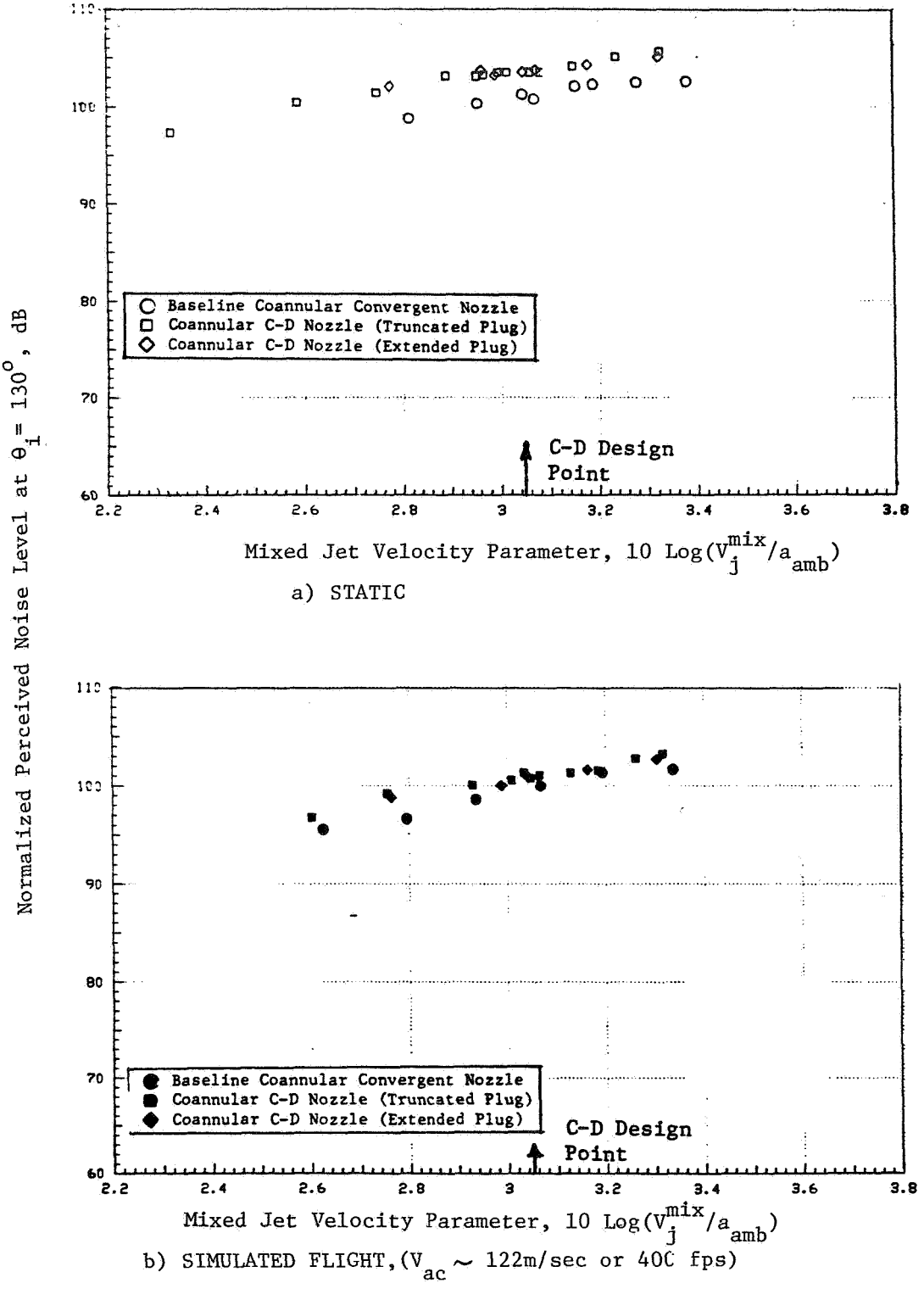

FIGURE 3-8. NORMALIZED PNL_{130} DATA OF CONVERGENT AND C-D UNSUPPRESSED COANNULAR PLUG NOZZLES (DFSC-1,-2 AND -3)

SPL data of a large number of fixed area-ratio coannular plug nozzles with convergent terminations and having different outer stream radius ratios. Based on these experimental observations reported in References 5, 17 and 21, some of the increment observed in the aft angle acoustic data of the C-D coannular plug nozzles relative to the convergent configuration can be attributed to the lower radius ratios of the C-D nozzle.

3.2.4 Directivity and Spectral Data Comparisons Between C-D and Convergent Coannular Plug Nozzles at C-D Design Conditions

In this subsection, static and simulated flight PNL- and OASPL-directivites and front quadrant spectral data of the three unsuppressed coannular nozzles DFSC-1 through DFSC-3 are presented and compared to one another. The aerodynamic flow conditions correspond to the design conditions of the C-D terminations of the DFSC-2 and DFSC-3 nozzles. The diagnostic data for the static test cases were presented earlier in the Subsection 3.2.2.

Static and simulated flight PNL- and OASPL-directivites of the three unsuppressed coannular configurations are presented in Figures 3-9 and 3-10, respectively. The data indicate clearly the front quadrant shock noise reductions obtained with the convergent-divergent terminations (DFSC-2) and the additional benefit measured with the extended plug (DFSC-3). These benefits are more significant in flight relative to the reductions noted under static tests.

Typical static and simulated flight spectral characteristics at $\theta_i = 60°$ are presented in Figure 3-11 for the C-D design conditions of Figures 3-8 and 3-9. As before, the data of C-D coannular nozzles (DFSC-2 and -3) are compared with those of the convergent coannular nozzles (DFSC-1). In order to characterize the spectral frequencies associated with the two shock structures identified on and downstream of plug, shock-cell related broadband peak frequencies for DFSC-1 were calculated using the measured (LV) average shock-cell spacings. The predictions are based on the following equation (Reference 1) for the peak frequency for static tests:

MODEL	TEST PT.	P_r^o	T_T^o, °R	V_j^o, ft/s	P_r^i	T_T^i, °R	V_j^i, ft/s	V_j^{mix}, ft/s	T_T^{mix}, °R	V_{ac}, ft/s
1	119	3.32	1686	2441	3.12	855	1688	2287	1517	0
2	219	3.32	1679	2436	3.12	862	1696	2268	1494	0
3	319	3.32	1688	2442	3.13	861	1696	2272	1500	0

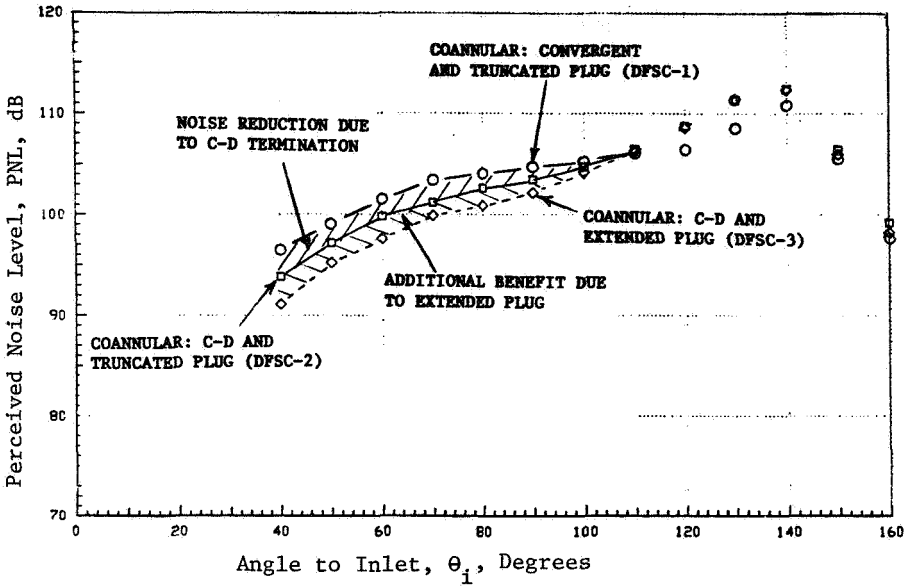

a) PNL - DIRECTIVITY

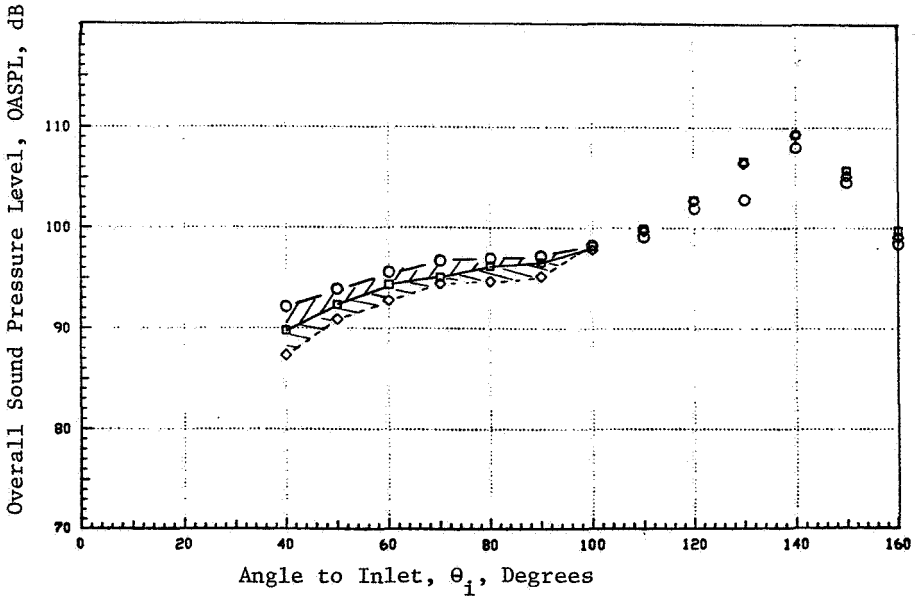

b) OASPL - DIRECTIVITY

FIGURE 3-9. COMPARISON OF PNL- AND OASPL -DIRECTIVITIES OF COANNULAR C-D NOZZLES HAVING TRUNCATED AND EXTENDED PLUGS WOTH THAT OF BASELINE COANNULAR CONVERGENT NOZZLE WITH TRUNCATED PLUG (STATIC).

MODEL	TEST PT.	P_r^o	T_T^o, °R	V_j^o, ft/s	P_r^i	T_T^i, °R	V_j^i, ft/s	V_j^{mix}, ft/s	T_T^{mix}, °R	V_{ac}, ft/s
1	120	3.33	1699	2452	3.13	869	1703	2300	1530	400
2	220	3.33	1695	2450	3.12	873	1705	2282	1509	400
3	320	3.33	1689	2451	3.13	875	1710	2283	1511	400

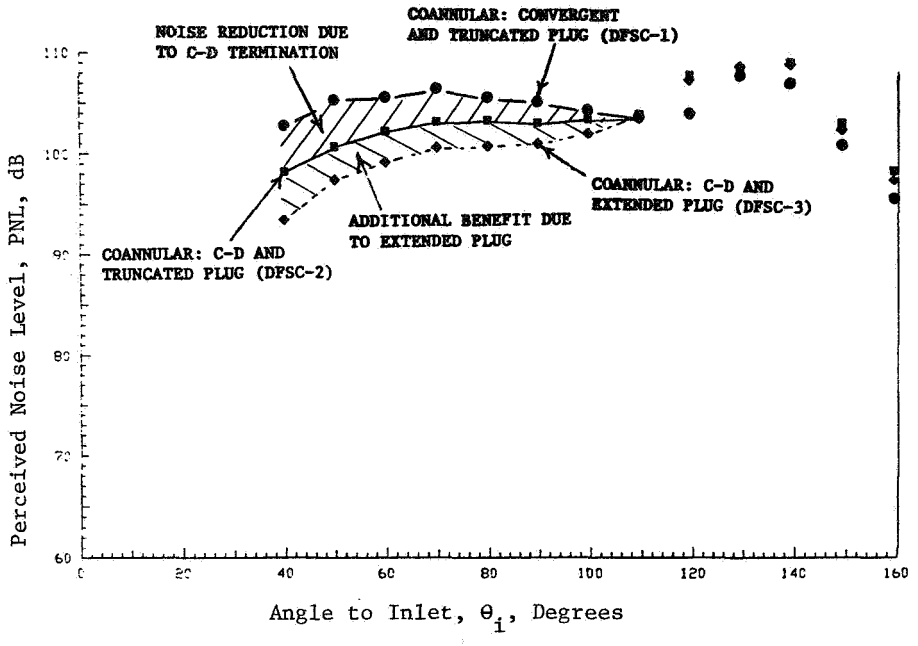

a) PNL - DIRECTIVITY

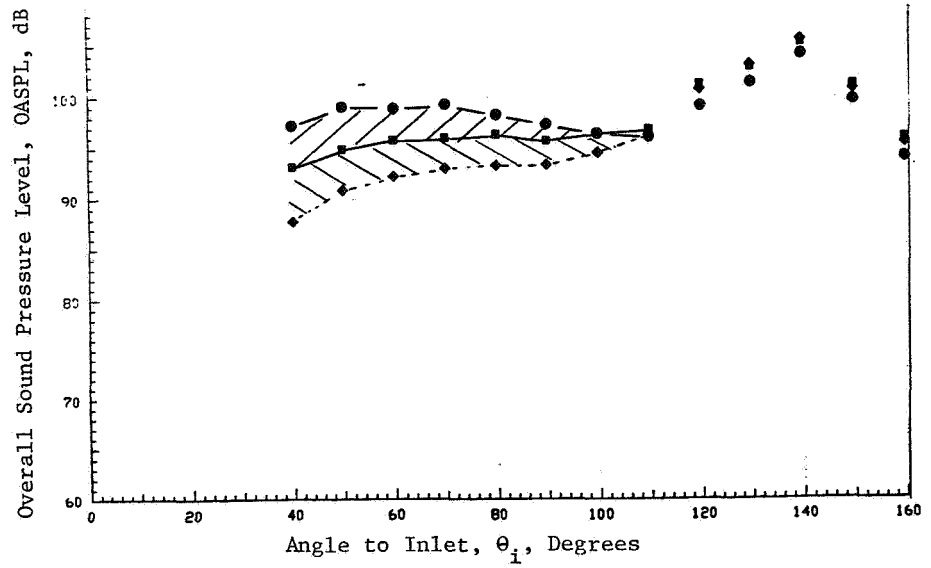

b) OASPL - DIRECTIVITY

FIGURE 3-10. COMPARISON OF PNL- AND OASPL- DIRECTIVITIES OF COANNULAR C-D NOZZLES HAVING TRUNCATED AND EXTENDED PLUGS WITH THAT OF BASELINE COANNULAR CONVERGENT NOZZLE WITH TRUNCATED PLUG (FLIGHT).

DATA SCALED TO TOTAL NOZZLE AREA OF 0.903 m^2 (1400 $In.^2$)
AND EXTRAPOLATED TO 731.5 m (2400 Ft.) SIDELINE

$P_r^o \approx 3.33$; $T_T^o \sim 1700^oR$

$P_r^i \approx 3.13$; $T_T^i \sim 875^oR$

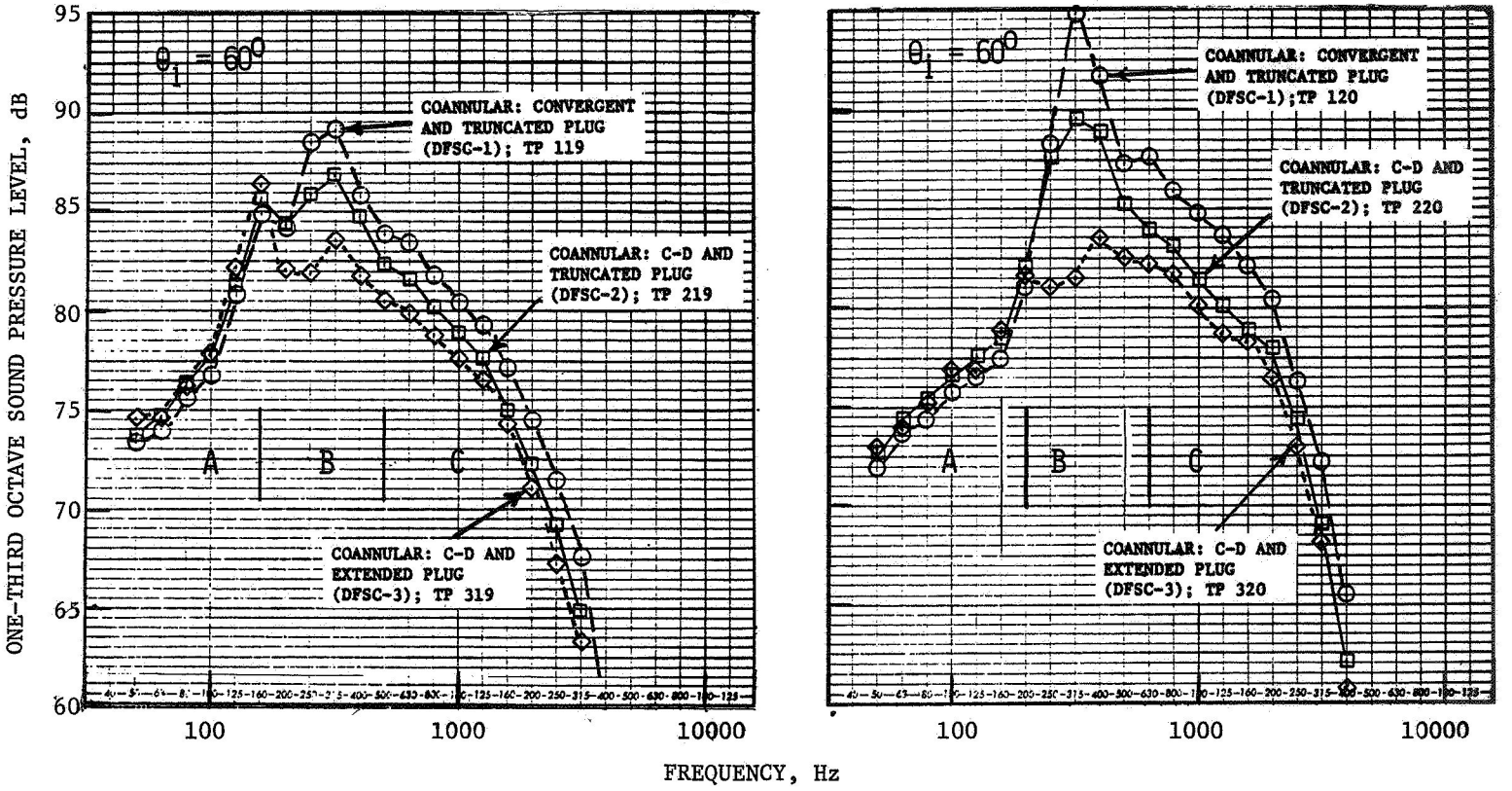

a) STATIC

b) SIMULATED FLIGHT, $V_{ac} \simeq 122$m/sec (400 fps)

FIGURE 3.11. TYPICAL FRONT QUADRANT SPECTRAL COMPARISON OF COANNULAR C-D NOZZLES HAVING TRUNCATED AND EXTENDED PLUGS WITH THAT OF BASELINE COANNULAR NOZZLE WITH TRUNCATED PLUG.

$$\left(f_p\right)_{static} = \frac{U_c}{L_{avg}\,(1 + M_c\,\mathrm{Cos}\,\Theta_i)} \qquad (3.1)$$

In the above equation, U_c is the convection velocity of the eddy which is taken as equal to 0.65 x jet velocity V_j, $M_c = U_c/a_{amb}$ with a_{amb} being the ambient speed of sound and Θ_i is the observer angle with respect to upstream axis. The jet velocity associated with shock-cells on the plug and downstream of the plug were taken to be V_j^o and V_j^{mix}, respectively. The shock broadband peak frequency corresponding to a flight Mach number of M_{ac} was calculated by applying the Doppler shift to the predicted static data as follows:

$$\left(f_p\right)_{flight} = \frac{\left(f_p\right)_{static}}{1 - M_{ac}\,\mathrm{Cos}\,\Theta_i} \qquad (3.2)$$

The needed average shock-cell spacings on and downstream of the plug, as determined from the static LV measurements at the matching aerodynamic flow conditions, were found to be 1.778 (2.5 x h°) inch and 5.623 (1.08 D_{eq}) inch, respectively. The static broadband peak frequencies associated with noise due to shock-cells on and downstream of the plug of the model scale nozzle are predicted then to be 6,270 Hz and 1,910 Hz, respectively. These frequencies fall within the 1/3-octave-bands having center frequencies of 6,300 Hz and 2,000 Hz. When extrapolated to the typical product size of 1,400 sq. in., the shock-cell associated broadband peak frequencies correspond to 1/3-octave-bands having center frequencies of 800 Hz and 250 Hz (nine 1/3-OB shifts) for the static case, and 1,000 Hz and 315 Hz (one 1/3-octave shift relative to the static case) for the flight case, respectively. Using the above information, three distinct frequency ranges designated as A, B and C are indicated in Figure 3-11. They are:

- Region - A: the low frequency spectra of f $\leq$ 160 Hz ($\leq$ 200 Hz for flight),

- Region - B: the middle frequency spectra of 160 Hz < f < 500 Hz that contains the broadband peak frequency of noise associated with shock-cells downstream of plug (200 Hz < f < 630 Hz for flight), and

- Region - C: the high frequency spectra of f > 500 Hz (f > 630 Hz for flight) that contains the broadband peak frequency of noise associated with shock-cells on the plug.

The spectra of Region - A is jet mixing noise related and hence no significant differences are observed between the data of the three configurations operating at identical flow conditions. Comparison of the spectra among the three configurations in Region - B indicates that the C-D coannular nozzle with extended plug (DFSC-3) has the lowest level. Since this is the region dominated by noise due to downstream shock-cells, this observation in spectral data is in accordance with the LV measurements that indicated almost complete elimination of shock-cells downstream of the extended plug of DFSC-3. The level reduction noted with the data of the C-D coannular nozzle with truncated plug (DFSC-2) compared to that of DFSC-1 is due to a relatively weakened shock-cell structure downstream of the plug [see LV data in Figure 3-5i] of DFSC-2. Finally, in Region - C, a significant reduction in the spectral levels is noted with the data of DFSC-2 compared to the data of DFSC-1. Since this is the region governed mainly by the noise due to shock-cells on the plug, this observation from spectral data conforms the earlier noted LV measurement that indicated elimination of shock-cells on the plug by the convergent-divergent termination of DFSC-2 (see LV data in Figure 3-5ii). As the difference between the C-D configurations DFSC-2 and -3 is only in their plug terminations and thus both have identical flows without shock-cells on the plug, no significant differences are noted between their spectra in this region. Similar observations can be made from spectral comparisons between the data of the three configurations at other front quadrant locations. A set of data at Θ_i = 40°, 50° and 60° are presented in Figures 3-12 and 3-13, for static and simulated flight cases, respectively.

All of these observations from the front quadrant spectral data of DFSC-1, -2 and -3 configurations are valid for both static and simulated flight cases at the matching C-D design conditions. However, due to the front

	MODEL	TEST PT.	P_r^o	T_T^o, °R	V_j^o, ft/s	P_r^i	T_T^i, °R	V_j^i, ft/s	V_j^{mix} ft/s	T_T^{mix}, °R	V_{ac}, ft/s
○	1	119	3.32	1686	2441	3.12	855	1688	2287	1517	0
□	2	219	3.32	1679	2436	3.12	862	1696	2268	1494	0
◇	3	319	3.32	1688	2442	3.13	861	1696	2272	1500	0

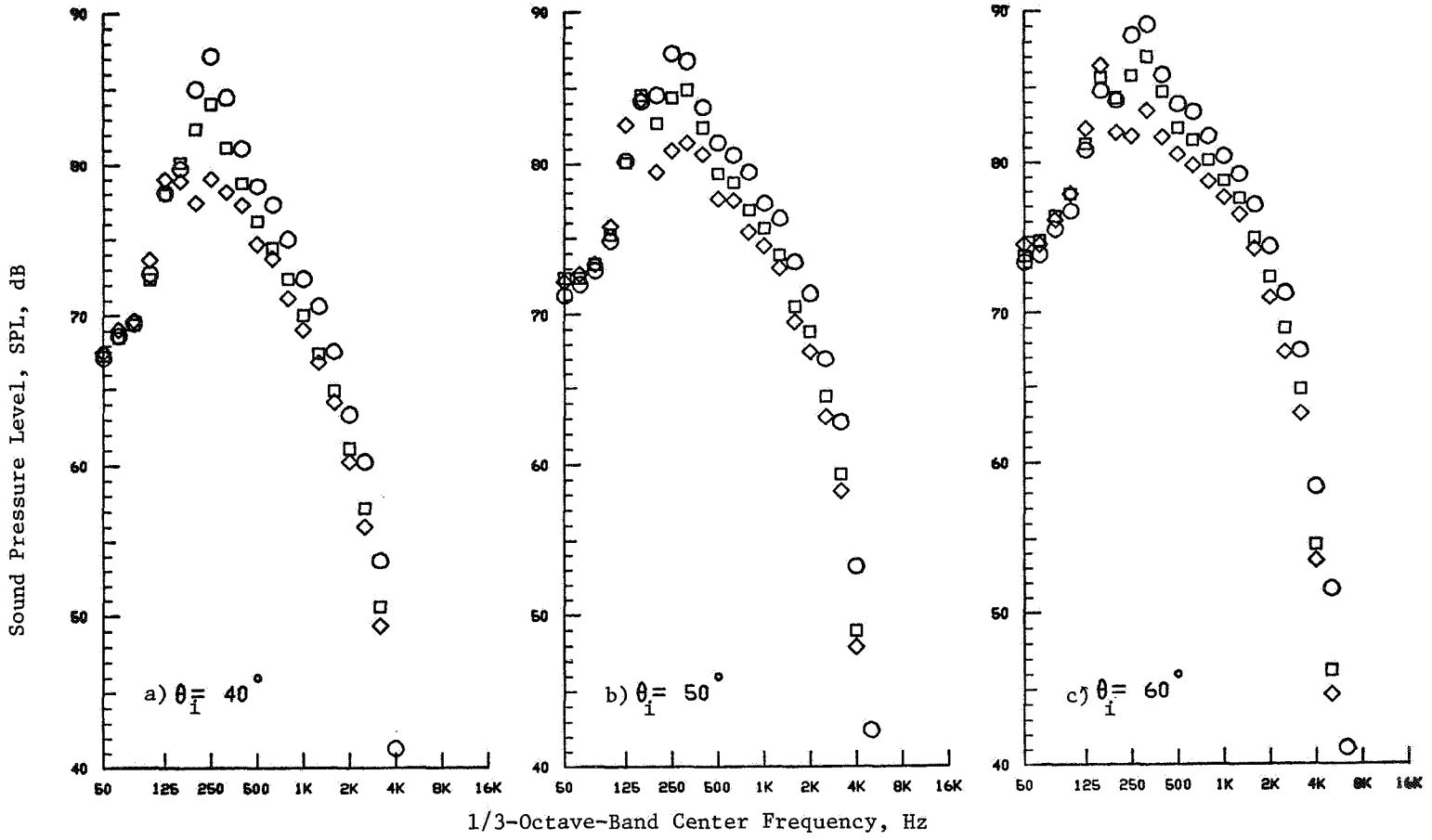

FIGURE 3-12. SPECTRAL COMPARISON AT THREE FRONT QUADRANT LOCATIONS BETWEEN COANNULAR C-D NOZZLES HAVING TRUNCATED AND EXTENDED PLUGS WITH THAT OF BASELINE COANNULAR NOZZLE WITH TRUNCATED PLUG (STATIC).

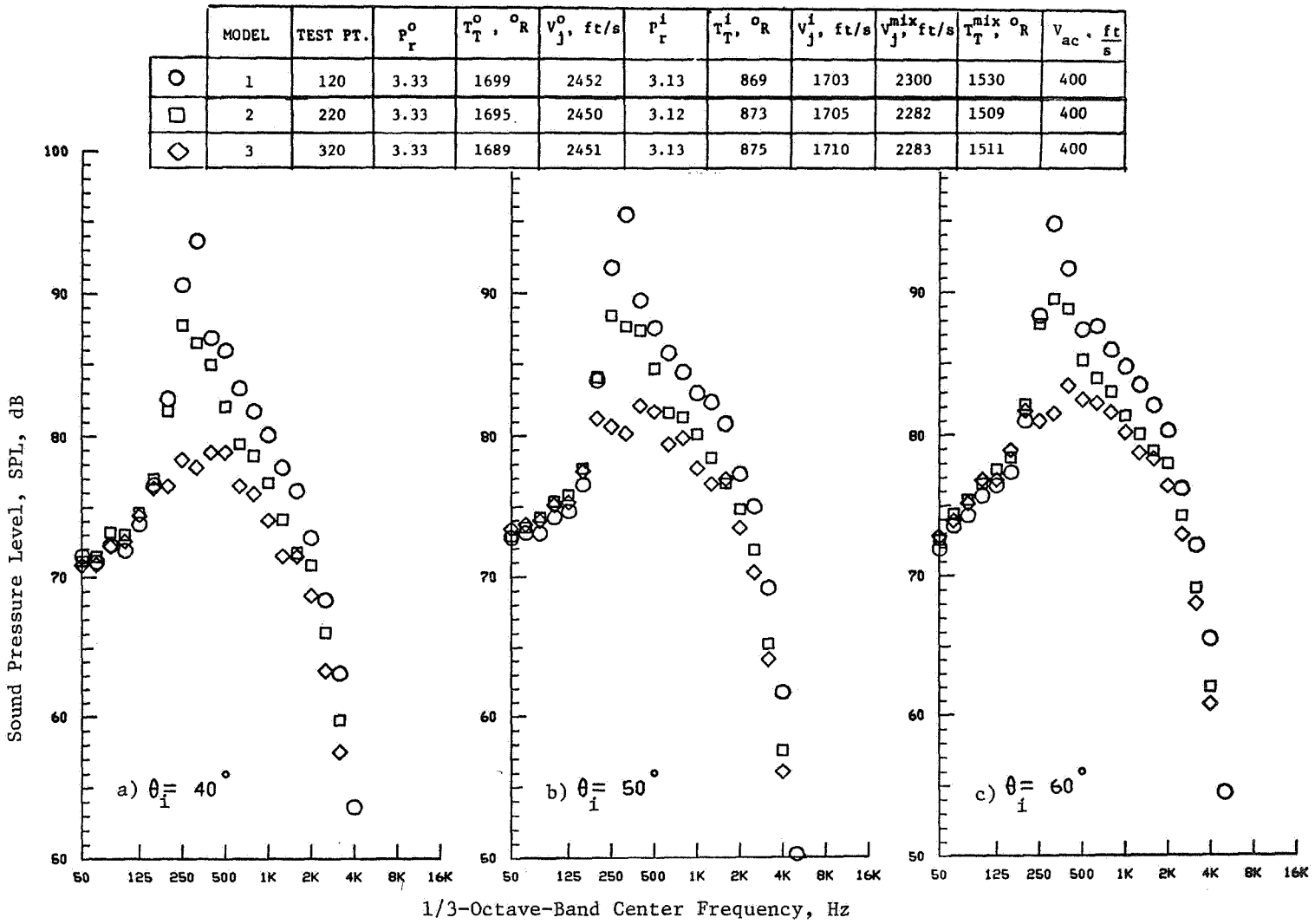

FIGURE 3-13. SPECTRAL COMPARISON AT THREE FRONT QUADRANT LOCATIONS BETWEEN COANNULAR C-D NOZZLES HAVING TRUNCATED AND EXTENDED PLUGS WITH THAT OF BASELINE COANNULAR NOZZLE WITH TRUNCATED PLUG (FLIGHT).

quadrant flight amplification of shock-cell noise, the spectral levels in middle and high frequency ranges B and C of shock-cell infested DFSC-1 and -2 in flight are higher that their corresponding values under static conditions. A discussion on the effect of flight is presented in the next subsection.

3.2.5 Effect of Flight on Convergent and C-D Coannular Nozzle Front-Quadrant Noise at C-D Design Conditions

The static measured acoustic and LV data of Configurations DFSC-1 through DFSC-3 are compared in this subsection to their respective simulated flight (V_{ac} = 122 m/sec or 400 fps) results. The data in Figure 3-14 first summarizes the effect of flight on measured PNL data of convergent circular (References 5, 6 and 7), convergent coannular nozzle with truncated plug (DFSC-1) and C-D coannular nozzle with truncated (DFSC-2) and extended (DFSC-3) plugs at a typical forward quadrant angle of Θ_i = 60°. The data are plotted as a function of effective shock strength parameter β^{eff}. An examination of this figure indicates that the amount of amplification of the front quadrant static data of convergent circular nozzle due to flight is larger than that of the three coannular nozzles, for a given operating condition.

The static measured PNL- and OASPL-directivities of DFSC-1 through DFSC-3 at C-D design conditions are compared to their corresponding simulated flight data in Figures 3-15 and 3-16, respectively. The data indicate that the forward quadrant PNL amplifications due to the simulated flight are 4.1, 2.5, and 1.6 dB and the forward quadrant OASPL amplifications are 3.3, 1.6 and -0.4 dB (at Θ_i = 60°) for configurations DFSC-1 through -3, respectively. The minimal forward quadrant flight amplification noted with the C-D coannular nozzle with extended plug (DFSC-3) is indicative of the elimination of significant shock-cell structure with this configuration. This fact has been ascertained earlier from independent analyses of the static diagnostic results (Figures 3-5 and 3-6). The static LV data of Figure 3-5 are repeated in Figure 3-17 and compared with the corresponding LV data obtained under simulated flight condition. Unlike the effect of free-jet on convergent circular nozzle shock-cell structure (References 5 and 7), the shock-cell pattern of DFSC-1 is not stretched significantly by the free-jet.

DATA SCALED TO TOTAL NOZZLE AREA OF 0.903 m^2 (1400 $In.^2$)
AND EXTRAPOLATED TO 731.5 m (2400 Ft.) SIDELINE

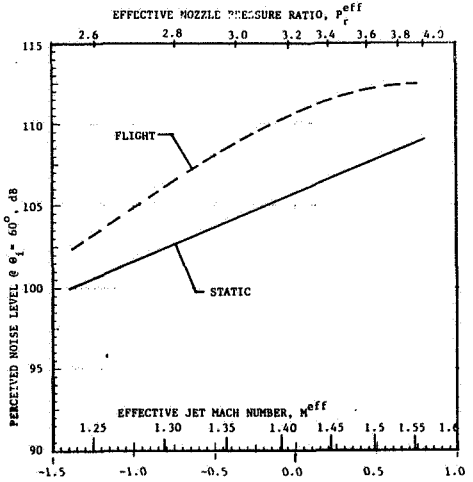

a) CIRCULAR: CONVERGENT

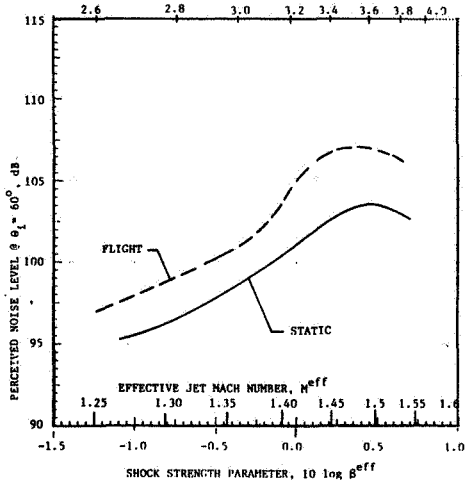

b) COANNULAR: CONVERGENT AND TRUNCATED PLUG (DFSC-1)

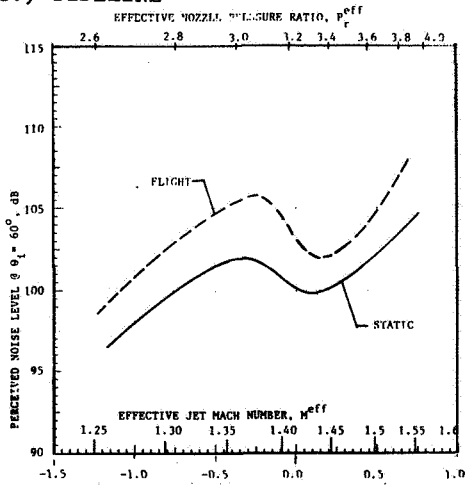

c) COANNULAR: C-D AND TRUNCATED PLUG (DFSC-2)

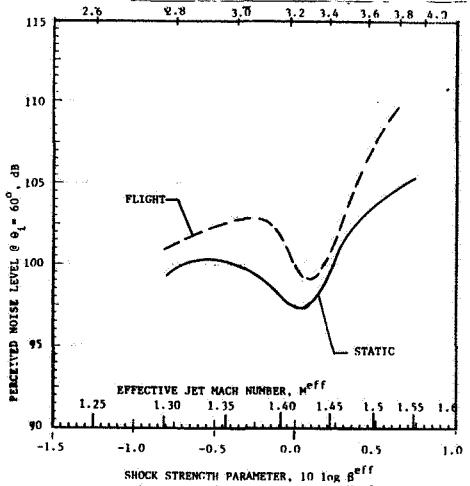

d) COANNULAR: C-D AND EXTENDED PLUG (DFSC-3)

FIGURE 3-14. EFFECT OF SIMULATED FLIGHT ON FRONT QUADRANT PNL DATA OF CONVERGENT CIRCULAR, COANNULAR WITH TRUNCATED PLUG, AND C-D COANNULAR WITH TRUNCATED AND EXTENDED PLUG NOZZLES.

(See Figures 3-12 and 3-13 for Aerodynamic Conditions)

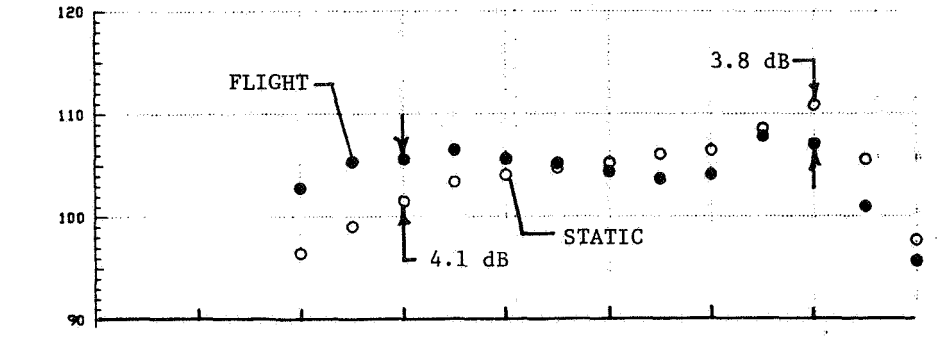

a) COANNULAR: CONVERGENT AND TRUNCATED PLUG (DFSC-1)

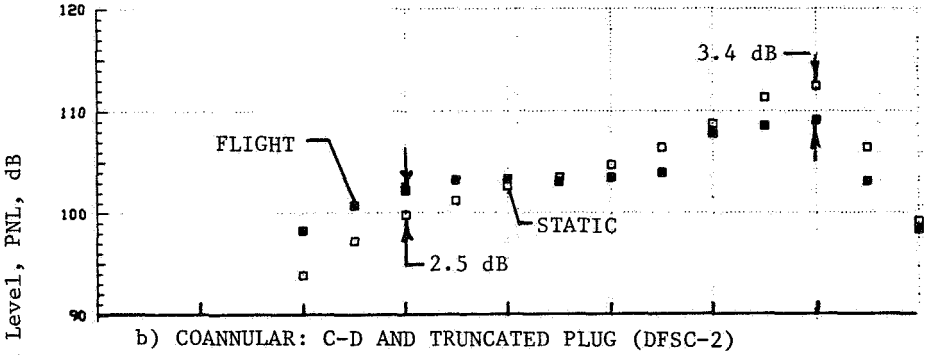

b) COANNULAR: C-D AND TRUNCATED PLUG (DFSC-2)

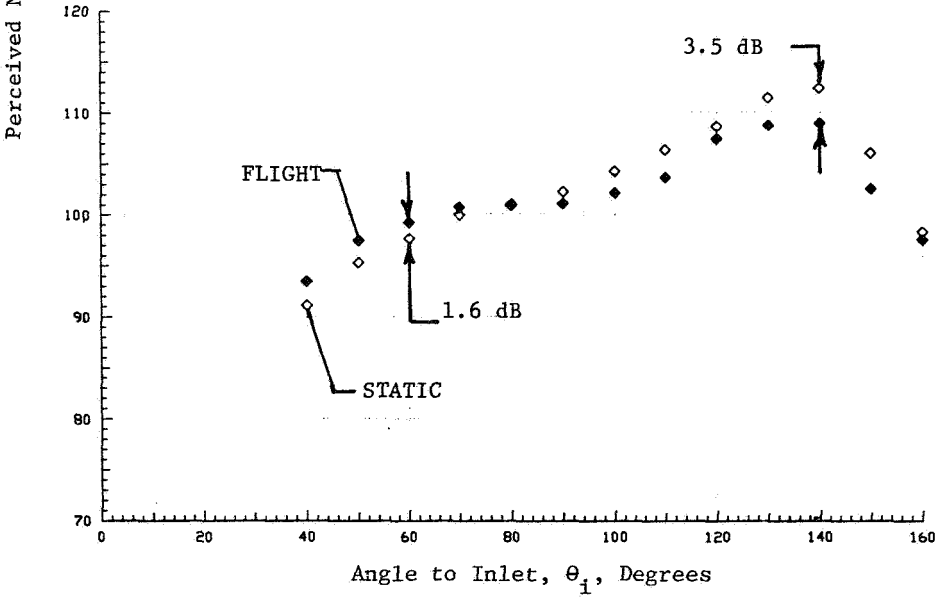

c) COANNULAR: C-D AND EXTENDED PLUG (DFSC-3)

FIGURE 3-15. EFFECT OF SIMULATED FLIGHT ON PNL DIRECTIVITY OF CONVERGENT AND C-D COANNULAR PLUG NOZZLES AT C-D DESIGN CONDITIONS.

(See Figures 3-12 and 3-13 for Aerodynamic Conditions)

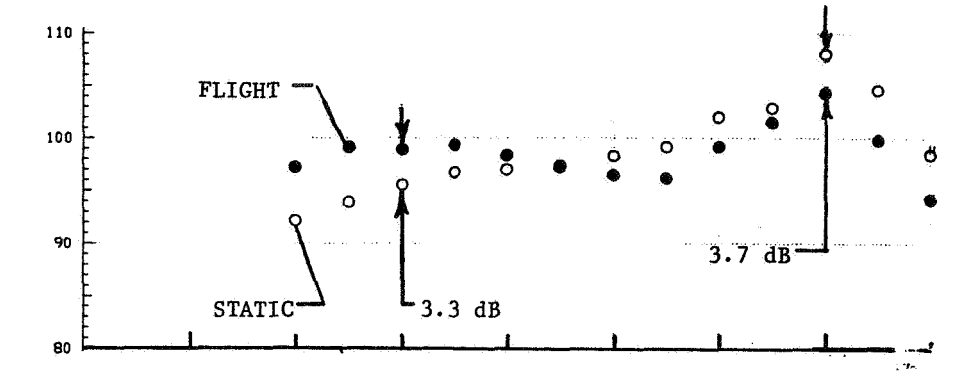

a) COANNULAR: CONVERGENT AND TRUNCATED PLUG (DFSC-1)

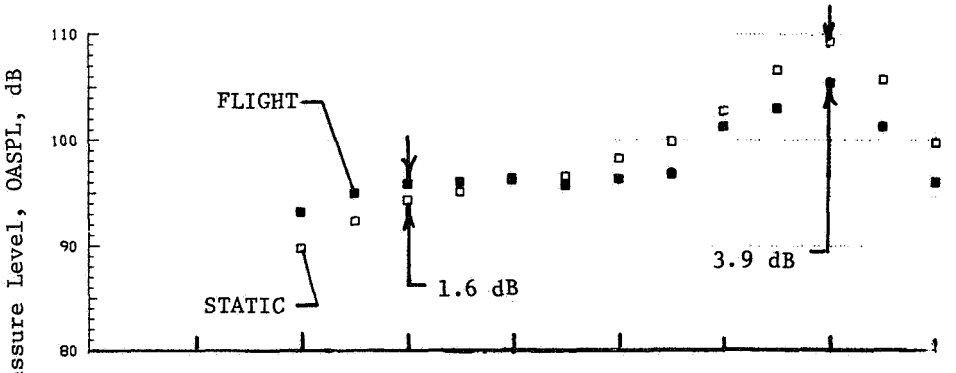

b) COANNULAR: C-D AND TRUNCATED PLUG (DFSC-2)

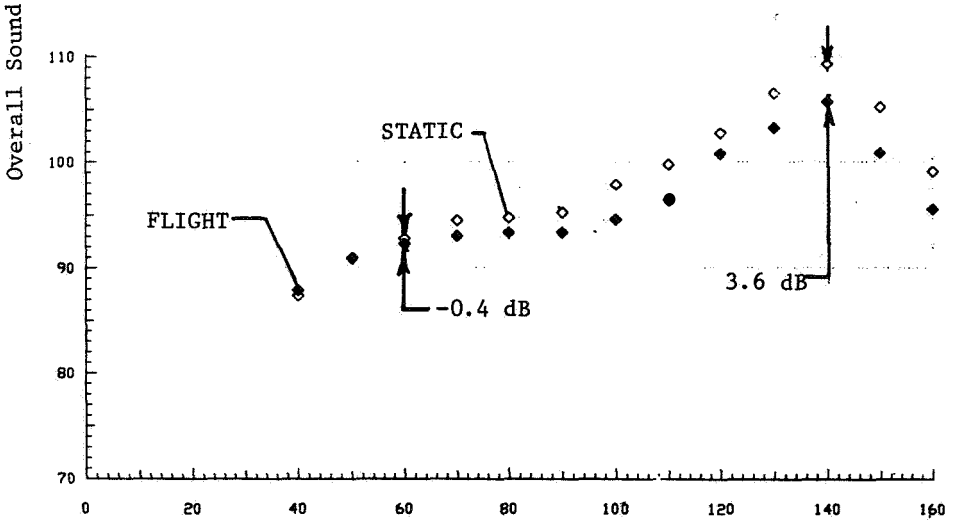

c) COANNULAR: C-D AND EXTENDED PLUG (DFSC-3)

FIGURE 3-16. EFFECT OF SIMULATED FLIGHT ON OASPL DIRECTIVITY OF CONVERGENT AND C-D COANNULAR PLUG NOZZLES AT C-D DESIGN CONDITIONS.

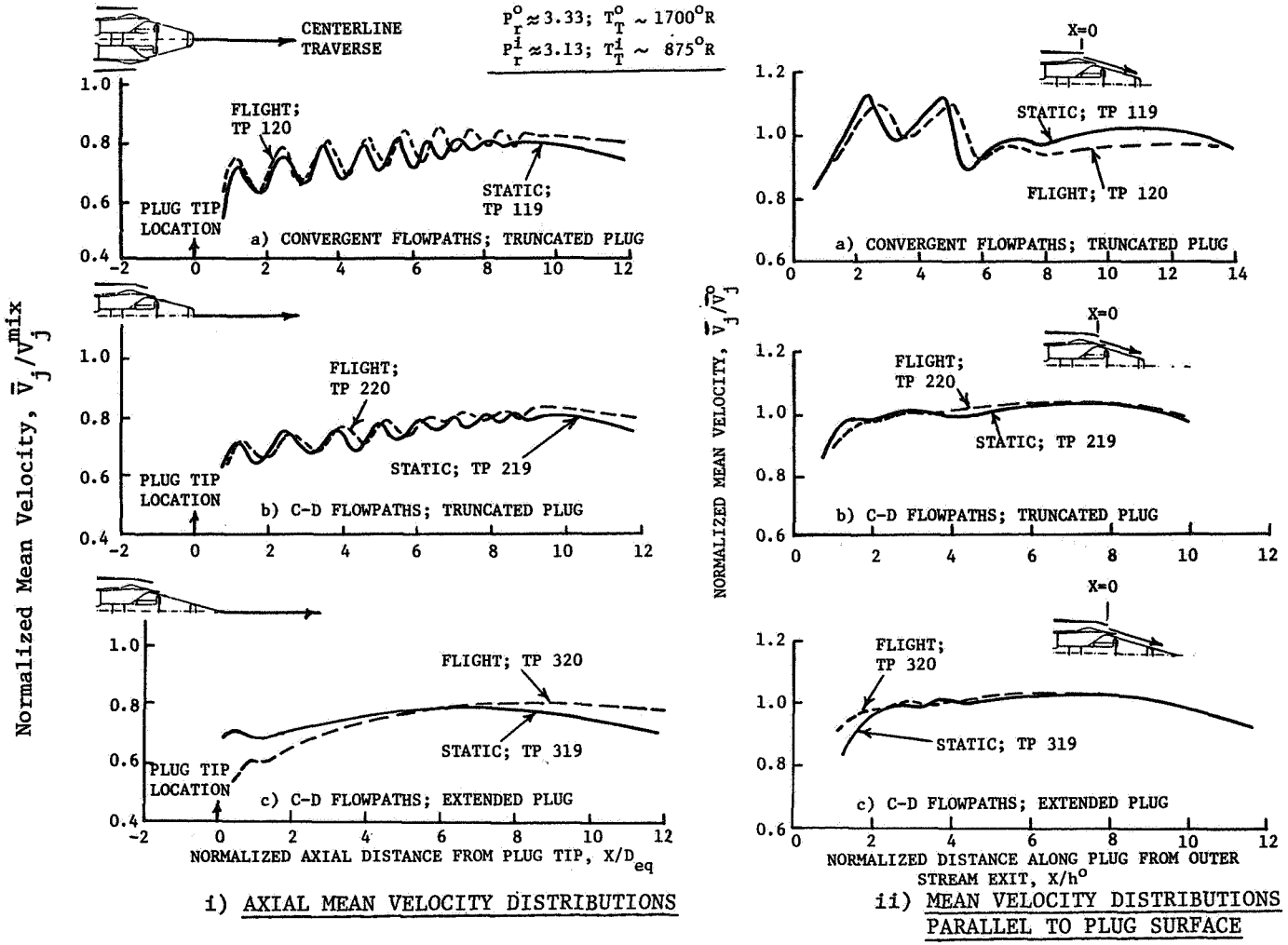

FIGURE 3-17. COMPARISON OF STATIC WITH SIMULATED FLIGHT MEAN VELOCITY DISTRIBUTIONS OF CONVERGENT COANNULAR NOZZLE WITH TRUNCATED PLUG (DFSC-1), CONVERGENT-DIVERGENT COANNULAR NOZZLES WITH TRUNCATED (DFSC-2) AND EXTENDED (DFSC-3) PLUGS.

The directivity data of Figures 3-15 and 3-16 indicate also the expected aft quadrant jet noise suppression due to the simulated flight. For example, at the peak aft angle of Θ_i = 140°, the jet noise reduction in PNL and OASPL for each of the three configurations is noted to be approximately equal to 3.6 dB. Minimal changes in the static data when compared to flight data are observed in the neighborhood of Θ_i = 90°.

Static to flight comparison of the front quadrant spectral data at Θ_i = 40°, 50° and 60° for the three configurations DFSC-1 through DFSC-3 are presented in Figures 3-18 through 3-20, respectively. An examination of these figures at, for example, Θ_i = 60° indicates that maximum and minimum amplification in the frequency ranges of interest (Ranges B and C) occurs with the convergent coannular nozzle (DFSC-1) and C-D coannular nozzle with extended plug (DFSC-3), respectively. This is made clear in Figure 3-21 by plotting the differences between the flight and static SPL levels against frequency at a typical forward quadrant angle of Θ_i = 60° for the three configurations at the C-D design point. Positive SPL differences indicate flight amplification. An examination of this figure indicates that

- Except in the very high frequency range, shock-cell noise in Region-C of C-D coannular nozzle with truncated plug (DFSC-2) is significantly less amplified indicating the benefit of C-D terminations in the elimination of shock-cells on the plug.

- Shock-cell noise of C-D coannular nozzle with extended plug has additional decrease in amplification in Region-B that is associated with shock-cells downstream of plug indicating the benefit of the extended plug.

3.3 ALTERNATIVE APPROACHES TO REDUCTION OF SHOCK-CELL NOISE OF CONVERGENT COANNULAR PLUG NOZZLES

The data presented under subsection 3.2 demonstrate the substantial shock-cell noise reduction that could be obtained by proper C-D design of the flowpaths along with the added benefit that could be achieved by an extended plug. In order to determine whether a somewhat similar additional benefit

MODEL	TEST PT.	P_r^o	T_T^o, °R	V_j^o, ft/s	P_r^i	T_T^i, °R	V_j^i, ft/s	V_j^{mix}, ft/s	T_T^{mix}, °R	V_{ac}, ft/s
1	119	3.32	1686	2441	3.12	855	1688	2287	1517	0
1	120	3.33	1699	2452	3.13	869	1703	2300	1530	400

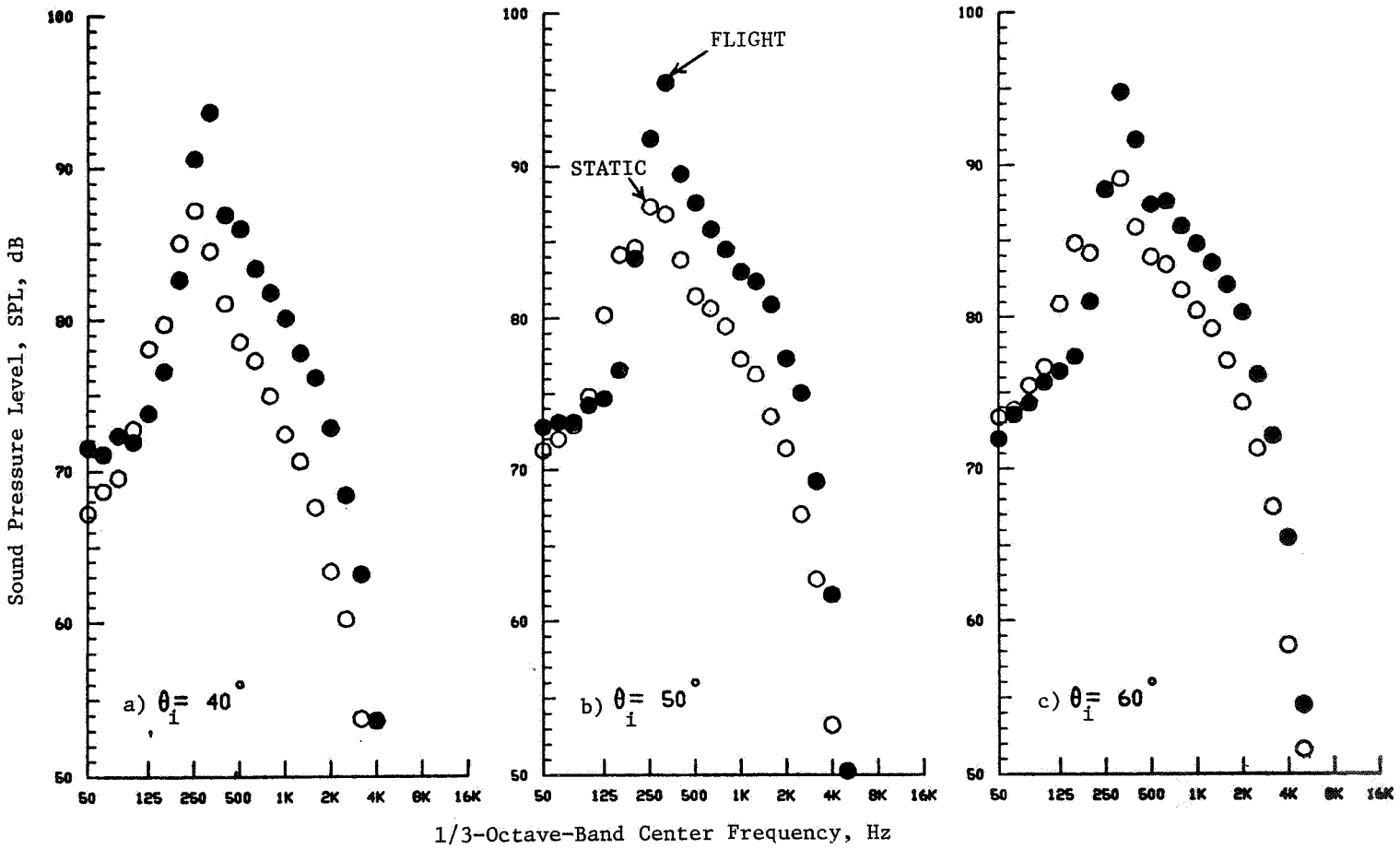

FIGURE 3-18. EFFECT OF SIMULATED FLIGHT ON FRONT QUADRANT SPECTRAL DATA OF CONVERGENT COANNULAR NOZZLE WITH TRUNCATED PLUG (DFSC-1).

MODEL	TEST PT.	P_r^o	T_T^o, °R	V_j^o, ft/s	P_r^i	T_T^i, °R	V_j^i, ft/s	V_j^{mix}, ft/s	T_T^{mix}, °R	V_{ac}, ft/s
2	219	3.32	1679	2436	3.12	862	1696	2268	1494	0
2	220	3.33	1695	2450	3.12	873	1705	2282	1509	400

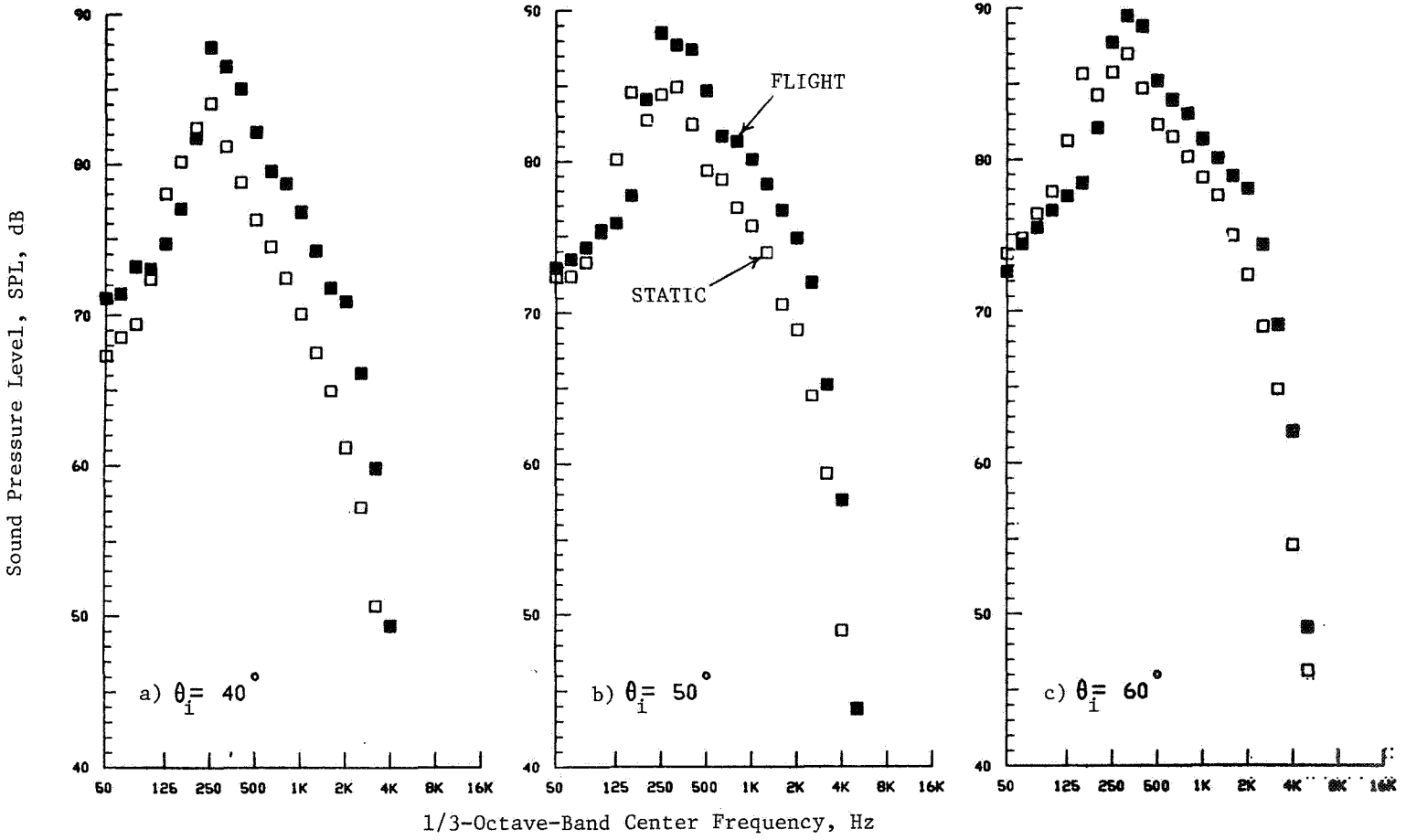

FIGURE 3-19. EFFECT OF SIMULATED FLIGHT ON FRONT QUADRANT SPECTRAL DATA OF C-D COANNULAR NOZZLE WITH TRUNCATED PLUG (DFSC-2).

MODEL	TEST PT.	P_r^o	T_T^o, °R	V_j^o, ft/s	P_r^i	T_T^i, °R	V_j^i, ft/s	V_j^{mix}, ft/s	T_T^{mix}, °R	V_{ac}, ft/s
3	319	3.32	1688	2442	3.13	861	1696	2272	1500	0
3	320	3.33	1698	2451	3.13	875	1710	2283	1511	400

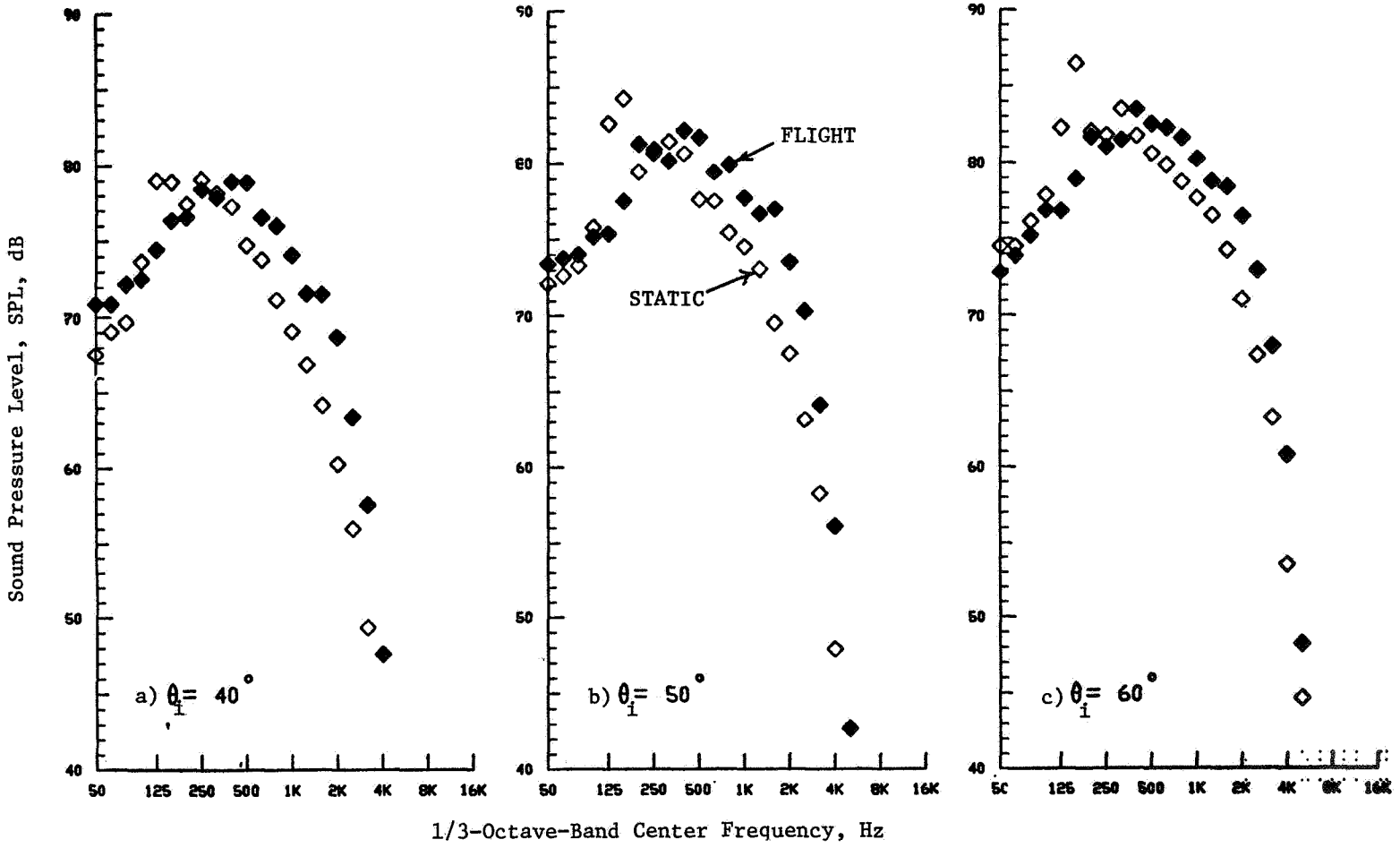

FIGURE 3-20. EFFECT OF SIMULATED FLIGHT ON FRONT QUADRANT SPECTRAL DATA OF C-D COANNULAR NOZZLE WITH EXTENDED PLUG (DFSC-3).

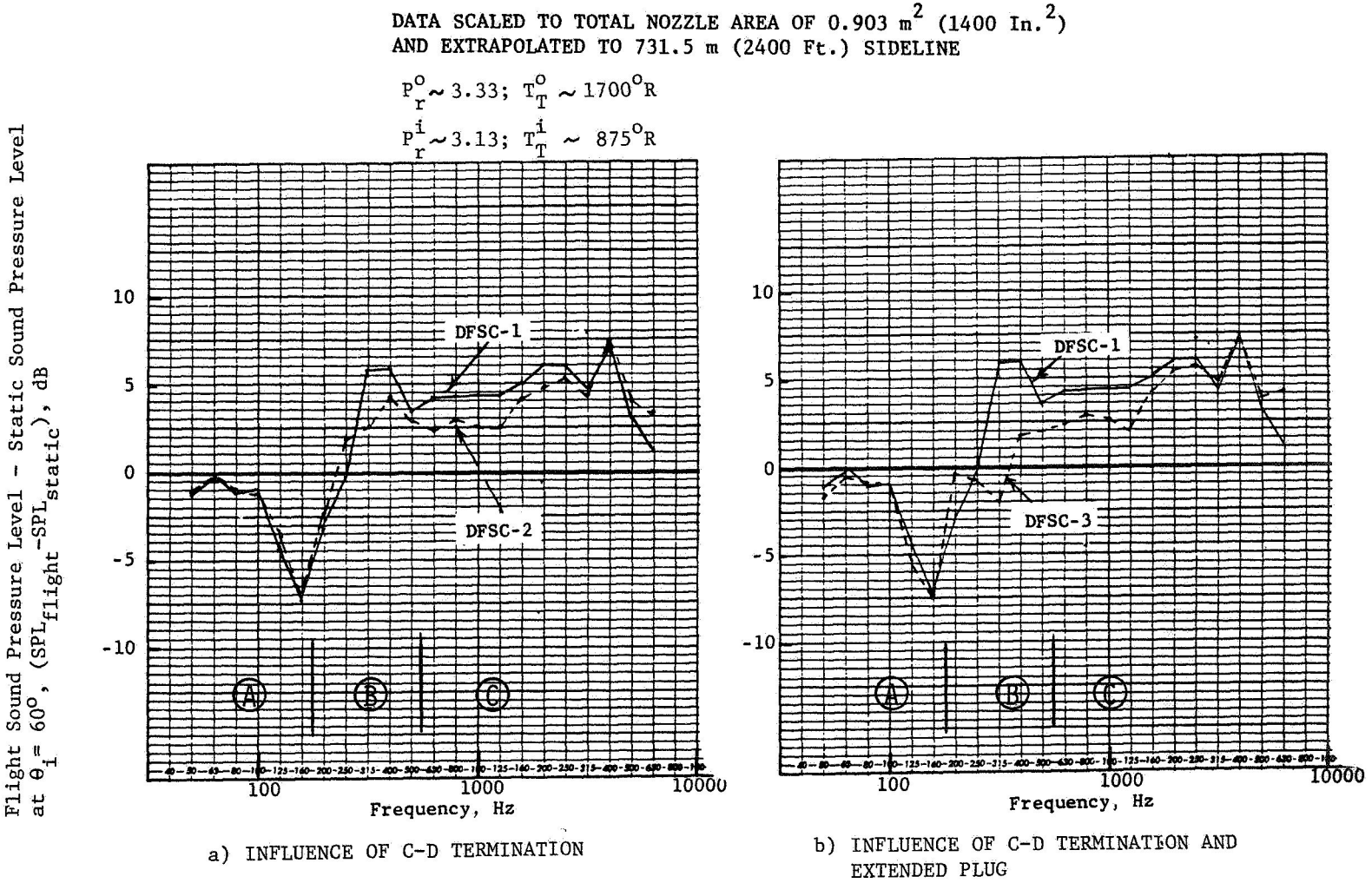

a) INFLUENCE OF C-D TERMINATION

b) INFLUENCE OF C-D TERMINATION AND EXTENDED PLUG

FIGURE 3-21. FLIGHT AMPLIFICATION (ATTENUATION) COMPARISON BETWEEN BASELINE COANNULAR CONVERGENT PLUG NOZZLE (DFSC-1) AND COANNULAR C-D NOZZLE WITH TRUNCATED PLUG (DFSC-2) AND EXTENDED PLUG (DFSC-3) AT C-D DESIGN CONDITIONS.

could be obtained by an extended sharp plug on a convergent coannular nozzle, tests were conducted with DFSC-1 nozzle having its truncated plug replaced by an extended plug. This configuration, referred to as DFSC-6, was tested (as per Table 2-IX) over an outer stream pressure ratio range of $2.5 < P_r^o < 4.0$ for two fixed inner flow conditions, namely, (a) supersonic stream at $P_r^i \simeq 3.13$ and $T_T^i \simeq 850°R$ and (b) subsonic stream at $P_r^i \simeq 1.81$ and $T_T^i \sim 1300°R$. The acoustic and limited diagnostic data obtained under the above conditions are presented in this subsection and compared with those of the convergent coannular nozzle with truncated plug (DFSC-1).

3.3.1 Effect of the Extended Plug With Convergent Coannular Nozzle

The static and simulated flight measured front quadrant PNL data of the DFSC-6 configuration having a fixed supersonic inner stream are presented in Figure 3.22. For values of $\beta^{eff} > 1.0$ (i.e., $\log \beta^{eff} > 0$ and $P_r^o < 3.33$), the static data indicates a small front quadrant, acoustic benefit with the extended plug relative to the truncated plug on the convergent coannular nozzle.

Normalized PNL data at $\Theta_i = 130°$ obtained with the extended plug nozzle (DFSC-6) are compared in Figure 3-23 with those of the truncated plug nozzle to determine the effect of the extended plug on jet mixing noise. The data indicates that, for the test conditions, the truncated/extended nature of plug had no effect on the jet mixing noise under both static and simulated flight conditions.

3.3.2 Benefit of Subsonic Inner Stream in Shock-Cell Noise Reduction

In most of the acoustic tests conducted in this program, the aerodynamic flow conditions were such that both outer and inner flow speeds were supersonic and corresponded to typical AST/VCE cycle conditions. During an earlier investigation (Reference 5), very limited acoustic and diagnostic tests were conducted with a coannular nozzle, similar to DFSC-1, but operating with a supersonic outer and a subsonic inner stream. The data, summarized in Figure 3-24, indicates a significant acoustic benefit with a subsonic inner

DATA SCALED TO TOTAL NOZZLE AREA OF 0.903 m^2 (1400 $In.^2$)
AND EXTRAPOLATED TO 731.5 m (2400 Ft.) SIDELINE

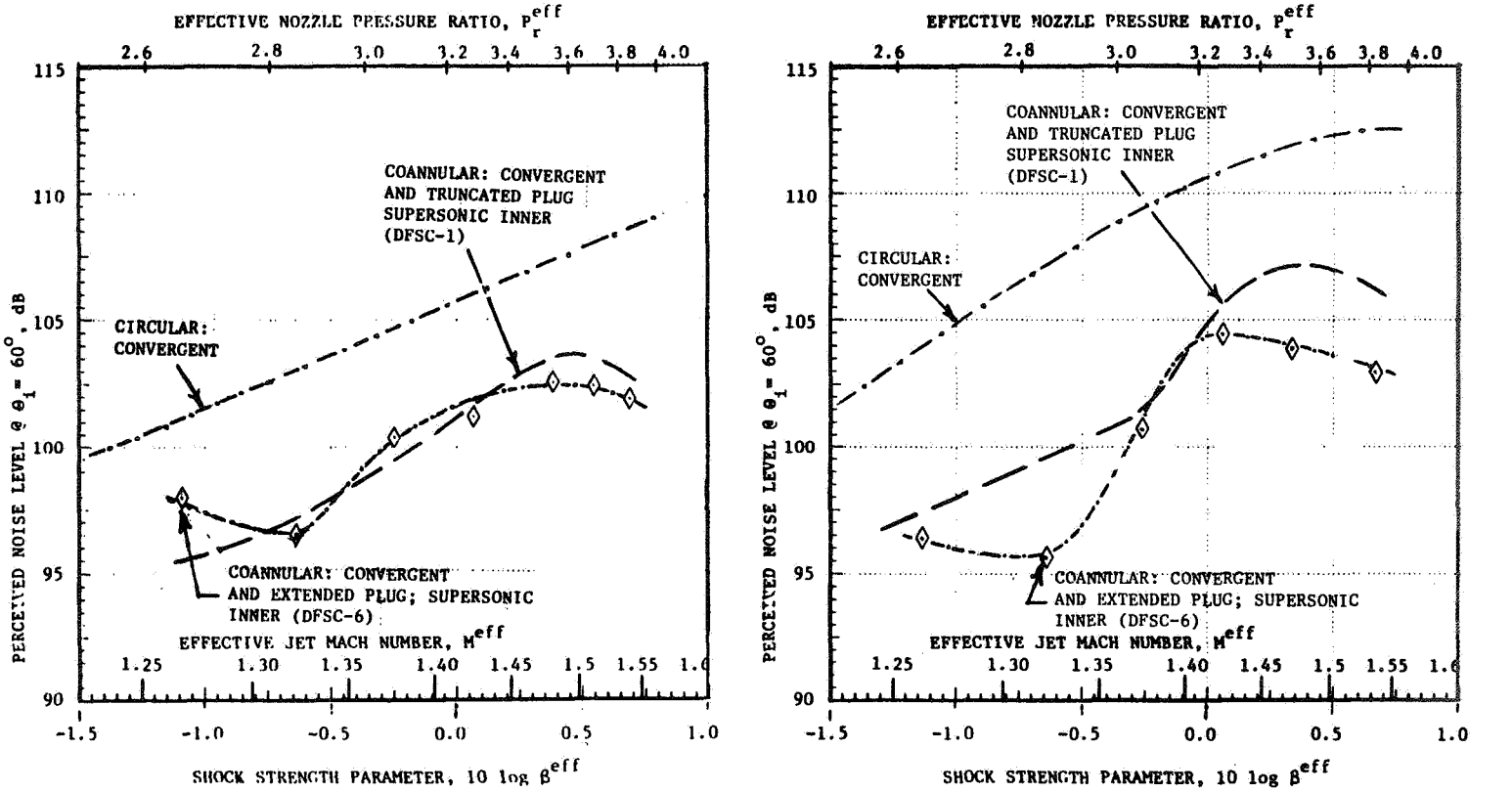

FIGURE 3-22. COMPARISON OF FORWARD QUADRANT PERCEVED NOISE LEVEL DATA OF CONVERGENT COANNULAR NOZZLES WITH TRUNCATED (DFSC-1) AND EXTENDED (DFSC-6) PLUGS.

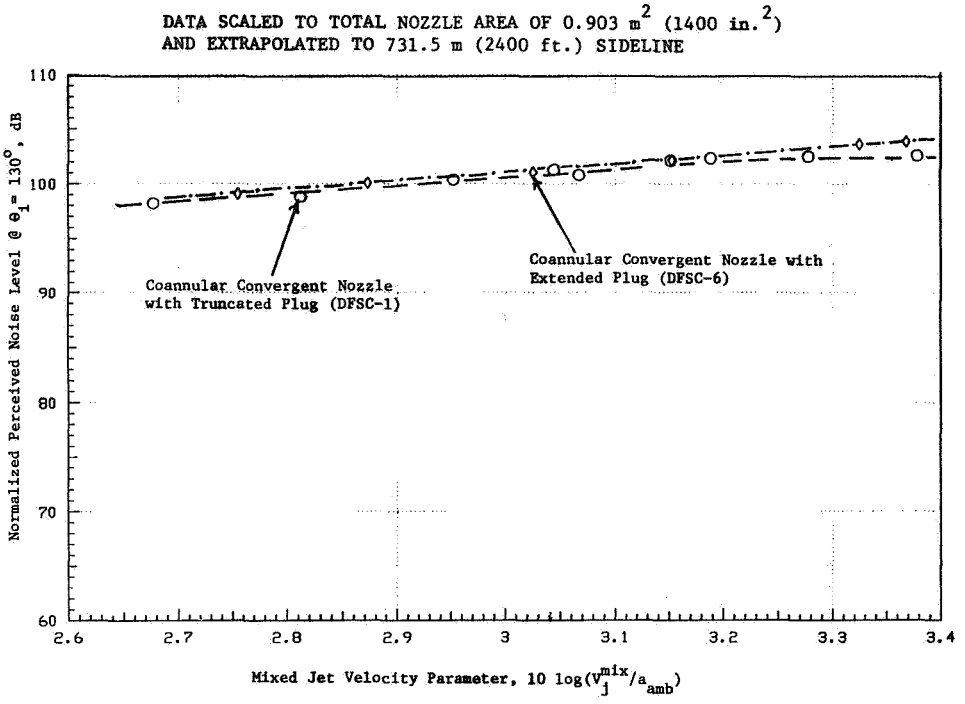

a) STATIC

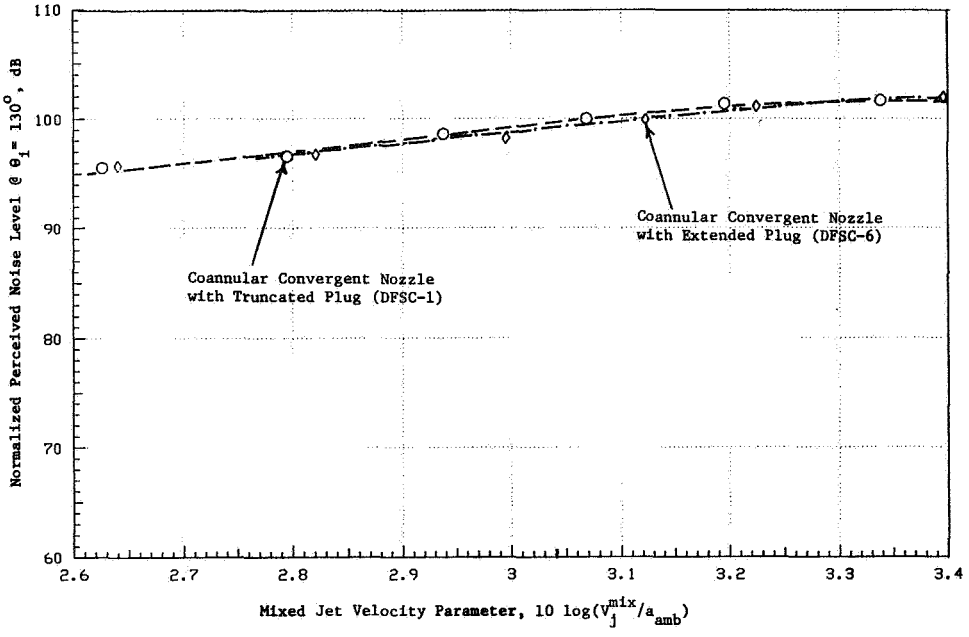

b) SIMULATED FLIGHT (V_{ac} = 122 mps or 400 fps)

FIGURE 3-23. EFFECT OF EXTENDED PLUG ON AFT QUADRANT DATA OF CONVERGENT COANNULAR NOZZLE.

Test Point	V^o fps	P_r^o	T_T^o	V^i fps	P_r^i	T_T^i °R	V^{mix} fps	P_r^{mix}	T_T^{mix} °R
204	2555	3.78	1693	1644	3.21	794	2378	3.60	1521
216	2563	3.78	1708	1109	1.57	854	2416	3.42	1621

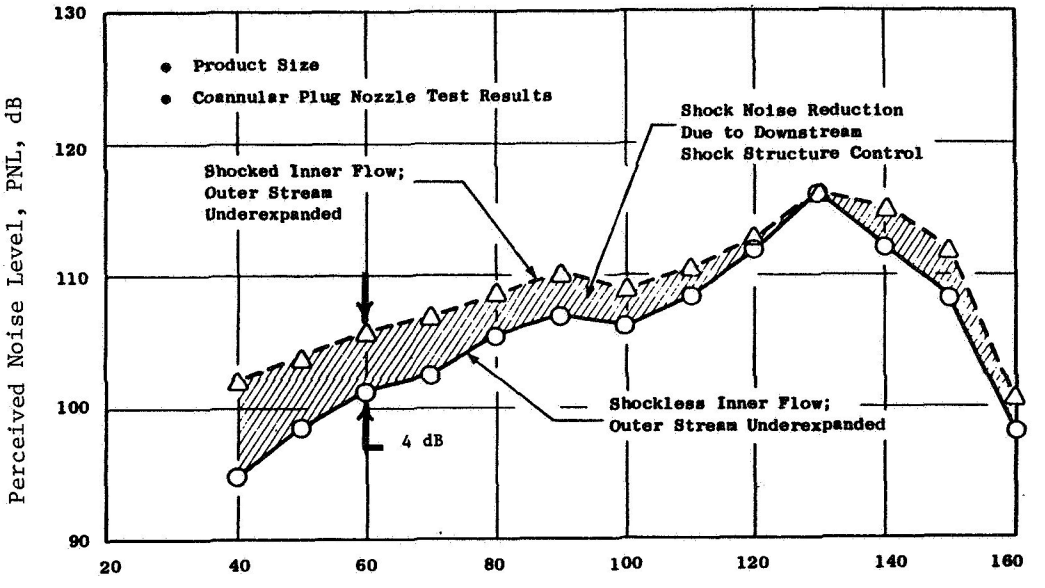

a) PNL - DIRECTIVITY

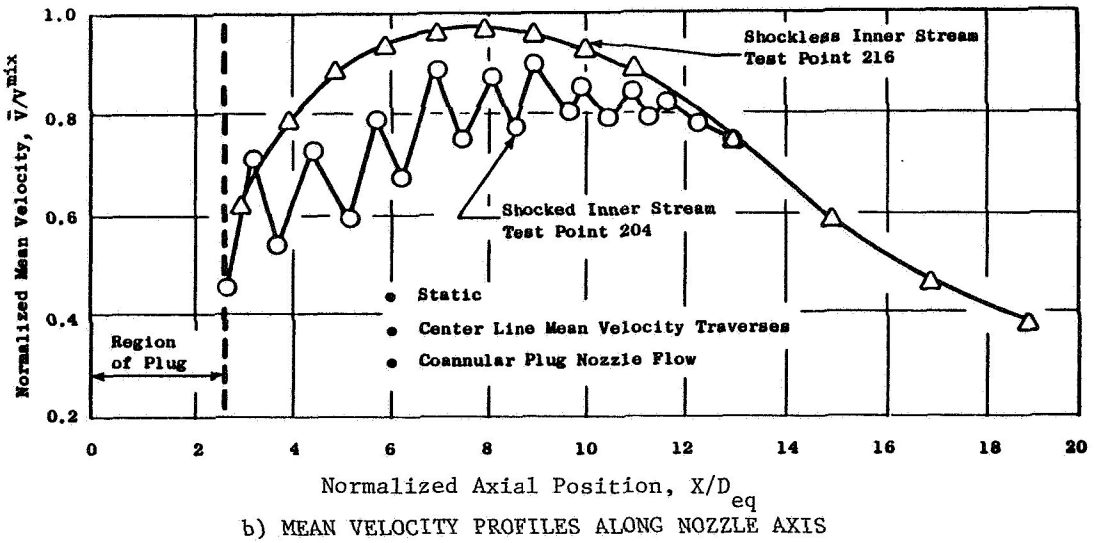

b) MEAN VELOCITY PROFILES ALONG NOZZLE AXIS

FIGURE 3-24. INFLUENCE OF INNER STREAM ON COANNULAR NOZZLE ACOUSTIC AND MEAN VELOCITY DATA (REF. 5).

stream relative to a supersonic inner stream in lowering the front quadrant shock-cell noise level of a convergent coannular nozzle by eliminating the downstream shock-cells.

In order to obtain additional such data over a range of outer stream pressure ratios ($2.5 < P_r^o < 4.0$), tests were conducted with the convergent coannular nozzle with extended plug (DFSC-6) with the inner stream maintained at a subsonic condition ($P_r^i \sim 1.80$). The PNL data so obtained at $\theta_i = 60°$ are presented in Figure 3-25 and compared with those obtained from convergent coannular nozzles with truncated and extended plugs (DFSC-1 and -6) and having fixed supersonic inner streams ($P_r^i \sim 3.13$). The data indicates that significant front quadrant noise benefit with the subsonic inner stream, noted under one outer stream test condition in Reference 5 (see Figure 3-24), is obtained over a full range of outer stream conditions.

Diagnostic data that compare the axial mean velocity traces obtained along three axial traverses (one on the nozzle centerline and the other two on parallels to the centerline but offset by $R/D_{eq} = 0.25$ and 0.5) with the convergent coannular nozzle with extended plug and operating with supersonic and subsonic inner streams, for a given underexpanded outer stream condition, and presented in Figure 3-26. An examination of this figure indicates a reduction in the number of shock-cells and a weakening of the remaining shock-cells with subsonic inner stream for all regions downstream of the plug. Since this is a convergent coannular configuration, the shock-cells are present on the plug. The front quadrant acoustic benefit due to the subsonic inner stream, that is demonstrated in Figure 3-25, therefore, is due to significant weakening precipitated by the subsonic inner flow on the downstream shock-cell structure.

Similar acoustic and LV tests with a subsonic inner stream were not conducted with the convergent coannular nozzle with the truncated plug (DFSC-1). However, limited diagnostic shadowgraph tests were conducted on DFSC-1 with both supersonic and subsonic inner streams, for a given underexpanded outer stream. These data, presented in Figure 3-27, indicate that the subsonic inner stream on the truncated plug configuration has the effect of minimizing the expansion fan which is noted with supersonic inner

DATA SCALED TO TOTAL NOZZLE AREA OF 0.903 m^2 (1400 $In.^2$)
AND EXTRAPOLATED TO 731.5 m (2400 Ft.) SIDELINE

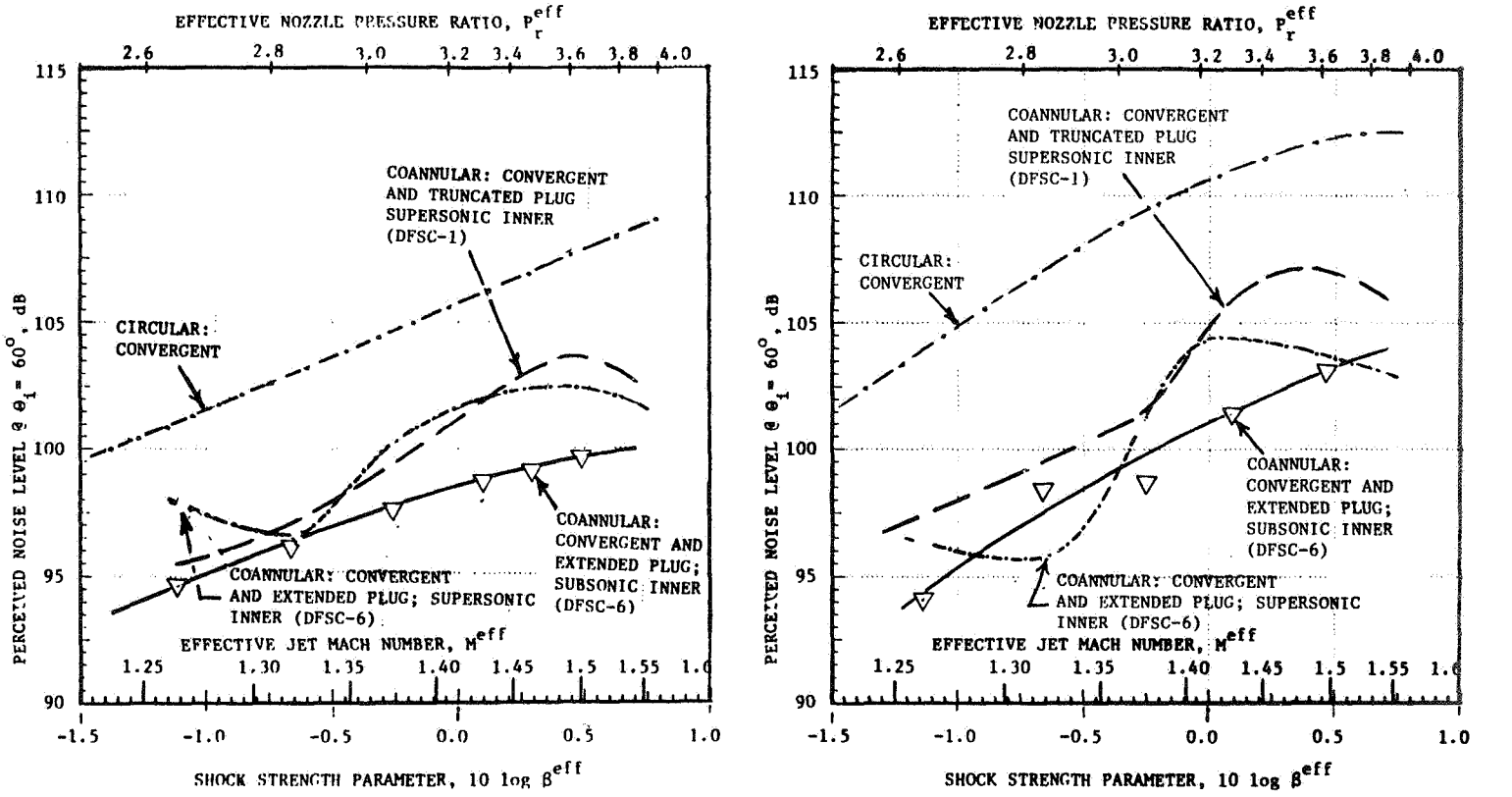

FIGURE 3-25. COMPARISON OF FORWARD QUADRANT PERCEIVED NOISE LEVEL DATA OF CONVERGENT COANNULAR NOZZLES (DFSC-1&6) WITH SUPERSONIC AND SUBSONIC INNER STREAMS.

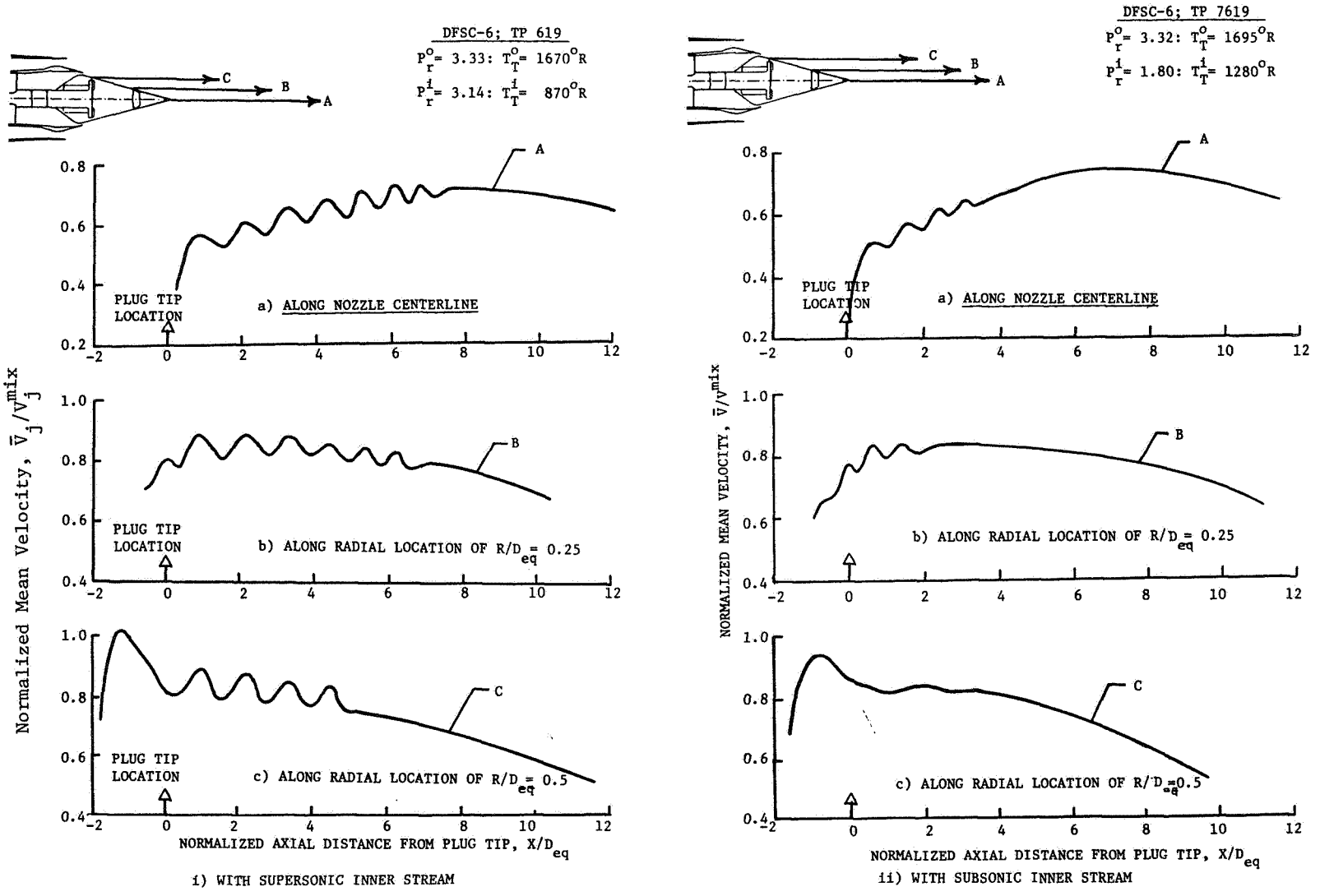

FIGURE 3-2ℓ. COMPARISON OF AXIAL MEAN VELOCITY DISTRIBUTIONS OF CONVERGENT COANNULAR NOZZLE WITH SUPERSONIC AND SUBSONIC INNER STREAMS.

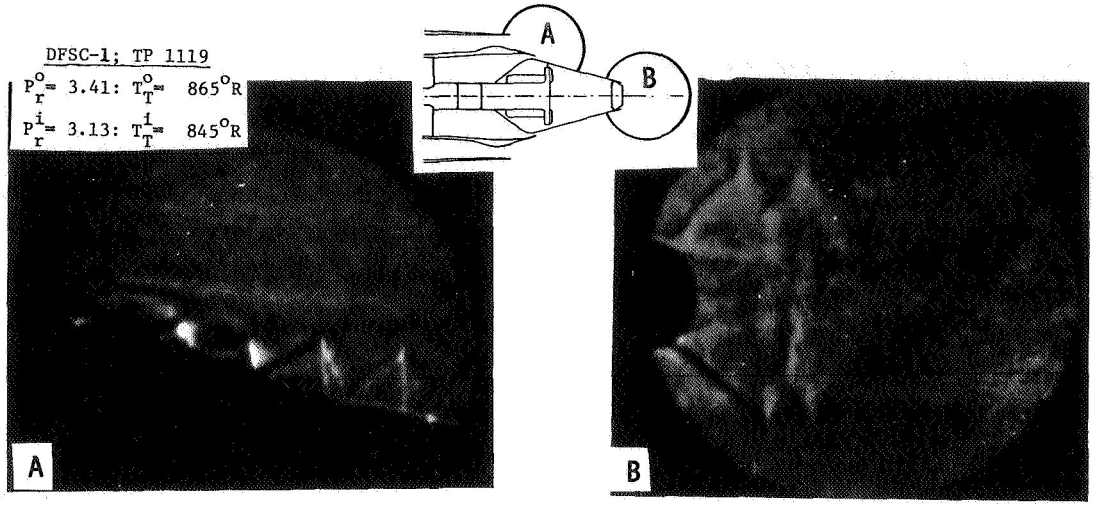

a) SUPERSONIC INNER STREAM

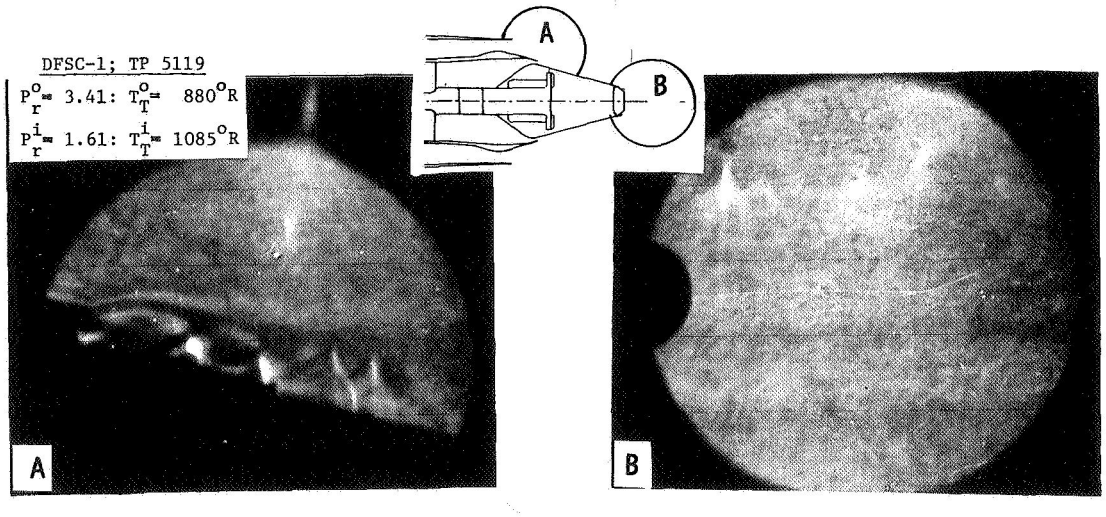

b) SUBSONIC INNER STREAM

FIGURE 3-27. COMPARISON OF PLUG REGION SHADOWGRAPHS OF CONVERGENT COANNULAR NOZZLE HAVING TRUNCATED PLUG (DFSC-1) WITH SUPERSONIC AND SUBSONIC INNER STREAMS.

stream. This, in turn, weakens the downstream shock-cell structure. Hence, it can be expected that the subsonic inner stream would be equally effective in the shock-cell noise reduction of convergent coannular nozzles with truncated plug.

Aft-quadrant normalized PNL data of convergent coannular nozzles DFSC-1 and DFSC-6 at Θ_i = 130° and operating with fixed supersonic and subsonic inner streams are presented in Figure 3-28. The data indicate that, for the convergent coannular nozzle and at a fixed V_j^{mix} (and hence equivalent thrust), the aft quadrant jet mixing noise is unaffected by the nature of the inner stream.

The static and simulated flight OASPL-directivities and a typical front quadrant spectral data are presented in Figures 3-29 and 3-30, respectively, for the convergent coannular plug nozzle (DFSC-6) with supersonic (TP-619 and -620) and subsonic (TP-7619 and -7620) inner streams. The underexpanded outer stream flow conditions for these test points are $P_r^o \sim 3.33$ and $T_T^o \sim 1680°R$. The diagnostic data for these test cases were discussed earlier in Figure 3-26. The directivity data of Figure 3-29 clearly indicate the front quadrant shock noise reduction obtained due to the presence of the subsonic inner stream. More significant benefit is noted in flight relative to the reductions under static tests. The typical front quadrant spectra presented in Figure 3-30 indicates significant SPL reduction in the mid frequency range that is due to the weakening of the downstream shocks by the subsonic inner flow (refer to Figure 3-26). Since the shock structure was more or less identical on the plug with both supersonic and subsonic inner streams (see Figure 3-27), no significant differences are noted between the corresponding high frequency spectra. Also, the low frequency spectra that are dominated by the jet mixing noise agree for the test cases as the mixed velocities are not significantly different.

It was noted, under Subsection 3.2.2, that significant shock-cell structures were eliminated with the C-D coannular nozzle with extended plug operating at the C-D design conditions (refer to Figure 3-5). In addition, a maximum PNL reduction of 8.9 dB and 12.2 dB were measured, under static and simulated flight conditions, respectively, relative to a convergent circular nozzle (refer to Figure 3-4). The PNL data of this C-D configuration

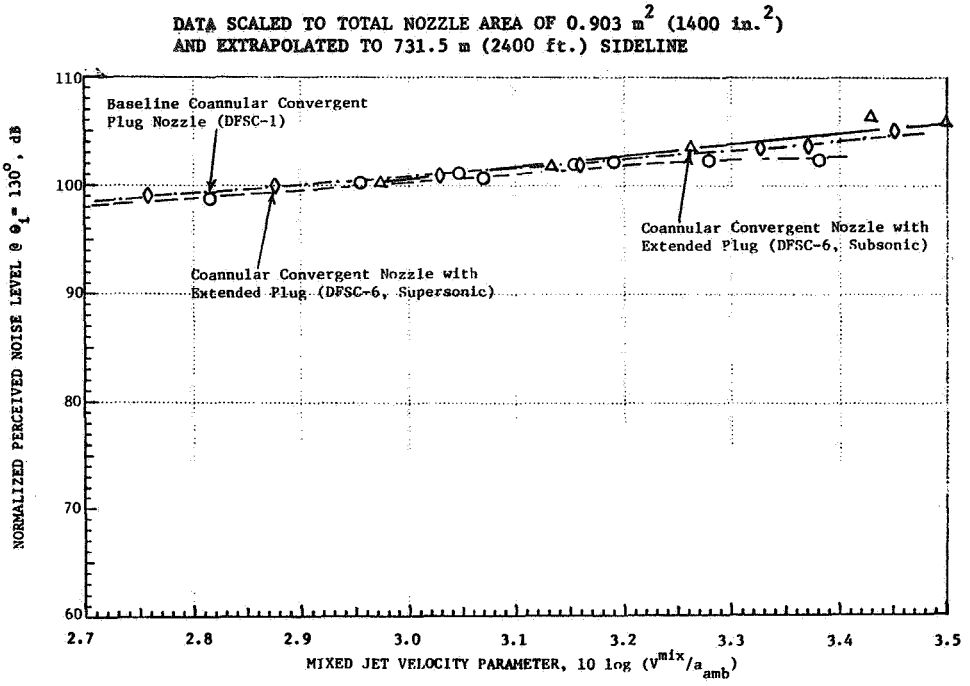

a) STATIC

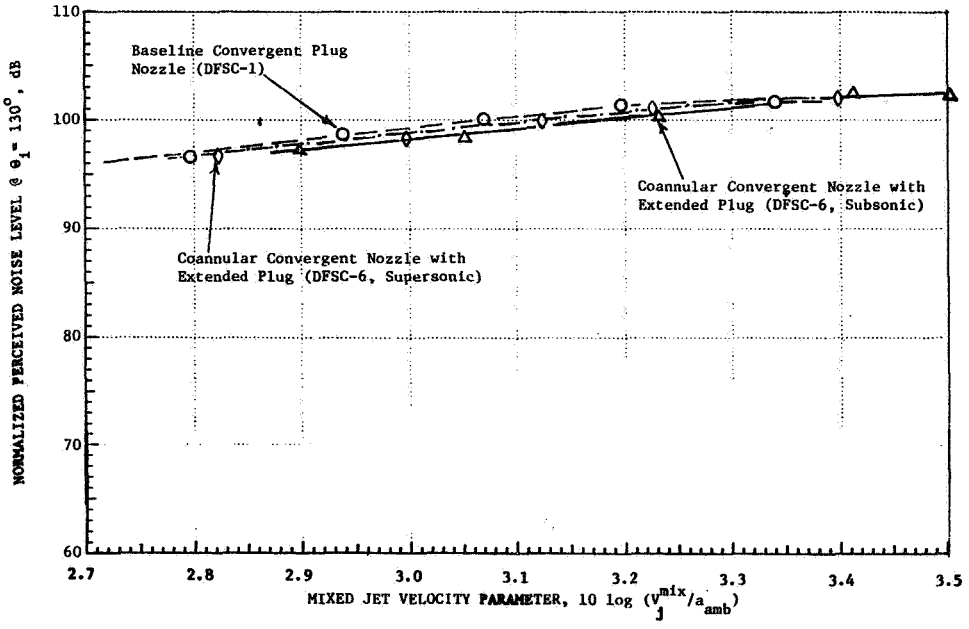

b) SIMULATED FLIGHT (V_{ac} = 122 mps or 400 fps)

FIGURE 3-28. EFFECT OF SUPERSONIC/SUBSONIC INNER STREAM ON TYPICAL AFT QUADRANT NORMALIZED ACOUSTIC DATA OF CONVERGENT COANNULAR PLUG NOZZLE.

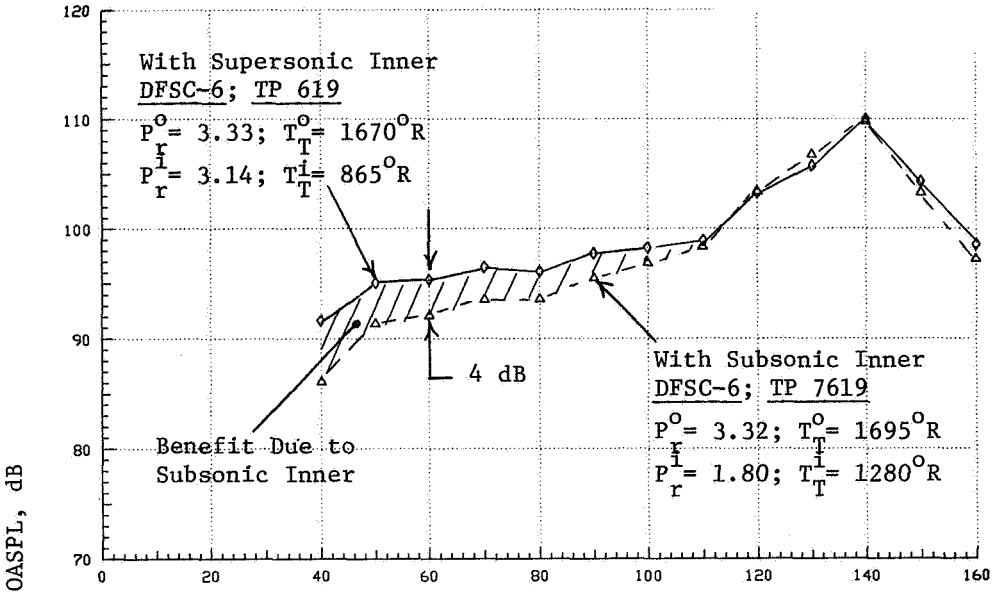

a) Static

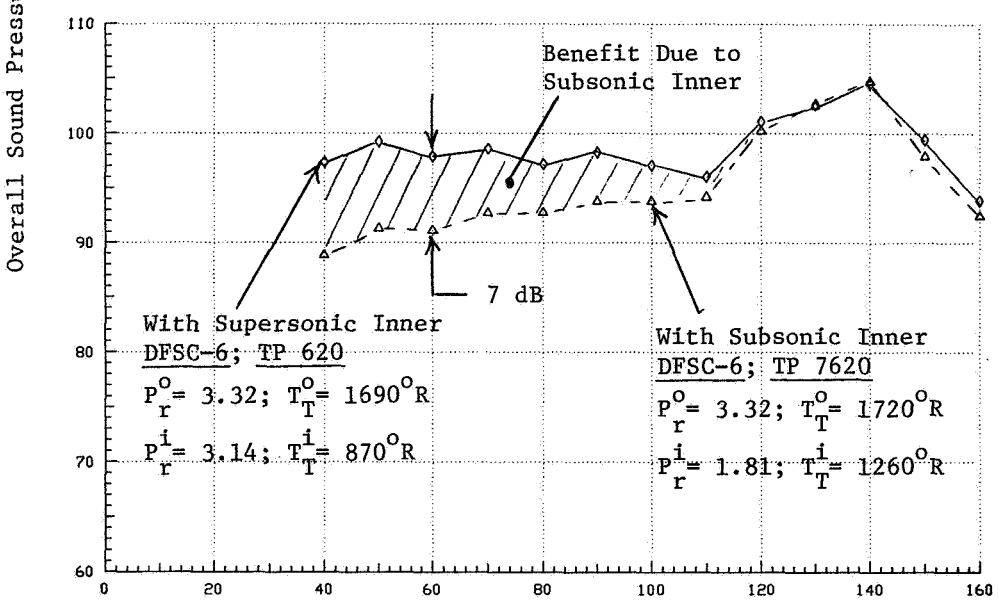

Overall Sound Pressure Level, OASPL, dB

Angle to Inlet, θ_i, Degrees

b) Simulated Flight (V_{ac}= 122m/Sec or 400 fps)

FIGURE 3-29. TYPICAL STATIC AND SIMULATED FLIGHT OASPL-DIRECTIVITIES OF CONVERGENT COANNULAR NOZZLE (DFSC-6) WITH SUBSONIC AND SUPERSONIC INNER STREAMS FOR A GIVEN UNDEREXPANDED OUTER STREAM.

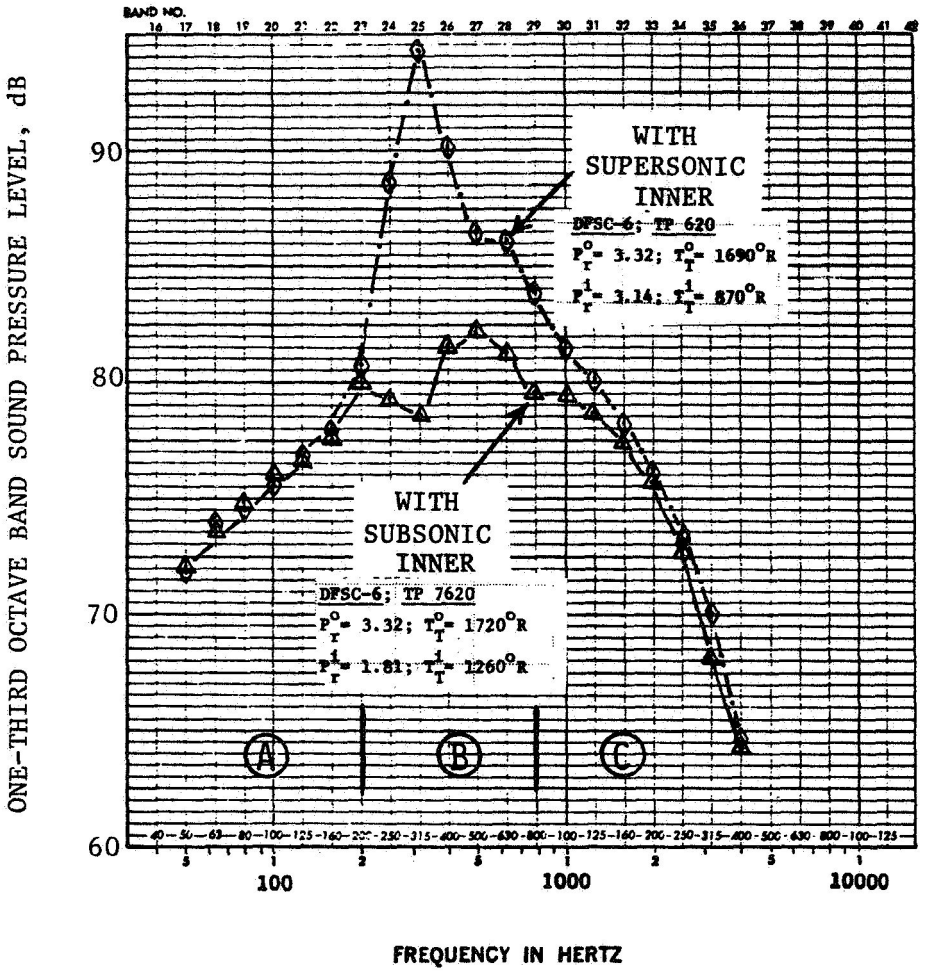

FIGURE 3-30. TYPICAL FRONT QUADRANT SPECTRA OF CONVERGENT COANNULAR NOZZLE (DFSC-6) WITH SUBSONIC AND SUPERSONIC INNER STREAMS FOR A GIVEN UNDEREXPANDED OUTER STREAM (SIMULATED FLIGHT).

are compared in Figure 3-31 with the data of convergent coannular nozzle, operating with the subsonic inner stream, in order to make a comparative estimate of the latter relative to the almost shock-free DFSC-3 configuration. An examination of this figure indicates that, at mixed flow conditions that match the design β^{eff} of the DFSC-3 configuration, the measured PNL reductions with the DFSC-6 nozzle operating with a subsonic inner stream relative to a convergent circular nozzle are 7.5 dB and 9.7 dB under static and simulated flight conditions, respectively. In addition, the significant front quadrant noise reduction with the fixed subsonic inner stream is observed over the entire test range of the outer stream ($2.5 < P_r^o < 4.0$). While the test cycle conditions with the subsonic inner stream differ from that of a typical AST/VCE cycle, future changes in VCE fan cycle could make this concept worthwhile in reducing the front quadrant noise over an entire operational range.

3.4 CONVERGENT-DIVERGENT SUPPRESSOR NOZZLE DATA

In this subsection, the acoustic and diagnostic data obtained with the multi-element suppressor nozzles (DFSC-4 and DFSC-5) are presented. The benefits of the convergent-divergent termination in the flowpaths of the multi-element suppressor nozzle relative to the convergent terminated suppressor are discussed.

As described in subsection 2.4, two multi-element suppressor nozzles were tested during the present shock-cell noise investigation. The convergent configuration (DFSC-4), with a 20-shallow-chute convergent flowpath suppressor in the outer stream and a convergent annular flowpath in the inner stream has a suppressor area ratio of 1.75 and equivalent exit diameters of 12.9 (outer) and 5.7 (inner) inches. The convergent-divergent configuration (DFSC-5), with a 20-shallow-chute C-D flowpath suppressor in the outer stream and a C-D annular flowpath in the inner stream, has suppressor area ratios of 1.75 (at throat) and 1.56 (at exit). It is designed for Mach numbers of 1.40 (outer) and 1.33 (inner). The equivalent diameters at the throat are 12.8 (outer) and 5.8 (inner) inches.

DATA SCALED TO TOTAL NOZZLE AREA OF 0.903 m^2 (1400 $In.^2$)
AND EXTRAPOLATED TO 731.5 m (2400 Ft.) SIDELINE

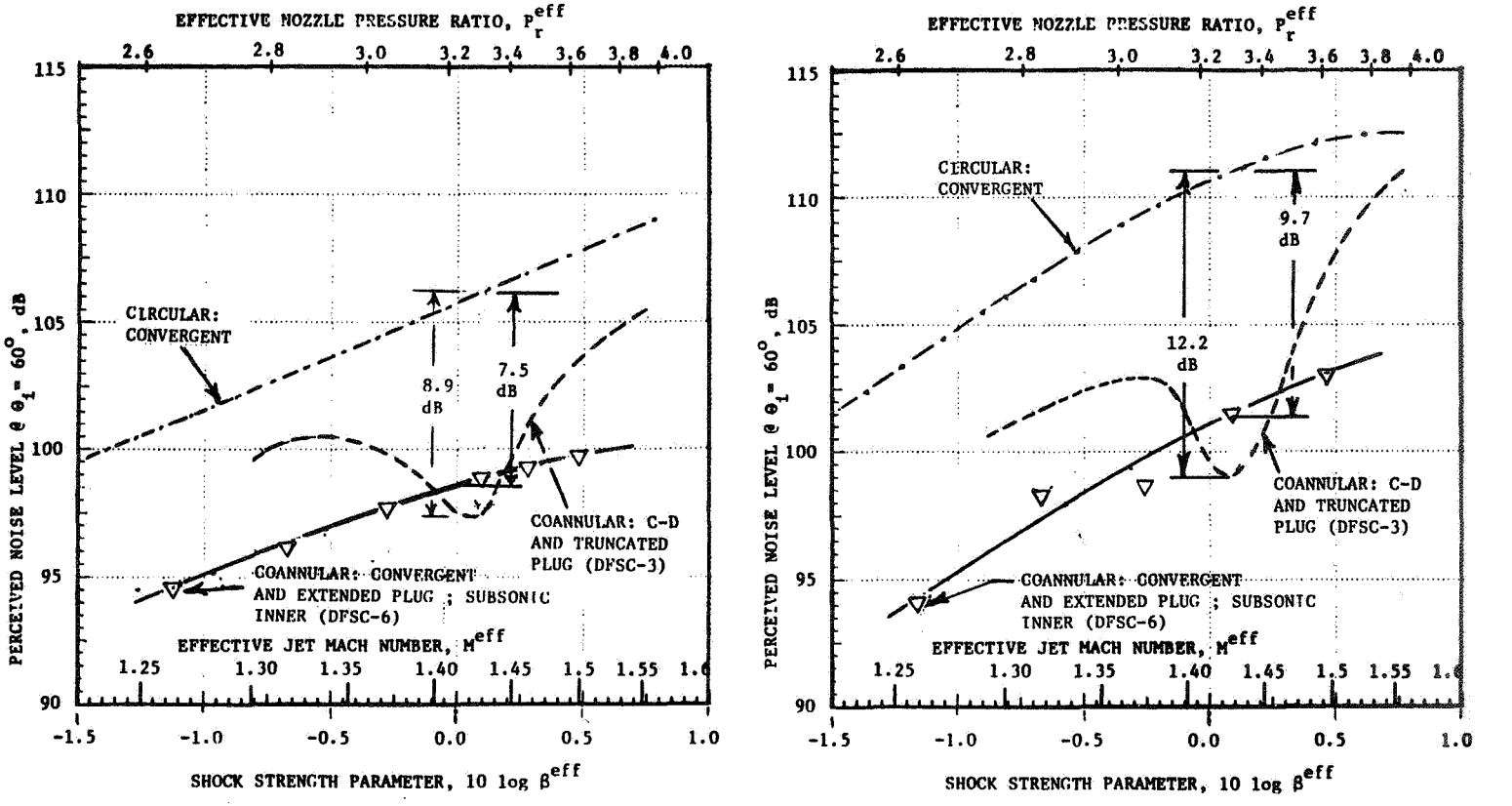

FIGURE 3-31. EFFECTIVENESS OF SUBSONIC INNER STREAM ON FRONT QUADRANT NOISE OF A CONVERGENT COANNULAR NOZZLE WITH EXTENDED PLUG (DFSC-6).

3.4.1 Effectiveness of C-D Flowpaths for Multi-Chute Suppressors

The static and simulated flight measured perceived noise levels of the convergent suppressor configuration (DFSC-4), at a typical forward quadrant angle of Θ_i = 60°, was presented earlier in Figure 3-2. These data are repeated in Figure 3-32 and compared with the corresponding results measured with the C-D suppressor configuration. The data presented as a function of the shock-cell parameter parameter 10 log β^{eff} were obtained over a range of flow variables that are typical of AST/VCE cycle conditions (refer to Table 2-VIII for Test Matrix). The measured data are compared also with the corresponding data of the convergent circular nozzle. An examination of the figure indicates a maximum reduction of 2.3 and 2 dB under static and simulated flight conditions, respectively, with the C-D nozzle relative to the convergent suppressor nozzle (DFSC-4) near the C-D design point which also corresponds to a typical AST takeoff condition. An examination of this figure also indicates a significant shock associated noise amplification in flight for each of the nozzles over the test range of pressure ratios. It should be noted that the relative magnitudes between the two suppressor nozzles remain almost unchanged under static and flight conditions indicating almost equal amount of flight amplification for each of the configurations. This suggests that the acoustic data for the C-D suppressor nozzle still contains shock noise components even at the C-D design condition.

Typical aft quadrant PNL comparisons between data of DFSC-4 and DFSC-5 are illustrated in Figure 3-33. In this figure normalized PNL measured at an angle of Θ_i = 130° are plotted against ideally expanded mixed stream jet velocity. The results indicate that, for a given thrust, the convergent suppressor configuration (DFSC-4) yields a lower jet mixing noise relative to the C-D suppressor nozzle (DFSC-5). As will be illustrated next in this subsection, the diagnostic LV measurements showed a faster decay rate of the mean velocity for the convergent suppressor nozzle (DFSC-4) compared to the data of the C-D suppressor nozzle (DFSC-5). This could be one of the reasons for the observed lower jet mixing noise with the convergent suppressor.

Some of the significant diagnostic data obtained with DFSC-4 and -5 configurations are presented in Figures 3-34 and 3-35. The aerodynamic flow conditions for the diagnostic tests match the design conditions of the C-D

DATA SCALED TO TOTAL NOZZLE AREA OF 0.903 m^2 (1400 $In.^2$)
AND EXTRAPOLATED TO 731.5 m (2400 Ft.) SIDELINE

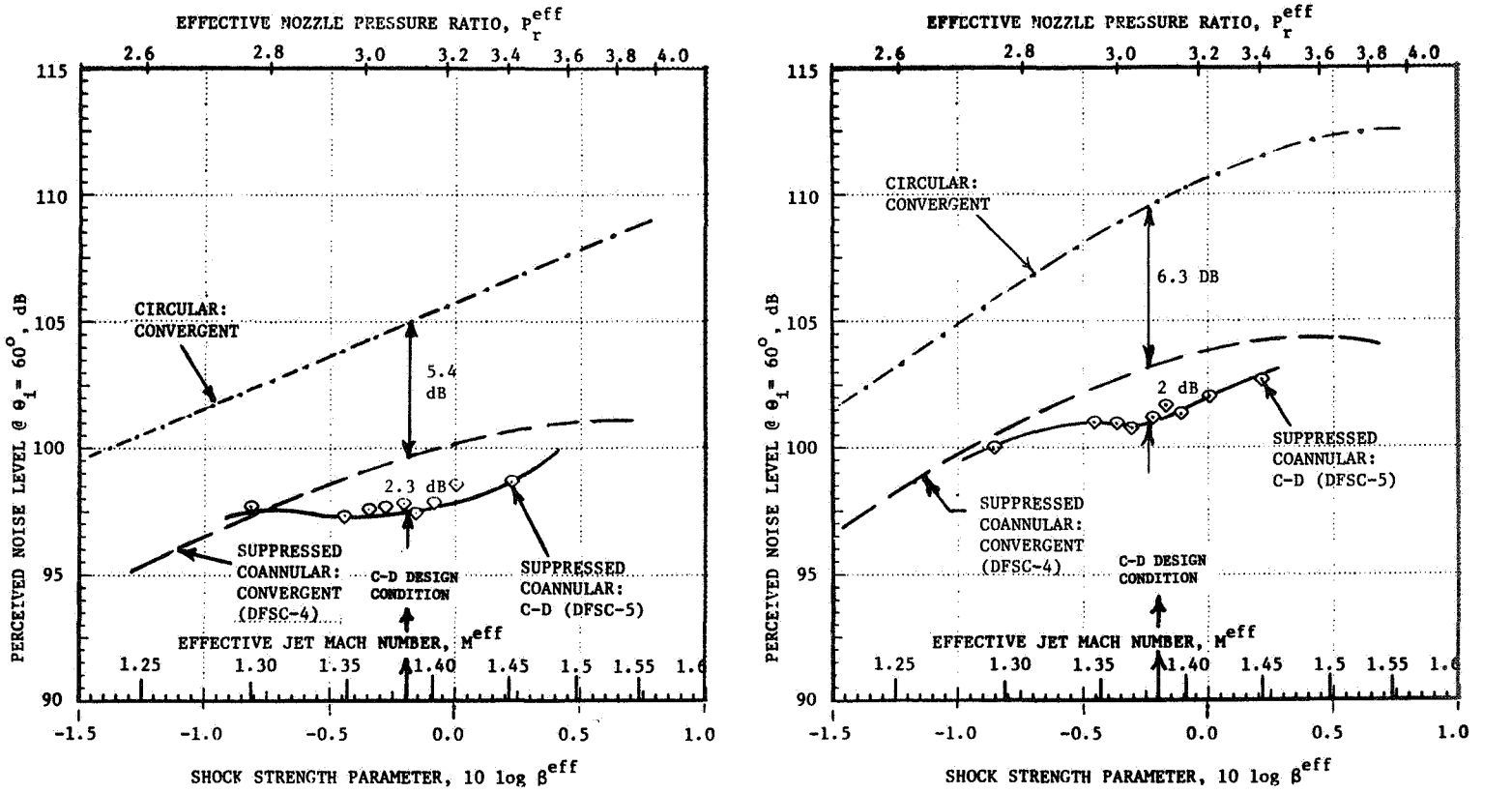

FIGURE 3-32. EFFECTIVENESS OF CONVERGENT-DIVERGENT INNER AND OUTER FLOWPATHS IN SHOCK-CELL NOISE REDUCTION FOR A SUPPRESSED COANNULAR NOZZLE (DFSC-5).

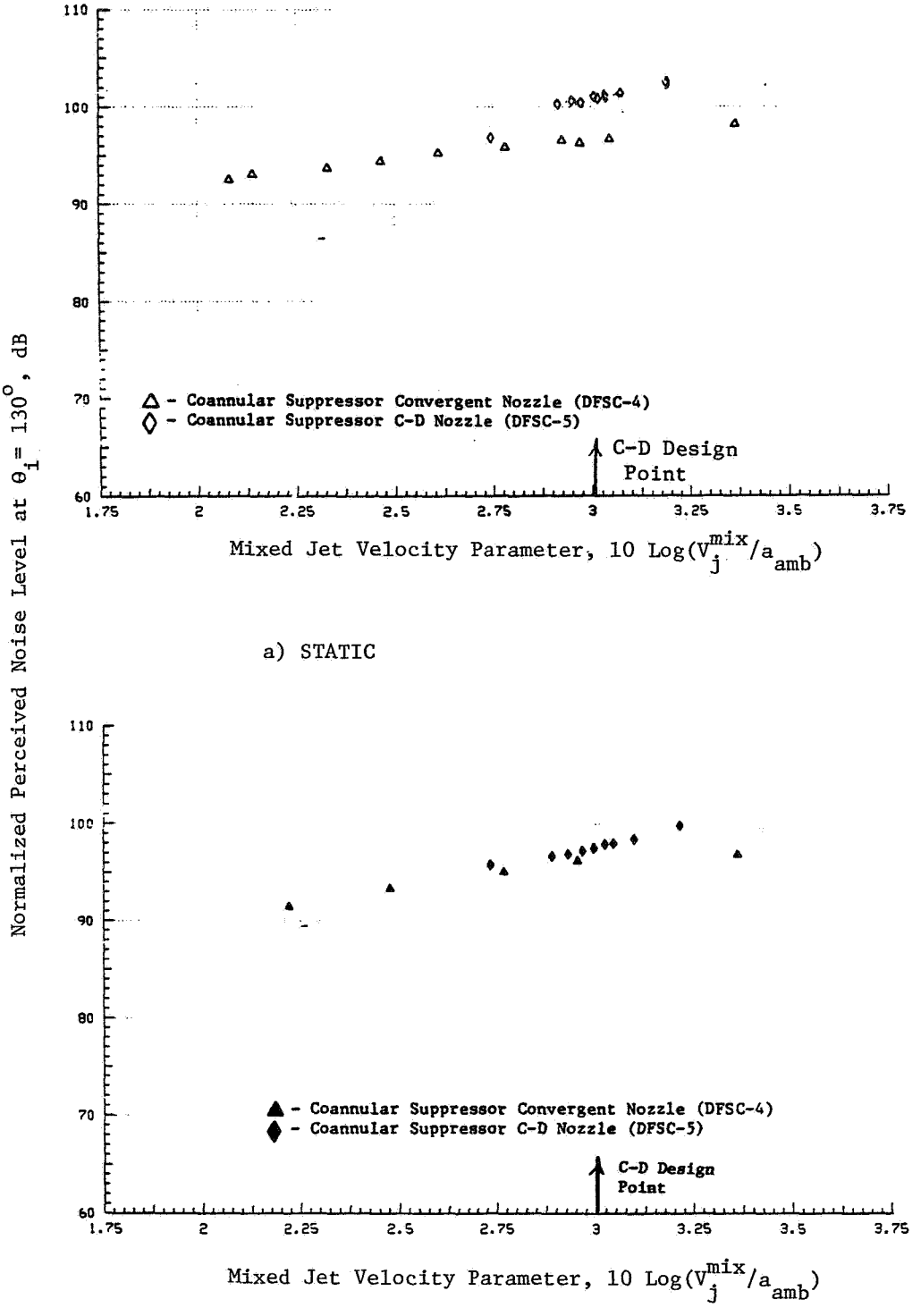

FIGURE 3-33. AFT QUADRANT COMPARISON OF NORMALIZED PNL DATA AT $\theta_i = 130^o$ OF COANNULAR SUPPRESSOR C-D NOZZLE WITH THOSE OF BASELINE COANNULAR SUPPRESSOR CONVERGENT NOZZLE.

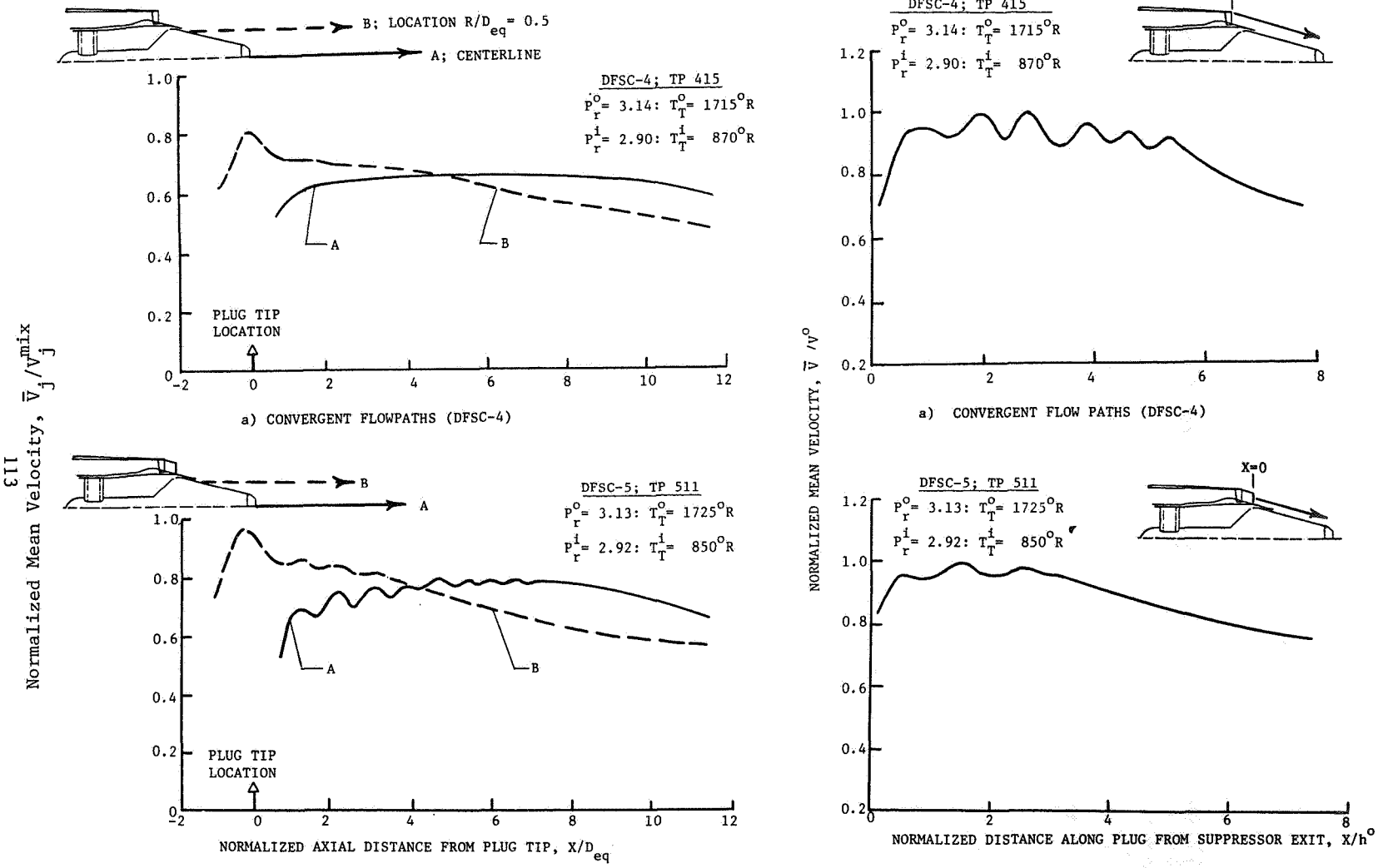

FIGURE 3-34. COMPARISON OF MEAN VELOCITY DISTRIBUTIONS OF CONVERGENT AND C-D SUPPRESSOR COANNULAR NOZZLES AT C-D DESIGN CONDITIONS (STATIC TESTS)

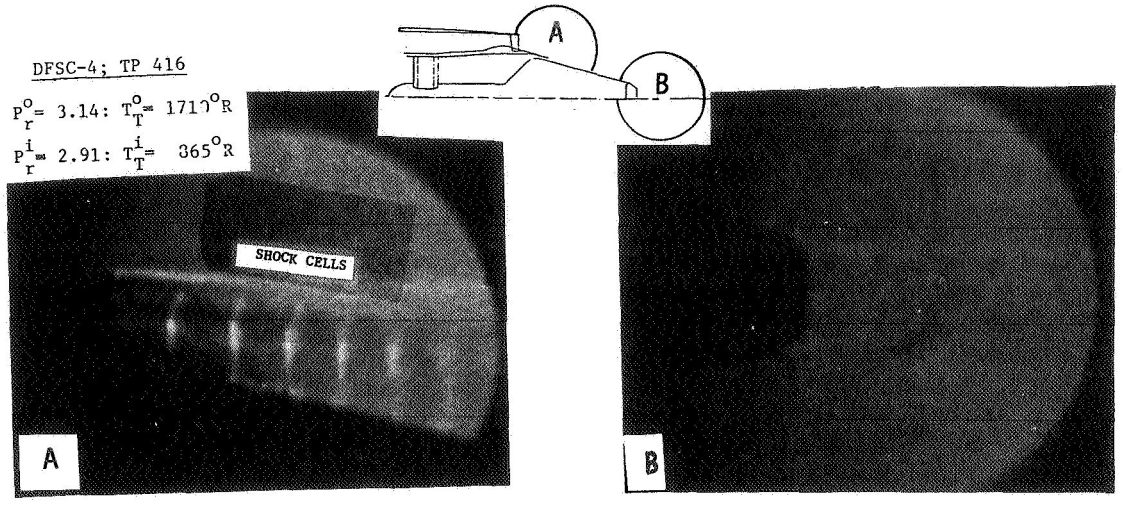

a) CONVERGENT FLOWPATHS

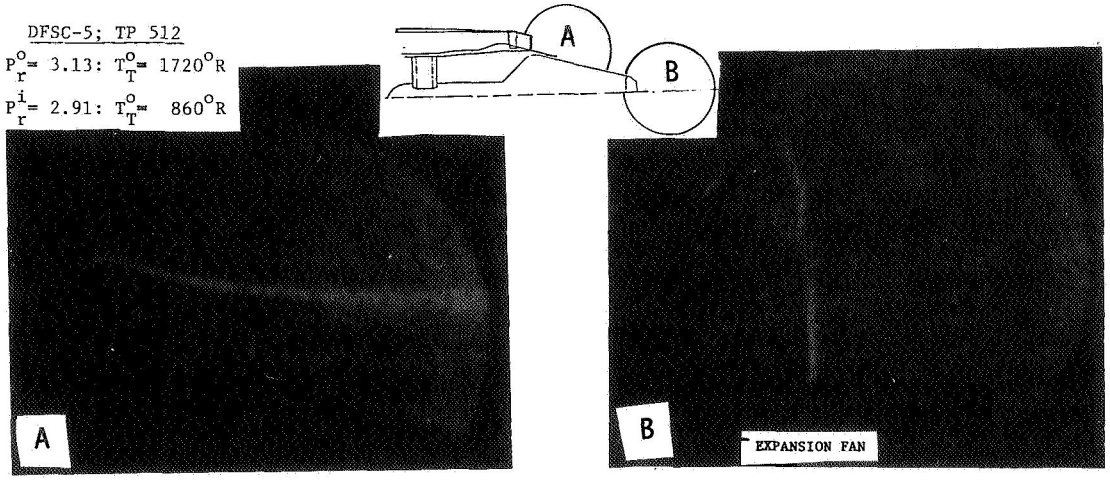

b) C-D FLOWPATHS

FIGURE 3-35. COMPARISON OF THE PLUG REGION SHADOWGRAPHS OF CONVERGENT AND C-D SUPPRESSOR COANNULAR NOZZLES AT C-D DESIGN CONDITIONS (SIMULATED FLIGHT TEST).

flowpaths of DFSC-5*. The laser velocimeter data of Figure 3-34 compare the mean velocity traces obtained along two axial traverses (one on the nozzle centerline and the other on a parallel to the centerline but offset by R/D_{eq} = 0.5) and a traverse parallel to the plugs for each of the two configurations. An examination of this figure indicates:

- Weakening of the shock structure on the plug surface of DFSC-5, relative to that on the plug of the convergent suppressor (DFSC-4) because of the C-D terminations.

- The normalized axial mean velocity for DFSC-4 is less than 0.70 for values of $X/D_{eq} > 2.0$ indicating a subsonic flow region and hence the observed absence of shock-cells downstream of the plug of the convergent suppressor configuration.

- Existence of supersonic flow over a significant region downstream of plug of DFSC-5 and the presence of shock-cells in that region.

The expansion of the supersonic flow at the plug truncation of DFSC-5 nozzle is indicated by the shadowgraphs presented in Figure 3-35. The pictures taken in the plug region confirm the presence of the expansion fan at the tip of the truncated plug of the DFSC-5 nozzle and the absence of the expansion fan at the tip of the truncated plug of the DFSC-4 nozzle. The shadowgraphs also substantiate the weakening of the shock-cells on the plug of the C-D terminated suppressor and the existence of 6 to 7 shock-cells on the plug of the convergent suppressor.

3.4.2 Directivity and Spectral Data Comparisons Between Convergent and C-D Suppressor Coannular Plug Nozzles at C-D Design Conditions

In this subsection, the static and simulated flight PNL- and OASPL-directivities and typical spectral comparisons of the two suppressed coannular nozzles DFSC-4 and DFSC-5 are presented and compared to one another. The aerodynamic flow conditions correspond to the design conditions of the C-D terminations of the DFSC-5 configuration. The diagnostic data obtained during static tests were presented in the previous subsection.

*For these conditions, the local Mach number in the mixed flow region is greater than unity for approximate values of $\bar{V}_j/\bar{V}_j^{mix} > 0.7$ to 0.8, approximately.

PNL- and OASPL-directivities of the two suppressed coannular configurations are presented in Figures 3-36 and 3-37, for static and simulated flight, respectively. The C-D benefit in terms of PNL are evident over the forward quadrant angles, while in the aft quadrant the convergent suppressor yields lower mixing noise compared to the C-D suppressor nozzle. The LV test data presented earlier in Figure 3-34 had indicated shock-cells on the plug for DFSC-4 and downstream of the plug for DFSC-5 and subsonic flow downstream of the plug of DFSC-4 while DFSC-5 had supersonic flow downstream of the plug. The two shock-cell structures, for example, have two different associated length scales and hence two different broadband peak frequencies. Similarly, the downstream subsonic/supersonic mixed flow velocities of DFSC-4/DFSC-5 affect the jet mixing noise spectra, particularly in the low and middle frequencies. In the PNL calculations, these SPL levels at different frequencies are weighted differently and this leads to the differences noticed between the levels and directivities of PNL and OASPL data.

Static and simulated flight spectral characteristics of DFSC-4 and DFSC-5 at the C-D design conditions are compared in Figures 3-38 through 3-40. While only the spectral data at $\Theta_i = 60°$ are presented in Figure 3-38, a set of data at all front quadrant angles are presented in Figures 3-39 and 3-40. In order to characterize the spectral frequencies associated with the shock-cells on the plug for DFSC-4 and downstream of the plug for DFSC-5, the respective shock-cell related broadband frequencies were calculated using Equations 3.1 and 3.2. The needed average shock-cell spacings on the plug of DFSC-4 and downstream of the plug of DFSC-5 configurations were obtained from the respective shadowgraph and LV axial mean velocity trace. For the static cases, they were determined to be 1.03 inch and 4.70 inch, respectively. The static broadband noise peak frequencies at $\Theta_i = 60°$ and associated with these shock-cells on the DFSC-4 and DFSC-5 model nozzles and at the test conditions are predicted then to be 10,700 Hz and 2,260 Hz, respectively. When extrapolated to the typical product size, these peak frequencies correspond to 1/3-octave-bands having center frequencies of 1,250 Hz and 315 Hz for the static cases and approximately 1,600 Hz and 400 Hz for the corresponding flight cases.

Using the above information, three distinct frequency ranges designated as A, B and C are defined as follows:

MODEL	TEST PT.	P_r^o	T_T^o, °R	V_j^o, ft/s	P_r^i	T_T^i, °R	V_j^i, ft/s	V_j^{mix}, ft/s	T_T^{mix}, °R	V_{ac}, ft/s
4	415	3.14	1715	2411	2.90	872	1658	2256	1541	0
5	511	3.13	1725	2419	2.92	852	1644	2254	1540	0

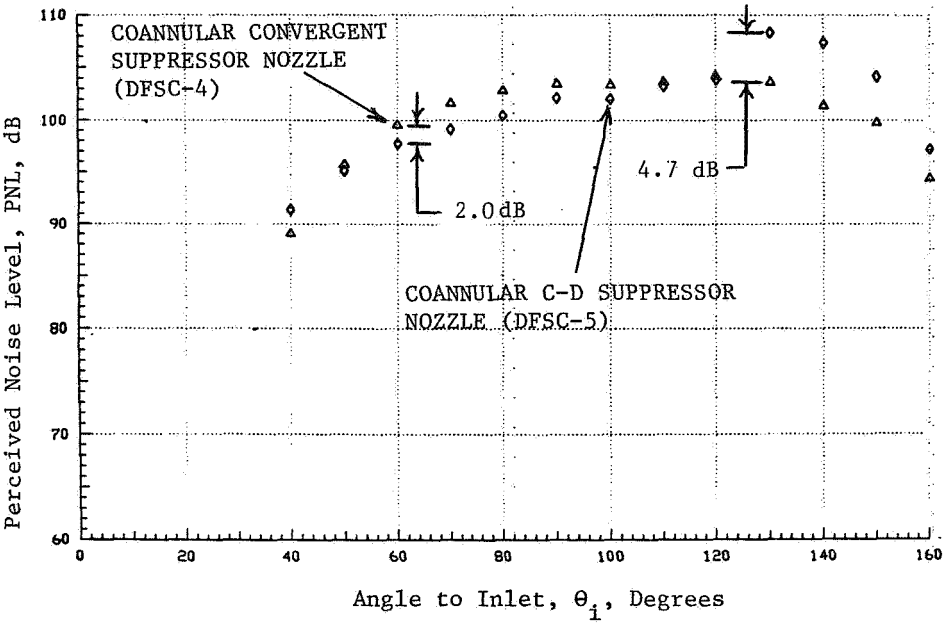

a) PNL-DIRECTIVITY

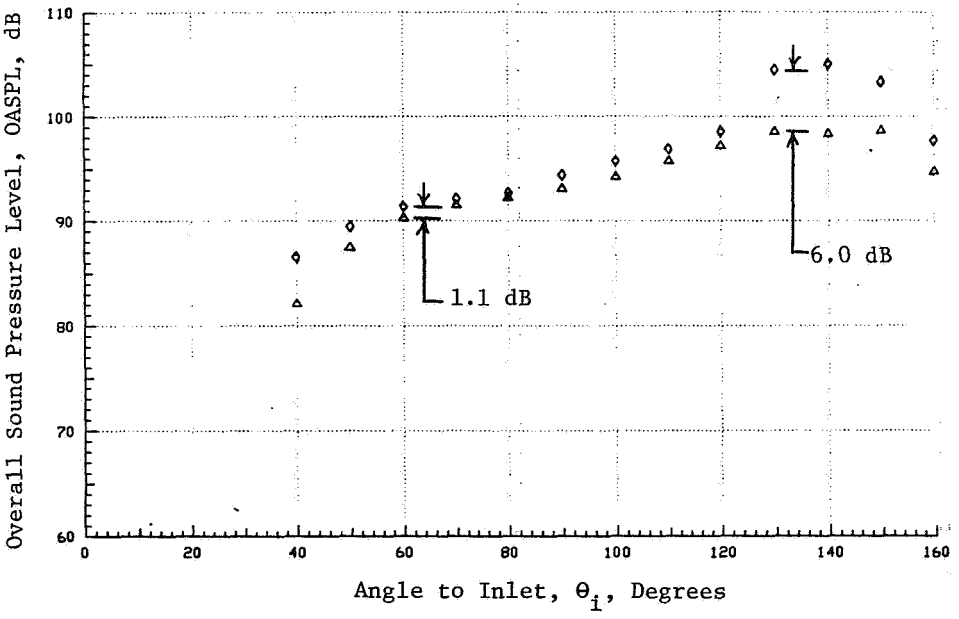

b) OASPL- DIRECTIVITY

FIGURE 3-36. COMPARISON OF PNL- AND OASPL- DIRECTIVITIES OF COANNULAR SUPPRESSOR C-D NOZZLE WITH THOSE OF COANNULAR SUPPRESSOR CONVERGENT NOZZLE (STATIC).

MODEL	TEST PT.	P_r^o	T_T^o, °R	V_j^o, ft/s	P_r^i	T_T^i, °R	V_j^i, ft/s	V_j^{mix}, ft/s	T_T^{mix}, °R	V_{ac}, ft/s
4	416	3.14	1708	2407	2.91	866	1654	2251	1535	400
5	512	3.13	1718	2412	2.91	857	1646	2250	1536	400

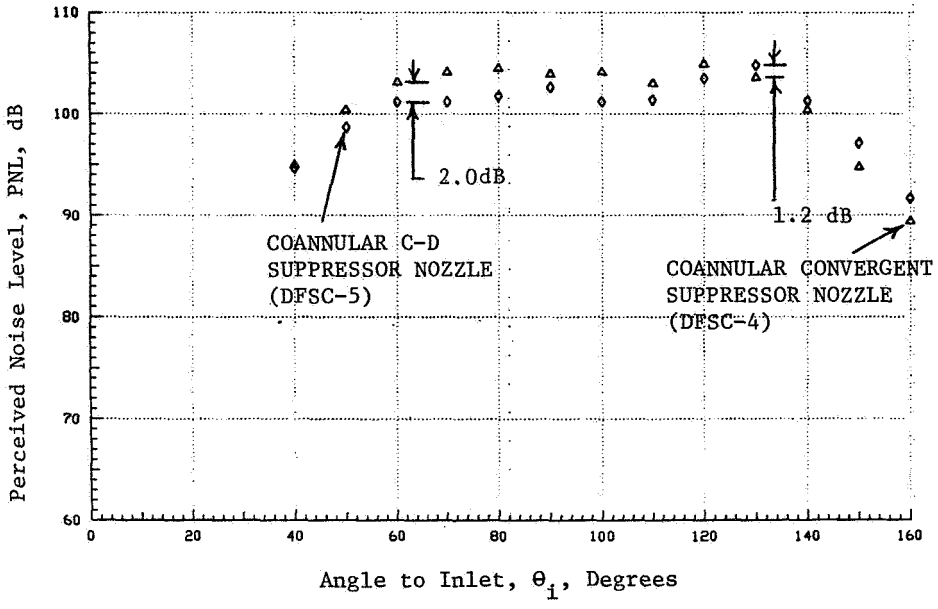

a) PNL - DIRECTIVITY

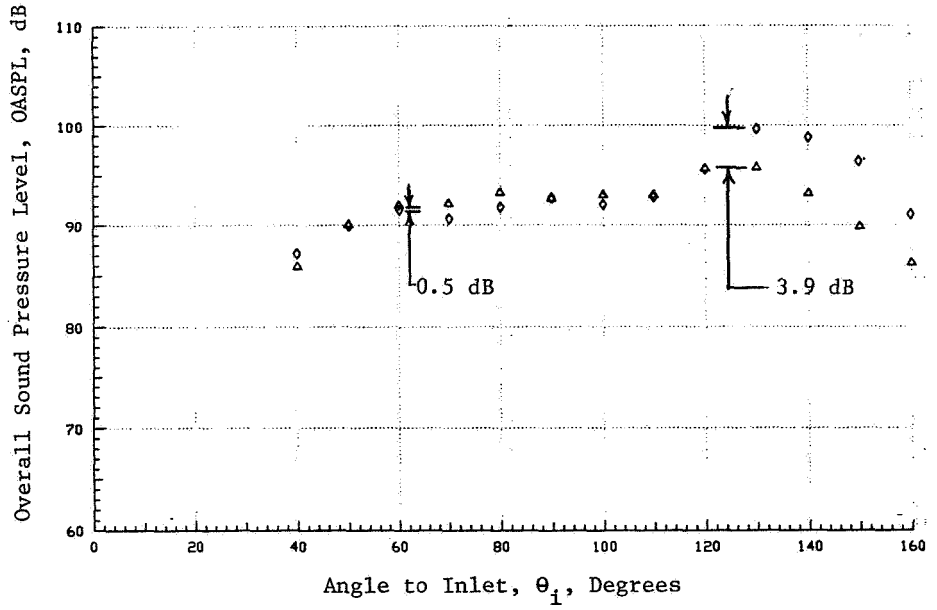

b) OASPL - DIRECTIVITY

FIGURE 3-37. COMPARISON OF PNL- AND OASPL-DIRECTIVITIES OF COANNULAR SUPPRESSOR C-D NOZZLE WITH THOSE OF COANNULAR SUPPRESSOR CONVERGENT NOZZLE (SIMULATED FLIGHT).

DATA SCALED TO TOTAL NOZZLE AREA OF 0.903 m^2 (1400 $In.^2$)
AND EXTRAPOLATED TO 731.5 m (2400 Ft.) SIDELINE

$P_r^o \sim 3.14$, $T_T^o \sim 1700^oR$

$P_r^i \sim 2.91$, $T_T^i \sim 860^oR$ $\quad \theta_i = 60^o$

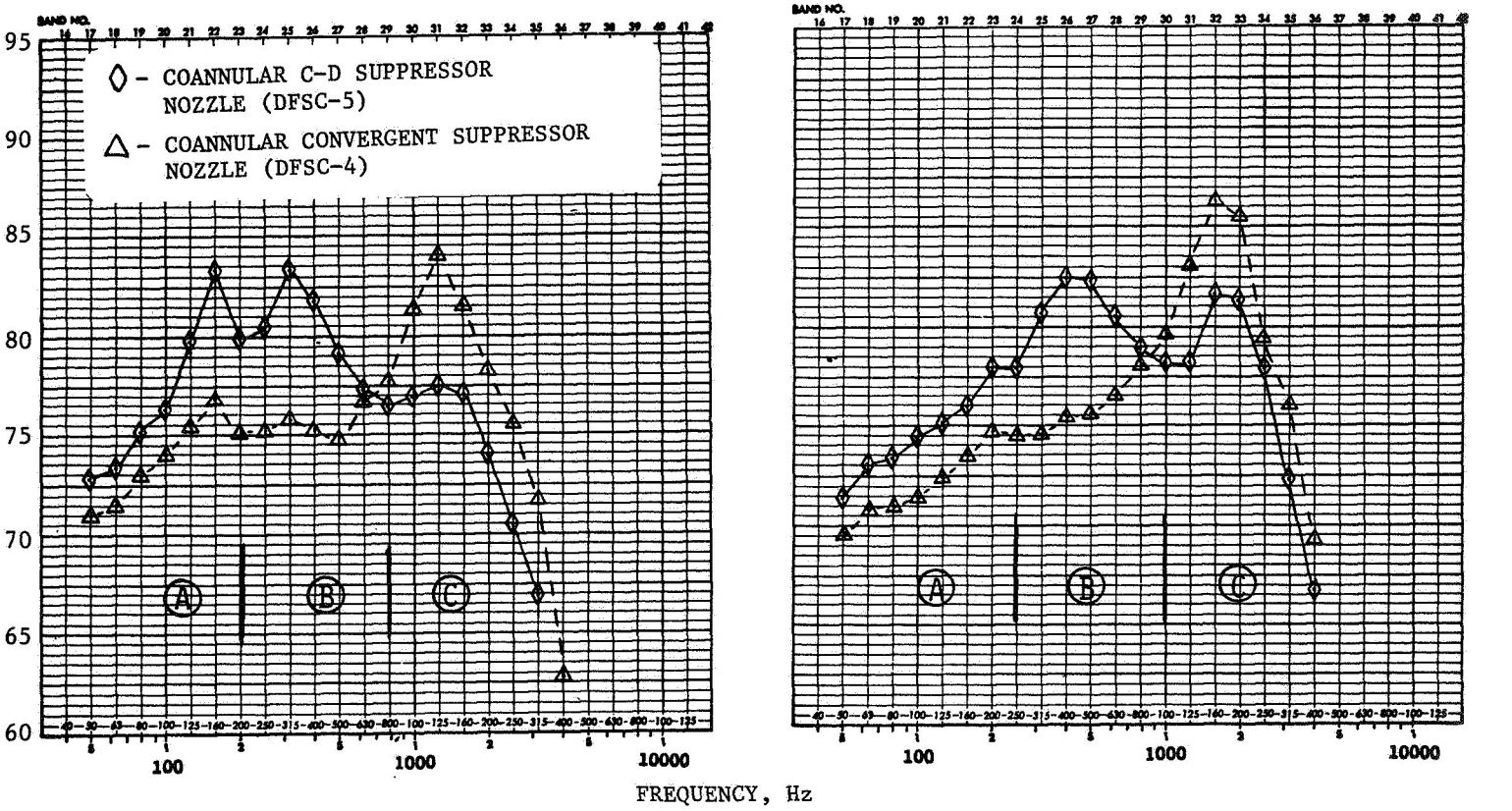

a) STATIC

b) SIMULATED FLIGHT, $V_{ac} \simeq 122$m/sec (400 fps)

FIGURE 3-38. TYPICAL STATIC AND SIMULATED FLIGHT FRONT QUADRANT SPECTRAL COMPARISON BETWEEN COANNULAR C-D AND CONVERGENT SUPPRESSOR NOZZLES AT C-D DESIGN CONDITIONS.

(See Figure 3-36 for Aerodynamic Conditions)

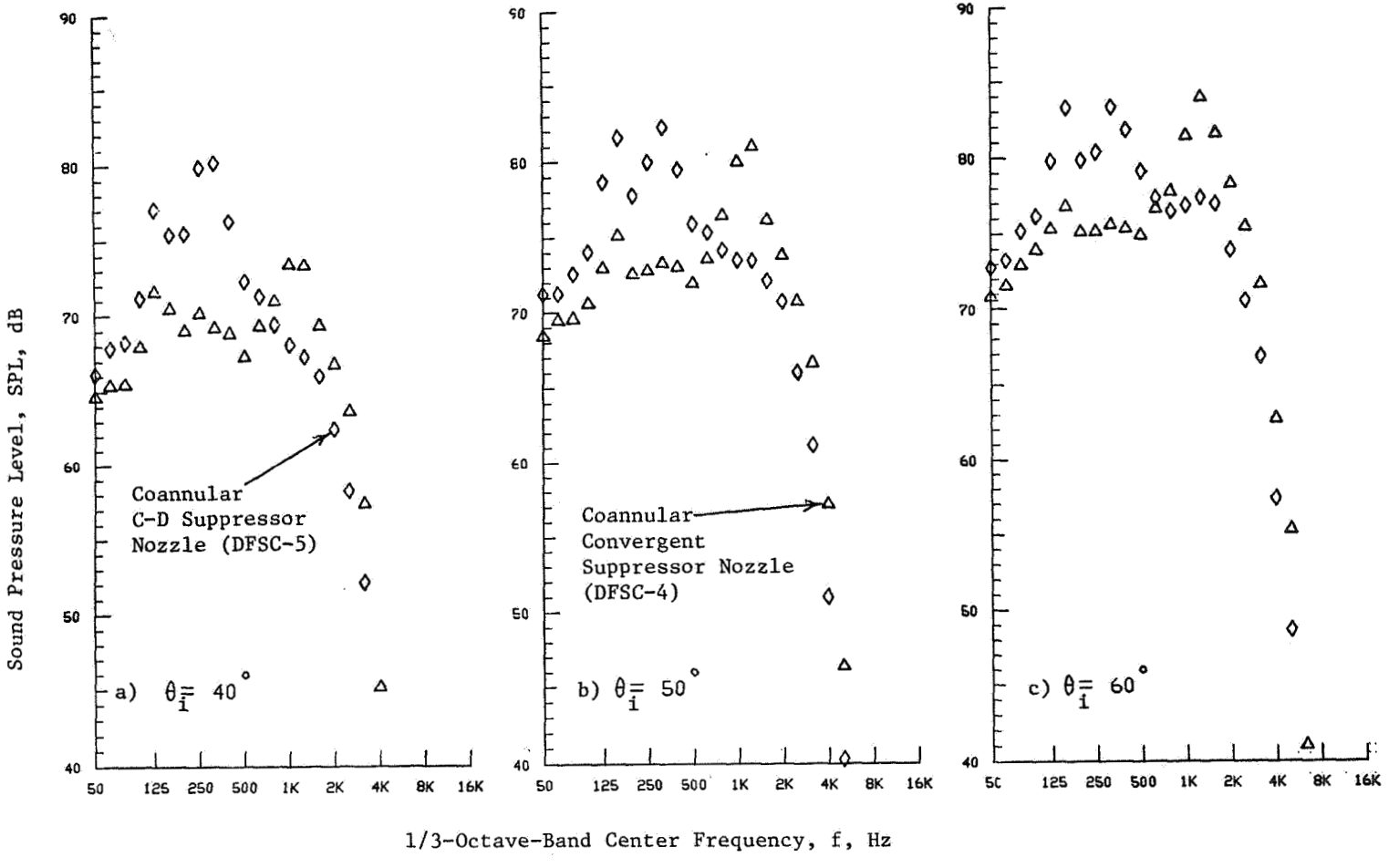

FIGURE 3-3.9. FRONT QUADRANT SPECTRAL COMPARISON BETWEEN COANNULAR C-D AND CONVERGENT SUPPRESSOR NOZZLES AT C-D DESIGN CONDITIONS (STATIC)

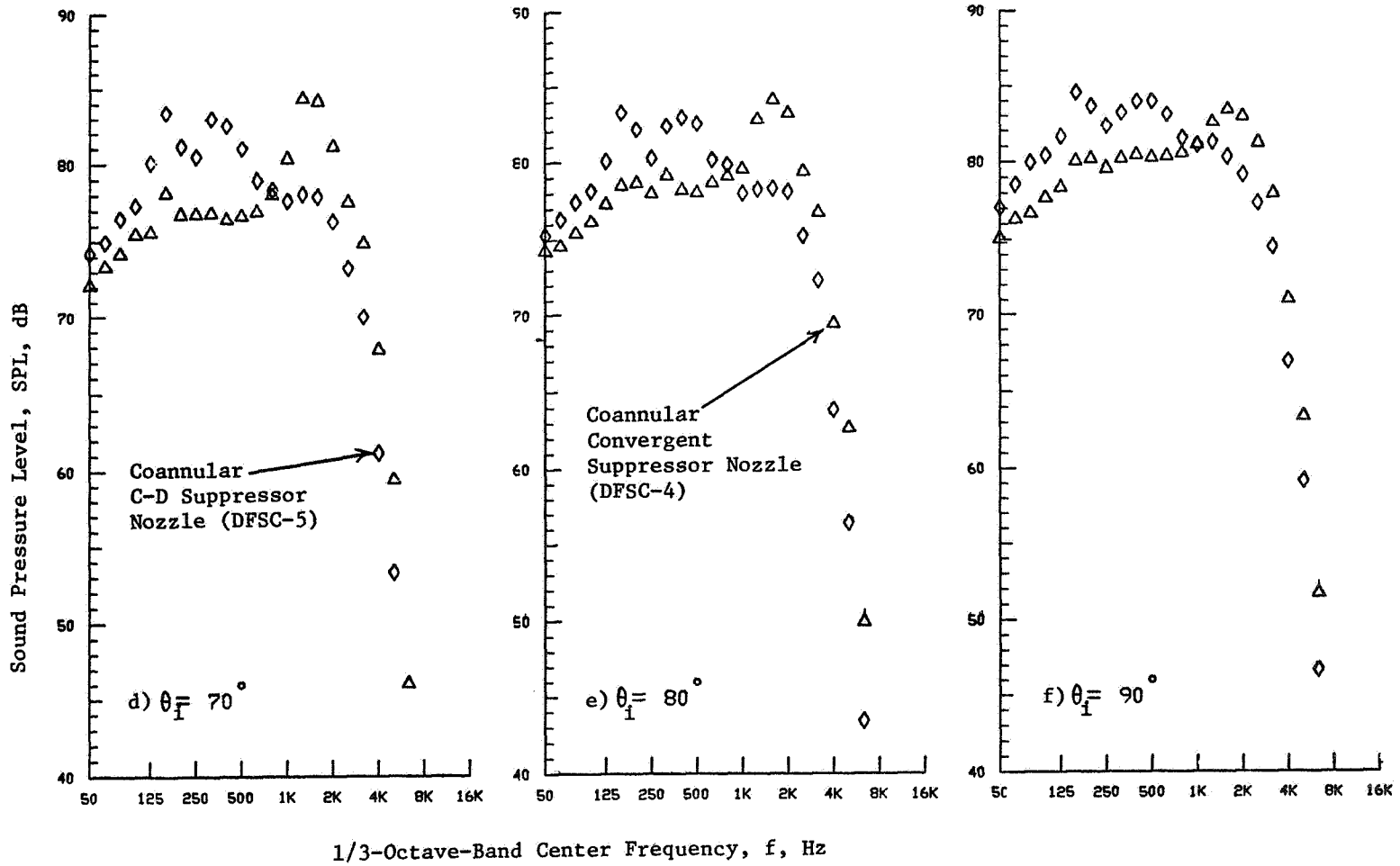

FIGURE 3-39. CONCLUDED.

(See Figure 3-37 for Aerodynamic Conditions)

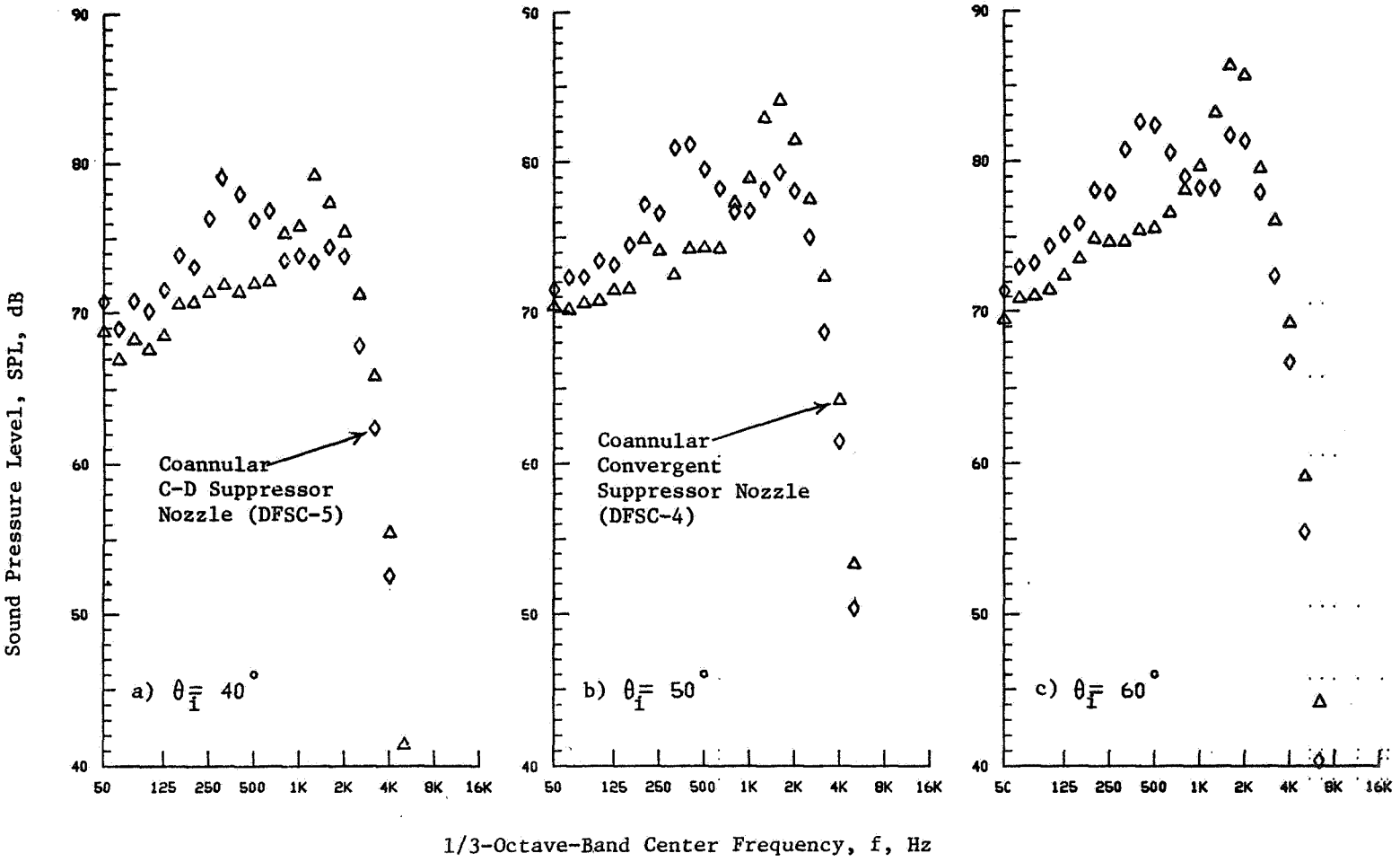

FIGURE 3-40. FRONT-QUADRANT SPECTRAL COMPARISON BETWEEN COANNULAR C-D AND CONVERGENT SUPPRESSOR NOZZLES AT C-D DESIGN CONDITIONS (SIMULATED FLIGHT).

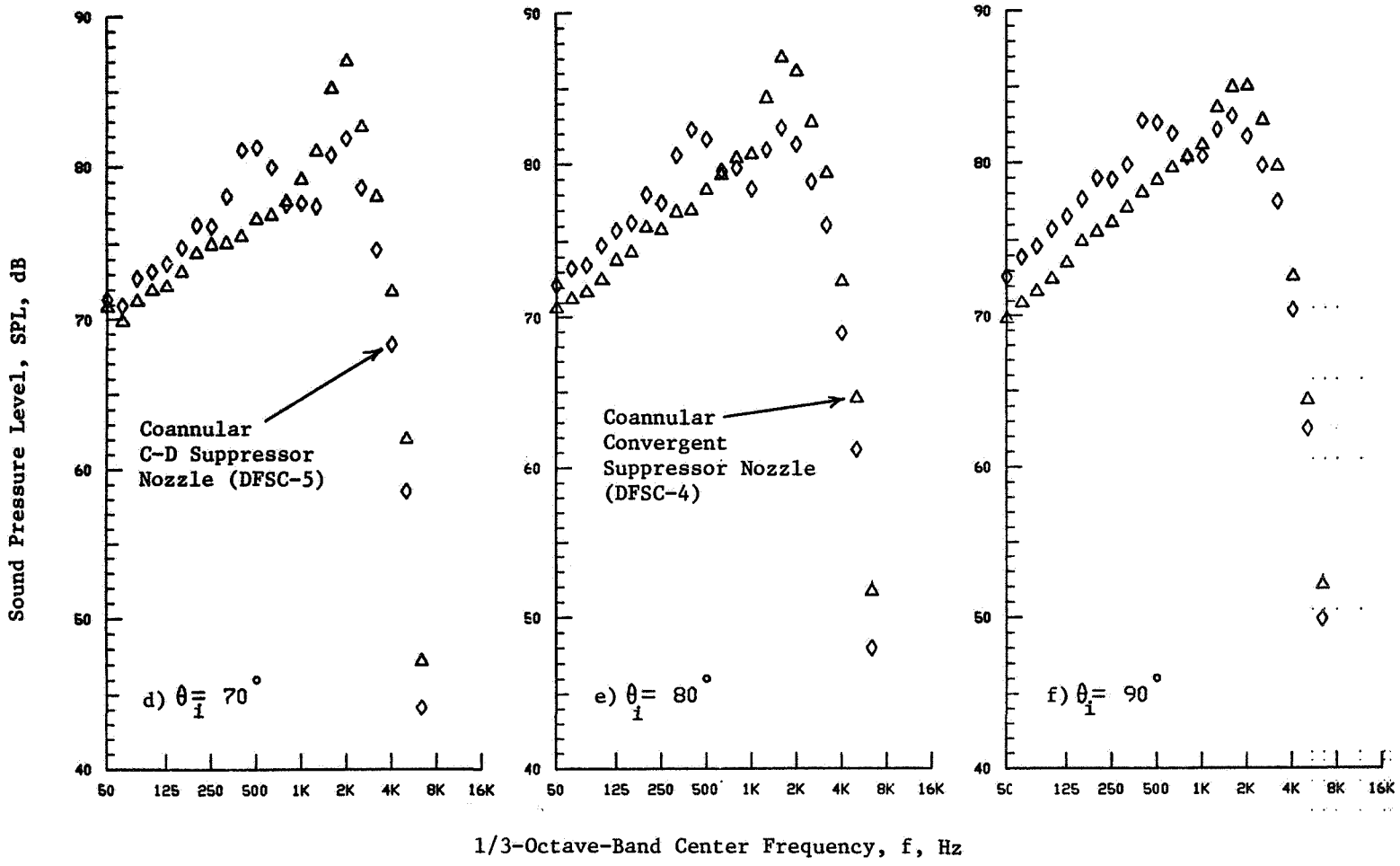

FIGURE 3-40. CONCLUDED.

- Region-A: The low frequency spectra of f $\leq$ 200 Hz ($\leq$ 250 for flight).

- Region-B: The middle frequency spectra of 200 Hz < f < 800 Hz that contains the broadband peak frequency of noise associated with shock-cells downstream of the plug of DFSC-5 (250 < f < 1,000 Hz for flight).

- Region-C: The high frequency spectra of f > 800 Hz (f > 1,000 Hz for flight) that contains the broadband peak frequency of noise associated with shock-cells on the plug of DFSC-4.

The spectra of Region-A is jet mixing noise related. The peak noted in the static spectra of the DFSC-5 nozzle at f = 160 Hz (Figure 3-38) is inferred to be a screech tone*. This tone is observed also to be invariant with the angle of observation as indicated by the front quadrant static data of Figure 3-39. Comparison of the spectra in the middle frequency Range-B in Figure 38 indicates (1) the presence of broadband peaks at f = 315 Hz and 400/500 Hz for the static and simulated flight cases of the C-D suppressor at θ_i = 60°, and (2) absence of such peaks in the spectra of convergent suppressor configuration. These observations in the spectral data of Range-B, that is dominated by noise due to shock-cells downstream of the plug,are in agreement with (1) the earlier calculated broadband peak frequencies due to the shock-cells downstream of the plug of DFSC-5 and (2) the absence of these downstream shock-cells with DFSC-4. Finally, in Region-C the spectral comparison indicates (1) a broadband peak at f = 1,250 Hz and 1,600 Hz for the static and simulated cases of the convergent suppressor at θ_i = 60° and (2) a significant reduction in the SPL values of these peaks with the C-D suppressor configuration. These observations, in the spectral region governed mainly by the noise due to shock-cells on the plug, again conforms with (1) the earlier estimated broadband peak frequencies due to the shock-cells on the plug of DFSC-4 and (2) a significant weakening of the plug shock-cells by the

---

* The screech tone frequency can be predicted from (Reference 23) $f_{screech} = U_c/L_{avg}(1+M_c)$. Using the measured L_{avg} of the downstream shock-cells, $f_{screech}$ = 200 Hz is obtained for the scaled DFSC-5 nozzle.

C-D termination of DFSC-5. Similar spectral observations at other front quadrant locations can be made from the set of data presented in Figures 3-39 and 3-40.

Sets of aft-quadrant spectral comparisons of the data of DFSC-4 and DFSC-5 are presented in Figures 3-41 and 3-42 for static and simulated flight conditions, respectively. The data indicate that, over the entire aft-quadrant, the convergent suppressor nozzle (DFSC-4) shows lower sound pressure levels than the C-D suppressor configuration except in the high frequency range. Since
low to middle frequency jet noise is produced in the region downstream of the plugs, this indicates higher rate of mean velocity decay downstream of the plug of the convergent suppressor nozzle. The LV measurements, presented in Figure 3-34(i), confirm the existence of subsonic flow in all regions downstream of the plug of DFSC-4 compared to the plume of the C-D suppressor nozzle which maintains supersonic speed up to ten equivalent diameters downstream of the plug.

3.4.3 Effect of Flight on Convergent and C-D Suppressor Coannular Shock-Cell Noise Data at C-D Design Conditions

The static measured acoustic data of coannular suppressor configurations DFSC-4 and DFSC-5 are compared in this subsection to their respective simulated flight (V_{ac} = 122 m/sec or 400 fps) results. The data in Figure 3-43 first summarizes the effect of flight on the measured PNL data at a typical forward-quadrant angle of Θ_i = 60° as a function of effective shock strength parameter β^{eff}. For comparison, similar data of convergent coannular nozzle with truncated plug (DFSC-1) and the C-D coannular nozzle with extended plug (DFSC-3) that were presented earlier in Figure 3-14 are repeated in this figure. An examination of this figure indicates that the amount of flight amplification of the front quadrant static PNL data of both of the suppressor configurations, for a given β^{eff}, are approximately equal to one another and to the amplification obtained with the convergent coannular configuration (DFSC-1). Minimum flight amplification in the vicinity of the C-D design conditions is observed only with C-D coannular nozzle with the extended plug (DFSC-3).

(See Figure 3-36 for Aerodynamic Conditions)

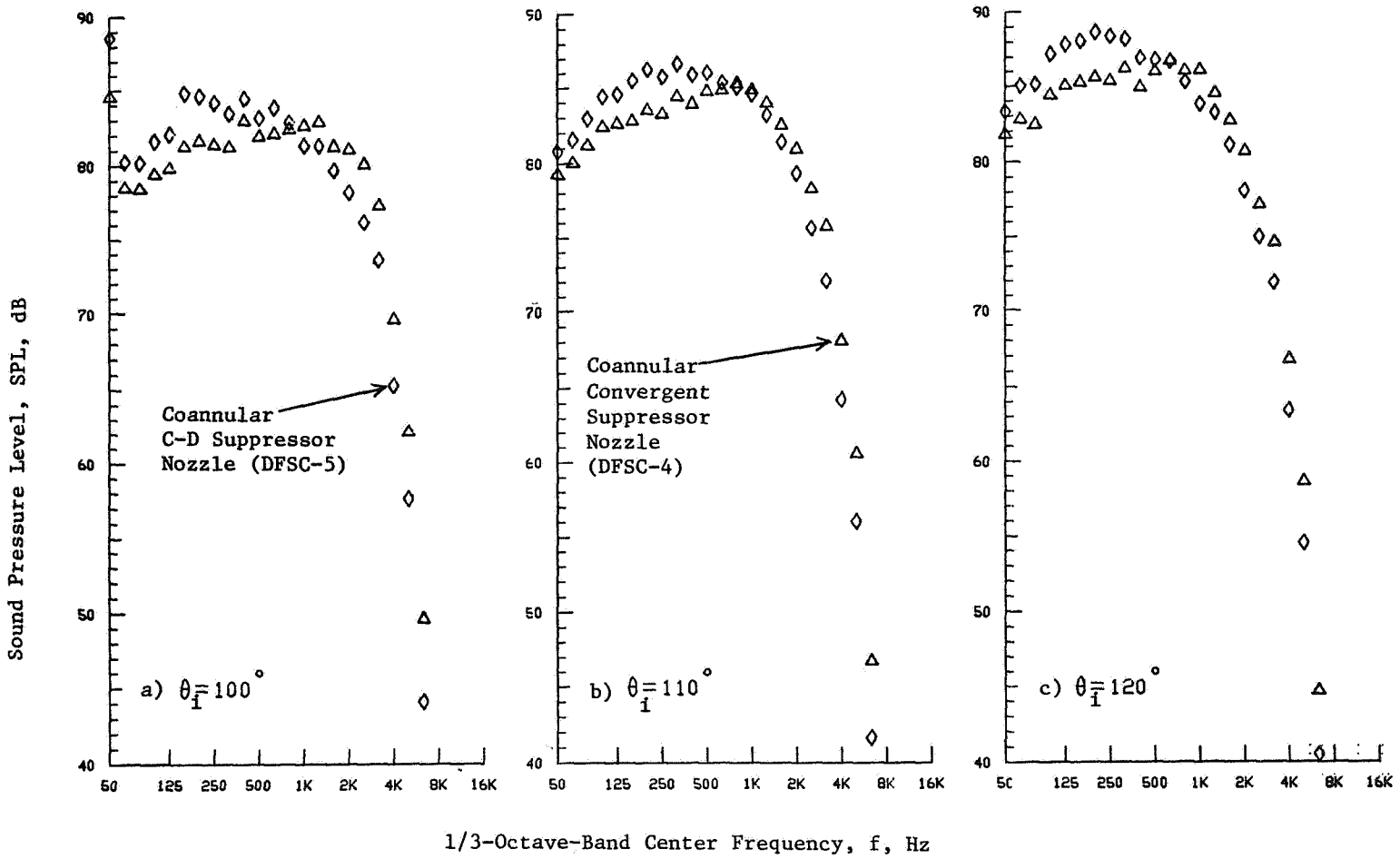

FIGURE 3-41. AFT-QUADRANT SPECTRAL COMPARISON BETWEEN COANNULAR C-D AND CONVERGENT SUPPRESSOR NOZZLES AT C-D DESIGN CONDITIONS (STATIC).

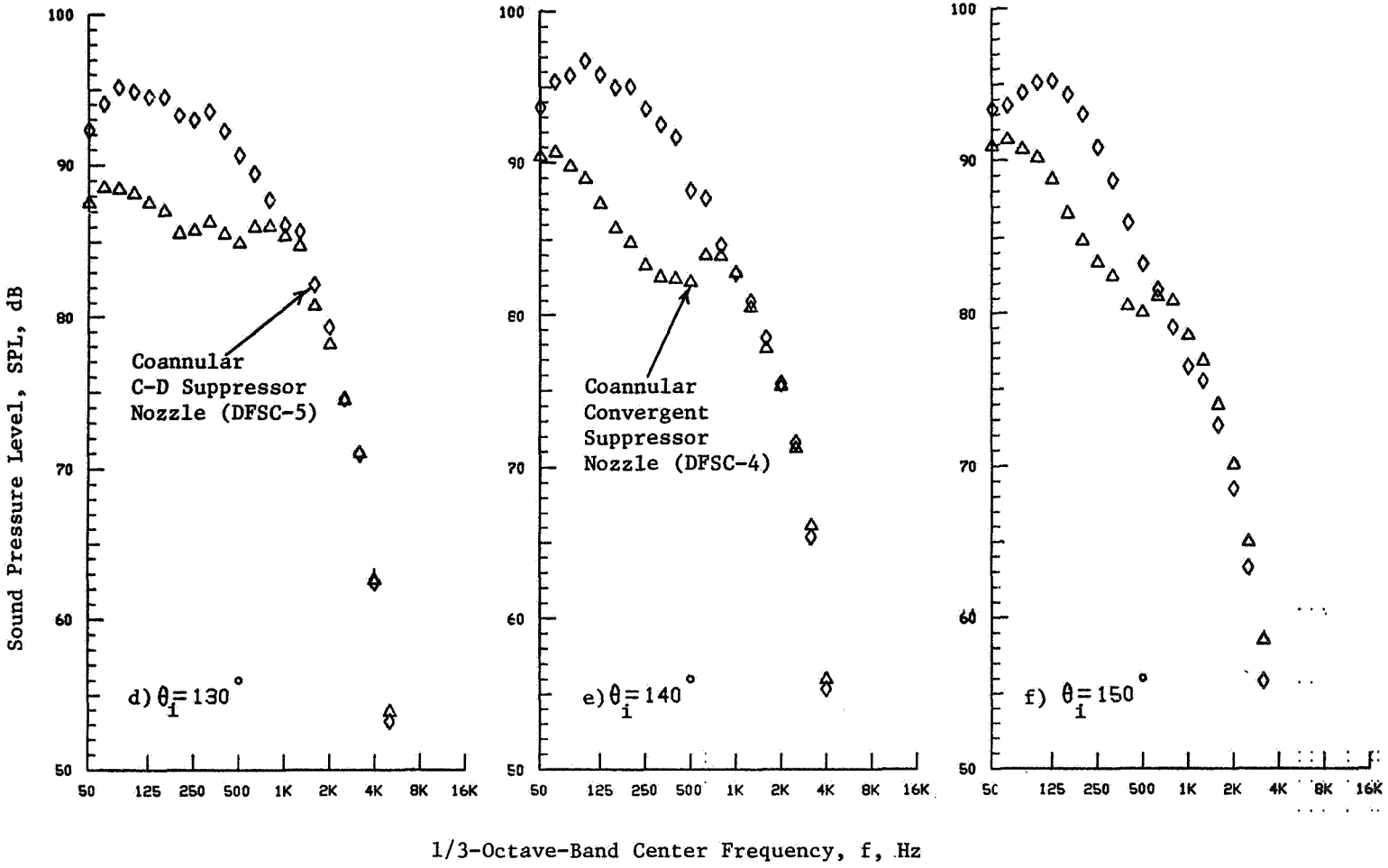

Figure 3-41. CONCLUDED.

(See Figure 3-37 for Aerodynamic Conditions)

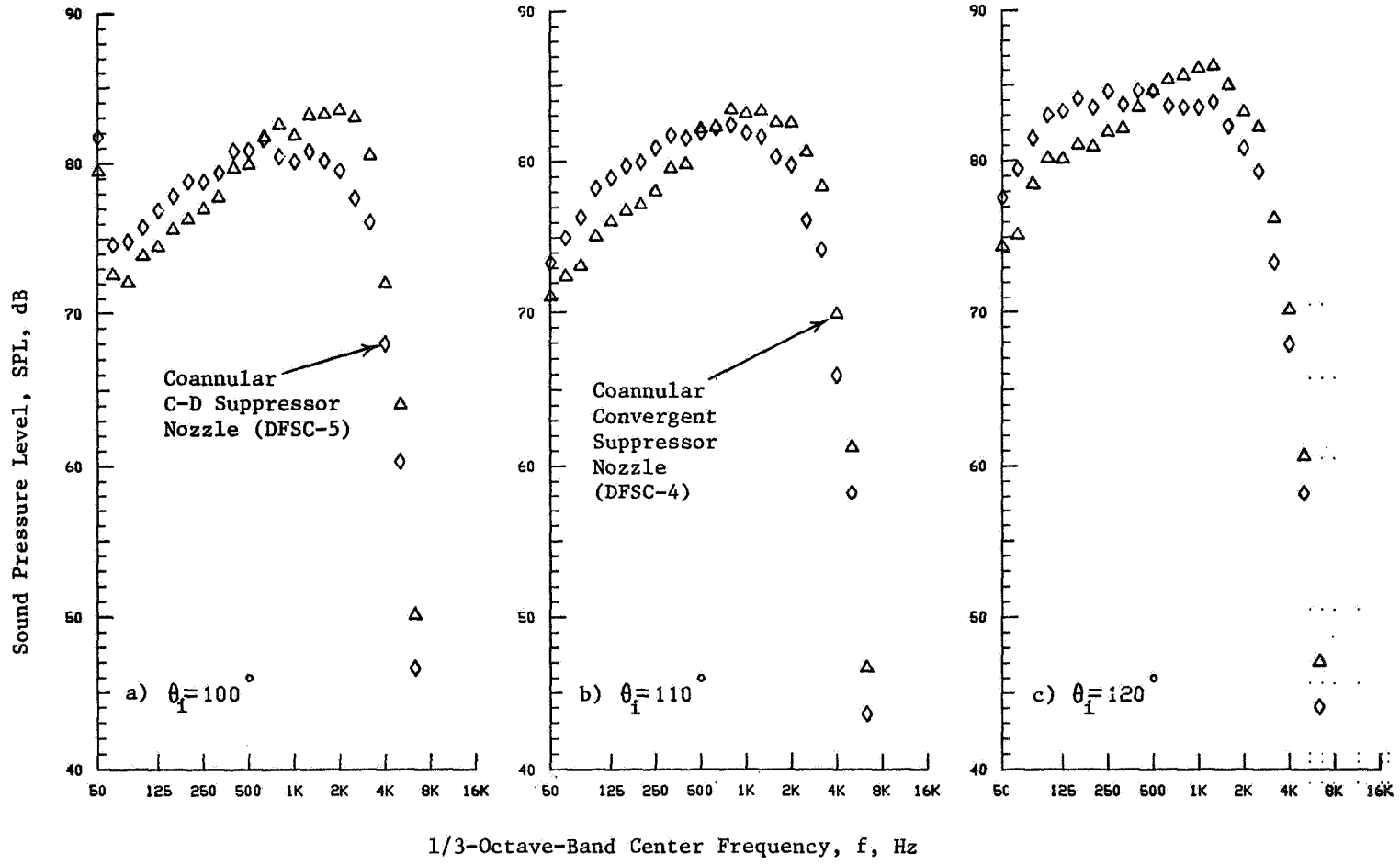

FIGURE 3-42. AFT-QUADRANT SPECTRAL COMPARISON BETWEEN COANNULAR C-D AND CONVERGENT SUPPRESSOR NOZZLES AT C-D DESIGN CONDITIONS (SIMULATED FLIGHT).

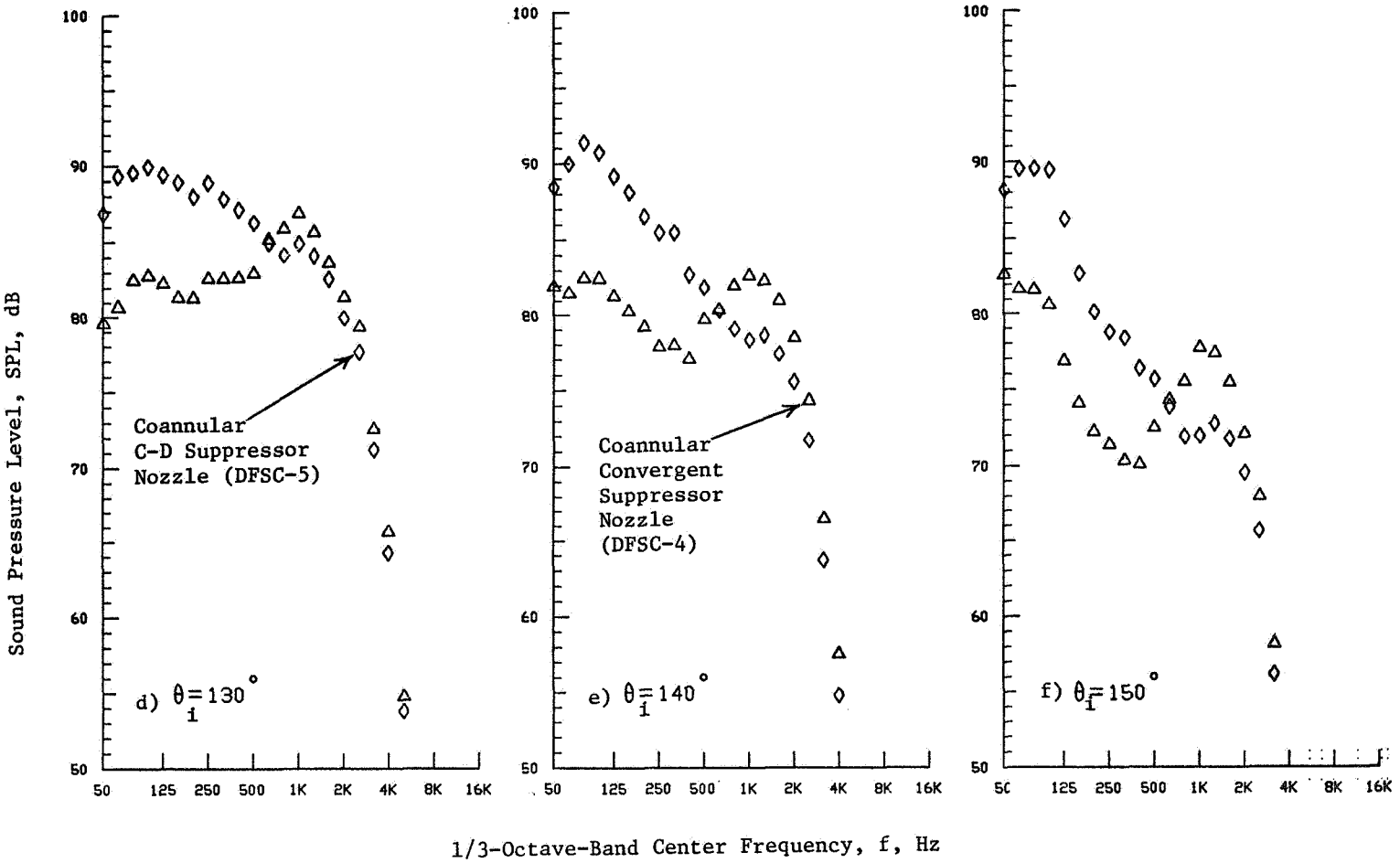

FIGURE 3-4.2. CONCLUDED.

DATA SCALED TO TOTAL NOZZLE AREA OF 0.903 m^2 (1400 $In.^2$)
AND EXTRAPOLATED TO 731.5 m (2400 Ft.) SIDELINE

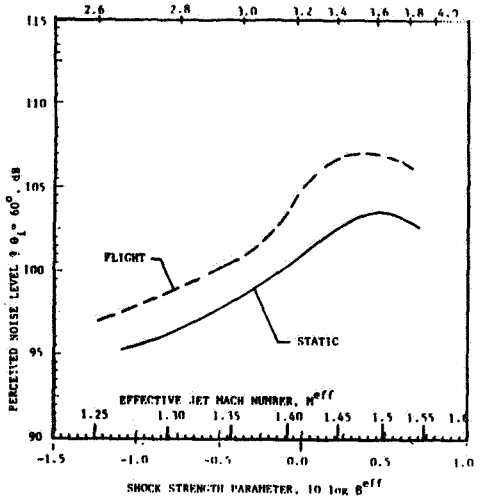

a) COANNULAR: CONVERGENT AND TRUNCATED PLUG (DFSC-1)

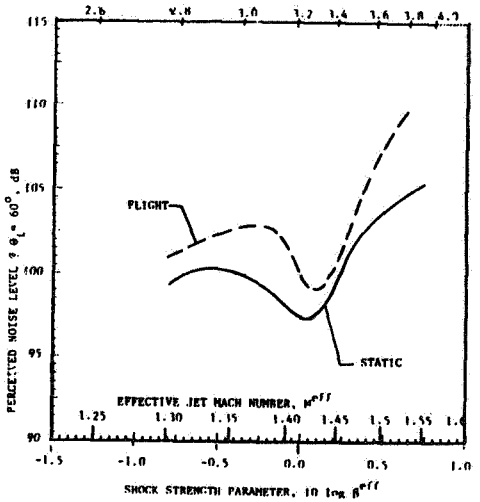

b) COANNULAR: C-D AND EXTENDED PLUG (DFSC-3)

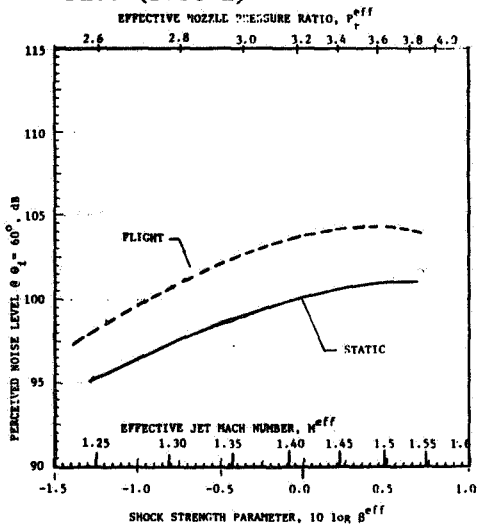

c) CONVERGENT SUPPRESSED COANNULAR (DFSC-4)

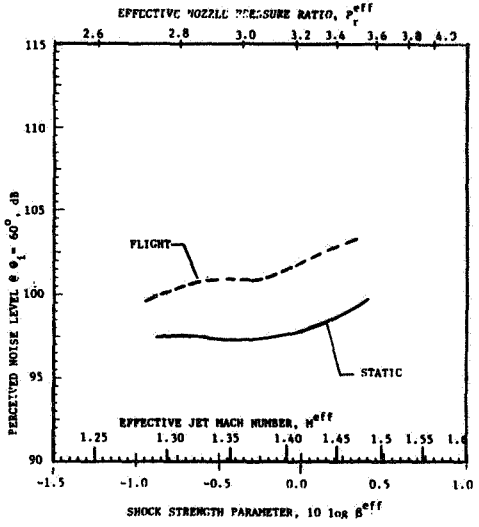

d) C-D SUPPRESSED COANNULAR (DFSC-5)

FIGURE 3-43. EFFECT OF FLIGHT ON FRONT-QUADRANT PNL DATA OF CONVERGENT COANNULAR, C-D COANNULAR WITH EXTENDED PLUG, AND CONVERGENT AND C-D SUPPRESSOR NOZZLES

The static measured PNL- and OASPL-directivities of the two coannular suppressor nozzles of this study at the design conditions of the C-D configuration are compared to their corresponding simulated flight data in Figures 3-44 and 3-45, respectively. The corresponding DFSC-4 and -5 selected front quadrant spectral comparisons are presented in Figures 3-46 and 3-47. The directivity data indicate that the front quadrant (at Θ_i = 60°) PNL amplifications are 3.6 and 3.4 dB and corresponding OASPL amplifications are 1.6 and ~0 dB for convergent and C-D suppressor configurations, respectively, due to flight.

3.5 EFFECT OF JET TEMPERATURE ON SHOCK-CELL NOISE

In this section, discussions on the influence of plume temperature for a given Mach number of the flow on the shock-cell noise of convergent unsuppressed and suppressed configurations (DFSC-1 and DFSC-4, respectively) are presented.

One of the items relevant to shock associated noise is the effect of jet plume temperature on shock-turbulence interactions. Based upon his work on shock associated noise from imperfectly expanded jets, Tanna (Reference 3) concluded that the overall intensity of shock associated noise is essentially independent of the jet efflux temperature. However, the analytical work by Howe and Ffowcs-Williams (Reference 24) on the noise generated by an imperfectly expanded supersonic jet predicted that the total radiated sound power, P, of shock associated noise is approximated by

$$P = \frac{\Pi a^2 \beta^2 p^2 U_c}{2\rho V_j^2}$$

where p is the excess pressure at the jet exit, β is the shock strength parameter, V_j and U_c represents the jet efflux velocity and the convection velocity, respectively, and ρ corresponds to the local flow density which is inversely proportional to the local flow temperature.

The complexity of the issue lies in the fact that the shock-cell noise component of imperfectly expanded supersonic jet noise is not isolated easily from the jet mixing noise component during the measurements. Since the jet

(SEE FIGURES 3-36 AND 3-37 FOR AERO-CONDITIONS.)

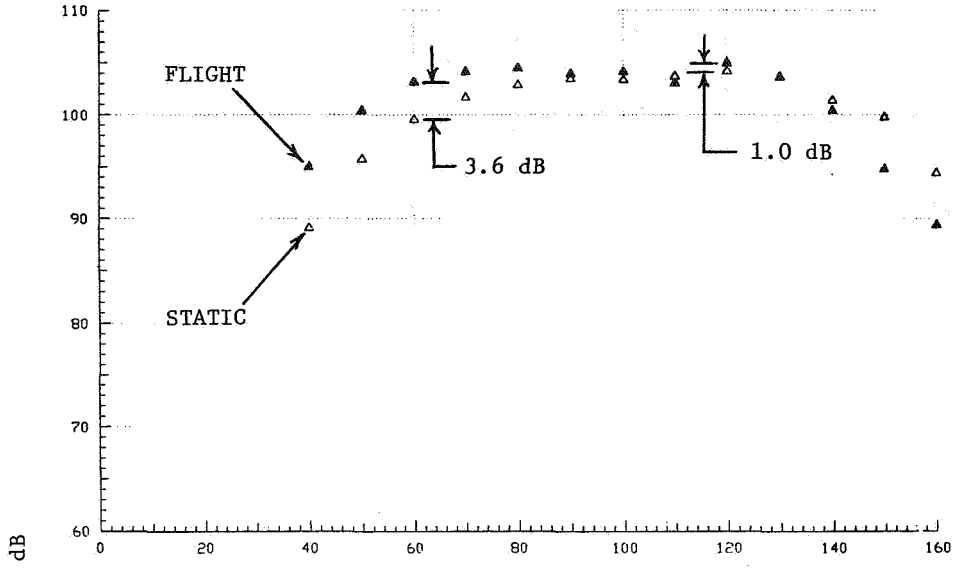

a) CONVERGENT SUPPRESSED COANNULAR NOZZLE (DFSC-4)

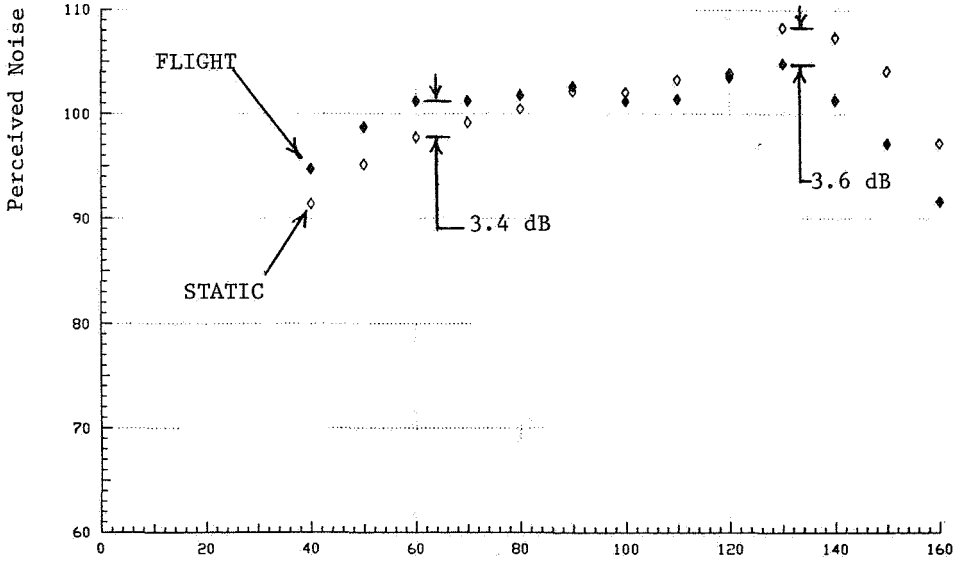

Perceived Noise Level, PNL, dB

b) C-D SUPPRESSED COANNULAR NOZZLE (DFSC-5)

FIGURE 3-44. EFFECT OF SIMULATED FLIGHT ON THE PNL-DIRECTIVITY OF CONVERGENT AND C-D SUPPRESSOR NOZZLES AT C-D DESIGN CONDITIONS.

(SEE FIGURES 3-36 AND 3-37 FOR AERO-CONDITIONS.)

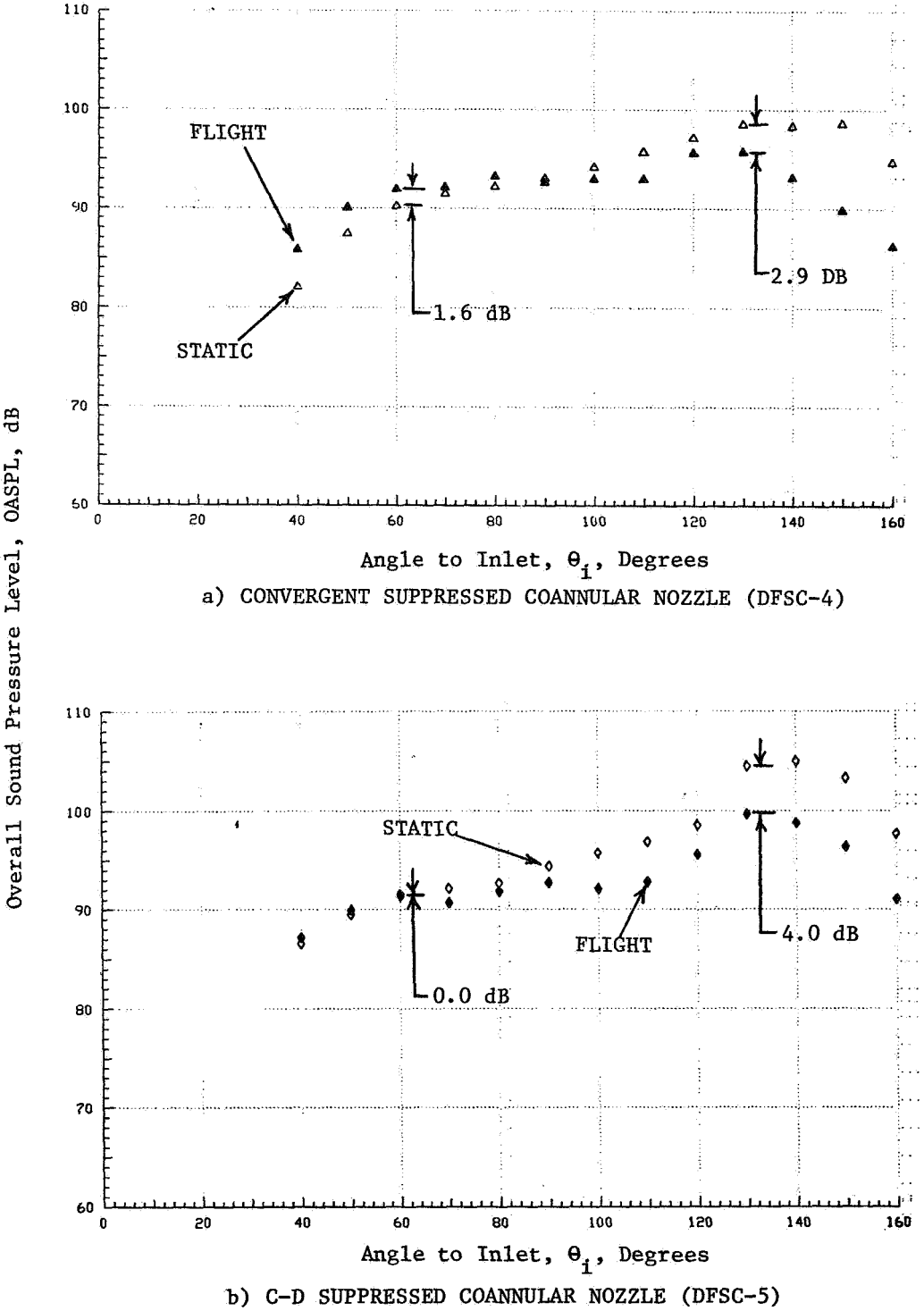

FIGURE 3-45: EFFECT OF SIMULATED FLIGHT ON THE OASPL-DIRECTIVITY OF CONVERGENT AND C-D SUPPRESSOR NOZZLES AT C-D DESIGN CONDITIONS.

(SEE FIGURES 3-36 AND 3-37 FOR AERO-CONDITIONS.)

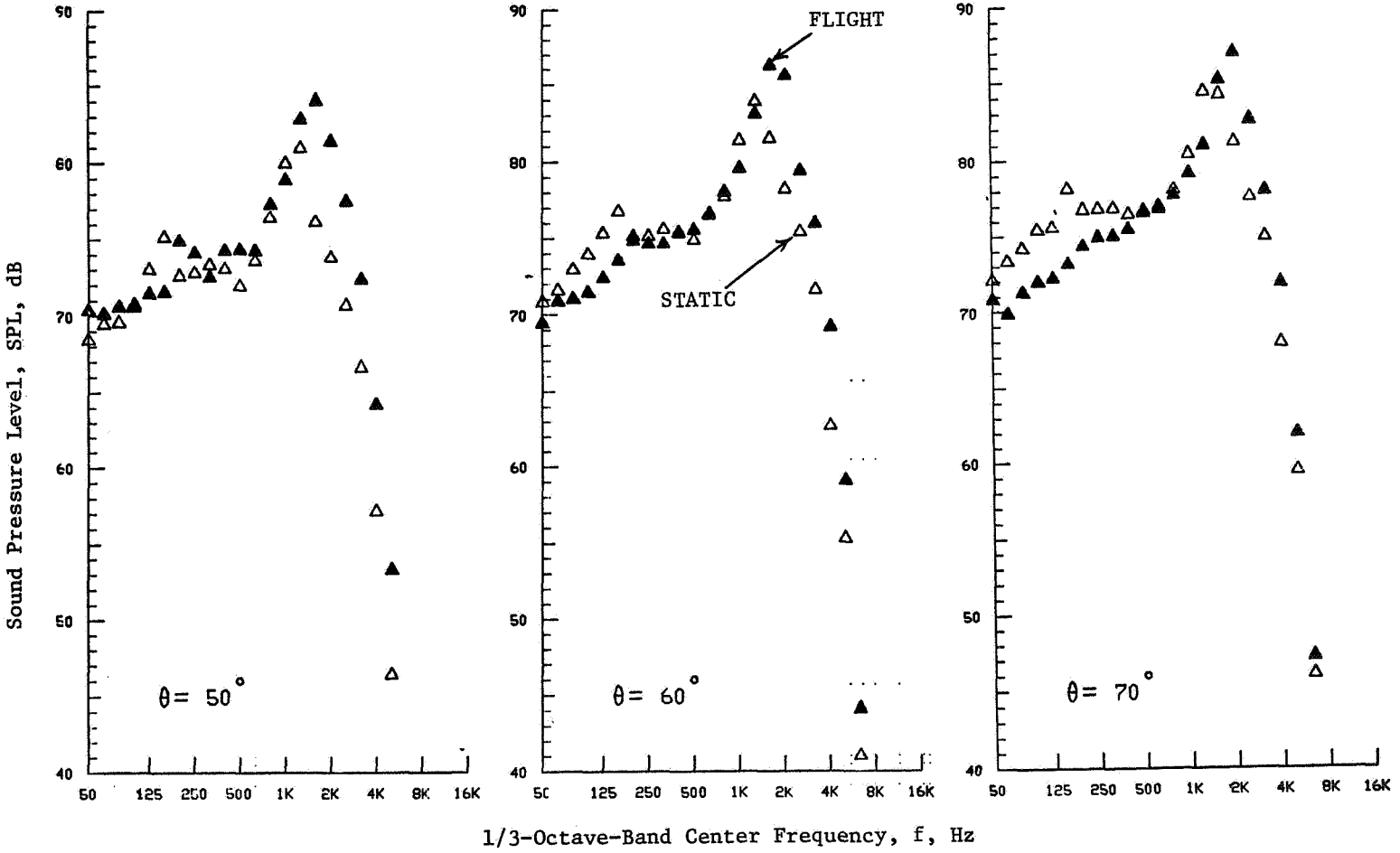

FIGURE 3-46. EFFECT OF SIMULATED FLIGHT ON TYPICAL FRONT QUADRANT SPECTRA OF CONVERGENT SUPPRESSOR NOZZLE AT C-D DESIGN CONDITION OF DFSC-5.

(SEE FIGURES 3-36 AND 3-37 FOR AERO-CONDITIONS.)

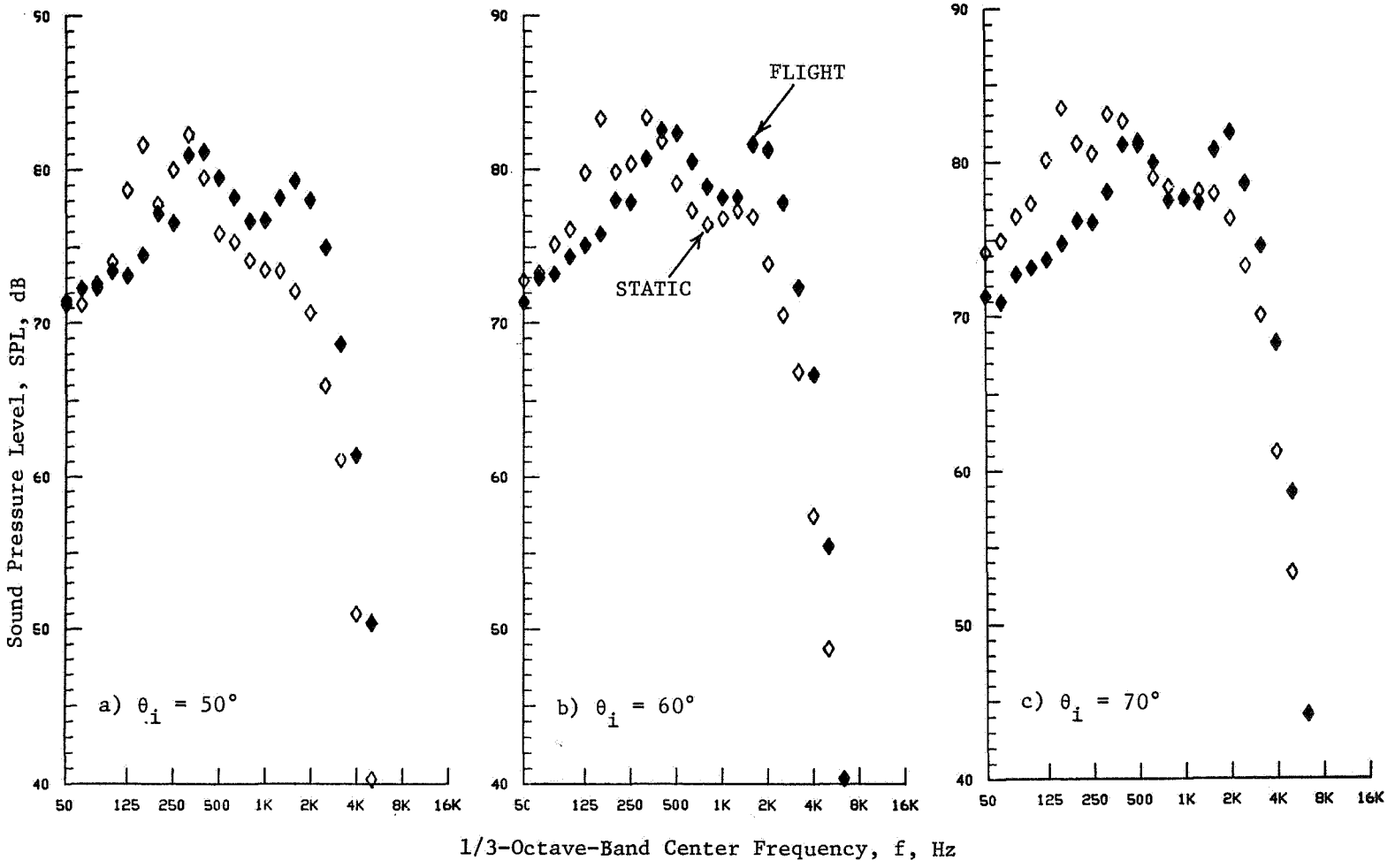

FIGURE 3-47. EFFECT OF SIMULATED FLIGHT ON TYPICAL FRONT QUADRANT SPECTRA OF C-D SUPPRESSOR NOZZLE (DFSC-5) AT C-D DESIGN CONDITION.

mixing noise follows the V^8 law, and increasing jet temperature (at a given pressure ratio) increases jet velocity, heated jets are generally noisier than their cold counterparts.

In this subsection results of a comparative study of shock-cell noise characteristics between moderately heated (T_T^o ~ 870°R) and high temperature (T_T^o ~ 1700°R) jets are presented. The overall and spectral characteristics of shock-cell noise produced under different flow temperatures by the baseline convergent coannular nozzle with a truncated plug (DFSC-1) and the convergent coannular suppressor plug nozzle (DFSC-4) are discussed.

Forward quadrant PNL at θ_i = 60°, as a function of the effective shock strength parameter (β^{eff}) and obtained under static and simulated flight conditions with the baseline convergent coannular plug nozzle (DFSC-1), are presented in Figure 3-48. Two sets of data, which correspond to the moderately heated and high temperature cases, are presented. Since the inner flow aerodynamic conditions were maintained identical during both the series of tests, the presented data can be regarded to indicate the effect of outer stream temperature on PNL_{60}. An examination of Figure 3-48 indicates no appreciable difference between the two sets of data except at high pressure ratios of the flight case. Similar comparison of the data for the convergent coannular suppressor nozzle (DFSC-4) is made in Figure 3-49, indicating a similar conclusion regarding the effect of the temperature. This result is consistent with the conclusion derived from the test data with the single flow nozzles (Reference 25).

PNL- and OASPL-directivity of DFSC-1 configuration operating at the two temperatures, under static and simulated flight conditions, are illustrated in Figures 3-50 and 3-51. The data indicate, that in the forward quadrant, the moderately heated jet is associated with a relatively higher PNL and OASPL under both static and simulated flight conditions. This partially could be due to the screech which was identified to be present with most of the moderately heated model jets and generally absent with the high temperature streams. The on-line narrowband data at θ_i = 60° (filter bandwidth = 25 Hz) obtained during these tests are presented in Figure 3-52 to indicate the presence of the screech fundamental during the cold tests. The first harmonic of the screech coincides with the shock-cell broadband peak frequency associated with the shock-cells downstream of the plug and hence is not identified in this figure.

DATA SCALED TO TOTAL NOZZLE AREA OF 0.903 m^2 (1400 $In.^2$)
AND EXTRAPOLATED TO 731.5 m (2400 Ft.) SIDELINE

$P_r^i \sim 3.13$, $T_T^i \sim 860^oR$

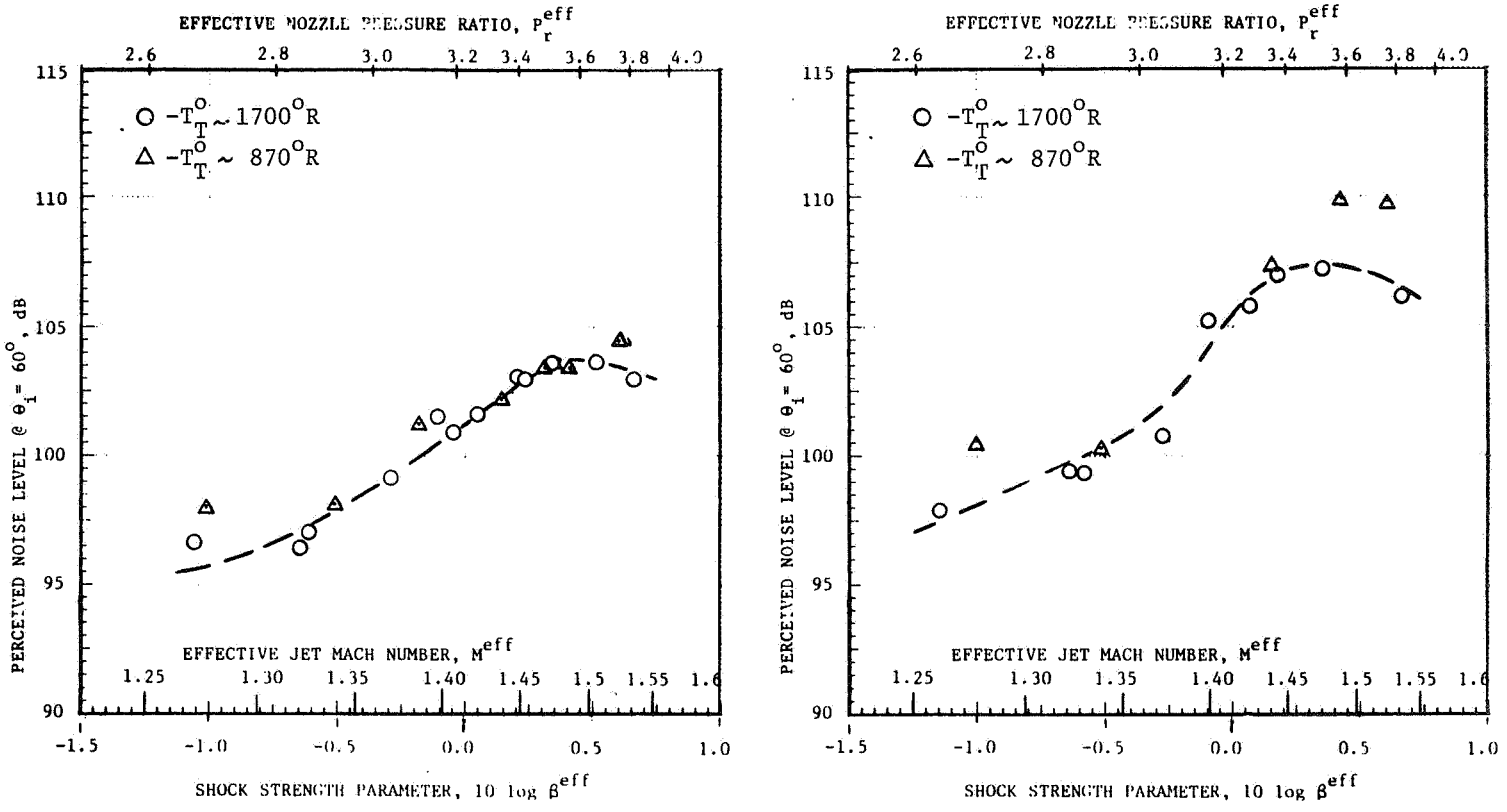

FIGURE 3-48. EFFECT OF OUTER STREAM TEMPERATURE ON THE FRONT QUADRANT PERCEIVED NOISE LEVEL DATA (AT θ_i=60°) OF CONVERGENT COANNULAR NOZZLE WITH TRUNCATED PLUG (DFSC-1).

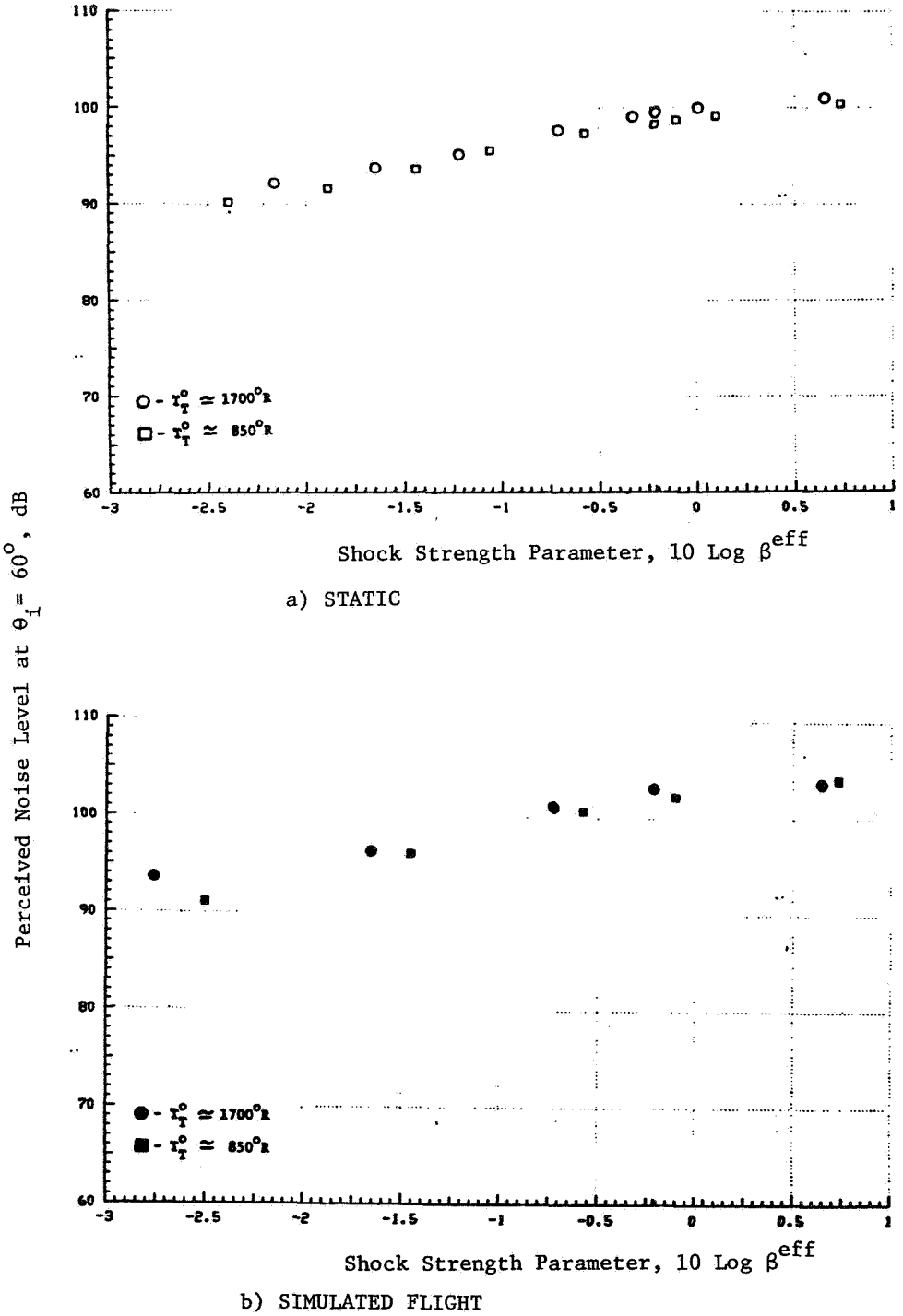

FIGURE 3-49. EFFECT OF OUTER STREAM TEMPERATURE ON THE FRONT QUADRANT PERCEIVED NOISE LEVEL DATA (AT $\theta_i = 60^o$) OF CONVERGENT COANNULAR SUPPRESSOR NOZZLE (DFSC-4).

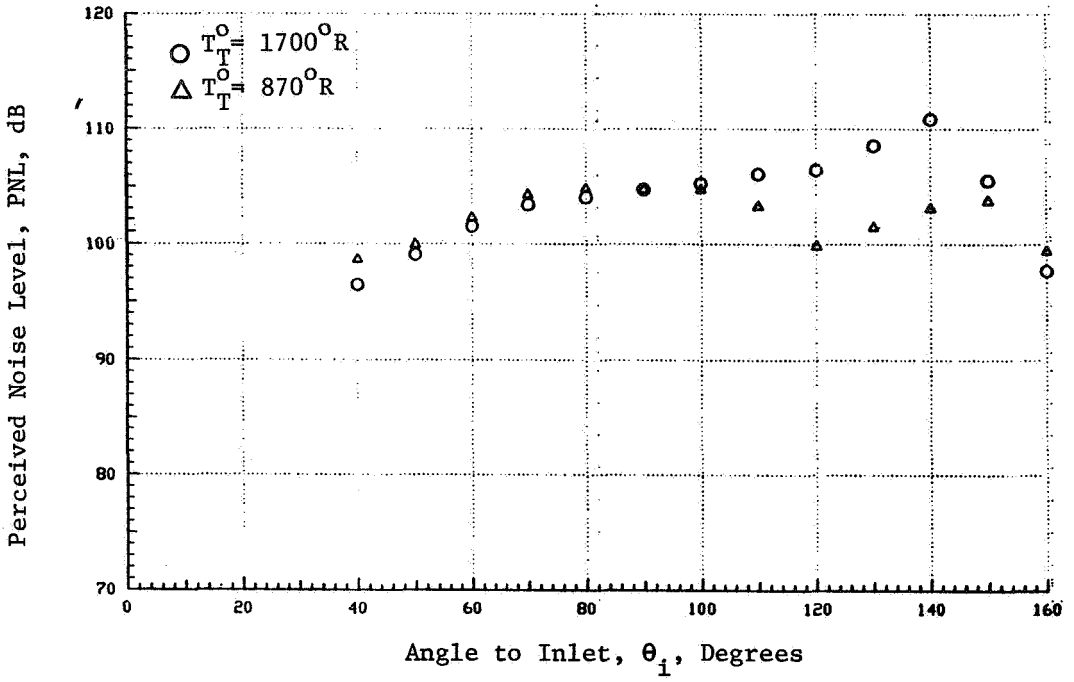

a) PNL - DIRECTIVITY

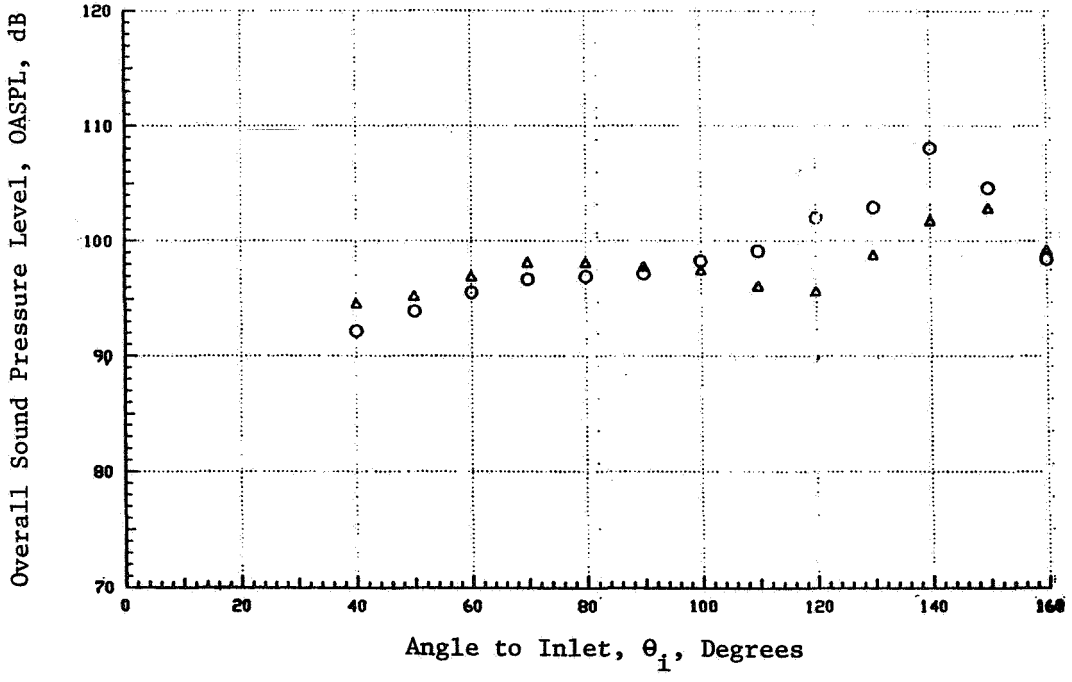

b) OASPL - DIRECTIVITY

FIGURE 3-50. EFFECT OF OUTER STREAM TEMPERATURE ON PNL - OASPL - DIRECTIVITY OF CONVERGENT COANNULAR NOZZLE WITH TRUNCATED PLUG (DFSC-1, STATIC).

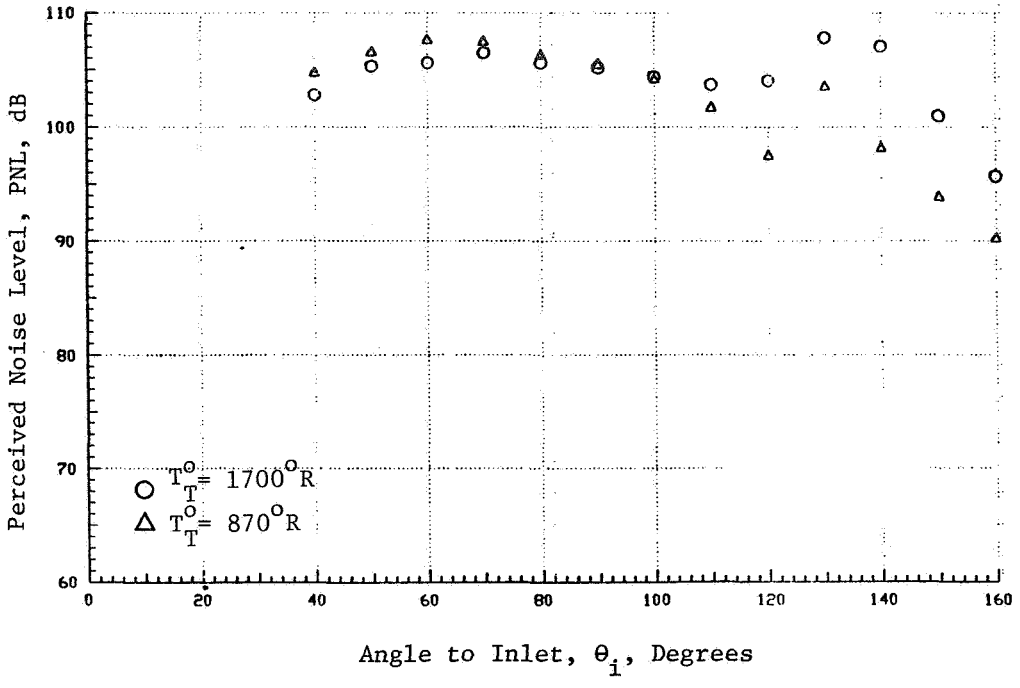

a) PNL - DIRECTIVITY

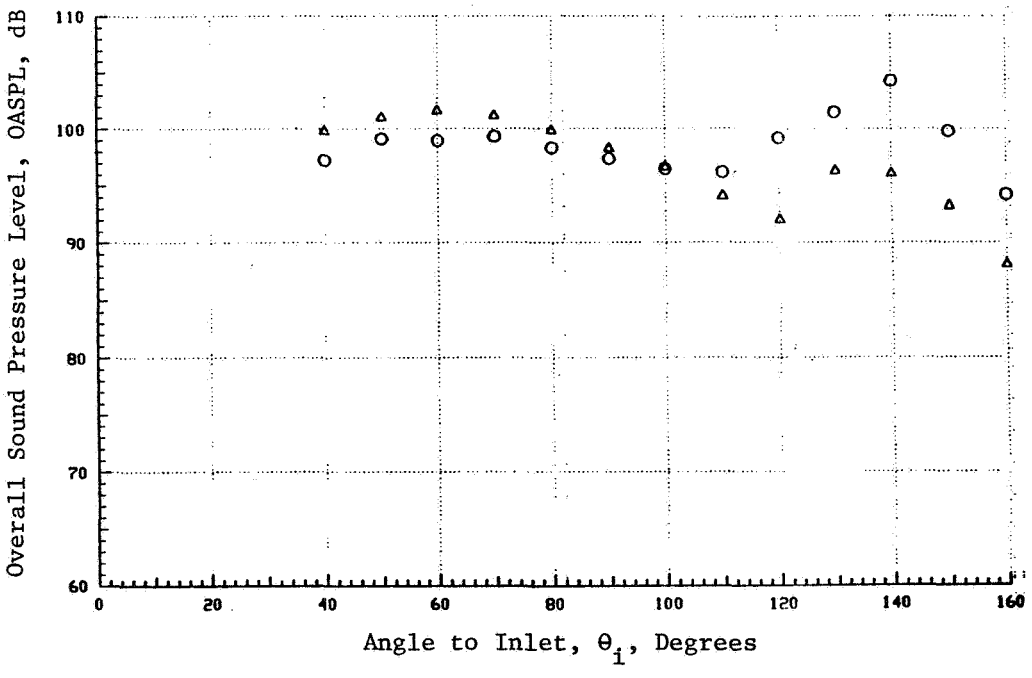

b) OASPL - DIRECTIVITY

FIGURE 3-51. EFFECT OF OUTER STREAM TEMPERATURE ON PNL- AND OASPL-DIRECTIVITY OF CONVERGENT COANNULAR NOZZLE WITH TRUNCATED PLUG (DFSC-1, SIMULATED FLIGHT).

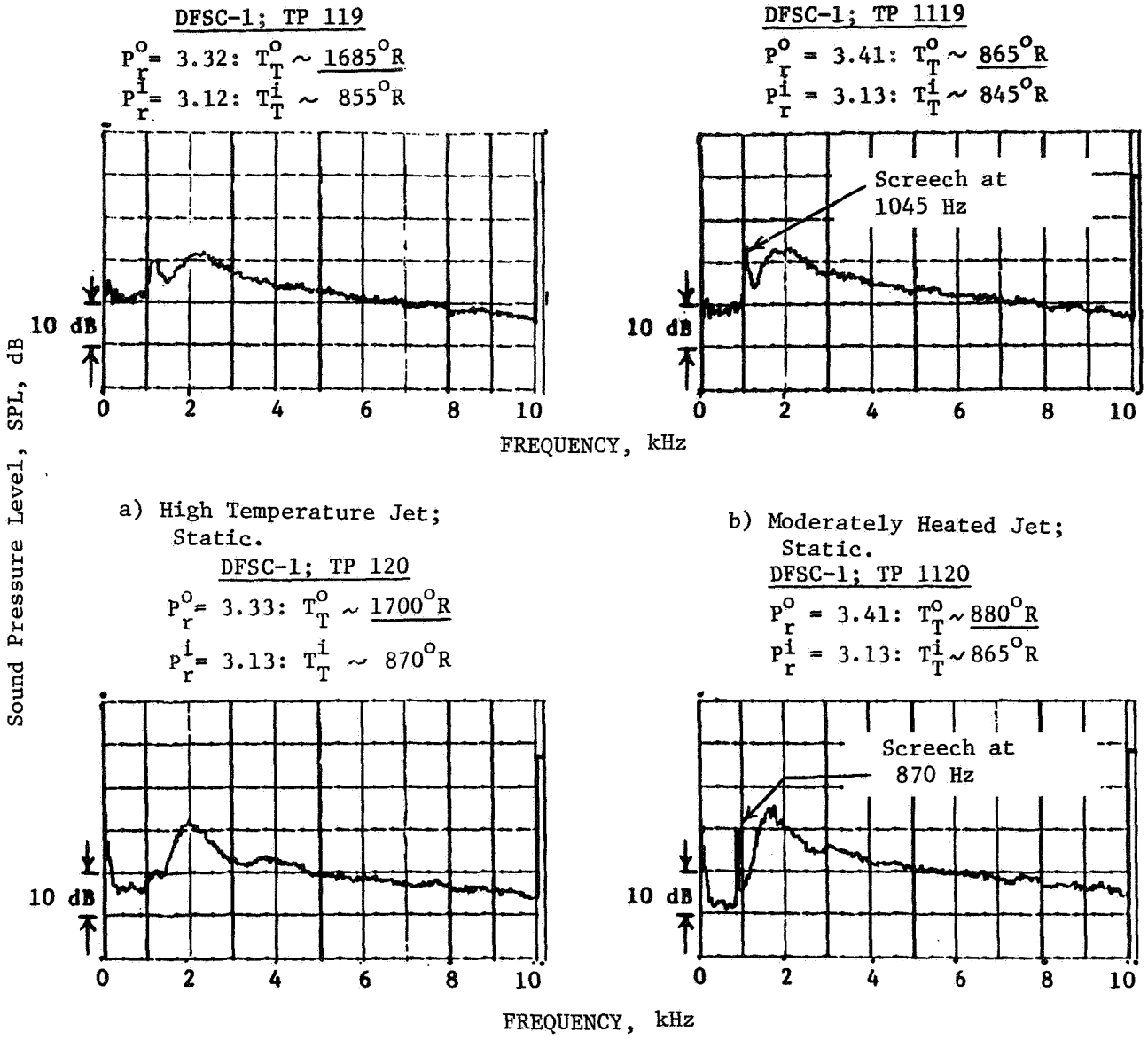

FIGURE 3-5.2. ON-LINE NARROWBAND DATA OBTAINED WITH CONVERGENT COANNULAR NOZZLE AT TWO OUTER STREAM TEMPERATURES.

Selected diagnostic LV test results obtained under these test conditions are presented in Figure 3-53. This figure indicates the earlier observed (Figure 3-5) two shock-cell structures for both the test conditions. The one on the plug, governed by the outer stream, is observed to be very similar in profile for the two temperatures outer stream indicating identical shock-cells on the plug. Because of the significant differences in the outer stream temperatures, the mean velocities are different between the two test points. The downstream shock-cell structure along the centerline of the nozzle appears not to be affected over a considerable axial distance from the plug tip by the change in the outer stream temperature indicating that it is basically a function of the inner stream flow.

Typical front quadrant spectra of the convergent coannular nozzle with truncated plug obtained with the two outer stream temperatures are presented in Figures 3-54 and 3-55 for the static and simulated flight cases, respectively. The figure indicates that in the high frequency region (similar to Region-C of Figure 3-11), the spectral data agree with one another indicating equivalent shock-cell structures on the plug. The higher SPL at the peak frequency in the mid-frequency region (similar to Region-B of Figure 3-11), observed with the moderately heated outer stream, probably is due to the first harmonic of the observed screech that coincided with the shock broadband peak frequency due to the downstream shock-cells. The lower frequency spectra which is jet mixing noise related, indicates the differences in levels due to the different stream velocites.

Based on the above observations it is concluded that variation in the plume temperatures of convergent coannular plug nozzles has negligible effect on shock-cell noise.

3.6 EFFECT OF SIMULATED FLIGHT ON LOCATION OF SONIC LINE NEAR THE JET EXIT

A limited number of LV radial traverses were conducted during the present study with the aim to identify the effect of flight on the sonic line near the jet exit. It is appropriate, at the outset, to review the significance of the sonic line in the shock-cell noise generation. A shock-cell is defined as a segment of the jet plume between the two consecutive intersections between a shock and the sonic line. A sonic line is located within the shear layer, and the embedded shock system in the jet plume

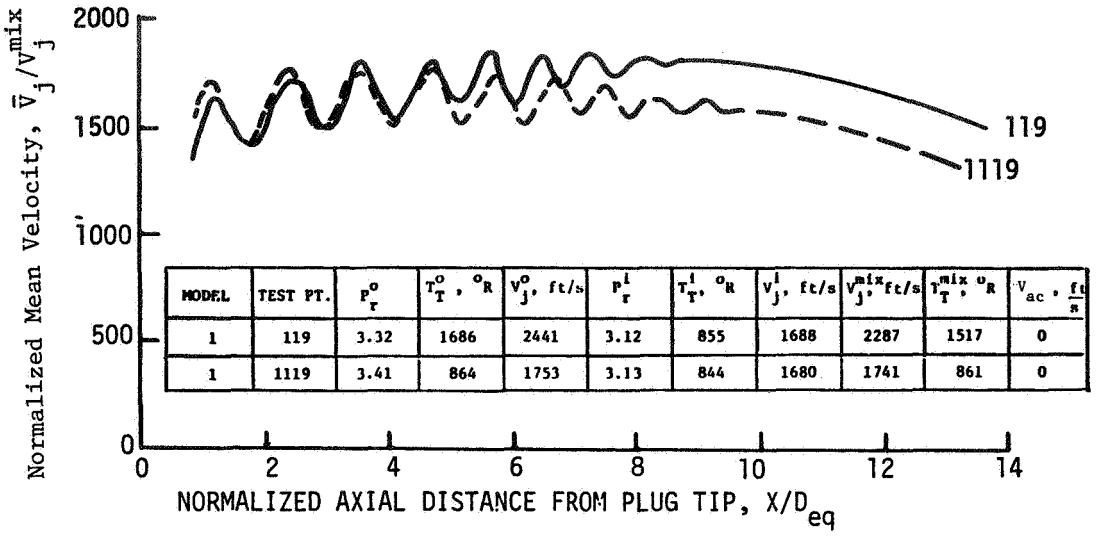

MODEL	TEST PT.	P_r^o	T_T^o, °R	V_j^o, ft/s	P_r^i	T_T^i, °R	V_j^i, ft/s	V_j^{mix} ft/s	T_T^{mix}, °R	V_{ac}, ft/s
1	119	3.32	1686	2441	3.12	855	1688	2287	1517	0
1	1119	3.41	864	1753	3.13	844	1680	1741	861	0

a) CENTERLINE AXIAL TRAVERSE

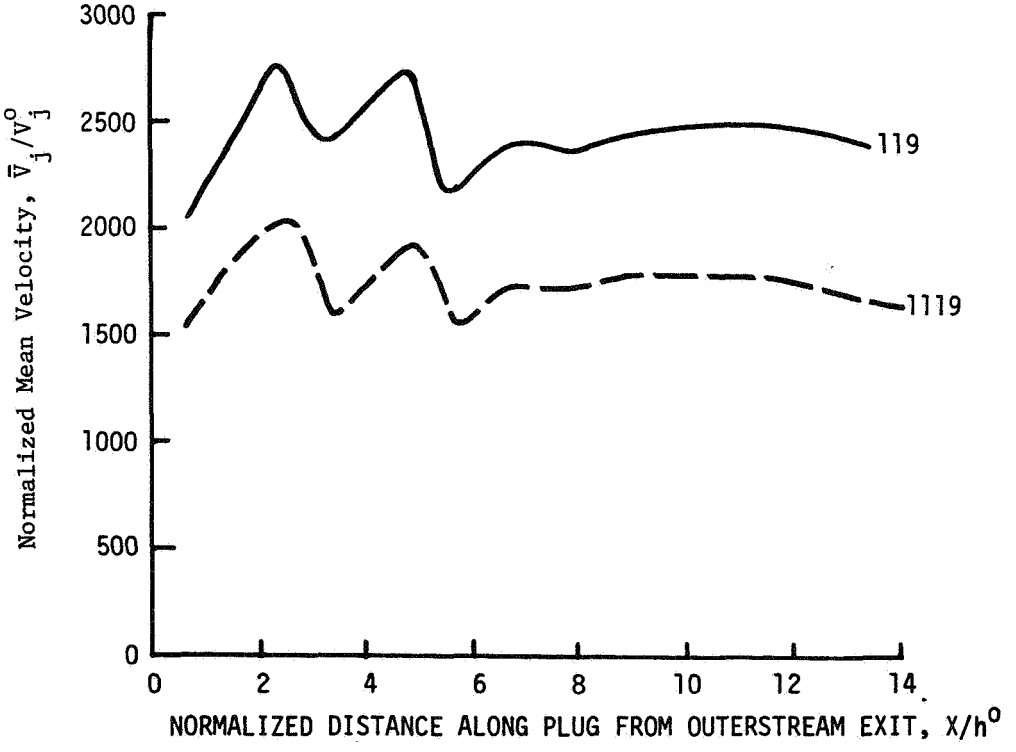

b) TRAVERSE PARALLEL TO PLUG SURFACE

FIGURE 3-53. COMPARISON OF MEAN VELOCITY DISTRIBUTIONS OF CONVERGENT COANNULAR PLUG NOZZLE AT TWO OUTER STREAM TEMPERATURES (STATIC).

MODEL	TEST PT.	P_T^o	T_T^o, °R	V_j^o, ft/s	P_T^i	T_T^i, °R	V_j^i, ft/s	V_j^{mix}, ft/s	T_T^{mix}, °R	V_{ac}, ft/s
1	119	3.32	1686	2441	3.12	855	1688	2287	1517	0
1	1119	3.41	864	1753	3.13	844	1680	1741	861	0

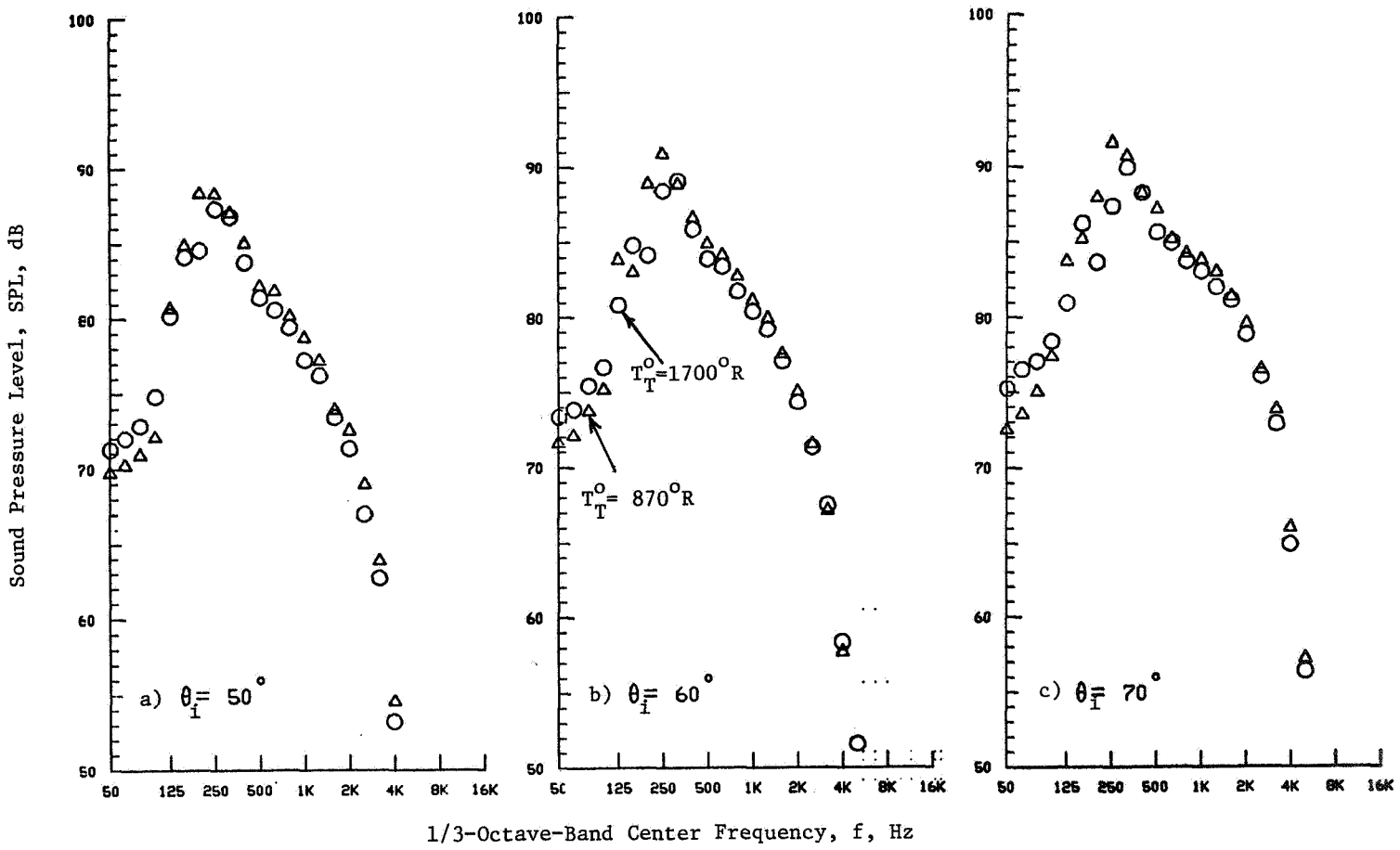

FIGURE 3-54. EFFECT OF OUTER STREAM TEMPERATURE ON THE FRONT QUADRANT SPECTRA OF CONVERGENT COANNULAR NOZZLE WITH TRUNCATED PLUG (DFSC-1, STATIC).

MODEL	TEST PT.	P_T^o	T_T^o, °R	V_j^o, ft/s	P_r^i	T_T^i, °R	V_j^i, ft/s	V_j^{mix} ft/s	T_T^{mix}, °R	V_{ac}, ft/s
1	120	3.33	1699	2452	3.13	869	1703	2300	1530	400
1	1120	3.41	880	1768	3.13	866	1701	1758	878	400

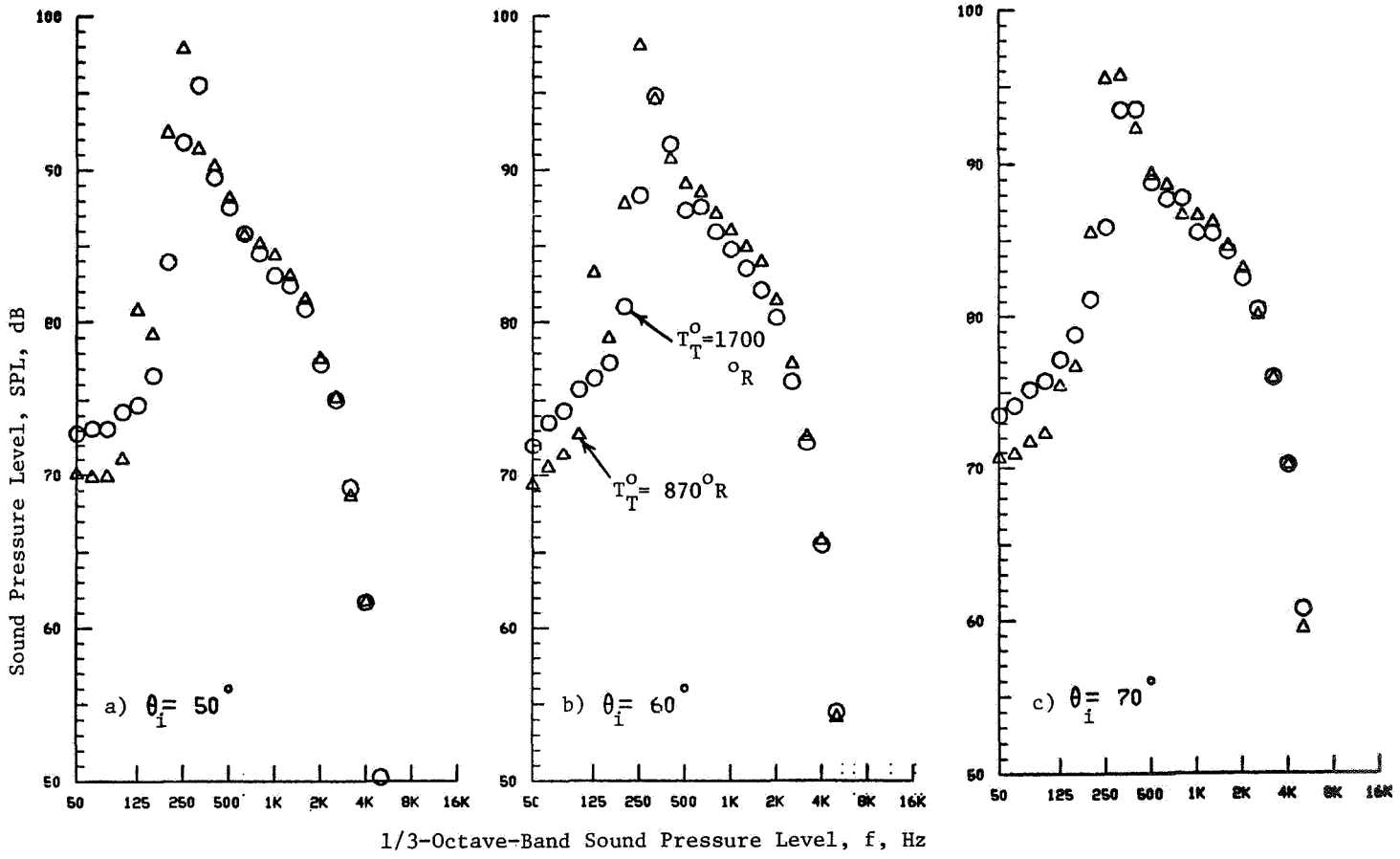

FIGURE 3-55. EFFECT OF OUTER STREAM TEMPERATURE ON THE FRONT QUADRANT SPECTRA OF CONVERGENT COANNULAR NOZZLE WITH TRUNCATED PLUG (DFSC-1, SIMULATED FLIGHT).

will not extend beyond this line. From a detailed nearfield study of shock containing supersonic flows, Seiner and Norum (Reference 10) indicated that the locations of the minimum Mach number agree well with the locations of closest approach of the sonic line to the jet centerline. That is to say, the points on a wavy sonic line which approach closest to the jet axis correspond to the locations where shock waves (or expansion waves) terminate. As is known, free-jet addition to an imperfectly expanded supersonic jet flow tends to stretch the shock-cell spacing, and, therefore, it may be reasonable to suspect that the sonic line may be shifted by the presence of the free-jet. Based on these considerations, a limited number of LV radial traverses near the jet exit (and on the plug surface) was performed. Some representative results of this survey are presented in this section. Selected nozzles for this study included:

- DFSC-2: C-D coannular nozzle with truncated plug.
- DFSC-4: Multi-element suppressor nozzle with convergent terminations in outer/inner flowpaths.

Figures 3-56 and 3-57 illustrate composite flow field pictures near the jet exit of these two nozzles. Figures 3-56a and 3-57a compare the static with simulated flight measured axial mean velocity distributions along the outer nozzle lip-line obtained with point-histograms. Turbulence intensity distributions measured with these histograms on the outer nozzle lip-line are compared in Figures 3-56b and 3-57b. The sonic lines determined from the radial mean velocity profiles near the plug surface are presented in Figures 3-56c and 3-57c.

The selected test points have the following aerodynamic conditions:

Model	Test Point	P_r^o	T_T^o (^oR)	P_r^i	T_T^i (^oR)	V_{ac} (fps)	P_r^{mix}	T_T^{mix}	Remarks
DFSC-2	219	3.32	1679	3.12	862	0	3.22	1494	C-D design conditions
DFSC-2	220	3.33	1695	3.12	873	400	3.23	1509	
DFSC-4	1415	3.32	844	2.90	848	0	3.17	844	Matched to C-D design condition of DFSC-5
DFSC-4	1416	3.22	871	2.91	846	400	3.17	867	

MODEL	TEST PT.	P_r^o	T_T^o, °R	V_j^o, ft/s	P_r^i	T_T^i, °R	V_j^i, ft/s	V_j^{mix}, ft/s	T_T^{mix}, °R	V_{ac}, ft/s
2	219	3.313	1681	2436	3.130	859	1695	2297	1494	0
2	220	3.318	1700	2451	3.129	852	1688	2308	1506	400

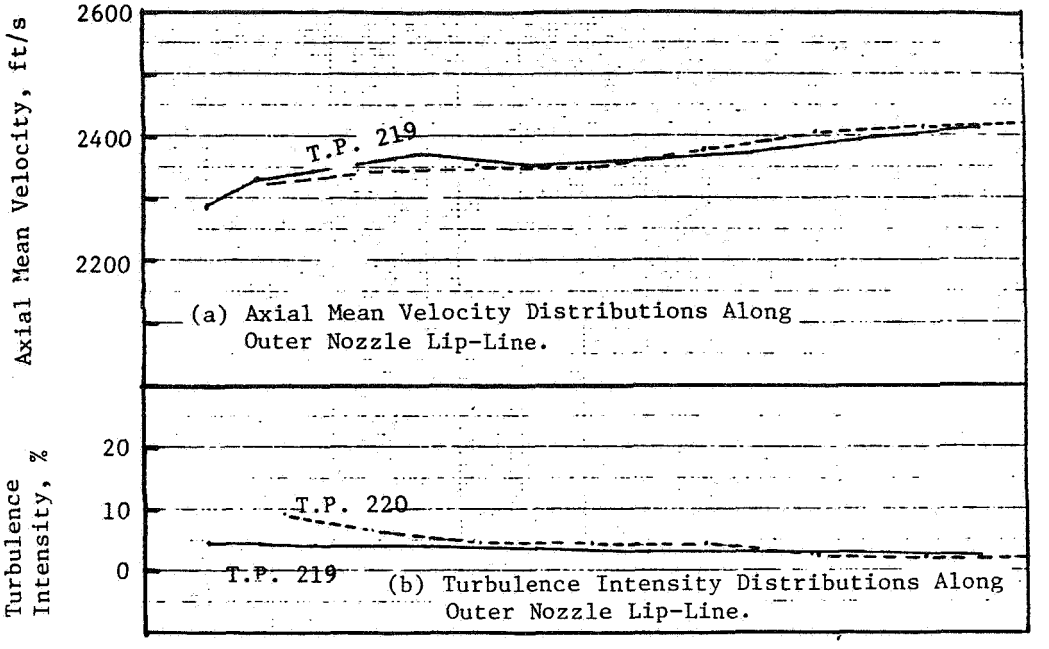

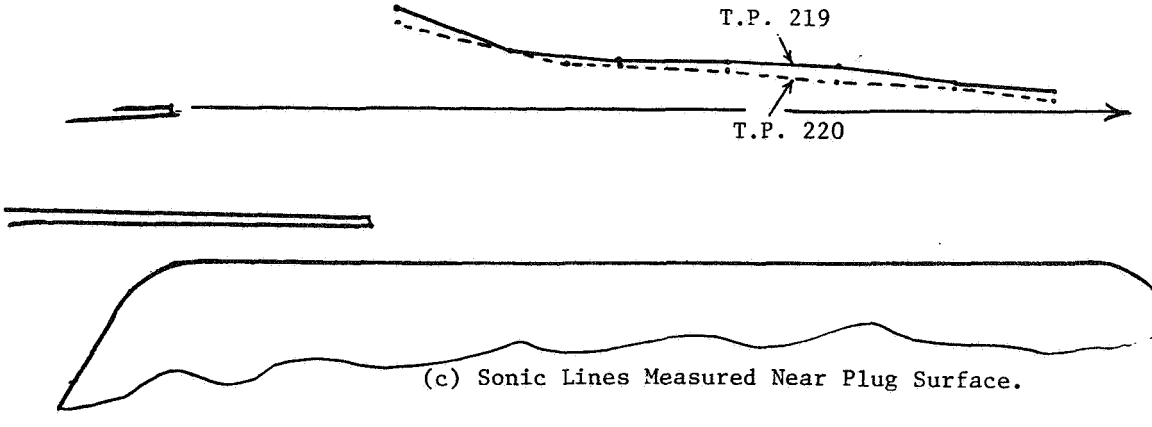

FIGURE 3-56. LV MEASURED FLOW FIELD NEAR EXIT OF COANNULAR C-D NOZZLE (TRUNCATED PLUG, DFSC-2)

MODEL	TEST PT.	P_r^o	T_T^o, °R	V_j^o, ft/s	P_r^i	T_T^i, °R	V_j^i, ft/s	V_j^{mix}, ft/s	T_T^{mix}, °R	V_{ac}, ft/s
4	1415	3.202	853	1703	2.910	855	1644	1694	853	0
4	1416	3.216	878	1730	2.909	847	1636	1716	873	400

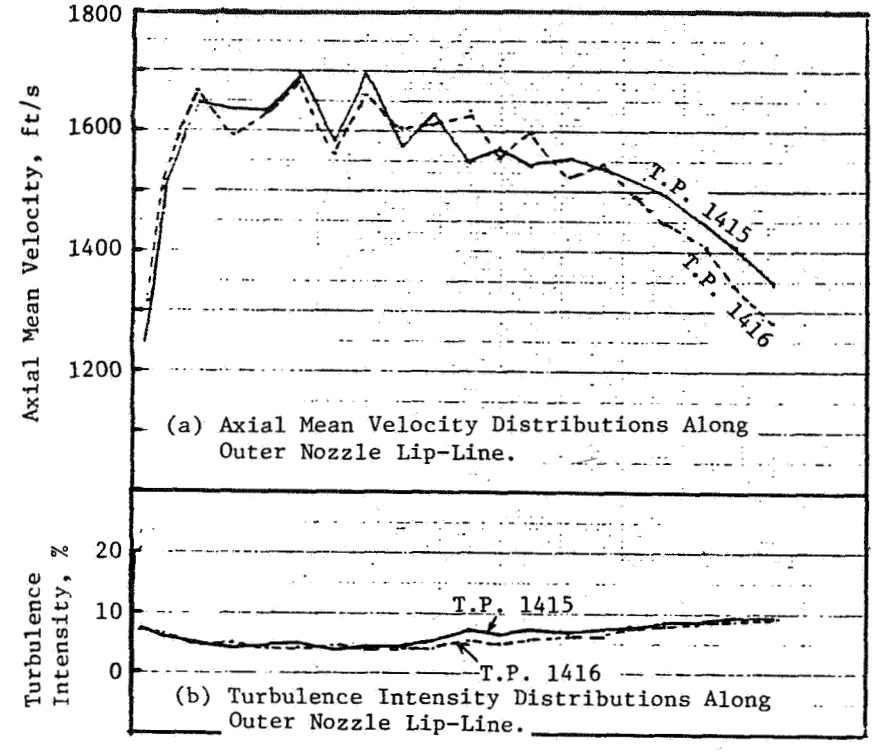

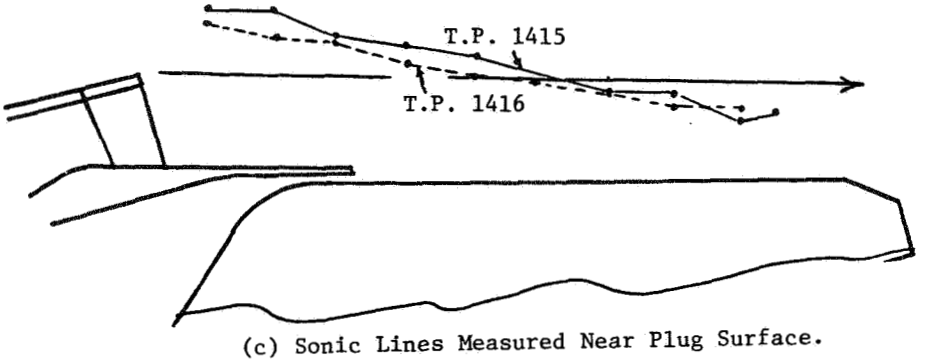

(c) Sonic Lines Measured Near Plug Surface.

FIGURE 3-57. LV MEASURED FLOW FIELD NEAR EXIT OF COANNULAR SUPPRESSOR CONVERGENT NOZZLE (DFSC-4).

In view of the fact that the test points in Figure 3-56 correspond to the C-D design condition for DFSC-2, relatively smooth profiles of the mean velocity and turbulence intensity distributions are obtained. The sonic lines near the outer lip-line that are depicted in Figure 3-56c for this nozzle are observed to be not affected appreciably. The locations of the sonic lines are observed not to match with the location of the lip-line, although they are close to each other.

Similar flow field pictures for the convergent DFSC-4 nozzle are presented in Figure 3-57. Because of the imperfect expansion on the plug, the mean velocity profiles indicate the shock-cell structure. However, because of the high rate of mean velocity decay on the plug, sharply inclined sonic lines are observed under both static and simulated flight conditions.

This discussion on the effect of the free-jet on the sonic line is concluded with the observation that the free-jet does not significantly affect the supersonic shear layer close to the nozzle exit.

4.0 SHOCK-CELL NOISE PREDICTION FOR COANNULAR PLUG NOZZLES

One of the objectives of this study is to develop a semi-empirical prediction method for predicting the shock-cell noise of coannular plug nozzles. As discussed in Section 3.0, diagnostic laser velocimeter measurements and shadowgraphs indicated two shock-cell structures (i.e., on and downstream of the plug) for a high radius ratio coannular plug nozzle with convergent terminations on both outer and inner flowpaths.

Two of the significant diagnostic observations of Section 3.0 are:

- The shock-cell structure on the plug is essentially due to the imperfect expansion of the supersonic outer stream; and,

- The supersonic flow over the truncated plug results in an expansion fan in the region of the truncated plug, which results in a pattern of shock waves and expansion waves, resulting in the observed shock-cell structure downstream of the plug of a convergent coannular nozzle.

Bhutiani (References 5 and 26) developed a semi-empirical method for predicting the jet-mixing and shock-cell noise of coannular plug nozzles. That method employed the Harper-Bourne and Fisher model applicable to circular nozzles (Reference 1) with certain modifications to predict the shock-cell noise of coannular plug nozzles. Only shocks downstream of the plug were considered in the prediction of shock-cell noise. Also, a shock strength parameter, β^{eff} (which equals $\sqrt{(M^{eff})^2-1}$, where M^{eff} is the Mach number obtained from an effective pressure ratio, given by $P_r^{eff} = (P_r^o + A_r P_r^i)/(1 + A_r)$, was defined and used in computing the shock-cell noise.

The method developed in Reference 26 has been extended in this study to calculate the shock-cell noise due to the identified two shock-cell structures, by defining appropriate and different length scales and shock strength parameters that characterize the two shock-cell system. The convergent-divergent coannular nozzle, operating at the design supersonic Mach number, has been shown to result in a reduction of shock-cell noise due to

weakened shock-cell structures on the plug and downstream of the plug (refer to Section 3.2). In order to estimate the effectiveness of convergent-divergent flowpath at the design and slightly off-design conditions, the extended model has been empirically modified.

The presence of a subsonic inner stream for a convergent coannular nozzle resulted in a significant weakening of the shock-cell structure downstream of the plug and hence yielded a reduction of shock cell noise (Section 3.3). This essentially was due to the subsonic flow over the truncated plug which in a way "insulated" the supersonic outer flow from the base of the truncated plug. The method developed in this study is extended to account also for the presence of a subsonic inner stream and to predict the shock-cell noise of convergent coannular nozzles operating with this modified cycle condition.

The following subsections summarize the methodology developed based on the above concepts and compare selected predicted results with the corresponding experimental data.

4.1 PREDICTION PROCEDURE

Figure 4-1 schematically illustrates the behavior of supersonic flow of a high radius ratio, low area ratio (A^i/A^o) coannular plug nozzle. The shock-cells on the plug are created due to the non-isentropic expansion of the outer stream. Due to the small area ratio ($A^i/A^o \simeq 0.2$) and large radius ratio ($R_r^o \simeq 0.85$), the inner stream has a very small annulus height ($h^i/D_{eq} \simeq 0.03$) and, as such, does not have a noticeable shock structure (see Figure 3-6). The typical half-cone angle for the plugs for variable cycle engine nozzles (VCE) has been 15° (Reference 27). Since the flow separates for such plugs after some distance downstream of the plug, truncated plugs were employed to minimize the plug length, so as to minimize the weight. A supersonic flow over such a truncated plug undergoes expansion. The expansion waves impinge on the shear layer and get reflected as oblique shock waves. The oblique shock waves are reflected in the like sense from the nozzle centerline (line of symmetry). They in turn are reflected as expansion waves by the shear layer. This process continues until the static pressure in the flow equalizes the ambient pressure. This process results in the shock-cell structure downstream of a truncated plug.

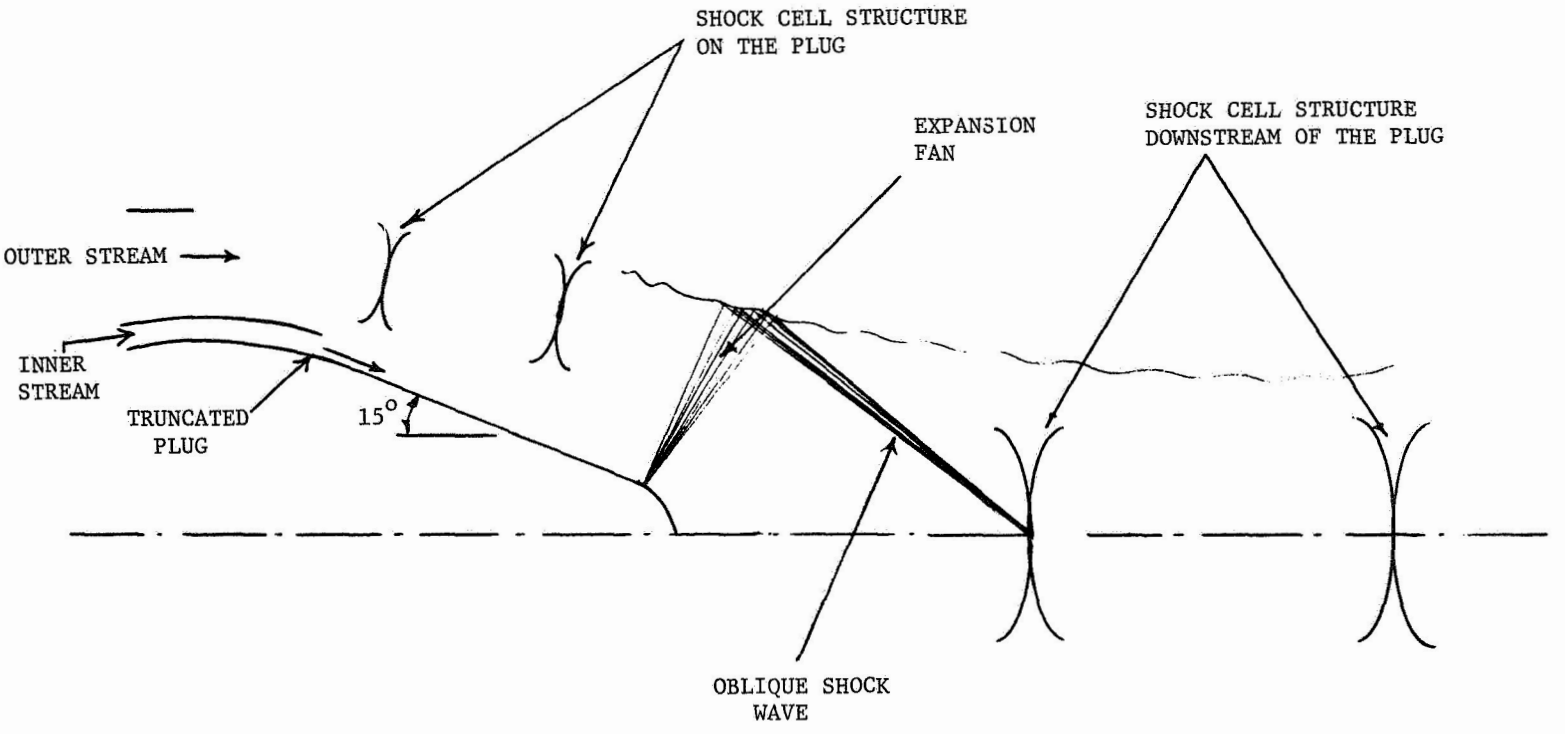

FIGURE 4-1. A SCHEMATIC REPRESENTATION OF SUPERSONIC FLOW OF A COANNULAR PLUG NOZZLE.

4.1.1 Selection of Shock Structure Parameters for Convergent Coannular Plug Nozzles

A review of the front quadrant acoustic data of the coannular plug nozzle with convergent terminations (configuration DFSC-1) clearly shows the presence of two regions of broadband shock-cell noise (e.g., see Figure 3-7) which can be attributed to the two shock-cell structures. The selection of the length scales and the shock strength parameters for the two shock structures was based on the review of the measured acoustic and diagnostic data. The characteristic dimension for predicting the shock-cell noise of shocks on the plug has been chosen to be the hydraulic diameter of the outer stream, D^o_{hyd}, defined as:

$$D^o_{hyd} = \frac{4 \times \text{Outer Stream Area}}{\text{Outer Noise Radiating perimeter}}$$

$$= \frac{4 \times \pi \left[(R^o_o)^2 - (R^i_o)^2\right]}{2\pi (R^o_o)}$$

$$= 2 \times h^o \times (1 + R^o_r) \qquad (4.1)$$

where R^o_o is the outer radius of outer stream,

R^i_o is the inner radius of outer stream,

R^o_r is the outer stream radius ratio (R^i_o/R^o_o), and

h^o is the annulus height of the outer stream.

Since the shocks on the plug are mainly due to the imperfect expansion of the outer stream, the shock strength parameter is calculated based on the ideally expanded Mach number of the outer stream. In other words, the shock strength parameter is given by:

$$\beta^o = \sqrt{(M^o)^2 - 1}$$

where

$$M^o = \sqrt{\frac{2}{\gamma - 1}\left[\left(P^o_r\right)^{\frac{\gamma-1}{\gamma}} - 1\right]} \qquad (4.2)$$

where M^o is the outer stream ideally expanded Mach number,
P_r^o is the outer stream pressure ratio, and
γ is the ratio of specific heats.

The LV measurements on the plug have indicated that there are typically 2 shock-cells on the plug (see Figure 3-5). This number of shock-cells is prescribed as an input in predicting the shock-cell noise due to shocks on the plug.

Next, the characteristic dimension for shocks downstream of the plug has been chosen to be the equivalent convergent circular nozzle diameter based on the total flow area, i.e.,

$$D_{eq} = \sqrt{\frac{4 \times (A^i + A^o)}{\pi}} \tag{4.3}$$

where A^i is the inner stream flow area
and A^o is the outer stream flow area.

The front quadrant acoustic data of coannular convergent configuration, DFSC-1 indicated that the shock-cell noise due to downstream shock structure is sensitive to the relative magnitudes of the inner and outer pressure ratios. During these acoustic tests, the inner stream pressure ratio, P_r^i was maintained at about 3.1 and the outer stream pressure ratio, P_r^o was varied from 2.5 to 4.0. A distinct change in front quadrant noise was observed when P_r^o was equal to or greater than P_r^i (i.e., for 10 log $\beta^{eff} > -.2$), (see Figure 3-1). It can be seen in Figure 3-1 that for $P_r^o \geq P_r^i$, PNL at $\Theta_i = 60°$ approaches a steady value and for $P_r^o \leq P_r^i$, (i.e., for 10 log $\beta^{eff} < -.2$) the PNL at $\Theta_i = 60°$ reduces rapidly. The shadowgraphs for $P_r^o \geq P_r^i$ also showed very little mixing of the inner and outer streams in the vicinity of plug tip indicating that for $P_r^o \geq P_r^i$, the inner stream seems to control the shock structure downstream of the plug (see Figure 3-6a). Hence, the shock strength parameter for downstream shock structure is to be based on the inner stream pressure ratio, for the case when $P_r^o \geq P_r^i$. When $P_r^o < P_r^i$, it is probable that the outer stream is fully expanded by the time it reaches the plug tip and hence the inner stream is exposed to a

different "ambient" condition compared to when the outer stream had not fully expanded. This would result in a possible interaction between the two streams. An area-weighted effective pressure ratio (P_r^{eff}) is chosen to be used in calculating the shock strength of shock structure downstream of the plug when $P_r^o < P_r^i$. P_r^{eff} is defined as:

$$P_r^{eff} = \frac{P_r^o A^o + P_r^i A^i}{A^o + A^i} \tag{4.4}$$

Figure 4-2 illustrates the above selection of the characteristic pressure ratio for calculation of the shock-cell noise due to shocks downstream of the plug for the series of acoustic tests performed with the convergent coannular configuration DFSC-1.

The LV measurements have indicated that there are typically 8 shock-cells downstream of the plug when $P_r^o > P_r^i$ (see Figure 3-5). For $P_r^o < P_r^i$, no such diagnostic information is available. Number of shock-cells for $P_r^o < P_r^i$ has been selected to be 2 so as to provide reasonable agreement with the acoustic data.

Table 4-I summarizes the selection of length scale, the pressure ratio which in turn determines the shock strength parameter, β and number of shock-cells for coannular plug nozzles.

The LV and shadowgraph diagnostic measurements have indicated that the presence of a subsonic inner stream effectively minimized shock structure downstream of the plug (see Figures 3-25 and 3-26). The choice of P_r^i as the pressure ratio governing the shocks downstream of the plug, if any, when $P_r^o \geq P_r^i$ may be reasonable when the inner stream is subsonic, since in such a case, only shock-cell noise due to shocks on the plug will be computed.

The computer program of Reference 26 was modified suitably to predict the shock-cell noise due to shocks on the plug and downstream of the plug separately, utilizing the appropriate shock structure parameters listed in Table 4-I. Next, the broadband shock-cell noise spectra of these two shock structures are assumed to be uncorrelated and are summed on a mean square pressure basis to yield the total shock-cell noise spectrum of coannular plug nozzles.

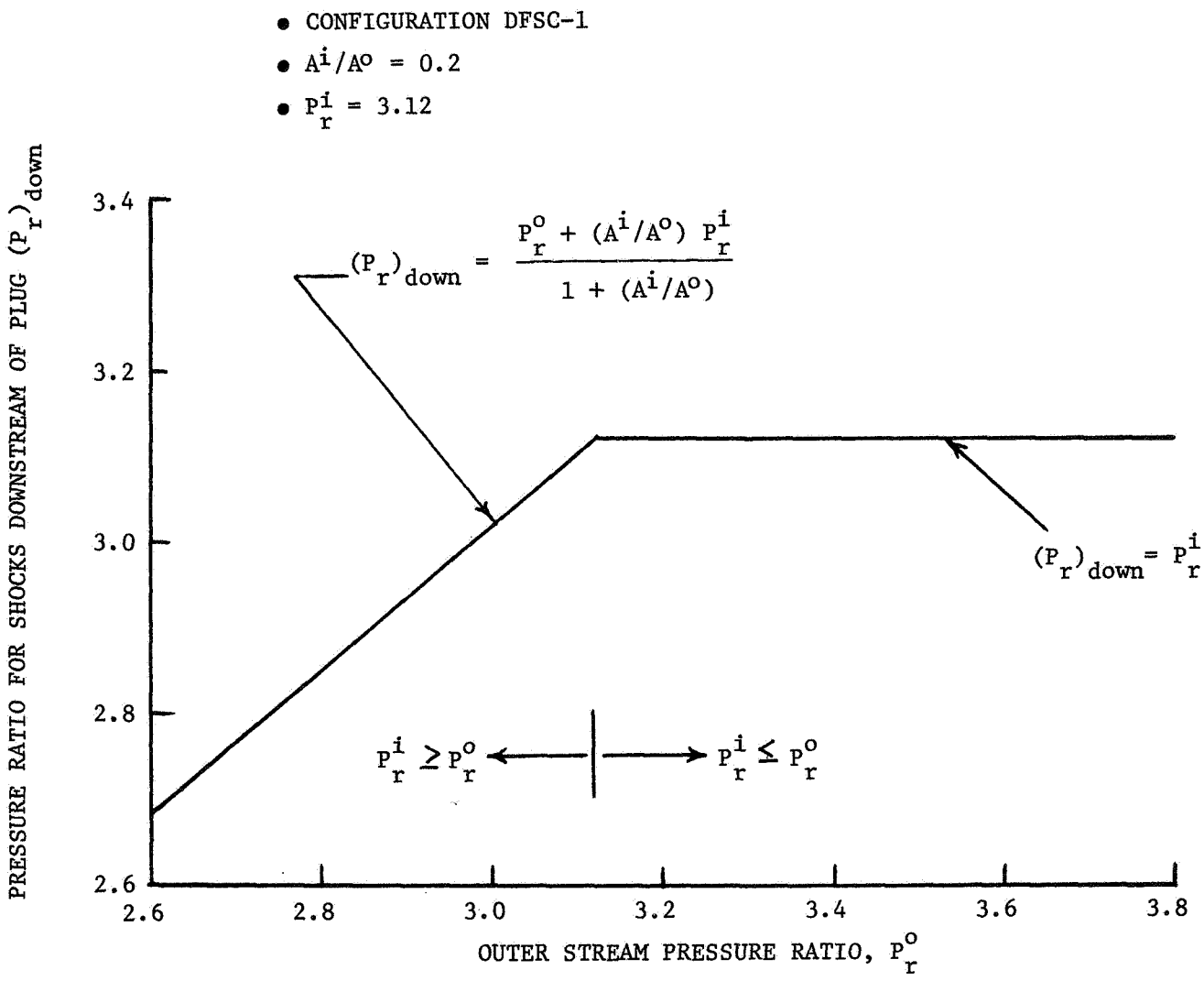

FIGURE 4-2. PREDICTION MODEL EMPLOYED FOR THE SELECTION OF CHARACTERISTIC PRESSURE RATIO FOR SHOCKS DOWNSTREAM OF THE PLUG.

TABLE 4-I

SHOCK STRUCTURE PARAMETERS FOR COANNULAR PLUG NOZZLES

Type of Shock Structure	Length Scale	Pressure Ratio	No. of Shock Cells
On the plug	D^o_{hyd} (see Eq. 4.1)	P^o_r	2
Downstream of the Plug	D_{eq} (see Eq 4.3)	P^i_r if $P^o_r \geq P^i_r$	8
		P^{eff}_r if $P^o_r < P^i_r$ (See Eq. 4.4)	2

4.1.2 Effectiveness of Convergent-Divergent Flowpath and Plug Tip Shape for Coannular Plug Nozzles

It has been shown in Section 3.2 that the application of a convergent-divergent flowpath for the inner and outer streams and a sharp tipped plug reduced shock strength of the shocks on the plug and downstream of the plug, respectively, and hence the observed minimum shock-cell noise in the vicinity of the C-D design condition. A simple empirical method is described in this subsection to compute the combined effectiveness of C-D flowpaths and sharp tipped plug in reducing the shock-cell noise in the vicinity of the C-D design condition.

Figure 4-3 conceptually illustrates the effect of the C-D termination and the sharp tipped plug in the vicinity of the design condition on the spectrum in the forward quadrant. The coannular plug nozzle with convergent termination and truncated plug typically exhibits two broadband peaks in the front quadrant spectrum. The peak at lower frequency corresponds to the shocks downstream of the plug, and the peak at higher frequency corresponds to

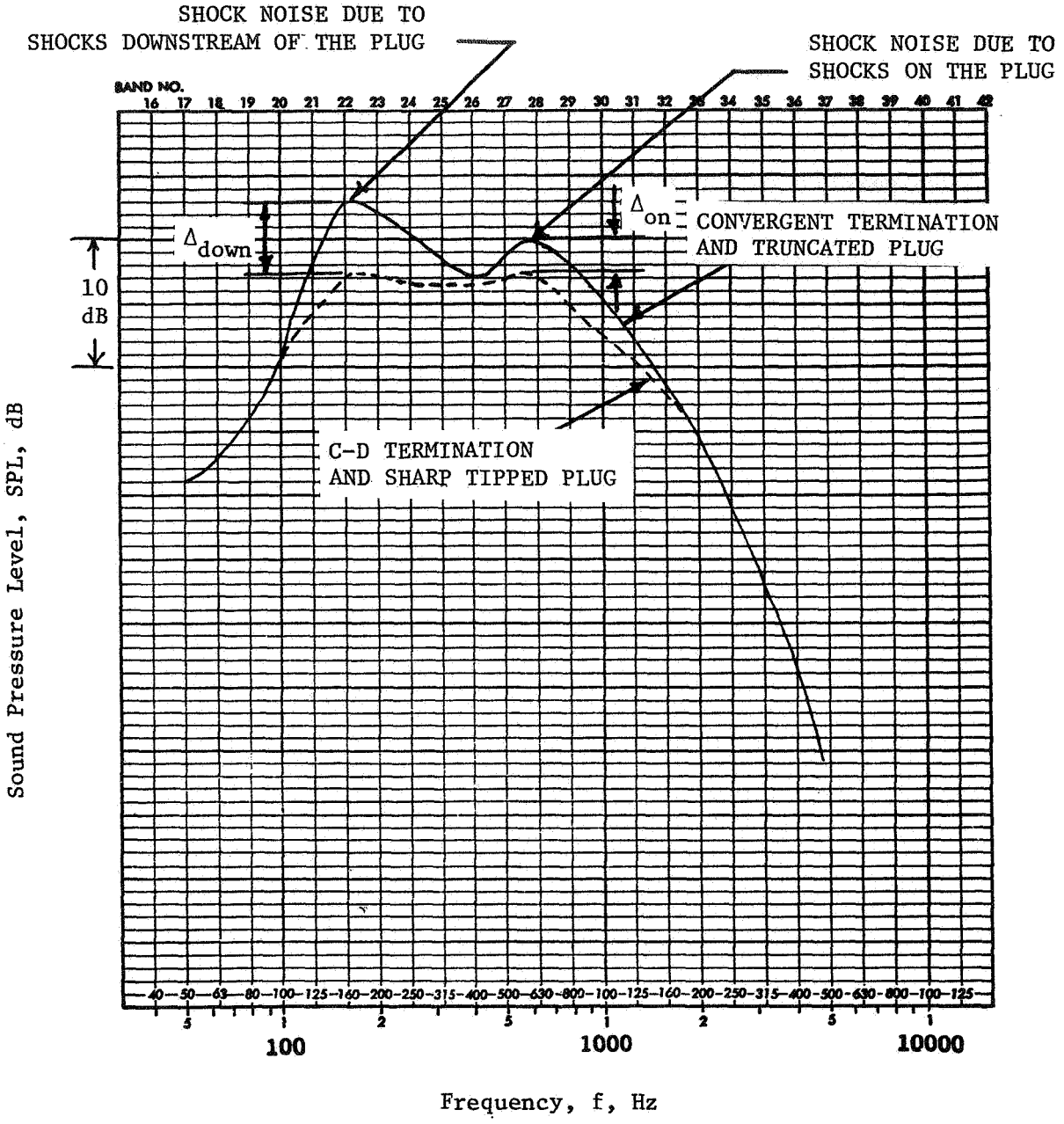

FIGURE 4-3. CONCEPTUAL ILLUSTRATION OF THE SPECTRAL SHOCK CELL NOISE REDUCTION OF COANNULAR PLUG NOZZLES DUE TO THE C-D TERMINATION AND THE SHARP TIPPED PLUG IN THE VICINITY OF THE DESIGN CONDITION IN THE FORWARD QUADRANT.

the shocks on the plug since the length scale of shocks downstream of the plug is larger than that of shocks on the plug. The application of a C-D flowpath results in a weakening of shocks on the plug yielding a noise reduction, Δ_{on}. The application of a sharp tipped plug results in a weakening of the shocks downstream of the plug yielding a noise reduction, Δ_{down}. The acoustic data at $\Theta_i = 60°$ of configuration DFSC-1 (coannular plug nozzle with convergent termination and truncated plug) and configuration DFSC-3 (coannular plug nozzle with convergent-divergent termination and sharp tipped plug) at design and slightly underexpanded and slightly overexpanded conditions were utilized in determining the variation of Δ_{down} and Δ_{on} with the β^{eff} which is calculated from P_r^{eff} through standard isentropic gas dynamic relationships. Figure 4-4 shows the deduced variation of Δ_{down} and Δ_{on} under static and simulated flight conditions. The equations describing Δ_{down} and Δ_{on} are given below:

Equations for Δ_{down}

Static Case

$$\Delta_{down} = 6.0 - 160 \log [\beta^{eff}/\beta_d^{eff}], \text{ for } \beta^{eff} > \beta_d^{eff} \text{ (Underexpanded)}$$

$$= 6.0 + 140 \log [\beta^{eff}/\beta_d^{eff}], \text{ for } \beta^{eff} < \beta_d^{eff} \text{ (Overexpanded)} \quad (4.5)$$

Simulated Flight Case

$$\Delta_{down} = 11.0 - 160 \log [\beta^{eff}/\beta_d^{eff}], \text{ for } \beta^{eff} > \beta_d^{eff} \text{ (Underexpanded)}$$

$$= 11.0 + 650 \log [\beta^{eff}/\beta_d^{eff}], \text{ for } \beta^{eff} < \beta_d^{eff} \text{ (Overexpanded)} \quad (4.6)$$

Equations for Δ_{on}

Static Case

$$\Delta_{on} = 4.0 - 60 \log [\beta^{eff}/\beta_d^{eff}], \text{ for } \beta^{eff} > \beta_d^{eff} \text{ (Underexpanded)}$$

$$= 4.0 + 140 \log [\beta^{eff}/\beta_d^{eff}], \text{ for } \beta^{eff} < \beta_d^{eff} \text{ (Overexpanded)} \quad (4.7)$$

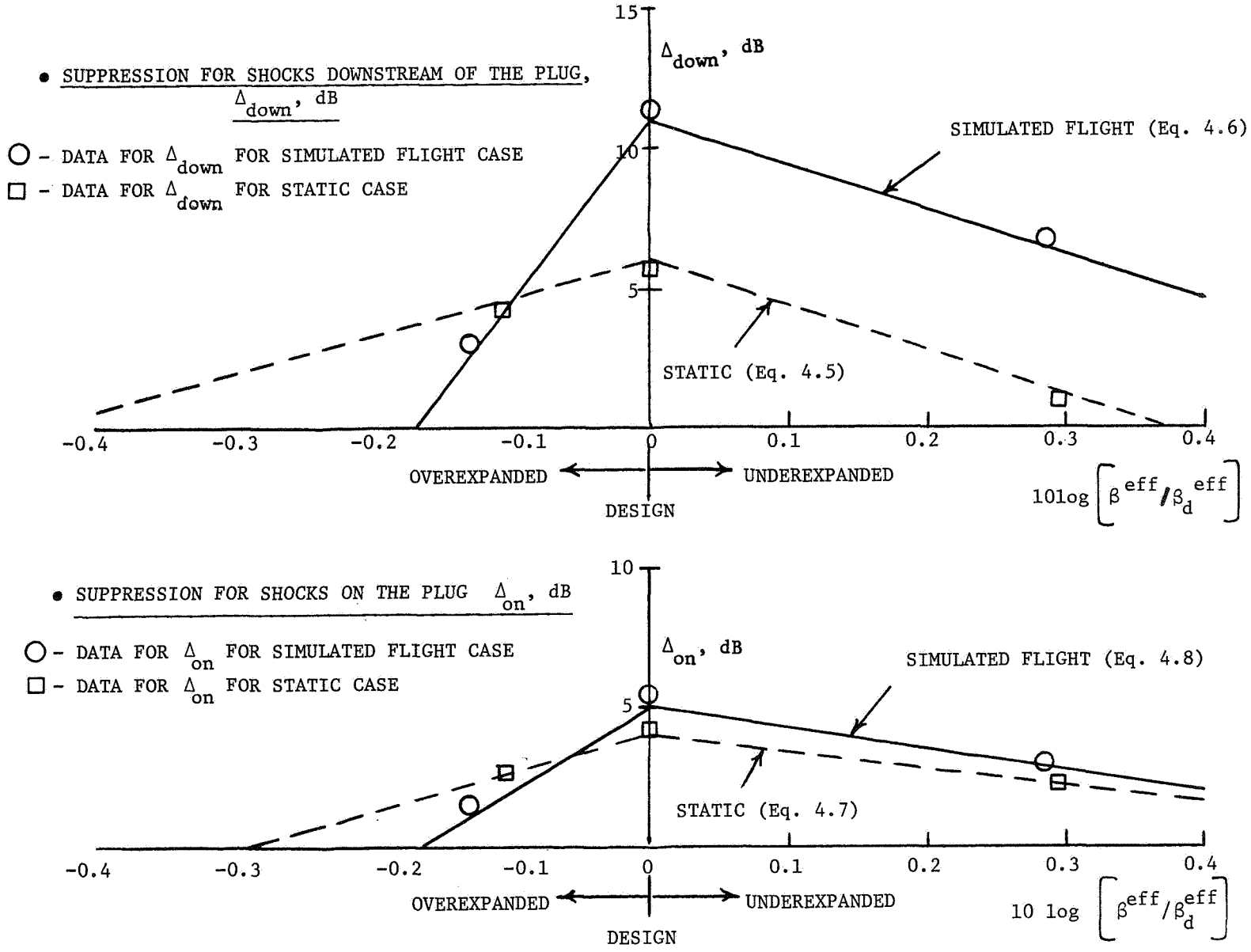

FIGURE 4-4. DEDUCED EFFECTIVENESS OF THE C-D TERMINATION AND SHARP TIPPED PLUG IN THE VICINITY OF THE DESIGN CONDITION FOR BOTH THE SHOCK STRUCTURES UNDER STATIC AND SIMULATED FLIGHT CONDITIONS.

Simulated Flight Case

$$\Delta_{on} = 5.0 - 80 \log [\beta^{eff}/\beta_d^{eff}], \text{ for } \beta^{eff} > \beta_d^{eff} \text{ (Underexpanded)}$$

$$= 5.0 + 300 \log [\beta^{eff}/\beta_d^{eff}], \text{ for } \beta^{eff} < \beta_d^{eff} \text{ (Overexpanded)} \quad (4.8)$$

where $\beta^{eff} = \sqrt{(M^{eff})^2 - 1}$ and M^{eff} is based on P_r^{eff}

and $\beta_d^{eff} = \sqrt{(M_d^{eff})^2 - 1}$ and $(M_d)^{eff}$ is based on $(P_r)_d^{eff}$.

$(P_r)_d^{eff}$ is the effective pressure at design condition and is given by:

$$(P_r)_d^{eff} = \frac{A^o (P_r)_d^o + A^i (P_r)_d^i}{A^o + A^i} \quad (4.9)$$

where $(P_r)_d^o$ is the design outer stream pressure ratio

and $(P_r)_d^i$ is the design inner stream pressure ratio.

A lower limit of zero is prescribed for both Δ_{down} and Δ_{on} values. The Δ_{down} and Δ_{on} values calculated as above are subtracted from the appropriate shock-cell noise spectra uniformly (i.e., at all frequencies and at all observer angles) to simulate the effect of C-D termination empirically and sharp tipped plug at design and slightly off-design conditions. The computer program has the option to include either the convergent termination with truncated plug or convergent-divergent termination with sharp tipped plug. In the case of C-D termination, one has to prescribe the design inner and outer stream Mach numbers also.

4.2 COMPARISON WITH EXPERIMENTAL DATA

Comparisons of the experimental data of configurations DFSC-1 (coannular plug nozzle with convergent terminations and truncated plug), DFSC-3 (coannular plug nozzle with C-D terminations and sharp plug) and DFSC-6 (coannular plug nozzle with convergent terminations and sharp plug) with

subsonic inner stream, with the predictions based on the semi-empirical method described in Section 4.1 are contained in this section.

Figure 4-5 compares the measured and predicted PNL directivities of configurations DFSC-1 and DFSC-3 under static and simulated flight conditions near the C-D design condition. A good agreement between data and predictions for DFSC-1 and DFSC-3 under simulated flight condition at all the observer angles is noted. In the static case, the agreement is acceptable. However, the measured ΔPNL values between DFSC-1 and DFSC-3 are equal to the predicted ΔPNL values at all observer angles in the front quadrant, for the static case.

Figure 4-6 compares the measured and predicted spectra of configuration DFSC-1 and DFSC-3 at Θ_i = 60° under static and simulated flight conditions near the C-D design condition. The measured and predicted location of low frequency peak for configurations DFSC-1 and DFSC-3 agree within one 1/3-octave-band under both static and simulated flight conditions. The predicted and measured peak sound pressure levels agree within 2 dB for the low frequency peak. Both the data and predictions for the configuration DFSC-1 indicate that the high frequency peak is not very easily discernable, implying that the shock noise created by the shocks on the plug is not that significant compared to the shock noise due to shocks downstream of the plug. In the case of configuration DFSC-3, the data indicate a fairly flat spectrum (within 3 dB) for frequencies in the range of 200 Hz - 630 Hz for the static case and 200 Hz - 1,000 Hz for the simulated flight case. The predictions for DFSC-3 also show similar trend indicating that the simple empirical model employed to estimate the effectiveness of the C-D termination and sharp tipped plug is reasonable.

Figure 4-7 compares the measured and predicted spectra of configurations DFSC-1 and DFSC-3 at Θ_i = 90° under static and simulated flight conditions near the C-D design condition. For configuration DFSC-1, the shock-cell noise dominates the spectra at Θ_i = 60° whereas, at Θ_i = 90°, jet noise becomes significant (cf. Figures 4-6 and 4-7). The measured and predicted spectra at Θ_i = 90° for configuration DFSC-1 show a relatively larger contribution of low frequency jet noise to the total noise compared to the spectra at Θ_i = 60°. The differences noted in the data

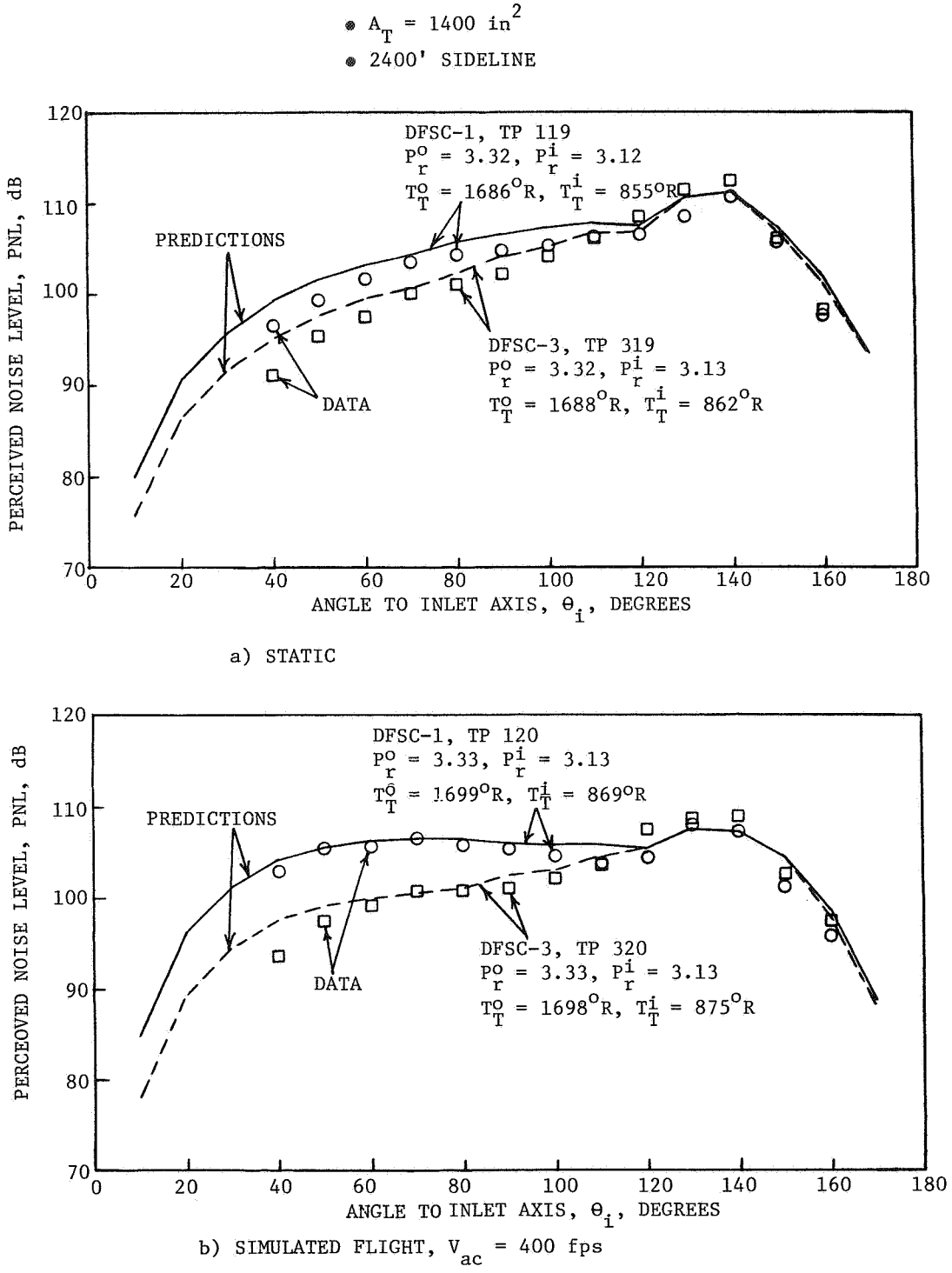

FIGURE 4-5. COMPARISON OF THE MEASURED AND PREDICTED PNL DIRECTIVITIES OF CONFIGURATIONS DFSC-1 (CONVERGENT NOZZLE WITH TRUNCATED PLUG) AND DFSC-3 (C-D NOZZLE WITH SHARP TIPPED PLUG) NEAR THE DESIGN CONDITION, UNDER STATIC AND SIMULATED FLIGHT CONDITIONS.

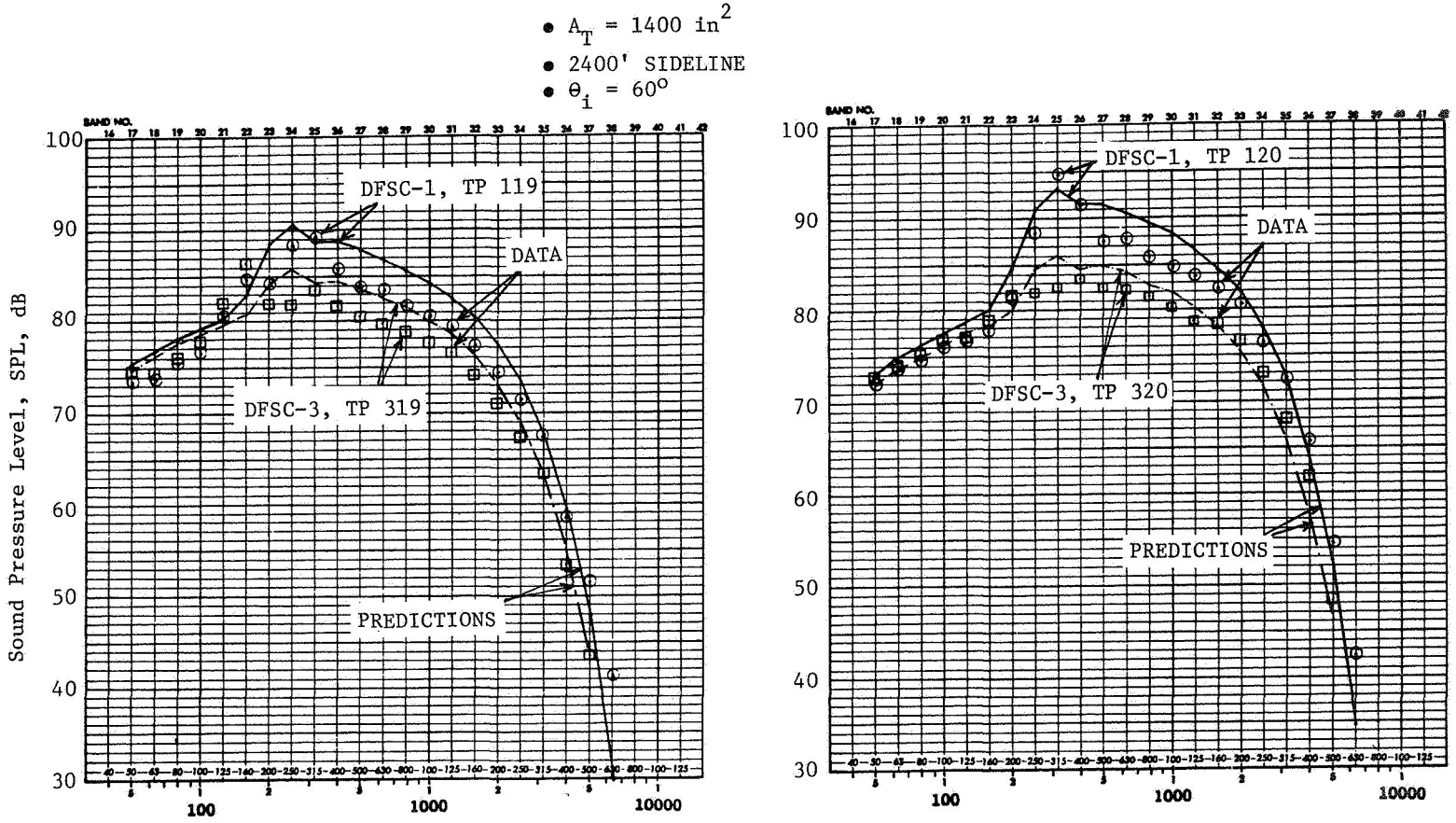

FIGURE 4-6. COMPARISON OF THE MEASURED AND PREDICTED SPECTRAL CONTENT AT θ_i = 60° OF CONFIGURATIONS DFSC-1 (CONVERGENT NOZZLE WITH TRUNCATED PLUG) AND DFSC-3 (C-D NOZZLE WITH SHARP TIPPED PLUG) NEAR THE DESIGN CONDITION, UNDER STATIC AND SIMULATED FLIGHT CONDITIONS.

- A_T = 1400 in^2
- 2400' SIDELINE
- θ_i = 90°

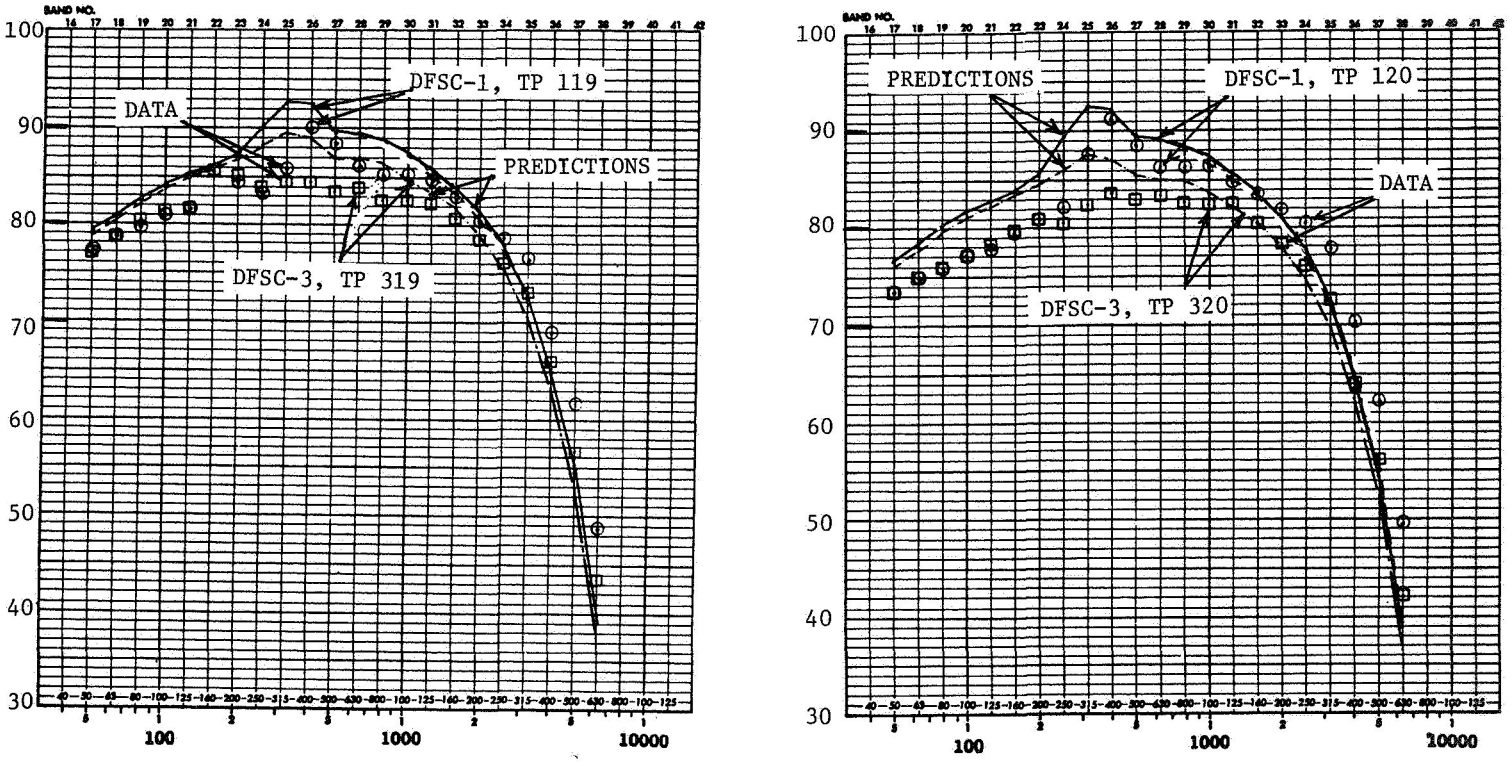

a) STATIC

b) SIMULATED FLIGHT, V_{ac} = 400 fps

FIGURE 4-7. COMPARISON OF THE MEASURED AND PREDICTED SPECTRAL CONTENT AT θ_i = 90° OF CONFIGURATIONS DFSC-1 (CONVERGENT NOZZLE WITH TRUNCATED PLUG) AND DFSC-3 (C-D NOZZLE WITH SHARP TIPPED PLUG) NEAR THE DESIGN CONDITION, UNDER STATIC AND SIMULATED FLIGHT CONDITIONS.

and prediction for the low frequencies (i.e., f < 200 Hz) for configurations DFSC-1 and DFSC-3 can be attributed to the overprediction of jet noise. Modifications to the prediction of jet noise (Reference 26) was beyond the scope of this effort. However, note that both data and predictions show that there is little modification in spectra for frequencies less than 200 Hz due to the geometric differences between configurations DFSC-1 and DFSC-3. The peak broadband shock noise still stands out clearly at Θ_i = 90°. The predictions of the location of the low frequency shock noise peak for DFSC-1 agree with data within one 1/3-octave-band. The predicted levels of the low frequency peak agree with data within 1-2 dB. The data and predictions of configuration DFSC-1 indicate a flat spectrum from 630 Hz to 1,000 Hz for both static and simulated flight cases which can be inferred as the contribution from the shocks on the plug to the shock-cell noise. As at Θ_i = 60°, the data and predictions of configuration DFSC-3 show a flat spectrum over the mid-frequency range.

The next series of data and theory comparisons are concerned with the modeling of the effects of subsonic inner stream on the coannular plug nozzle shock noise. The procedure presented in Section 4.1 would calculate only shock noise due to shocks on the plug in the presence of a subsonic inner stream. Figure 4-8 compares the measured and predicted PNL directivities of configurations DFSC-1 (coannular convergent nozzle with truncated plug) and DFSC-6 (coannular convergent nozzle with sharp tipped plug) with subsonic inner, for a simulated flight case. The data and predictions for configuration DFSC-1 are repeated from Figure 4-5b. The predicted PNL values in the front quadrant for the configuration DFSC-6 with subsonic inner are lower compared to the data indicating that the assumption that the subsonic inner stream removes all the shock structure downstream of the plug is not completely correct. In fact, the LV measurements (see Figure 3-26) indicate the presence of a weak shock structure and not a complete elimination of shock structure downstream of the plug. Hence, the predictions with only shocks on the plug for the case of a subsonic inner stream can be viewed as a limiting case.

Figure 4-9 compares the measured and predicted spectral content at Θ_i = 60° of configurations DFSC-1 and DFSC-6 with subsonic inner stream. At Θ_i = 60°, both the data and predictions show the conspicuous absence of

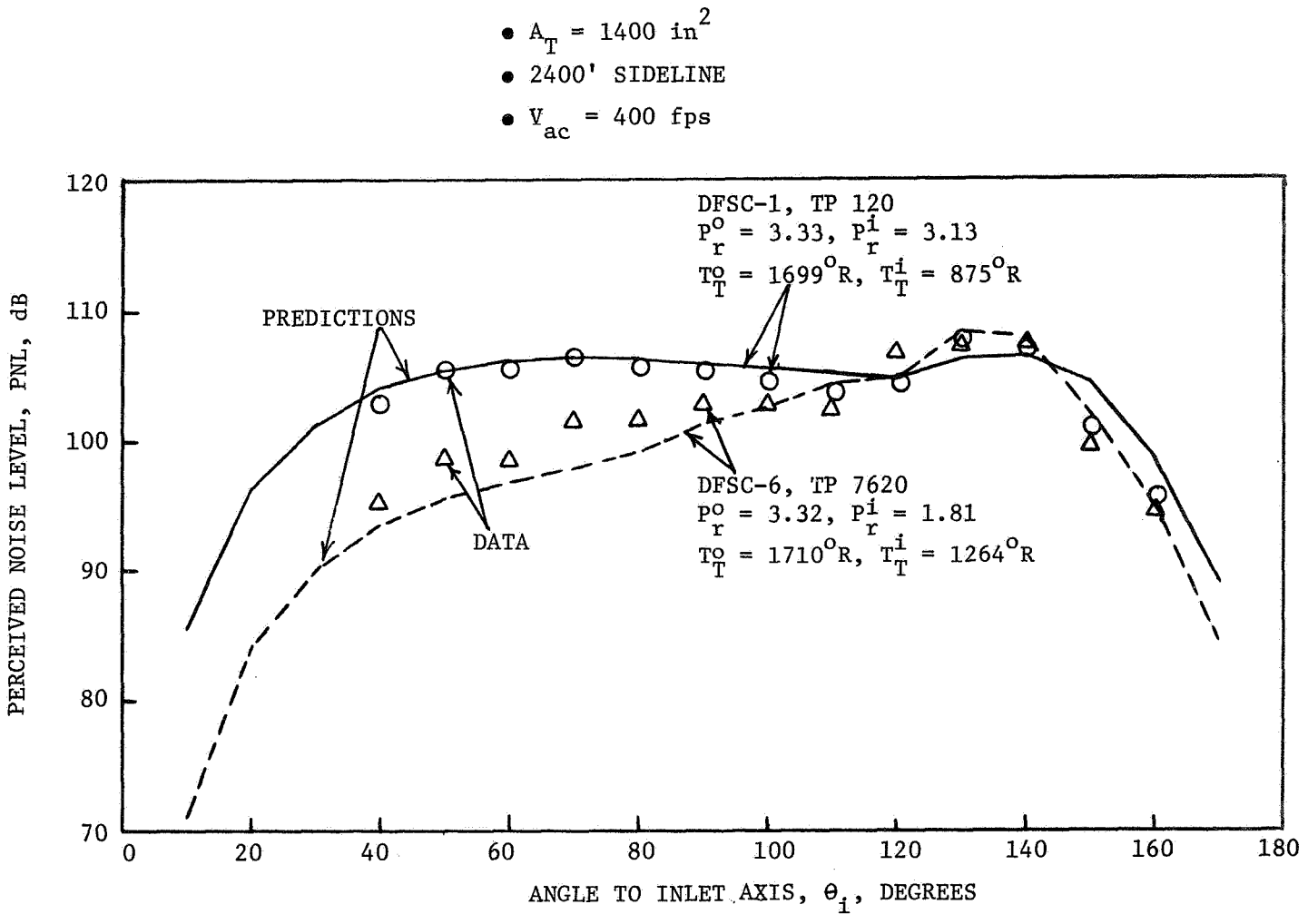

FIGURE 4-8. COMPARISON OF THE MEASURED AND PREDICTED PNL DIRECTIVITIES OF CONFIGURATIONS DFSC-1 (CONVERGENT NOZZLE WITH TRUNCATED PLUG) AND DFSC-6 (CONVERGENT NOZZLE WITH SHARP TIPPED PLUG) WITH SUBSONIC INNER STREAM FOR SIMULATED FLIGHT CONDITION (V_{ac} = 400 fps).

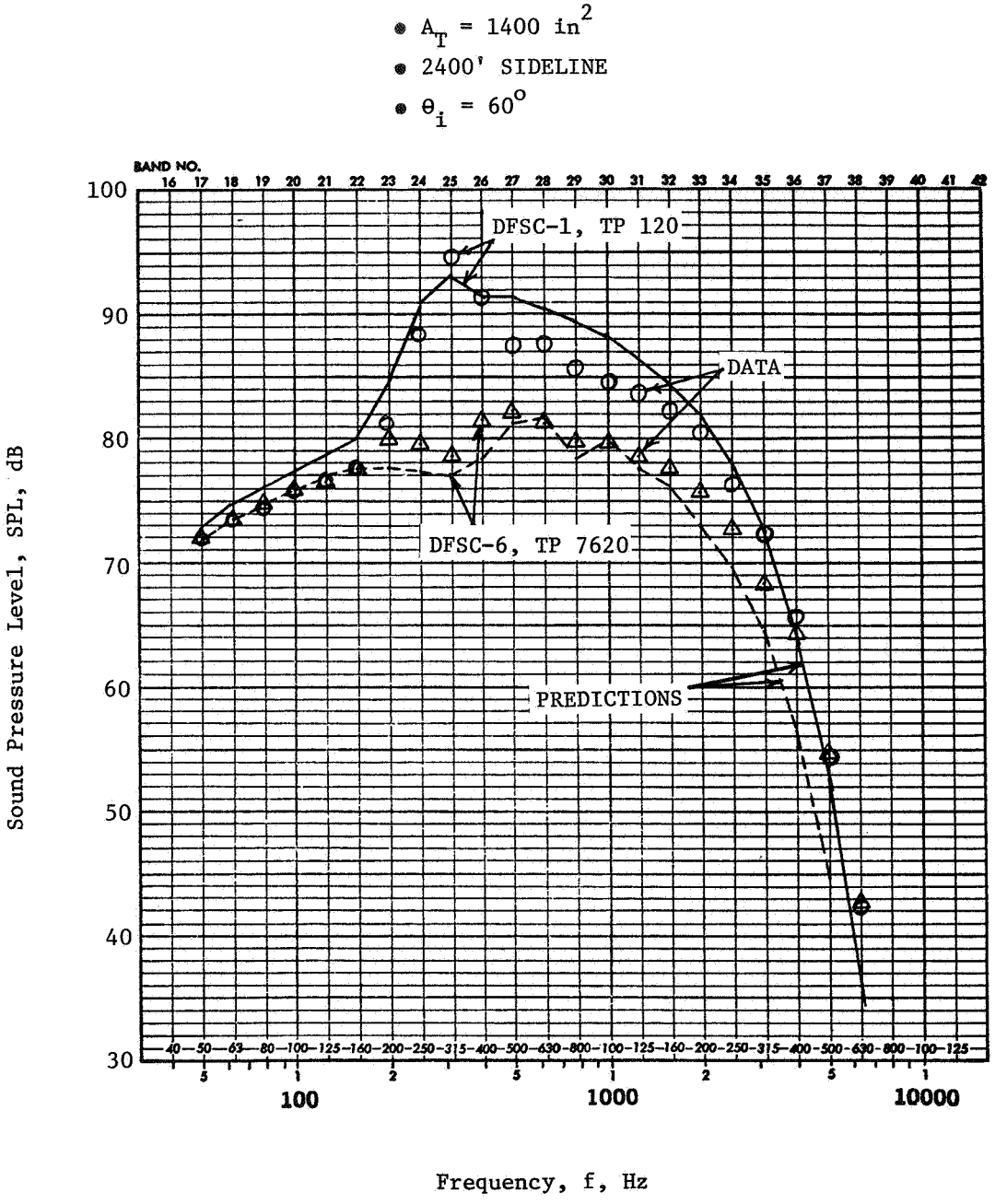

FIGURE 4-9. COMPARISON OF THE MEASURED AND PREDICTED SPECTRAL CONTENT AT θ_i = 60° OF CONFIGURATIONS DFSC-1 (CONVERGENT NOZZLE WITH TRUNCATED PLUG) AND DFSC-6 (CONVERGENT NOZZLE WITH SHARP TIPPED PLUG) WITH SUBSONIC INNER STREAM FOR SIMULATED FLIGHT CONDITION (V_{ac} = 400 fps).

the low frequency shock noise peak for configuration DFSC-6 with subsonic inner, which is due to a very weak shock structure downstream of the plug. The data and predictions for configuration DFSC-6 with subsonic inner are in good agreement over the entire frequency range. The predicted and measured location of the peak frequency of noise associated with shocks on the plug are 630 Hz and 500 Hz, respectively. The peak levels agree within 1 dB. A comparison of the data and/or predictions of configurations DFSC-1 and DFSC-6 with subsonic inner stream indicates the relatively minor role the shocks on the plug play in determining the total shock noise of coannular plug nozzles.

The next set of data-theory comparisons are aimed at comparing configurations DFSC-1, DFSC-3, and DFSC-6 with subsonic inner stream and a reference conic nozzle over a range of effective pressure ratios. Figure 4-10 compares the measured and predicted variation of PNL at $\Theta_i = 60°$ with respect to 10 log β^{eff} for a reference conic nozzle, configurations DFSC-1 and DFSC-3 under static and simulated flight conditions. The predictions for conic nozzle have been made utilizing the M-S (Motsinger-Siekmann) empirical method developed under a DOT contract (see Reference 28). This procedure utilizes the Harper-Bourne, Fisher method (Reference 1) without any modifications for the computation of shock-cell noise. The data for conic nozzle are taken from Reference 7. An examination of the figure indicates good agreement between data and predictions for conic nozzle for both static and simulated flight conditions. The predictions for configuration DFSC-1 agree with the data reasonably well at high and low values of P_r^{eff} (viz., for $P_r^{eff} > 3.1$ and $P_r^{eff} < 2.8$ or for 10 log $\beta^{eff} > -0.21$ and 10 log $\beta^{eff} < -0.74$). For $2.8 \leq P_r^{eff} \leq 3.1$, both the data and predictions show similar trend but do not agree in absolute levels. The prediction method employs a rather simple model for the selection of the characteristic pressure ratio for calculating the shock-cell noise due to shocks downstream of the plug (see Figure 4-2). The interaction between the inner and outer streams when $P_r^o \simeq P_r^i$ is quite complicated (see Reference 29). Hence, characterization of this complex interaction by the simple model employed is thought to be the reason for the discrepancy noted between data and prediction when $P_r^o \simeq P_r^i$. The empirical model employed for estimating the effectiveness of C-D termination predicts reasonably well in the vicinity of the C-D design condition. The shock structure of C-D nozzles at highly underexpanded and highly overexpanded

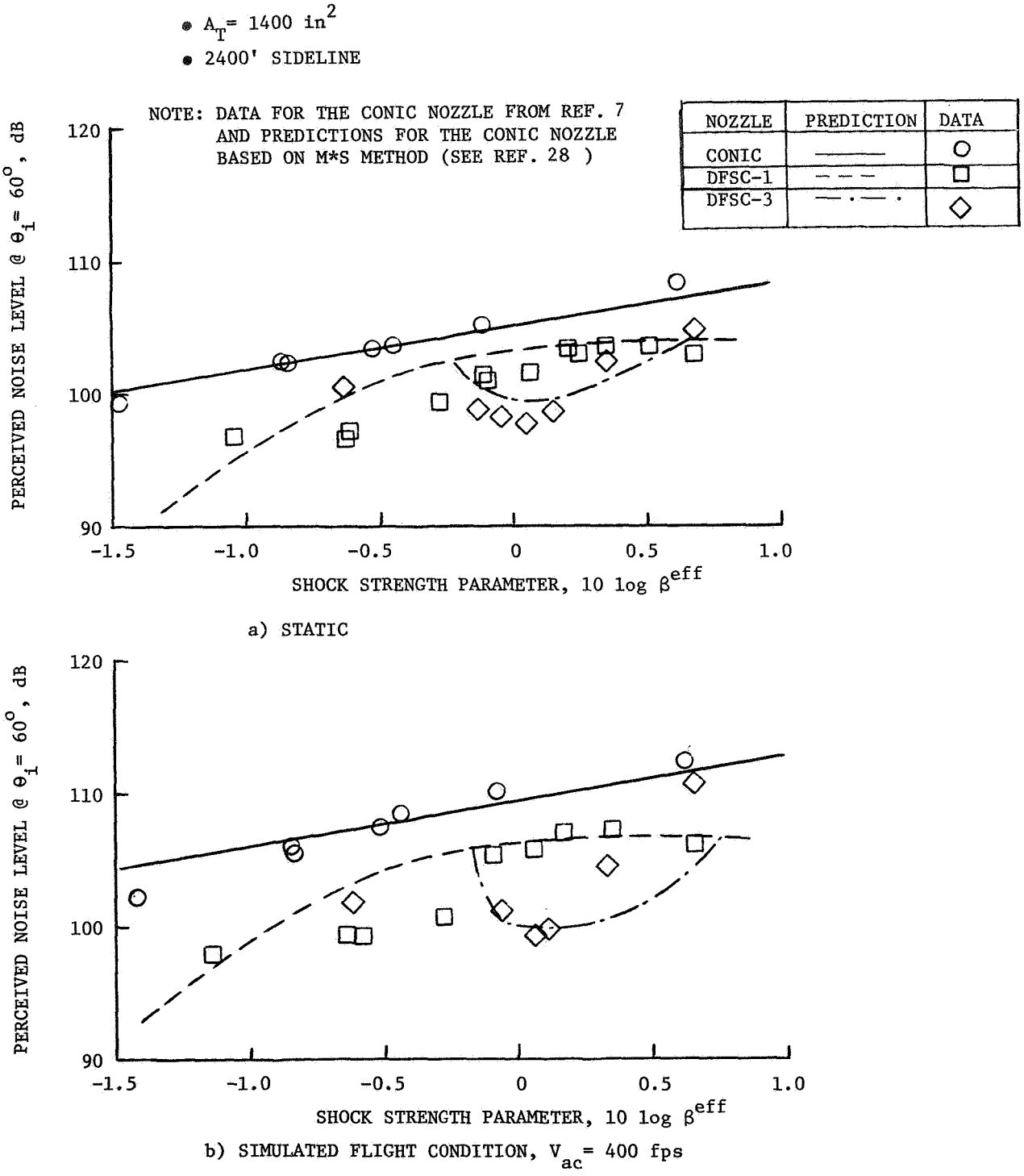

FIGURE 4-10. COMPARISON OF THE MEASURED AND PREDICTED VARIATION OF PNL AT θ_i= 60° WITH β^{eff} FOR CONIC NOZZLE, CONFIGURATIONS DFSC-1 (CONVERGENT COANNULAR PLUG NOZZLE WITH TRUNCATED PLUG) AND DFSC-3 (C-D COANNULAR PLUG NOZZLE WITH SHARP TIPPED PLUG) UNDER STATIC AND SIMULATED FLIGHT CONDITIONS.

conditions is quite different compared to the case of small pertubations from the design condition. The empirical model is based on data near the design condition and as such is valid only in the vicinity of the design condition.

Figure 4-11 compares the measured and predicted variation of PNL at $\Theta_i = 60°$ with respect to 10 log β^{eff} for a reference conic nozzle, configurations DFSC-1 and DFSC-6 with subsonic inner under static and simulated flight conditions. The data and predictions for configuration DFSC-6 with subsonic inner show similar trends. However, the predictions are lower than the data since the predictions assumed no shocks downstream of the plug in the presence of a subsonic inner stream and the laser velocimeter data shows a weak shock structure.

In summary, a semi-empirical prediction procedure that incorporates various features of supersonic flows observed in the case of coannular plug nozzles has been developed and the influence of these features on shock associated noise has been studied.

The prediction procedure has been shown to evaluate the contribution of shocks on the plug and shocks downstream of the plug individually and collectively to yield a good agreement with the measured data. The different length scales and shock strength parameters associated with these two shock structures have been identified and included in the prediction procedure. Both the predicted and measured data indicate that for coannular plug nozzles with convergent terminations, the shock structure downstream of the plug is the significant contributor to the total shock-cell noise. The application of a subsonic inner stream has been shown to be a simple and effective means of reducing the shock noise of coannular plus nozzles over a range of outer stream pressure ratios, as indicated by the measured and predicted data.

The prediction procedure also empirically models the effectiveness of the C-D terminations in the vicinity of the C-D design condition.

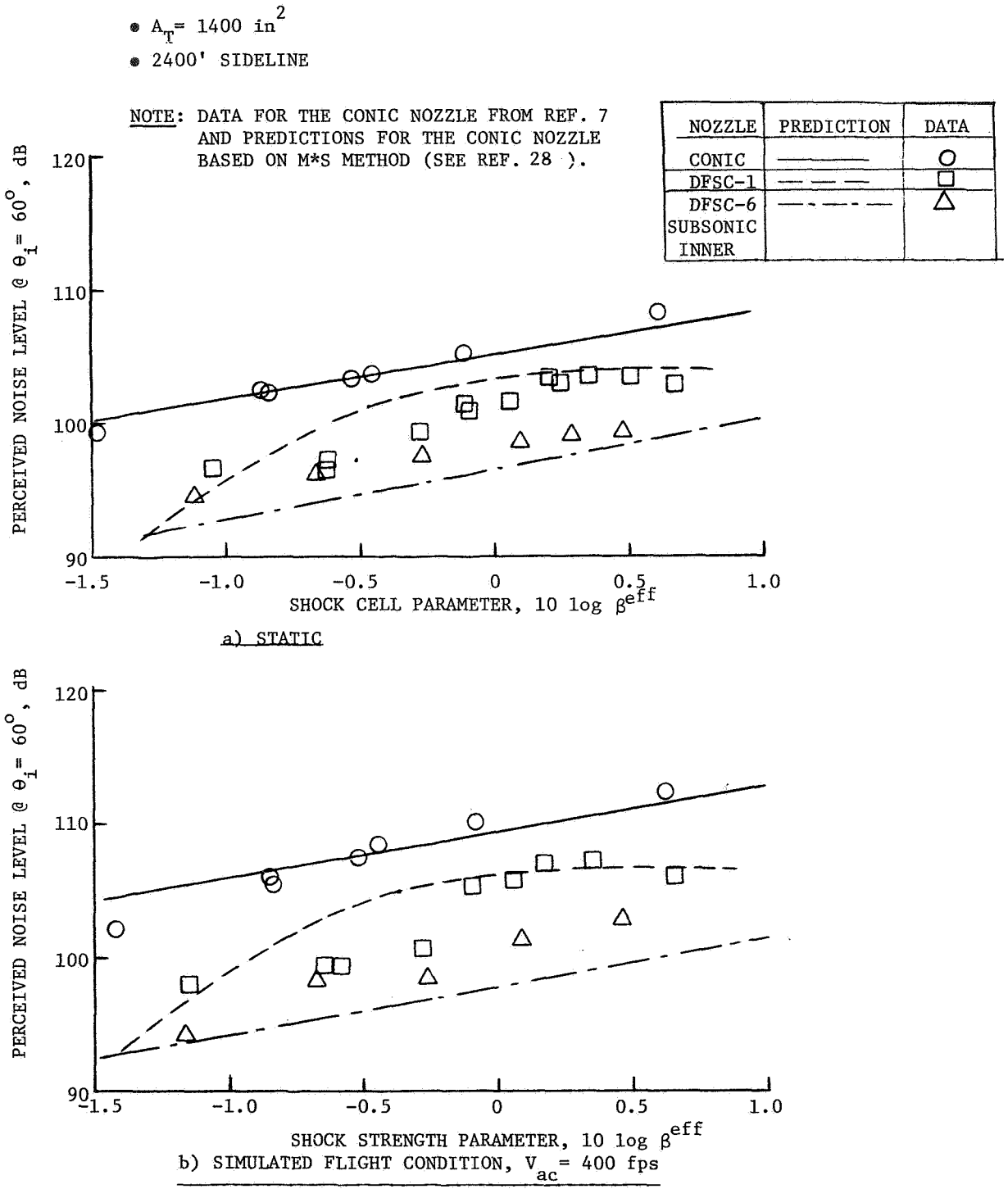

FIGURE 4-11. COMPARISON OF THE MEASURED AND PREDICTED VARIATION OF PNL AT θ_i = 60° WITH β^{eff} FOR CONIC NOZZLE, CONFIGURATIONS DFSC-1 (CONVERGENT COANNULAR PLUG NOZZLE WITH TRUNCATED PLUG) AND DFSC-6 (CONVERGENT COANNULAR PLUG NOZZLE WITH SHARP TIPPED PLUG) WITH SUBSONIC INNER STREAM FOR STATIC AND SIMULATED FLIGHT CONDITIONS.

5.0 CONCLUSIONS

During this investigation, six scale-model nozzles were tested in the Anechoic Free-Jet Facility for the evaluation of the effectiveness of convergent-divergent terminations on unsuppressed and mechanically suppressed coannular plug nozzles under both static and simulated flight conditions. The tested nozzles included (a) convergent terminated unsuppressed coannular plug nozzles with truncated and extended plugs (DFSC-1 and DFSC-6), (b) convergent-divergent terminated unsuppressed coannular plug nozzles with truncated and extended plugs (DFSC-2 and DFSC-3), (c) convergent terminated coannular plug nozzle with 20-chute convergent suppressor in the outer stream (DFSC-4), and (d) convergent-divergent terminated coannular plug nozzle with 20-chute C-D suppressor in the outer stream (DFSC-5).

A total of one hundred fifty-three acoustic test points, with inverted velocity profiles, were conducted over the six test configurations for a wide range of velocities. Diagnostic flow visualization with a shadowgraph and aerodynamic plume measurements with a laser velocimeter were performed on plumes of both convergent and C-D terminated configurations at test conditions that match with the design conditions of the corresponding C-D nozzles. In addition, most of the diagnostic tests were conducted at two outer stream temperatures of 1700°R and 870°R to determine the effect of temperature on shock-cell structure.

The significant results from the analyses of the measured acoustic and diagnostic data are:

- Available unsuppressed and suppressed convergent coannular baseline nozzle acoustic results and the corresponding measured data of this investigation agree demonstrating repeatability.

- From the diagnostic data of the unsuppressed convergent coannular nozzle with truncated plug (DFSC-1) shock-cell structures were identified on the plug and downstream of the plug. The predicted broadband peak frequencies associated with the two shock-cell

structures were correlated with the measured spectra using the average shock-cell spacings assessed from the LV-determined mean velocity profiles.

- Effectiveness of convergent-divergent terminations in the flowpaths of unsuppressed and suppressed coannular nozzles in the reduction of shock-cell noise has been measured. The front-quadrant acoustic benefit at $\Theta_i = 60°$ with the various configurations at corresponding C-D design conditions, relative to a baseline convergent circular nozzle, are summarized in Figure 5-1.

- The PNL_{60} data of unsuppressed and suppressed C-D coannular nozzles with truncated plug (DFSC-2 and 5) indicate, relative to a baseline convergent circular nozzle, a reduction of (1) 6.5 dB and 9.2 dB with unsuppressed C-D coannular nozzle (DFSC-2) and (2) 7.7 dB and 8.3 dB with suppressed C-D coannular nozzle (DFSC-5) under static and simulated flight conditions, respectively. The front quadrant acoustic benefit of the C-D configurations was observed over a range of pressure ratios in the vicinity of the C-D design condition.

- Diagnostic data obtained with the unsuppressed C-D coannular nozzle with truncated plug (DFSC-2) operating at the C-D design condition indicated (1) elimination of shock structure on the plug and (2) presence of an expansion fan at the plug termination with the resulting shock structure downstream of the plug. The effect of the expansion fan and the downstream shock-cell structure was minimized by replacing the truncated plug with a smooth extension (DFSC-3) to obtain an additional 2.4 dB and 3 dB reduction in PNL_{60} data, under static and simulated flight conditions, respectively. This additional reduction resulted in a total maximum acoustic benefit relative to a convergent circular nozzle of 8.9 dB and 12.2 dB with the unsuppressed C-D coannular nozzle with extended plug (DFSC-3) under static and simulated flight conditions, respectively.

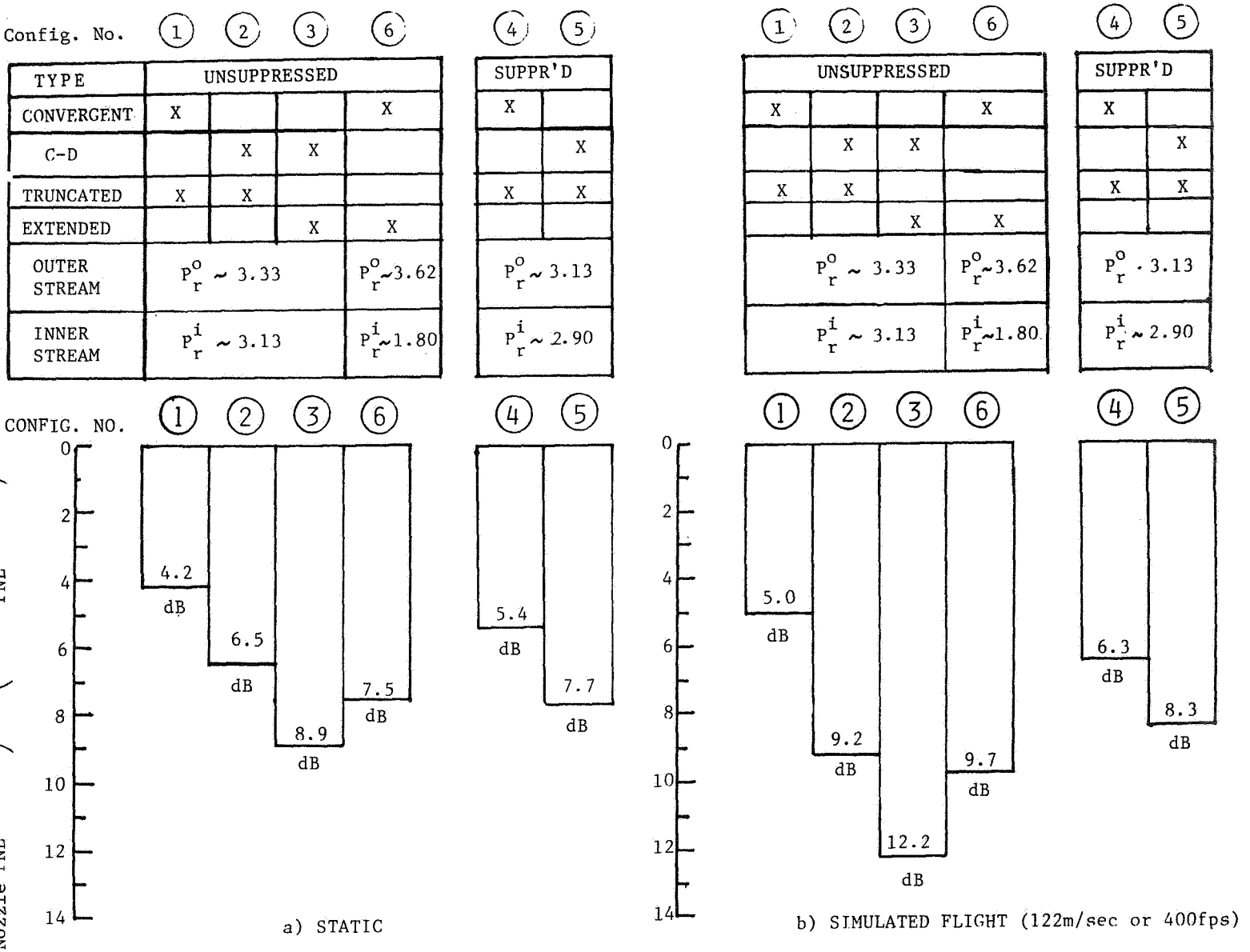

FIGURE 5-1. SUMMARY OF FRONT-QUADRANT NOISE REDUCTION MEASURED WITH COANNULAR NOZZLES OF THIS PROGRAM RELATIVE TO CONVERGENT CIRCULAR NOZZLE

- Significant front quadrant noise benefit was noted with a subsonic inner stream relative to a supersonic inner stream for the unsuppressed convergent coannular plug nozzle over an underexpanded range of outer stream conditions. At a shock strength parameter equal to that at the design condition of the unsuppressed C-D coannular nozzle with extended plug (DFSC-3), a maximum acoustic benefit of 7.5 and 9.7 dB were obtained at θ_i = 60° with the convergent coannular plug nozzle with a subsonic inner stream relative to a convergent circular nozzle, under static and simulated flight conditions.

- Diagnostic data that compare the axial mean velocities of convergent coannular nozzle obtained with supersonic and subsonic inner streams, for a given underexpanded outer stream, indicate a significant reduction in the number and strength of shock-cells with the subsonic inner stream for all regions downstream of the plug.

- Diagnostic data with the convergent and C-D suppressor configurations (DFSC-4 and 5) indicate (1) weakening of shock-cell structure on the plug of the C-D suppressor relative to that of convergent suppressor, (2) a subsonic flow region and hence no shock-cells downstream of the plug of the convergent suppressor and (3) existence of a supersonic flow and shock-cells downstream of the plug of C-D suppressor configuration. Due to the existence of the supersonic flow over a considerable downstream distance, the C-D suppressor resulted in more aft quadrant noise than the convergent C-D suppressor.

- The predicted broadband frequencies associated with shock-cells on the plug of the convergent suppressor nozzle and downstream of the plug of the C-D suppressor nozzle were correlated with the measured spectra using the average shock-cell spacings assessed from the shadowgraph and LV measurements.

- Jet temperature was determined to have negligible effect on the shock-cell noise of unsuppressed and suppressed convergent coannular plug nozzles.

- The free-jet was determined not to affect the supersonic shear layer and the sonic-line close to the exit regions of the nozzles.

Based on the measured diagnostic data of the flow field of the unsuppressed convergent coannular plug nozzle, appropriate parameters that characterize the length scale and strength associated with the shock-cells on the plug and downstream of the plug were identified. An existing shock-cell noise predictive program based on Fisher-Harper and Bourne model for convergent circular nozzle was modified to account for the observed two shock-cell structures. An acceptable agreement has been indicated between the measured and predicted data. In addition, an empirical model has been developed to estimate the effectiveness of (1) a subsonic inner for a convergent coannular nozzle and (2) convergent-divergent terminations in the vicinity of the design conditions for a C-D coannular nozzle.

6.0 NOMENCLATURE

A	Area, in^2
a_{amb}	Ambient speed of sound, fps
A_r	Ratio of inner to outer stream flow area
C-D	Convergent-Divergent
D	Diameter, in
f	Frequency, hertz
F	Thrust, lbs
F_{ref}	Reference thrust, 5,130 lbs.
h	Flowpath annulus height, in
k_i	Number of velocity samples in a class interval
L	Shock-cell spacing
ℓ	Divergent flowpath length
LBM	Mixed shock strength parameter, defined in Section 2.5.1
LV	Laser velocimeter
LVM	Mixed jet velocity parameter, defined in Section 000.1
M	Mach number
M_c	Convention Mach Number, U_c/a_{amb}
N	Total number of data samples for a histogram
NF	Normalization Factor, defined in Section 2.5.1
OAPWL	Overall Sound Power Level, dB re 10^{-12} Watts
OASPL	Overall Sound Pressure Level, dB re 20 $\mu N/m^2$
P	Pressure, psia
$\mathcal{P}$	Power
PNL	Perceived Noise Level, dB
PNLN	Normalized Perceived Noise Level, dB
P_r	Pressure ratio = P_T/P_{amb}
PWL	Sound Power Level, dB re 10^{-12} Watts
R	Radial distance
RH	Relative Humidity, %
R_o^i	Inner radius of outer stream, in
R_o^o	Outer radius of outer stream, in
R_r	Radius ratio

R_r^o	Outer stream radius ratio, R_o^i/R_o^o
S	Throat Slant Height
SPL	Sound Pressure Level, dB
T	Temperature, °R
t	Time, sec.
U_c	Convection velocity of eddy, feet/sec
v'	Turbulent velocity, feet/sec
V	Velocity, feet/sec
$\bar{V}$	Mean velocity, feet/sec
VCE	Variable Cycle Engine
W	Weight flow rate, lbs/sec
X	Axial distance, in

Greek Symbols

α	Atmospheric attenuation correction, dB, (Reference 12)
β	Shock strength parameter, defined as $\sqrt{M^2-1}$
γ	Ratio of specific heats
Δ	Sound Pressue Level difference, dB
θ_1	Divergent flap angle, degree
θ_2	Plug angle, degree
θ_{chute}	Angle subtended by each chute, degree
θ_{flow}	Angle subtended by each flow element, degree
θ_i	Angle of observer relative to inlet axis, degree
ρ	Density, lb/ft^3
ω	Density exponent

Superscripts

eff	Effective condition for dual stream nozzles
i	Inner stream
mix	Mixed stream
o	Outer stream

Subscripts

1,2...8	Shock cell number
60	Evaluated at $\theta_i = 60°$
130	Evaluated at $\theta_i = 130°$
ac	Aircraft
amb	Ambient
avg	Average
d	Design condition for convergent-divergent flowpaths
down	Refers to shocks downstream of the plug
eff	Effective condition for dual stream nozzles
exit	At nozzle exit
eq	Equivalent conic nozzle
flight	In flight value
hyd	Hydraulic
i	Index
j	Jet
η	ηth shock cell
on	Refers to shocks on the plug
obs	Source to observer
p	Peak
r	Ratio
S	Static (thermodynamic)
screech	Related to shock screech
static	Static (without simulated flight)
std day	Standard day
T	Total
throat	At nozzle throat

7.0 REFERENCES

1. Harper-Bourne, M., and Fisher, M., "The Noise From Shock Waves in Supersonic Jets," Proceedings of the AGARD Conference on Noise Mechanisms, Brussels, Belgium, AGARD CP131, 1973.

2. Stringas, E. J., et. al., "High Velocity Jet Noise Source Location and Reduction, Task 2: Theoretical Development and Basic Experiments, Task 6: Noise Abatement Design Guide," Final Report, FAA-RD-76-79, 1979.

3. Tanna, H. K., "An Experimental Study of Jet Noise - Part II: Shock Associated Noise," Journal of Sound and Vibration, Volume 50, 1977, Pages 429-444.

4. Sarohia, V., "Some Flight Simulation Experiments on Jet Noise From Supersonic Under Expanded Flows," AIAA Journal, Volume 16, 1978, Pages 710-716.

5. Knott, P. R., Janardan, B. A., Majjigi, R. K., Bhutiani, P. K., and Vogt, P., "Free-Jet Acoustic Investigation of High Radius-Ratio Coannular Plug Nozzles," Final Report on Contract NAS3-20619, under preparation.

6. Janardan, B. A., Majjigi, R. K., Brausch, J. F., and Knott, P. R., "Free-Jet Investigation of Mechanically Suppressed, High Radius Ratio Coannular Plug Model Nozzles," Final Report on Contract NAS3-21608, NASA CR-3596, 1984.

7. Yamamoto, K., Brausch, J. F., Janardan, B. A., Hoerst, D. J., Price, A. O., and Knott, P. R., "Experimental Investigation of Shock-Cell Noise Reduction for Single Stream Nozzles in Simulated Flight," Comprehensive Data Report on Contract NAS3-22514, R82AEB491, 1984 (NASA CR-168234).

8. Benzakein, M. J., and Knott, P. R., "Supersonic Jet Exhaust Noise," AFAPL TR-72-52, 1972.

REFERENCES (Continued)

9. Seiner, J. M., Norum, T. D., and Maestrello, L., "Effects of Nozzle Design on the Noise from Supersonic Jets," Supersonic Cruise Research 1979, Proceedings, Langley Research Center, NASA CP-2108, pages 479-492.

10. Norum, T. D. and Seiner, J. M., "Location and Propagation of Shock Associated Noise From Supersonic Jets," AIAA 6th Aeroacoustic Conference, AIAA 80-0983, 1980.

11. Tam, C. K. W. and Tanna, H. K., "Shock Associated Noise of Supersonic Jets From Convergent-Divergent Nozzles," Journal of Sound and Vibration, Volume 81, 1982, Pages 337-358.

12. Shields, F. D. and Bass, H. E., "Atmospheric Absorption of High Frequency Noise and Application to Fractional Octave Bands," NASA CR-2760, 1977.

13. Clapper, W. S., et al., "High Velocity Jet Noise Source Location and Reduction; Task IV - Development/Evaluation of Techniques for Inflight Investigation," R77AEG189, Report No. FAA-RD-76-79, IV, Final Report, U. S. Department of Transportation, February 1977.

14. Vogt, P. G., Bhutiani, P. K., and Knott, P. R., "Free-Jet Acoustic Investigation of High Radius Ratio Coannular Plug Nozzles," General Electric Company, Comprehensive Data Report, Volume I, R81AEG212, Contract NAS3-20619, January 1981.

15. Yamamoto, K., Janardan, B. A., Brausch, J. F., Hoerst, D. J., and Price, A. O., "Experimental Investigation of Shock-Cell Noise Reduction for Dual-Stream Nozzles in Simulated Flight," Comprehensive Data Report for Contract NAS3-23166, R83AEB358, 1984 (NASA CR-168336).

16. Knott, P. R., et al., "Supersonic Jet Exhaust Noise Investigation," AFAPL-TR-74-25, June 1974.

17. Brausch, J. F., et al., "High Velocity Jet Noise Source Location and Reduction; Task III - Experimental Investigation of Suppression Principles," Volumes II and III, R78AEG627, U. S. Department of Transportation, December 1978.

18. Knott, P. R., "Supersonic Jet Exhaust Investigation - Volume I Summary Report," AFAPL-TR-76-78, July 1, 1976.

19. Brausch, J. F., "Model Hardware Design Report for an Experimental Investigation of Shock-Cell Noise Reduction for Dual Stream Nozzles in Simulated Flight," General Electric Company, R82AEBG327, May 1982.

20. Brausch, J. F., Whittaker, R. W., and Knott, P. R., "Acoustic and Aerodynamic Nozzle Performance Design Considerations for the NASA AST/VCE Core Drive (CDFS) Acoustic Nozzle Program," General Electric Company, TM80-216, March 1980.

21. Bediako, E. D., and Yamamoto, K., "Aerodynamic Design and Analysis for Shock-Cell Noise Reduction System," General Electric Company, R81AEG543, September 1981.

22. Knott, P. R., Blozy, J. T., and Staid, P. S., "Acoustic and Aerodynamic Performance Investigations of Inverted Velocity Profile Coannular Plug Nozzles," NASA CR-3149, June 1979.

23. Powell, A., "On the Mechanism of Choked Jet Noise," Proc. Phys. Soc., Volume 66, 1953, Pages 1039-1056.

24. Howe, M. S. and Ffowcs-Williams, J. E., "On the Noise Generated by an Imperfectly Expanded Supersonic Jet," Phil. Trans. Roy. Soc. London, Volume 289, Number 1358, Pages 271-314 (1978).

REFERENCES (Concluded)

25. Yamamoto, K., Brausch, J. F., Balsa, T. F., Janardan, B. A., and Knott, P. R., "Experimental Investigation of Shock-Cell Noise Reduction for Single Stream Nozzles in Simulated Flight," Final Report on NAS3-23166, 1984.

26. Bhutiani, P. K., "A Unique Coannular Plug Nozzle Jet Noise Prediction Procedure," General Electric Technical Information Series Report No. R79AEG481, October 1979.

27. Vdoviak, J. W., Knott, P. R., and Ebacker, J. J., "Aerodynamic/Acoustic Performance of YJ101/Double Bypass VCE with Coannular Plug Nozzle," NASA CR-159869, January 1981.

28. Clapper, W. S., Gliebe, P. R., Motsinger, R., Sieckmann, A., and Stringas, E. J., "High Velocity Jet Noise Source Location and Reduction, Task 3 - Experimental Investigation of Suppression Principles, Volume I - Verification of Suppression Principles and Development of Suppression Prediction Methods," General Electric Company Contractor Final Report Number FAA-RD-76-79, III-I, December 1978.

29. Dosanjh, D. S., Bhutiani, P. K., and Ahuja, K. K., "Supersonic Jet-Noise Reduction by Coaxial Cold/Heated Jet Flows," Final Report on Grant No. DOT-OS-20094, Syracuse University, New York, March 1977, Pages 52-66.

1. Report No.	2. Government Accession No.	3. Recipient's Catalog No.
NASA CR-3846		

4. Title and Subtitle	5. Report Date
Experimental Investigation of Shock-Cell Noise Reduction for Dual-Stream Nozzles in Simulated Flight	November 1984
	6. Performing Organization Code

7. Author(s)	8. Performing Organization Report No.
B. A. Janardan, K. Yamamoto, R. K. Majjigi, and J. F. Brausch	R83AEB358
	10. Work Unit No.

9. Performing Organization Name and Address	11. Contract or Grant No.
General Electric Company Aircraft Engine Business Group Cincinnati, Ohio 45215	NAS3-23166
	13. Type of Report and Period Covered
	Contractor Report

12. Sponsoring Agency Name and Address	14. Sponsoring Agency Code
National Aeronautics and Space Administration Washington, D. C. 20546	501-31-3B (E-2283)

15. Supplementary Notes

Final report. Project Manager, James R. Stone, Fluid Mechanics and Instrumentation Division, NASA Lewis Research Center, Cleveland, Ohio 44135.

16. Abstract

Six scale-model nozzles were tested in an anechoic facility to evaluate the effectiveness of convergent-divergent (C-D) terminations in reducing shock-cell noise of unsuppressed and mechanically suppressed coannular plug nozzles. One hundred fifty-three acoustic test points with inverted velocity profiles were conducted under static and simulated flight conditions. Diagnostic flow visualization with a shadowgraph and velocity measurements with a laser velocimeter were performed on selected plumes. Significant results from the analyses of the measured data include: (a) Shock-cells were identified on the plug and downstream of the plug of the unsuppressed convergent coannular nozzle with truncated plug. Broadband peak frequencies predicted with the two shock-cell structures were correlated with the observed spectra using the measured shock-cell spacings. (b) Relative to a convergent circular nozzle, the perceived noise level data at an observer angle of 60° relative to inlet, indicated a reduction of (1) 6.5 dB and 9.2 dB with unsuppressed C-D coannular nozzle with truncated plug and (2) 7.7 dB and 8.3 dB with suppressed C-D coannular nozzle under static and simulated flight conditions, respectively. (c) The unsuppressed C-D coannular nozzle with truncated plug, operating at the C-D design condition, had shock-cells downstream of the plug with no shock-cells on the plug. The downstream shock-cells were eliminated by replacing the truncated plug with a smooth extension to obtain an additional 2.4 dB and 3 dB front quadrant PNL reduction, under static and simulated flight conditions, respectively. (d) With an underexpanded outer stream, reduction in the number and strength of shock-cells were noted in regions downstream of the plug of the convergent coannular nozzle with a subsonic inner relative to a supersonic inner stream. This resulted in a significant front-quadrant noise reduction. (e) Suppressor configurations were noted to have a subsonic flow downstream of the plug of the convergent nozzle and a supersonic flow downstream of the plug of C-D nozzle. This resulted in a higher aft quadrant noise for the C-D suppressor for a given stream conditions. An existing convergent circular nozzle shock-cell noise predictive program was modified to account for the shock-cells on the plug and downstream of the plug of convergent coannular nozzle. An acceptable agreement was obtained between the predicted and measured acoustic data.

17. Key Words (Suggested by Author(s))	18. Distribution Statement
Shock-cell noise; Supersonic jet noise; Convergent-divergent nozzles; Coannular nozzles; Suppressor nozzles	Unclassified - unlimited STAR Category 71

19. Security Classif. (of this report)	20. Security Classif. (of this page)	21. No. of pages	22. Price*
Unclassified	Unclassified	188	A09

*For sale by the National Technical Information Service, Springfield, Virginia 22161 NASA-Langley, 1984

National Aeronautics and
Space Administration

Washington, D.C.
20546

Official Business
Penalty for Private Use, $300

SPECIAL FOURTH CLASS MAIL
BOOK

Postage and Fees Paid
National Aeronautics and
Space Administration
NASA-451

NASA

POSTMASTER: If Undeliverable (Section 158
Postal Manual) Do Not Return